

Electronic Thesis and Dissertation Repository

---

9-20-2011 12:00 AM

## Development of Single and Multimodality Imaging Probes for PET, SPECT and Fluorescence Imaging

Babak Behnam Azad  
*The University of Western Ontario*

Supervisor  
Dr. Leonard G. Luyt  
*The University of Western Ontario*

Graduate Program in Chemistry  
A thesis submitted in partial fulfillment of the requirements for the degree in Doctor of Philosophy  
© Babak Behnam Azad 2011

Follow this and additional works at: <https://ir.lib.uwo.ca/etd>

 Part of the [Medicinal-Pharmaceutical Chemistry Commons](#), and the [Other Chemistry Commons](#)

---

### Recommended Citation

Behnam Azad, Babak, "Development of Single and Multimodality Imaging Probes for PET, SPECT and Fluorescence Imaging" (2011). *Electronic Thesis and Dissertation Repository*. 274.  
<https://ir.lib.uwo.ca/etd/274>

This Dissertation/Thesis is brought to you for free and open access by Scholarship@Western. It has been accepted for inclusion in Electronic Thesis and Dissertation Repository by an authorized administrator of Scholarship@Western. For more information, please contact [wlsadmin@uwo.ca](mailto:wlsadmin@uwo.ca).

DEVELOPMENT OF SINGLE AND MULTIMODALITY IMAGING PROBES  
FOR PET, SPECT AND FLUORESCENCE IMAGING

(Spine title: Probe Development for PET, SPECT and Fluorescence Imaging)

(Thesis format: Integrated-Article)

by

Babak Behnam Azad

Graduate Program in Chemistry  
(in collaboration with the Graduate Program in Molecular Imaging)

A thesis submitted in partial fulfillment  
of the requirements for the degree of  
Doctor of Philosophy

The School of Graduate and Postdoctoral Studies  
The University of Western Ontario  
London, Ontario, Canada

© Babak Behnam Azad 2011

THE UNIVERSITY OF WESTERN ONTARIO  
SCHOOL OF GRADUATE AND POSTDOCTORAL STUDIES

**CERTIFICATE OF EXAMINATION**

Supervisor

\_\_\_\_\_  
Dr. Leonard G. Luyt

Examiners

\_\_\_\_\_  
Dr. Kim M. Baines

\_\_\_\_\_  
Dr. Brian L. Pagenkopf

\_\_\_\_\_  
Dr. Brigitte Guérin

\_\_\_\_\_  
Dr. Edith Arany

The thesis by

**Babak Behnam Azad**

entitled:

**Development of Single and Multimodality Imaging Probes  
for PET, SPECT and Fluorescence Imaging**

is accepted in partial fulfillment of the  
requirements for the degree of  
Doctor of Philosophy

Date \_\_\_\_\_

\_\_\_\_\_  
Chair of the Thesis Examination Board

## ABSTRACT

This dissertation is in an integrated format discussing three major projects centered around probe development. In the first project, novel metal-chelated and fluorinated GLP-1 derivatives were prepared all containing D-Ala-8, a modification known to improve resistance towards degradation by dipeptidyl-peptidase IV. The effect of increased distance between DOTA and the peptide chain was investigated using a spacer, in order to reduce steric effects imposed by DOTA. Placement of linker and DOTA moieties were varied within the GLP-1 sequence to test for optimal metal-complex location. Binding affinity of peptide derivatives was determined *in vitro* with CHO/GLP-1R cell line and shown to be in the nM range. *In vivo* imaging was carried out using C57BL/6 mice. Modifications made to the peptide backbone, based on charge distribution, were shown to improve pharmacokinetics. Our results suggest developed GLP-1 tracers to be potential candidates for the non-invasive imaging of pancreatic islets *in vivo*.

In the second project, Gallium-chelated protoporphyrin IX (PPIX) derivatives containing the tripeptide RGD  $\alpha_v\beta_3$ -targeting moiety were prepared and evaluated. Reaction conditions for both naturally occurring  $^{69/71}\text{Ga}$ -labeling as well as  $^{68}\text{Ga}$ -radiolabeling were optimized using a microwave reactor. Optical properties were evaluated in order to study the effects of ligand conjugation and gallium chelation on absorption/emission properties of PPIX. Quantum yields pre- and post gallium chelation were comparable, indicating that the presence of gallium does not quench the inherent fluorescence of PPIX. The targeted compound was preferentially taken up by  $\alpha_v\beta_3$  integrin-expressing cancer cells versus the non-targeted form, as assessed by fluorescence microscopy. Our results suggest that gallium-

PPIX conjugates could be used as dual modality positron emission tomography/fluorescence microscopy probes and can assist in bridging imaging agent discovery from *in vitro* microscopy through to *in vivo* imaging.

In the third and final project, a novel high-throughput cell-based technique was developed for screening one-bead-one-compound (OBOC) libraries. In order to validate this technique, a small library consisting of heptameric peptides, and the  $\alpha_v\beta_3$  integrins targeting RGD sequence, was synthesized on Tentagel beads via a photo-labile linker. Compounds were screened against the  $\alpha_v\beta_3$ -expressing MD 435 cell line. After fluorescent-based sorting, peptides were photolytically cleaved off resin and analyzed using MALDI-TOF/TOF. Deconvolution of all peptide sequences was carried out successfully indicating this screening process to be a facile and efficient technique for discovery of novel targeting entities.

Keywords: Radiochemistry, Gallium-68, Indium-111, Fluorine-18, PPIX, GLP-1, OBOC library, molecular imaging

## CO-AUTHORSHIP STATEMENT

For data presented in Chapter 2, all synthesis, purification, characterization, labeling ( $^{111}\text{In}$ ,  $^{113/115}\text{In}$ ,  $^{69/71}\text{Ga}$ ,  $^{68}\text{Ga}$ ,  $^{19}\text{F}$ ,  $^{18}\text{F}$ ), as well as *in vitro* binding affinity assays and statistical analysis for compounds **1-8** were carried out by Babak Behnam Azad. *In vitro* plasma stability experiments, for developed GLP-1 analogues, were carried out in collaboration between Babak Behnam Azad and Vanessa Rota. Binding affinity determination of compounds acyl-GLP-**7** and acyl-GLP-**8**, cAMP experiments, as well as *in vivo* PET/SPECT imaging, were carried out by Vanessa Rota. Dr. Michael Kovacs assisted with the use of the GE TRACERlab FX-N automated unit for the synthesis of 4- $^{18}\text{F}$ ]FB. Dan Breadner was co-author due to acquiring preliminary results, which are not included in this thesis.

For data presented in Chapter 3, all synthesis, purification, characterization, metal-chelation ( $^{69/71}\text{Ga}$ ,  $^{68}\text{Ga}$ ), optical measurements and statistical analysis were carried out by Babak Behnam Azad. Fluorescence microscopy and cell culture was carried out by Choi-Fong Cho.

For data presented in Chapter 4, library synthesis, characterization, as well as MADLI-TOF/TOF analysis and all sequence deconvolution procedures were carried out by Babak Behnam Azad. Cell sorting and fluorescence microscopy were carried out by Choi-Fong Cho.

“Nel mezzo del cammin di nostra vita  
mi ritrovai per una selva oscura  
ché la diritta via era smarrita.”

–*Dante Alighieri*

*Dedicated to my loving parents, Hossein and Zarrin Behnam Azad*



## ACKNOWLEDGMENTS

My most sincere gratitude is extended to my supervisor Dr. Leonard G. Luyt for providing me with the opportunity to peruse my research interest in radiotracer development and molecular imaging and for teaching me the key traits of a true leader.

I wish to thank Dr. Savita Dhanvantari for her continuous support and guidance throughout my research. It is truly a rare gift to have the opportunity to work with such an exceptional researcher who still remembers what it is like to be a graduate student. I would also like to thank her laboratory members, and in particular Vanessa Rota, for their collaboration and expertise.

I thank Dr. Michael Kovacs for allowing me the use of his radiochemistry facilities, and for his assistance with the use of GE TRACERlab FX-N automated synthesis unit, as well as his laboratory associates for their support. I would also like to extend my gratitude to Dr. John Lewis and members of his lab, in particular Choi-Fong Cho, for their expertise and collaboration.

I thank my colleagues and friends at the University of Western Ontario and London Regional Cancer Program for their support and for making my graduate studies more enjoyable. Special thanks go to my better half, Rania, for her unconditional love and for continuing to be my guiding light during difficult times. I also extend a special thank you to my best friend Parsian whose friendship has been invaluable throughout the years.

Above all, I am forever grateful to my parents and my brother for their everlasting love and support during all stages of my life. If not for their sacrifices, I would not be where I am today.

## TABLE OF CONTENTS

	Page
Certificate of Examination	ii
Abstract	iii
Co-Authorship Statement	v
Epigraph	vi
Dedication	vii
Acknowledgements	viii
Table of Contents	ix
List of Tables	xii
List of Figures	xiv
List of Schemes	xvi
List of Appendices	xvii
List of Abbreviations	xviii
CHAPTER 1 Molecular Imaging	
1.1 Introduction	1
1.2 Imaging Probes	2
1.3 Design of Molecular Imaging Probes	6
1.4 Targeting Component	8
1.5 Labeling Techniques	11
1.6 Imaging Modalities	19
1.7 Radioisotope Production	26
1.8 Imaging Probe Design: Overall Picture	34
1.9 Multimodality Imaging	34
1.10 References	40
CHAPTER 2 Design, Synthesis and In Vitro Characterization of Glucagon-Like Peptide-1 Derivatives for Pancreatic Beta Cell Imaging	
2.1 Introduction	60
2.2 Experimental Procedures	69
2.3 Results and Discussion	81
2.3.1 Design of GLP-1 analogues	81
2.3.2 Synthesis of Indium-GLP-1 analogues	84

2.3.3	<i>In vitro</i> studies	89
2.3.4	cAMP studies	91
2.3.5	<sup>111</sup> In-Labeling	92
2.3.6	Synthesis of Gallium-GLP-1 analogues	95
2.3.7	Gallium-68 radiolabeling of GLP-1 analogues	96
2.3.8	<i>In vivo</i> studies	101
2.3.9	Modifying the GLP-1 peptide backbone	104
2.3.10	Fluorination of GLP-1	107
2.4	Conclusions	114
2.5	Acknowledgments	115
2.6	References	116

### CHAPTER 3 Development of targeted Gallium-PPIX compounds for PET / Fluorescence dual modality imaging

3.1	Introduction	130
3.2	Experimental Procedures	134
3.3	Results and Discussion	139
3.3.1	Probe design	139
3.3.2	Synthesis of <sup>69/71</sup> Ga-PPIX analogues	141
3.3.3	Optical analysis	144
3.3.4	<i>In vitro</i> imaging	146
3.3.5	<sup>68</sup> Ga-labeling	148
3.4	Conclusions	150
3.5	References	150

### CHAPTER 4 A cell-based approach for OBOC combinatorial library screening against cell surface receptors

4.1	Introduction	157
4.2	Experimental Procedures	163
4.3	Results and Discussion	166
4.4	Conclusions	181
4.5	References	182

CHAPTER 5 Outlook and Concluding Remarks	189
APPENDIX	194
CURRICULUM VITAE	224

## LIST OF TABLES

Table	Description	Page
1.1	List of targeted compounds for oncologic applications	4
1.2	List of peptides targeting GPCRs	9
1.3	Commercially available fluorescein derivatives	12
1.4	Radiometal chelators for Indium-111 and Gallium-68	17
1.5	Radioisotopes used in PET/SPECT imaging	23
1.6	PET tracers used in oncology	24
1.7	Clinical applications of radiopharmaceuticals for SPECT imaging	26
1.8	Properties of cyclotron produced radionuclides used in this dissertation	29
1.9	Specifications of generators used in nuclear medicine	31
1.10	Optical imaging applications in living subjects	34
2.1	Examples of <sup>18</sup> F-labeled peptide-based imaging tracers	68
2.2	Basic requirements of ideal radiofluorination procedures	69
2.3	Analysis of synthesized In-GLP-1 analogues by ESI-MS and RP HLPC	87
2.4	Receptor binding and cAMP measurements for GLP-1 peptide analogues	90
2.5	Description of modular part notations	99
2.6	Optimization of radiometal labeling conditions for GLP-1 analogues	100
3.1	Analysis of PPIX-RGD analogues by RP-HLPC and ESI-MS	142
3.2	Photophysical data for PPIX derivatives <b>1-9</b>	145
4.1	A list of biological targets for which OBOC combinatorial library assays were employed	163
4.2	List of prepared peptide sequences for cell-based screening assay	168
4.3	Calculated and observed fragmentation patterns for untreated GRGDSPS peptide	176
4.4	Calculated and observed fragmentation patterns for GRGDSPS peptide post sorting	176
4.5	Experimental and calculated fragmentations for <b>2</b>	177
4.6	Experimental and calculated fragmentations for <b>3</b>	177

4.7	Experimental and calculated fragmentations for <b>4</b>	178
4.8	Experimental and calculated fragmentations for <b>5</b>	178
4.9	Experimental and calculated fragmentations for <b>6</b>	179
4.10	Experimental and calculated fragmentations for <b>7</b>	179

## LIST OF FIGURES

Figure	Description	Page
1.1	Classes of imaging probes and their interaction schemes	2
1.2	Localization mechanism of gold nanoparticles in tumors cells	3
1.3	Scheme of targeted imaging probes versus smart probes	5
1.4	Design of an imaging probe	6
1.5	General outline of a cell showing commonly targeted entities	7
1.6	Examples of biological barriers in imaging probe delivery	8
1.7	Examples of reactive group chemistry for conjugation of a prosthetic group or bifunctional chelator	16
1.8	Available <i>in vivo</i> imaging modalities for small animal models	20
1.9	Mechanism of photon detection in PET	22
1.10	Structure of $^{18}\text{F}$ -FDG	23
1.11	Schematic diagram of a gamma camera setup for SPECT	25
1.12	Schematic of a cyclotron setup and function	28
1.13	Illustration of a radionuclide generator set-up	30
1.14	Structure of a fluorescent/MR dual-modality imaging probe with a PAMAM dendrimer core	37
1.15	Structures of $^{111}\text{In}$ -DOTA-cypate and Gd-DO3A-spiro-naphthoxazine	39
2.1	Major proglucagon degradation products and role of GLP-1 in insulin production	61
2.2	Structure of tris-tBu-DOTA	67
2.3	Structure of $^{37}\text{Lys}$ -DOTA-GLP-1	81
2.4	A schematic of the structure activity relationship of GLP-1	83
2.5	UV and MS spectra for compound <b>7</b> post purification	88
2.6	Competitive Displacement of compounds <b>2</b> , <b>7</b> and <b>8</b> vs. $^{125}\text{I}$ -exendin-4 on CHO/GLP-1R cells	89
2.7	<i>In vitro</i> cAMP accumulation of GLP-1, <b>2</b> , <b>7</b> , or <b>8</b> in CHO/GLP-1R	92
2.8	HPLC chromatograms for [ $^{113/115}\text{In}$ ]- <b>8</b> and [ $^{111}\text{In}$ ]- <b>8</b>	93
2.9	HPLC chromatograms for [ $^{113/115}\text{In}$ ]- <b>2</b> and [ $^{111}\text{In}$ ]- <b>2</b>	94
2.10	<i>In vitro</i> gamma camera imaging study with INS-1 832/13 cells	95
2.11	Depiction of an Eckert and Ziegler modular lab system for $^{68}\text{Ga}$ -radiolabeling experiments	97
2.12	HPLC chromatograms of $^{69/71}\text{Ga}$ - <b>7</b> and $^{68}\text{Ga}$ - <b>7</b> post purification	101
2.13	PET images after injection of $^{68}\text{Ga}$ - <b>7</b> into a C57BL/6 mouse	102

2.14	Biodistribution of <sup>68</sup> Ga- <b>7</b> in C57BL/6 mice	103
2.15	Ex-vivo gamma camera images of pancreata, hearts and stomachs after injection of <sup>68</sup> Ga- <b>7</b>	103
2.16	PET images after intravenous injection of <sup>68</sup> Ga-acyl- <b>7</b> into a C57BL/6 mouse	106
2.17	HPLC chromatogram and ESI-MS spectrum of <b>9</b>	109
2.18	Competitive Displacement assay of <sup>37</sup> Lys-FB GLP-1 vs. <sup>125</sup> I-Exendin-4 and <i>in vitro</i> cAMP accumulation in CHO/GLP-1R cells	110
2.19	<sup>1</sup> H-NMR spectrum of purified TMABT	111
2.20	HPLC chromatograms for 4-[ <sup>19</sup> F]FBA and 4-[ <sup>18</sup> F]FBA	112
3.1	Structures of porphine, phthalocyanine, protoporphyrin IX, and heme	132
3.2	Structure of the proposed imaging probe	140
3.3	Absorption and emission data obtained for <b>8</b>	145
3.4	Fluorescence microscopy of <b>8</b> in GFP-expressing MDA-MB-435 cells	147
3.5	HPLC chromatograms of [ <sup>69/71</sup> Ga]- <b>8</b> and [ <sup>68</sup> Ga]- <b>8</b>	149
4.1	Structures of Tentagel, PEG-PS and ArgoGel-MB-NH <sub>2</sub> resins	160
4.2	Illustration of an OBOC screening assays	162
4.3	Illustrates design of prepared peptides	168
4.4	Mechanism of detection and isolation of fluorescent samples by a COPAS <sup>TM</sup> Biosorter	169
4.5	Images of MDA-MB-435 cells adhered to Tentagel beads containing <b>6</b>	170
4.6	Images of MDA-MB-435 cells adhered to peptide-conjugated tentagel beads	171
4.7	Common peptide fragmentation and notations	173
4.7	MS/MS spectrum of GRGDSPS peptide standard	174
4.9	MS/MS spectrum of GRGDSPS peptide post sorting	175



## LIST OF SCHEMES

Scheme	Description	Page
2.1	Synthetic scheme for preparation of <b>7</b> and <b>8</b>	85
2.2	Indium labeling of DOTA-GLP-1 derivatives	87
2.3	Synthetic scheme for <sup>69/71</sup> Ga-labeling of GLP-1 analogues	96
2.4	Schematic of a program written for <sup>68</sup> Ga-labeling of GLP-1 analogues	98
2.5	Synthetic scheme for preparation of <b>9</b>	108
2.6	Synthetic scheme for the radiofluorination of GLP-1 analogues via solid phase approach	111
2.7	Synthetic scheme for the radiofluorination of GLP-1 analogues via solution phase approach	114
3.1	Synthetic pathway for the preparation of PPIX-AEEA-RGD analogues	142
3.2	Synthetic scheme for the preparation of <b>8</b>	143
3.3	Radiolabeling scheme for compound <b>8</b>	149
4.1	Synthetic pathway for a randomized combinatorial library	160
4.2	Possible fragmentation patterns of the Arginine side chain	180

## LIST OF APPENDICES

Appendix	Description	Page
I	Supplementary data for Chapter 2	194
II	Supplementary data for Chapter 3	202
III	Supplementary data for Chapter 4	210
IV	Copyright approval	222
V	Ethics approval	223

## LIST OF ABBREVIATIONS

Abbreviation	Description
4-FB	4-fluorobenzoic acid
ACE	affinity capillary electrophoresis
AEEA	2-[2-(2-aminoethoxy)ethoxy]acetic acid
Alloc	allyloxycarbonyl
Fmoc-ANP	<i>N</i> -Fmoc-3-amino-3-(2-nitrophenyl) propionic acid
BI	bioluminescence imaging
BOC	t-butoxycarbonyl
BODIPY	boron dipyrromethene
cAMP	cyclic adenosine monophosphate
CHO	chinese hamster ovary
CT	computed tomography
DCHA	dicyclohexylamine
DCM	dichloromethane
DIPEA	<i>N,N</i> -diisopropylethylamine
DMEM	dulbecco's modified eagle's medium
DMF	dimethylformamide
DMSO	dimethylsulfoxide
DOTA	1,4,7,10-tetraazacyclododecane-1,4,7,10-tetraacetic acid
DPP-IV	dipeptidyl-peptidase-IV
DTPA	diethylene triamine pentaacetic acid
DTT	dithiothreitol
EPR	enhanced permeability and retention effect
ESI-MS	electrospray ionization mass spectrometry
FDA	food and drug administration
FDG	2-deoxy-2-[ <sup>18</sup> F]fluoro-D-glucose
FI	fluorescence imaging
FITC	fluorescein isothiocyanate
Fmoc	9-fluorenylmethoxycarbonyl
G	generation
GFP	green fluorescent protein
GLP-1	glucagon-like peptide-1
GLP-2	glucagon-like peptide-2
GLP-1R	glucagon-like peptide-1 receptor
GPCR	G-protein-coupled receptor
GRPP	glucagon-like peptide related pancreatic peptide

HATU	2-(1H-7-azabenzotriazol-1-yl)-1,1,3,3-tetramethyl uronium hexafluorophosphate methanaminium
HBSS	hank's buffered salt solution
HBTU	<i>O</i> -benzotriazole- <i>N,N,N',N'</i> -tetramethyl-uronium-hexafluoro-phosphate
HPLC	high-performance liquid chromatography
HSA	human serum albumin
INS	insulinoma
LOR	line of response
M	molar
MADLI	matrix-assisted laser desorption/ionization
MBq	megabecquerel
MCC	metal-chealtor complex
mCi	millicurie
MeV	megaelectron volts
MRI	magnetic resonance imaging
MS	mass spectrometry
Mtt	4-methyltrityl
NHS	N-hydroxysuccinimide
nM	nanomolar
NMR	nuclear magnetic resonance
NOC	1-Nal3-octreotide
NOTA	1,4,7-triazacyclononane-1,4,7-triacetate
OBOC	one-bead-one-compound
PAMAM	polyamidoamine
PDT	photodynamic therapy
PEG	polyethylene glycol
PET	positron emission tomography
pM	picomolar
PPIX	protoporphyrin-IX
ppm	parts per million
PS	polystyrene
ROS	reactive oxygen species
RP-HPLC	reverse-phase high-performance liquid chromatography
rpm	revolutions per minute
RT	room temperature
SFB	<i>N</i> -succinimidyl 4-fluorobenzoate
SPE	solid phase extraction
SPECT	single photon emission computed tomography

SPPS	solid-phase peptide synthesis
TBME	tert-butyl methyl ether
TETA	1,4,8,11-tetraazacyclotetradecane-1,4,8,11-tetraacetic acid
TFA	trifluoroacetic acid
THF	tetrahydrofuran
TMABT	<i>t</i> -butyl- <i>N,N,N</i> -trimethylammonium benzoate triflate
TOF	time-of-flight
TSTU	<i>O</i> -( <i>N</i> -Succinimidyl)-1,1,3,3-tetramethyluronium tetrafluoroborate
TM	targeting moiety
UV	ultraviolet

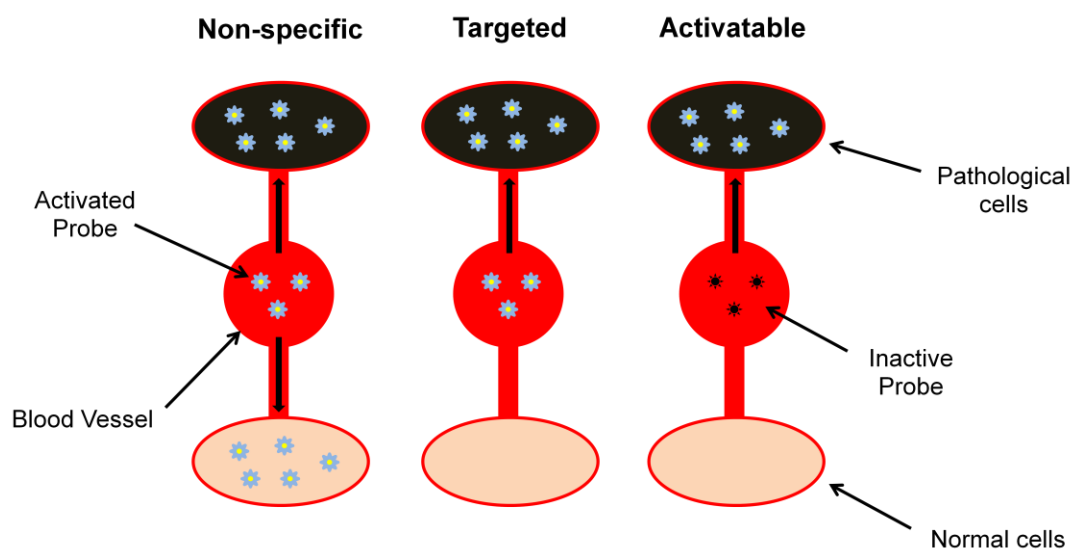
## **CHAPTER 1. Molecular Imaging**

### **1.1 Introduction**

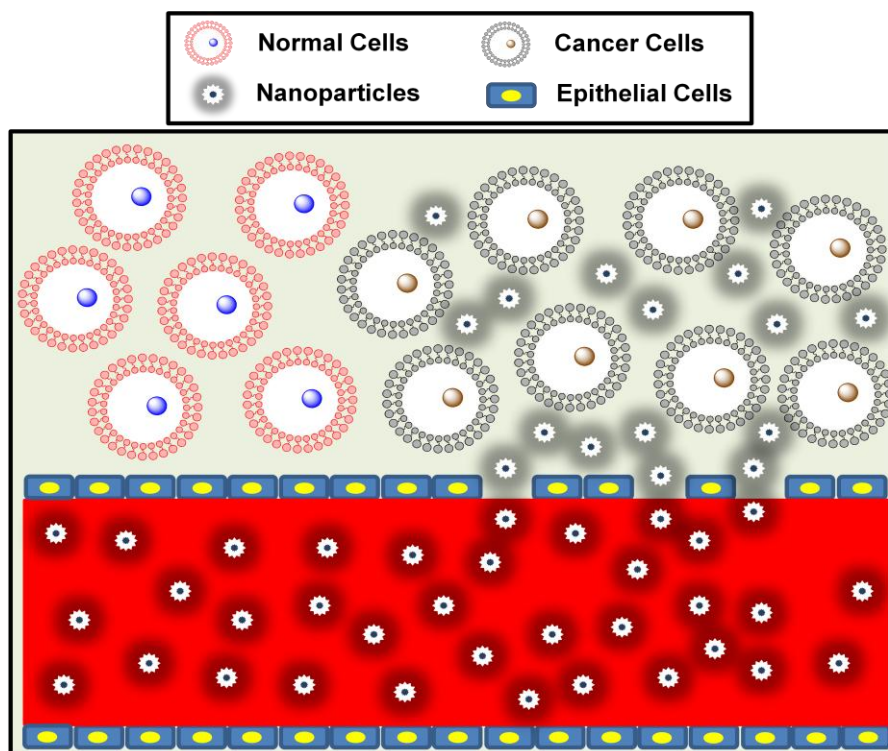
Over the past few decades, utilization of various imaging techniques has helped shape our understanding of numerous biological processes. Advances in the development of such techniques for small animals as well as human use, has increased the applications of imaging to include biomedical research, such as those in drug development and discovery. Historically, biomedical imaging methodologies relied on detection of disease processes or treatment effects as anatomical abnormalities and were therefore referred to as structural or conventional imaging. With the development of higher resolution instrumentation and discovery of improved imaging agents, it became possible to visualize physiological parameters in living subjects. This technique is commonly classified as functional imaging. More recently, however, it has become possible to image specific molecules and targets, which is a research discipline now referred to as molecular imaging.<sup>1, 2</sup> This research area provides a method for the non-invasive visualization, characterization and quantification of biological processes at cellular and sub-cellular levels. Furthermore, molecular imaging has also been shown to play a vital role in modern medicine as a result of its potential application in diagnostics and therapeutics.<sup>3-6</sup> Currently, two of the most important clinical applications of molecular imaging are in oncology and cardiac disease imaging. In oncology, significant breakthroughs have been achieved for treatment response assessment, cancer staging and early disease detection.<sup>7-10</sup> In the case of cardiovascular disease, imaging techniques have provided a route for plaque detection as well as analysis of cardiac repair.<sup>11, 12</sup> These applications were made possible largely due to the development of imaging probes.

## 1.2 Imaging Probes

The non-invasive visualization of biological processes *in vivo* requires the use of appropriately designed imaging probes. There are three main categories of imaging probes namely: non-specific, targeted and activatable (Figure 1.1). Non-specific probes, instead of interacting with specific molecular targets, accentuate differences between tissues in terms of permeability and perfusion levels. These probes are typically utilized in monitoring disease processes, which involve characterization of blood volume, flow or perfusion. Non-specific probes are commonly utilized in imaging practices. A recent example is a report on tumor drug delivery by non-covalently linked drug-gold nanoparticle. In this study the gold-nanoparticles, acting as non-specific probes, travel to the tumor site via enhanced permeability and retention (EPR) effect owing to the presence of leaky vasculature as demonstrated in Figure 1.2.<sup>2, 13-17</sup>



**Figure 1.1** Representative classes of imaging probes and their respective interaction schemes.<sup>14, 17</sup>

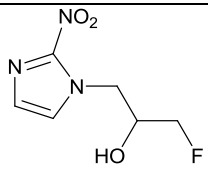
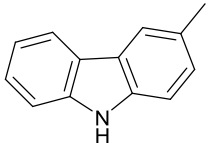
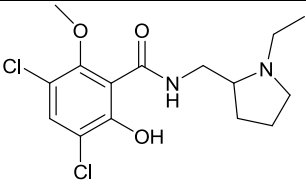
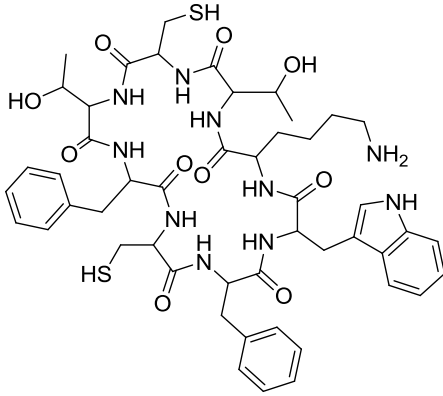
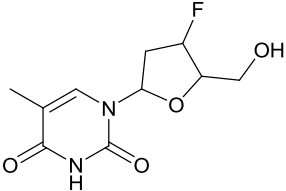


**Figure 1.2** A scheme demonstrating the localization of gold nanoparticles in tumors cells via enhanced diffusion through leaky vasculature.<sup>13</sup>

Visualization and monitoring of disease processes requires targeting of specific biological processes at cellular or sub-cellular levels. This requirement has led to the development of targeted and activatable imaging probes. In principle, targeted probes get localized on biomolecules of interest, thus allowing for the visualization of their distribution.<sup>14</sup> The mechanism of target-specific uptake is directly related to the biochemical processes involved since site directed probes could include enzyme substrates, inhibitors, transport protein ligands, membrane bound or cytosolic binding sites as well as mRNA or DNA components.<sup>18</sup> Targeted probes are detectable at all times, regardless of any interaction with the biological target, which leads to higher background

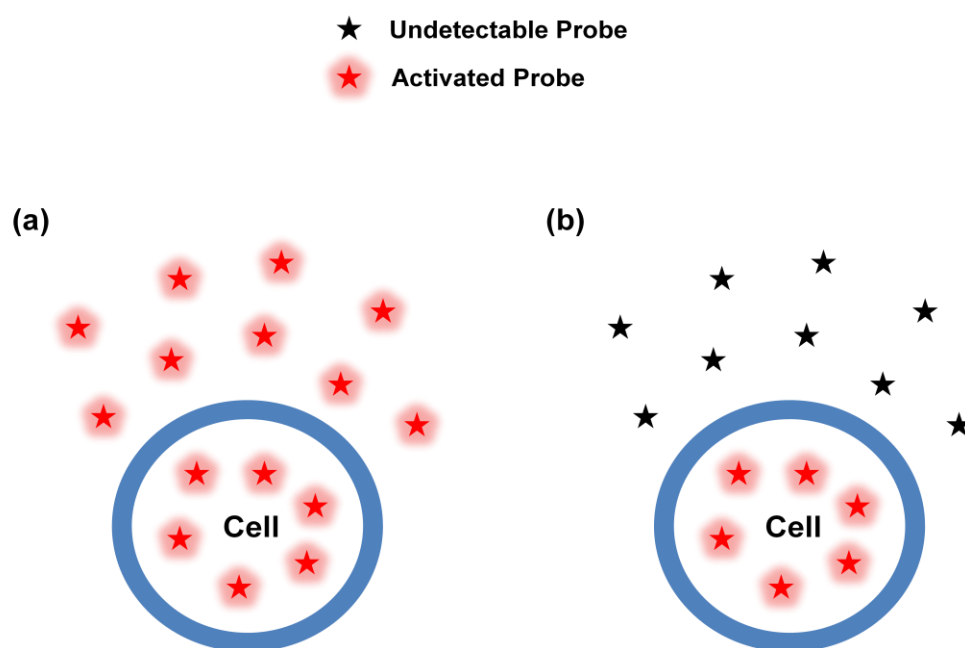


noise levels. However, considering that only the probes bound to the biological targets stay in the system, higher signal to noise ratios can be obtained if waiting periods are permitted prior to imaging. Targeted probes are utilized in several areas of oncology including heart, brain and tumor imaging as well as tumor therapy. Examples of such probes and their applications are given in Table 1.1.

Probe	Structure	Application
FMISO		Hypoxic marker for heart
Carazolol		$\alpha$ -Adrenergic receptor ligand (myocardial receptor present in many heart disease)
Raclopride		D2-dopamine receptor antagonist (dopamine activity in brain)
Octreotide (Sandostatin®)		Study somatostatin receptors found in a number of human tumors (eg. gastrinoma, insulinoma, carcinoid, neuroblastoma)
FLT		Monitoring tumor proliferation (eg. lymphoma)

**Table 1.1** Examples of targeted compounds for oncologic applications.<sup>19-24</sup>

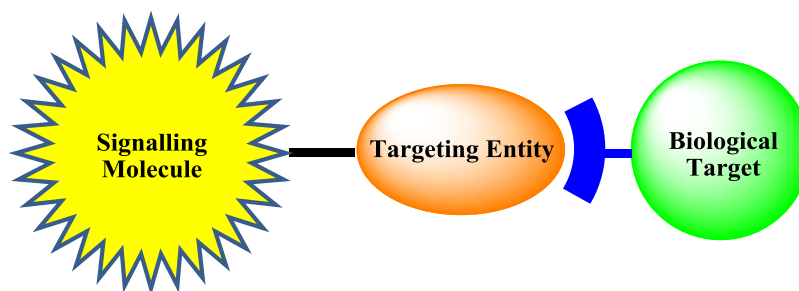
Activatable probes (also referred to as smart probes), do not produce a signal in their native state and, considering that their detection requires interaction with their intended biological targets, typically produce higher signal to noise ratios. Smart probes can be activated by ionic interactions or enzymatic cleavage, and thus can also be used to monitor the localization of molecular functions. Figure 1.3 illustrates the use of activatable probes compared to other categories of molecular probes. A recently reported class of smart probes includes the pH-activatable fluorescent probes used in molecular imaging of viable cancer cells.<sup>14, 25</sup> Pharmacokinetics of such probes, however, is not ideal in all cases, as interference from other biological entities (eg. enzymes) is likely to occur. Therefore, the choice of targeted versus smart probe is case dependent.



**Figure 1.3** Scheme of targeted imaging probes (a) versus activatable "smart" probes (b).

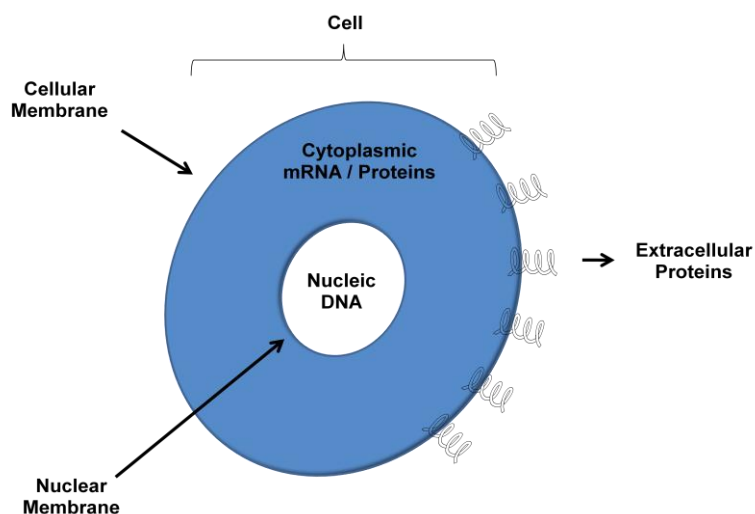
### 1.3 Design of molecular imaging probes

The design of a molecular imaging probe requires special attention to a number of key factors, the most important of which are 1) identification of a suitable biological molecular target, 2) identification of a targeting entity with optimal affinity for the target of interest, 3) labeling of the targeting entity with a suitable signaling molecule, thus the modality, 4) overcoming the barriers in the biological delivery of the designed probe, and 5) if possible, finding ways to amplify the observed probe signal.<sup>14</sup> Figure 1.4 illustrates the general design of a targeted molecular imaging probe.<sup>14</sup>



**Figure 1.4** Components of an imaging probe and its interaction with a biological target.

Finding the appropriate targeting ligand requires a screening process. Such techniques are currently employed in the drug development industry and include phage display, proteomics, robotics, recombinant techniques, and high throughput screening methods, which have only recently been widely employed to identify molecular imaging targets. Examples of potential molecular targets include nucleic acid sequences, proteins, carbohydrates and lipids (Figure 1.5). The design of imaging probes requires several considerations, which include: probe localization on the cell surface or within the cell, quantity of biological target per cell, and probable steric issues that may hinder probe delivery.<sup>14, 17</sup>

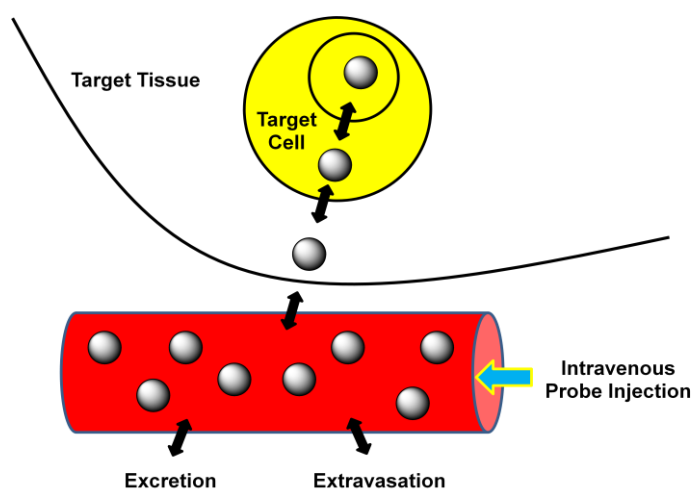


**Figure 1.5** General outline of a cell showing commonly targeted entities.

The next step in the design of an imaging probe, once a biological target has been selected, is the identification of a molecule that would specifically bind the target with optimal affinity. The targeting entity can range in size from a small molecule (eg. receptor ligand), to a larger molecule such as a monoclonal antibody. The identification of this entity is usually performed using library based screening, phage display or in silico (ligand screening).<sup>14, 26</sup> Depending on the properties of the molecule and the modality of choice, a signaling ligand is then bound to the selected targeting entity. For nuclear imaging, radioisotope labeling, typically carried out by chelation or covalent coupling reactions, is required.<sup>27</sup> Optical imaging on the other hand, requires organic fluorophores or inorganic compounds, such as quantum dots, for fluorescence imaging, or naturally occurring substrates for bioluminescence optical imaging.<sup>28</sup>

The designed imaging probe should also possess the appropriate characteristics in order to bypass all biological barriers (Figure 1.6) and reach the target of interest, within a reasonable time period, in sufficient concentration. The most important properties of the

developed probe *in vivo* are absorption, distribution, metabolism, and elimination (pharmacokinetics). In order to leave the vascular system, the vascular walls would need to be traversed. Lower molecular weight imaging probes can extravasate and be distributed in both target and non-target tissues, thus decreasing signal to noise ratios. Extravasation, however, is not always feasible. While tumors or inflammatory tissues with leaky vasculature are easier to traverse, traversing the blood brain barrier tends to be less permissible. Once the probe crosses over into the targeted tissue, it would have to overcome other barriers, such as steric issues preventing proper probe delivery, in order to reach the targeted cell.<sup>14, 17, 29, 30</sup>



**Figure 1.6** Examples of biological barriers that could prevent proper delivery of an imaging probe.<sup>2, 14, 17</sup>

#### 1.4 Targeting Component

As discussed earlier, the targeting entity can range in size from a small molecule (eg. receptor ligand), to a much larger molecule such as an antibody. The work presented in this dissertation concerns the use of peptide-based compounds as the targeting

component for the development of molecular imaging probes. The use of peptide derivatives and their applications are discussed in detail below.

Receptor targets used for peptide-based radiopharmaceuticals are most commonly among the family of seven transmembrane proteins, often referred to as G-protein-coupled receptors (GPCRs). This family contains the largest class of human receptors of pharmacological importance, consisting of approximately 50% of reported clinically relevant drugs acting on its protein members. Advances in proteomics and genomics have led to the discovery of several hundred GPCRs, some of which have been reported to have peptide-based endogenous ligands. Some of the most promising examples of peptide-based drugs and imaging agents are directed towards the somatostatin and bombesin receptor family. Peptides have been extensively utilized as drug candidates in two basic categories namely peptides directed towards tumor cell-surface receptors (Table 1.2) and those targeted towards tumor vasculature.<sup>31-44</sup>

<b>Peptide</b>	<b>GPCR</b>	<b>Cancer targets</b>
Bombesin / gastrin releasing peptide	GRP-R (BB2)	Prostate
Cholecystokinin	CCK2-R	Medullary thyroid
GLP-1	GLP-1R	Insulinomas
Neurotensin	NTR1	Pancreatic cancer
Somatostatin	SST2 (most common)	Neuroendocrine tumors
Neuropeptide Y	NPY1	Breast
Substance P	NK1R	Glioblastoma

**Table 1.2** Examples of peptides targeting GPCRs.

Tumor vasculature targeting is employed in monitoring processes involved in tumor growth. Tumor cell proliferation requires enhanced blood supply, making angiogenesis a necessity in tumor growth beyond 1-2 mm. Enhanced angiogenesis is

accompanied by over-expression of many biological factors such as integrins, growth factors and proteases. As a result, a large number of peptide-based imaging probes have been developed to monitor the over-expression of these biological factors during the progression of angiogenesis.<sup>45, 46</sup> Examples include peptides containing the  $\alpha_v\beta_3$ -integrin targeting moiety Arg-Gly-Asp.<sup>47</sup>

As targeting agents, peptides provide a number of advantages over other molecules, which is particularly accentuated when considering their synthetic route and diversity. Synthesis of peptides using automated solid-phase methodologies allows for rapid production of analogues in a reasonable time frame. The commercial availability of unnatural amino acids, further extends the chemical diversity of peptides prepared by this methodology. Furthermore, peptide-based probes have shown to have lower antigenicity, rapid access to tumors, enhanced tumor penetration, as well as faster clearance rates.<sup>31</sup>

Major drawbacks associated with using peptide-based compounds include poor oral bioavailability and poor metabolic stability. Fortunately, the former is not a major concern in oncology as most radiopharmaceuticals are administered intravenously. In addition, the metabolic stability of peptides *in vivo* has shown to improve using a variety of structural modifications known to prevent enzymatic degradation. The design of suitable and robust peptide-based probes therefore needs to account for the following considerations: biological stability, target affinity, target specificity, and pharmacokinetic characteristics. Steps in this methodology include design, synthesis and biological evaluation of the best peptide candidates. Initial biological evaluation analysis could consist of competitive binding assays or cell-based assays, with a focus to create probes with high affinity and specificity for the desired protein target. Additional studies will

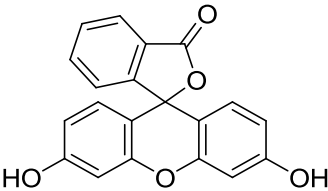
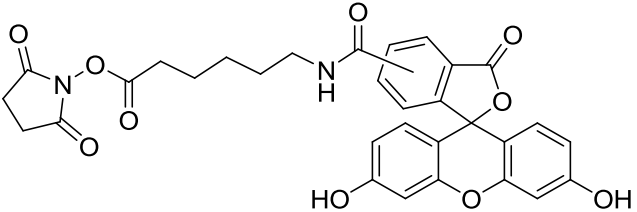
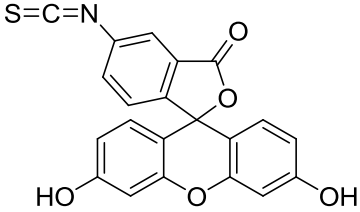
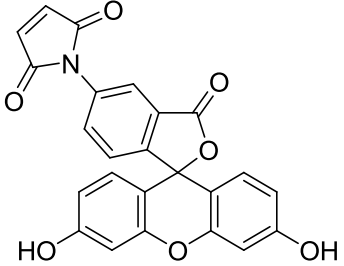
then aid in creating a molecule exhibiting biological stability. While results obtained from *in vitro* analyses do not necessarily reflect those from *in vivo* studies, they are certainly a reasonable starting point in screening for successful candidates. In the next stage, the pharmacokinetics of developed peptide candidates are evaluated *in vivo*.<sup>31</sup>

## 1.5 Labeling Techniques

### 1.5.1 Fluorophore Labeling

Fluorescent dyes are commonly conjugated onto biological compounds using either coupling reactions (eg. amine and an activated carboxylic acid), or direct nucleophilic reactions between a reactive group (eg. amine, thiol, alcohol) and a fluorophore. One of the most utilized groups, especially in peptide chemistry, are amines which are reasonably nucleophilic above pH 8.0 and can be reacted with activated fluorophore esters, such as N-hydroxysuccinimide (NHS) ester, with high yields and reproducibility.<sup>48</sup> Activated esters, such as the NHS esters, typically exhibit high selectivity towards aliphatic amines, while having low reaction rates with aromatic amines, alcohols and phenol. Fluorophore conjugation to amines can also be carried out using isothiocyanates, which are routinely employed in conjugation of fluorescein derivatives. In the absence of a reactive amine, thiols could also be utilized in such reactions. This is achieved via maleimide-thiol reaction at pH 7. Handling of thiol-containing compounds, however, is more tedious in the presence of multiple thiols, which could lead to the formation of disulfide bridges. In these situations, addition of a reducing agent such as dithiothreitol (DTT) is required.<sup>49</sup> Table 1.3 lists examples of commercially available dyes used for conjugation of fluorescein.<sup>50-54</sup>



Compound	Structure
Fluorescein	 <p>The structure shows the fluorescein molecule, which consists of a central carbon atom bonded to three rings: a benzoxazine ring with two hydroxyl groups at the 4 and 7 positions, and two phthalide rings. One of the phthalide rings has a carbonyl group at the 5-position.</p>
6-[Fluorescein-5(6)-carboxamido]hexanoic acid <i>N</i> -hydroxysuccinimide ester	 <p>The structure shows the fluorescein core with a hexanoic acid chain attached to the 5-position of the phthalide ring. The terminal carboxylic acid group of the hexanoic acid is converted to an <i>N</i>-hydroxysuccinimide ester.</p>
Fluorescein 5(6)-isothiocyanate	 <p>The structure shows the fluorescein core with an isothiocyanate group (-N=C=S) attached to the 5-position of the phthalide ring.</p>
N-(5-Fluoresceinyl)maleimide	 <p>The structure shows the fluorescein core with a maleimide ring attached to the 5-position of the phthalide ring.</p>

**Table 1.3** Examples of commercially available fluorescein derivatives directed towards reactions with amines and thiols.

### 1.5.2 Radionuclide labeling

Radioisotope labeling reactions can be organized into six general categories, which are isotope exchange, recoil labeling, excitation labeling, biosynthesis, direct, and

bifunctional chelator/prosthetic group labeling. In radioisotope exchange reactions, one or more atoms in a molecule are replaced by their radioactive counterparts. Considering that these molecules (pre and post labeling) are identical, with the only exception being an isotope effect, it is expected that they would possess the same biological and chemical properties. Examples of radiolabeled compounds produced by isotope exchange are  $^{125}\text{I}$ -triiodothyronine, and  $^{125}\text{I}$ -thyroxine.<sup>55</sup>

Recoil, excitation and biosynthesis labeling methods are not within the scope of this work. However, in brief, recoil labeling utilizes recoil atoms, produced in a nuclear reaction, to generate radiolabeled compounds. Unfortunately, the high energy of these particles results in poor yields and low specific activity. An example of such a reaction is  $^6\text{Li}(n,\alpha)^3\text{H}$ , where the compound to be labeled is mixed in with a lithium salt and subsequently irradiated in the nuclear reactor. Similarly, excitation labeling entails the utilization of radioactive daughter ions in a nuclear decay process to label compounds of interest. An example is the decay of  $^{77}\text{Kr}$  to  $^{77}\text{Br}$ . In this reaction, exposure of the compound of interest to  $^{77}\text{Kr}$  results in labeling with  $^{77}\text{Br}$ . Biosynthesis is a process where a living organism is grown in a culture medium containing the radioisotope of interest. In this methodology, the tracer is incorporated into the metabolites produced by the metabolic process of the organism and is subsequently separated. Examples of this process include  $^{60}\text{Co}$  and  $^{57}\text{Co}$ -labeled vitamin B12.<sup>55</sup>

Direct labeling methods entail the attachment of a radionuclide to the molecule of interest without the need for a prosthetic group. An example of such procedure includes the binding of radionuclides to thiol groups in the targeting molecule. This methodology, although easy to perform, is difficult to control and may lead to undesired changes in the

structure, stability, and pharmacokinetics of the labeled molecule.<sup>56, 57</sup> The characterization of compounds produced from this methodology is also extremely difficult owing to the lack of a complete understanding of the number of donor atoms and the possible geometry of the incorporated radionuclides.<sup>55</sup> A more precise approach, perhaps, is radiofluorination which is carried out via nucleophilic or electrophilic routes.<sup>58</sup>

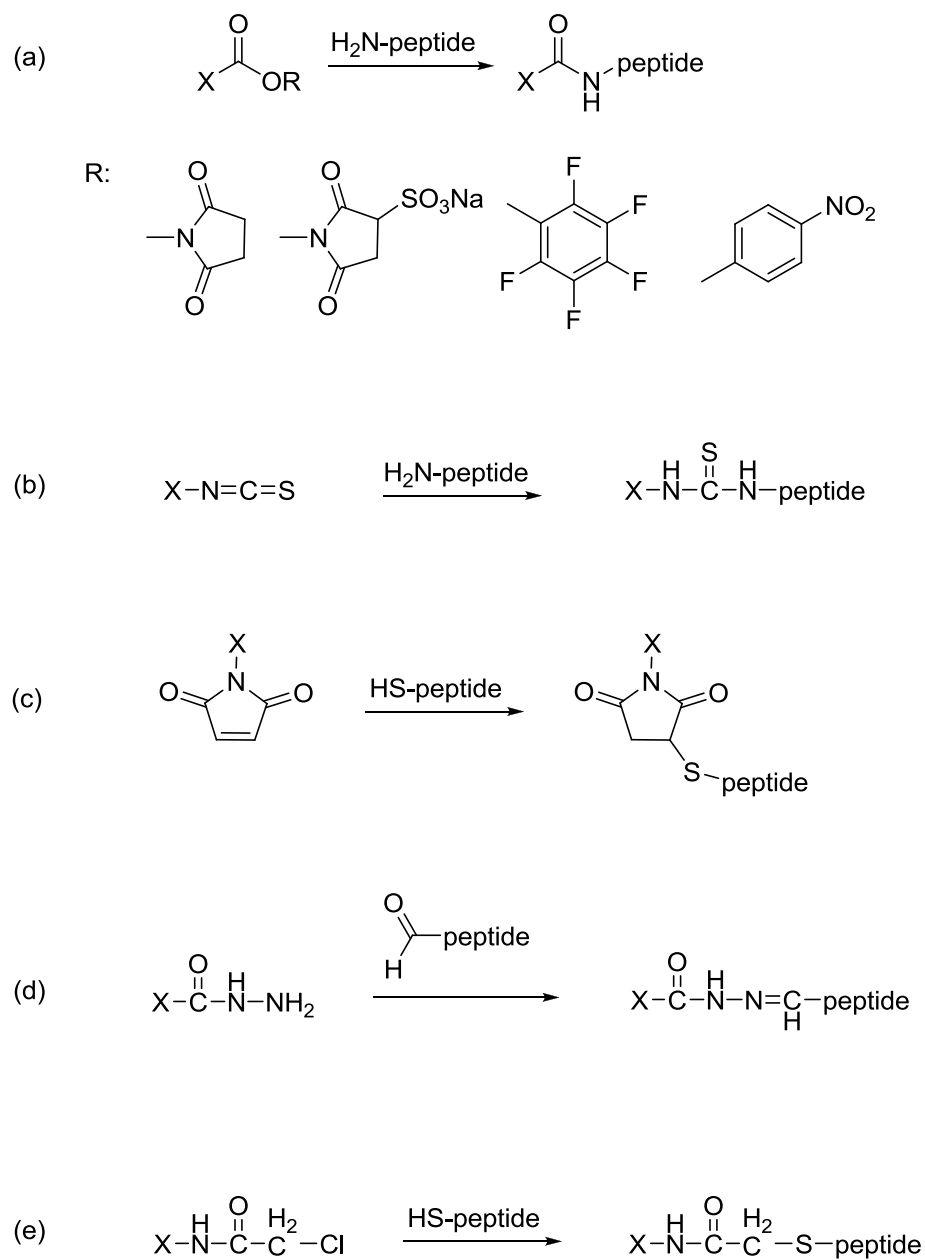
The last methodology, which is now the most utilized, is an indirect radiolabeling approach, where a prosthetic group or a radiometal chelator containing the radionuclide, is conjugated onto the biological compound of interest. This methodology, most widely employed in radiolabeling of peptides and proteins, takes advantage of reactive functional groups naturally present in these compounds for covalent attachment of the radionuclide containing moiety. Once again, several types of conjugation groups can be used such as active esters, isothiocyanates, maleimides, hydrazides, and  $\alpha$ -haloamides (Figure 1.7). The choice of the conjugation group is widely dependent on the reactivity and ease of product isolation. For instance, water soluble NHS-esters could be used for conjugation reactions to water insoluble peptides, in order to facilitate their removal. In the opposing case, the ether-soluble *p*-nitrophenyl esters could be used for water soluble peptides.<sup>59-61</sup>

Bifunctional chelator/prosthetic group methodology can be carried out using pre-labeling or post-labeling approaches. In the first approach, the radiolabeling of the prosthetic group/chelator is carried out initially, which is then followed by covalent conjugation of this entity to the biological molecule of interest. As the labeling and conjugation steps are separated, this procedure ensures the proper attachment of the radionuclide to the chelate moiety. However, the pre-labeling process could interfere with

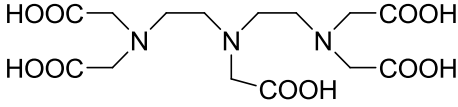
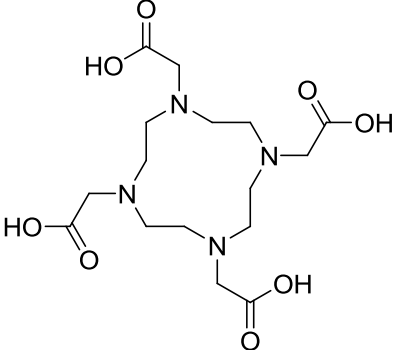
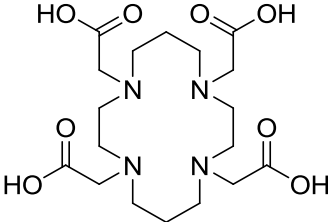
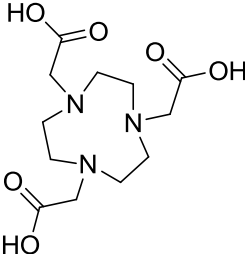
the conjugation process, thus further complicating the required purification steps. This process is also extremely time consuming and laborious and may not be optimal for short-lived radioisotope labeling. As a result, this approach is less commonly employed in radiolabeling procedures.<sup>59, 62, 63</sup>

In contrast, the post-labeling methodology, being most popular, requires the synthesis of a conjugate that is ready for radiolabeling (eg. metal-chelator peptide complex). This approach typically results in high yields and is compatible with solid-phase or solution phase chemistry. However, harsh conditions are required for effective labeling of conjugates, which could result in decomposition of starting materials.<sup>59</sup> A group of widely utilized bifunctional chelators are radiometal chelators, which have recently gained much interest. Examples of some well known chelators include DTPA, DOTA, TETA, and NOTA (Table 1.4).<sup>59</sup>

Bifunctional metal chelators are used to connect a radiometal to a targeting moiety. Metal-chelator complexes have been reported to be very stable both *in vitro* and *in vivo*. Many variations of caged metal chelators have also been reported in order to further enhance their respective biological stability. An ideal chelator is expected to coordinate the radionuclide with ease, great stability, and in high yields. The chelator must also be compatible with the radiometal of choice as it should not result in changes in oxidation states or redox potentials. DTPA, has been shown to be a strong chelating agent for trivalent metals such as indium-111.



**Figure 1.7** Examples of reactive group chemistry for conjugation of a prosthetic group or bifunctional chelator, X; (a) activated ester, (b) isothiocyanate, (c) maleimide, (d) hydrazide, (e)  $\alpha$ -haloamide.<sup>59</sup>

Chelator	Structure
DTPA	
DOTA	
TETA	
NOTA	

**Table 1.4** Examples of radiometal chelators commonly used with Indium-111 and Gallium-68.

There have been reports of DTPA conjugation to larger proteins (eg. albumins and antibodies), as well as smaller peptides such as somatostatin analogues.<sup>64-66</sup> The cyclen derivatives 1,4,7,10-tetraazacyclododecane-N,N',N'',N'''-tetracetic acid (DOTA),<sup>67-71</sup> 1,4,7-triazacyclononane-1,4,7-triacetic acid (NOTA),<sup>72, 73</sup> and their analogues, have played an important role in clinical applications as they form very stable complexes with a variety of trivalent radiometals such as <sup>66,67,68</sup>Ga, <sup>86,90</sup>Y, <sup>111</sup>In, <sup>149</sup>Pm, <sup>177</sup>Lu, as well as the divalent radiometals <sup>27</sup>Mg, <sup>47</sup>Ca, and <sup>64</sup>Cu. TETA (1,4,8,11-tetraazacyclotetradecane-1,4,8,11-tetraacetic acid), is one of the most well studied chelating agents for copper in peptide-based targeted radiotherapy (eg. somatostatin analogues).<sup>59, 74, 75</sup>

### 1.5.3 Important Considerations in Radiolabeling

Several factors need to be considered when preparing radiolabeled compounds. A high radiochemical yield is always desired, especially in cases utilizing short-lived radioisotopes. The employed radiolabeling approach should result in the formation of the most chemically stable conjugate, as the stability of the tracer is first and foremost determined by that of the radionuclide-conjugated entity. Optimization of labeling reaction conditions (eg. pH, temperature) is a necessity in order to prevent decomposition of the targeting entity. These conditions, to some extent, also dictate the most accessible approach for radiolabeling. Radiochemicals could be adsorbed on the inner walls of containers if they are in a carrier-free environment. In this case, low radiochemical yields can be avoided by using either silylated containers or those made of quartz. Storage conditions for the materials would also have to be determined based on the half-life of the

radioisotope and the overall stability of the compound. Another important variable is specific activity (the number of decays per amount of product), which is a measure of the ratio between radiolabeled and non-labeled compounds present in the final product (eg. non-radiolabeled starting materials). As a result, precautions should be taken to ensure optimal specific activity products. This value, however, is not always required to be high since, in certain cases, high levels could lead to product radiolysis (decomposition by radiation). Separation techniques would also have to be developed for the isolation and purification of the final labeled compounds as radioactive contaminants are often formed as byproducts of radioisotope decay.<sup>55</sup>

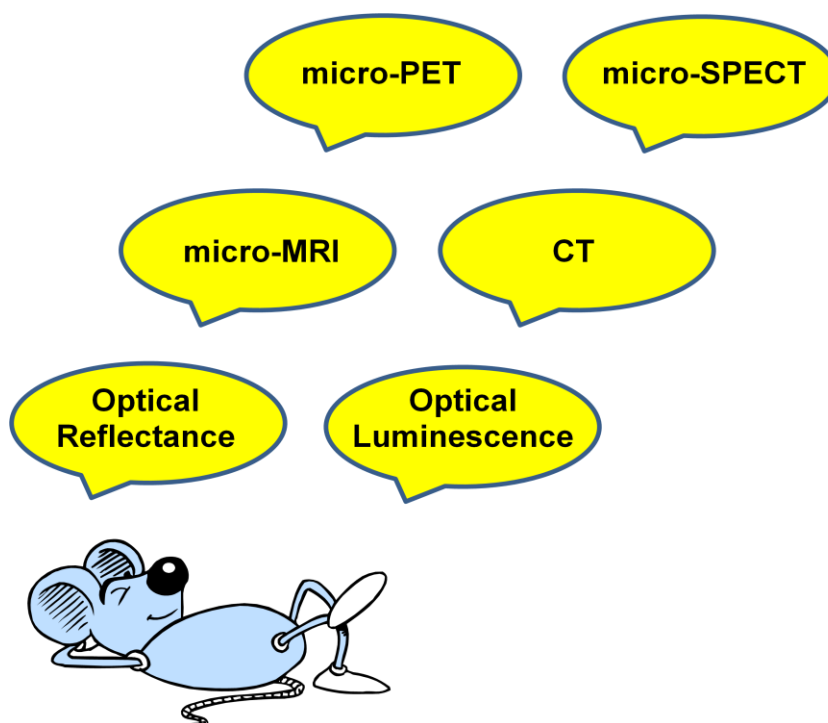
The choice of radionuclide is also important and requires consideration in determining the proper conjugating moiety. Important factors to consider are the half-life of the isotope, its mode of decay and availability. For diagnostic imaging, the half-life should be long enough to allow for the synthesis and purification of the desired probe, while still allowing for the administration of the tracer, its accumulation in the target tissues, and its clearance through non-targeted organs. At the same time, however, the half-life of the selected radioisotope should be as short as possible in order to prevent unnecessary radiation exposure.<sup>59</sup>

## **1.6 Imaging Modalities**

The most routinely used imaging techniques are nuclear, magnetic resonance, and optical, which are again categorized according to the type of signaling molecule used.<sup>1, 2, 76</sup> For instance, nuclear techniques use radioactive isotopes, while magnetic resonance and optical techniques utilize paramagnetic particles and fluorescent tags as



the signaling entity, respectively. The choice of the signaling entity, and therefore the modality, is dependent on the target of interest as it determines the most important imaging variables, such as sensitivity or resolution (Figure 1.8). The work presented in this thesis focuses on nuclear and optical techniques, which are discussed in more detail below.



**Figure 1.8** Examples of available *in vivo* imaging modalities for small animal imaging.

### 1.6.1 Nuclear Imaging

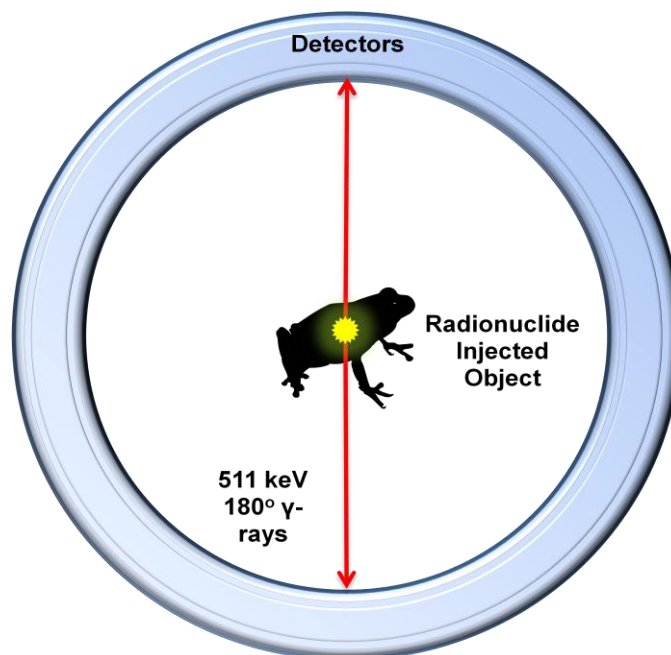
Nuclear imaging, or more specifically emission tomography, involves the use of radioactive isotopes as signaling entities. Two of the most commonly used modalities in

radionuclide imaging are positron emission tomography (PET) and single-photon emission computed tomography (SPECT). In both instances, a small quantity (pM) of a radiopharmaceutical is introduced into the body in order to non-invasively monitor the physiological functions of interest. The visualization of the radiopharmaceutical is made possible by detection of gamma rays that are emitted from the radionuclide.<sup>2</sup>

### 1.6.2 PET

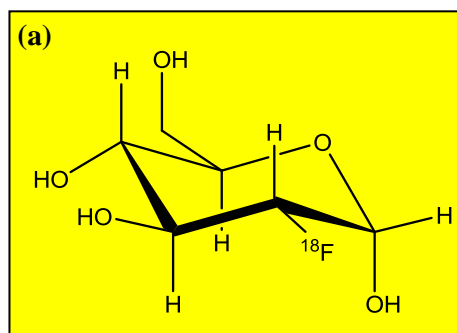
Radioisotopes that are used in PET decay by way of positron emission. The emitted positrons then travel a short distance through the body until they come in contact with electrons. The resulting electron-positron annihilation reaction then leads to the formation of a pair of anti-parallel 511 keV photons, which are simultaneously detected by a set of adjacent detectors. The lines outlining the traveled path of photons, and intersecting adjacent detectors, is referred to as the line of response (LOR). The cumulative LOR's are then used to reconstruct the 3D distribution of the positron-emitting radiopharmaceutical within the patient (Figure 1.9).<sup>77,78</sup>

The sensitivity of PET is in the pM range and is independent of the location and depth of the probe. Typically, several million cells containing the tracer are required for proper detection and recording of the event by the PET scanner. The high sensitivity of PET renders this imaging technique valuable for *in vivo* visualization of biological processes. It is worth noting, however, that because all emitted gamma rays in PET possess the same energy, if two imaging probes containing different radioisotopes were to be simultaneously injected, it would not be possible for PET detectors to distinguish them. As a result, imaging tracers have to be administered and processed individually.



**Figure 1.9** Mechanism of photon detection in PET.

As a result of the versatility of PET, there has been a tremendous increase in the number of PET radiotracers and clinical applications. The most frequently utilized PET radioisotopes are  $^{18}\text{F}$ ,  $^{82}\text{Rb}$ ,  $^{11}\text{C}$ ,  $^{15}\text{O}$ , and  $^{13}\text{N}$ , (Table 1.5) while the most notable PET radiotracer is  $^{18}\text{F}$ -FDG (Figure 1.10).<sup>79</sup> Considered the golden standard in PET imaging,  $^{18}\text{F}$ -FDG is used in the evaluation of several neoplasms and radiotherapy planning in various cancers such as those in lung, head and neck. A large number of other radiotracers are also currently being used in oncologic PET imaging. Some examples of such probes are listed in Table 1.6.<sup>77, 78</sup>



**Figure 1.10** Structure of  $^{18}\text{F}$ -FDG.

Radioisotope	Half-life	Modality
Rubidium-82	1.25 min	PET
Oxygen-15	124 sec	PET
Nitrogen-13	9.96 min	PET
Carbon-11	20.4 min	PET
Fluorine-18	110 min	PET
Technetium-99m	6.02 hours	SPECT
Iodine-123	13.2 hours	SPECT
Indium-111	2.83 days	SPECT
Gallium-67	3.26 days	SPECT
Iodine-131	8.02 days	SPECT

**Table 1.5** Common radioisotopes used in PET/SPECT imaging.

Tracer	Measured Variables
$^{11}\text{C}/^{18}\text{F}$ -thymidine	DNA synthesis
$^{11}\text{C}$ -methionine	Protein synthesis
$^{11}\text{C}/^{18}\text{F}$ -choline	Cell-membrane metabolism
$^{11}\text{C}/^{18}\text{F}$ /tyrosine, ethyltyrosine	Natural amino acid transport
$^{18}\text{F}$ -fluoro-dihydroxyphenylalanine	Dopamine synthesis, natural amino acid transport
$^{18}\text{F}$ -fluoro-misonidazole	Tissue hypoxia
$^{18}\text{F}$ -fluoro-17- $\beta$ -estradiol	Estrogen-receptor status
$^{18}\text{F}$ -fluorouracil	Tumor uptake of 5-fluoro-uracil
$^{11}\text{C}$ -acetate	Lipid synthesis

**Table 1.6** Examples of PET tracers used in oncology.<sup>77, 79-88</sup>

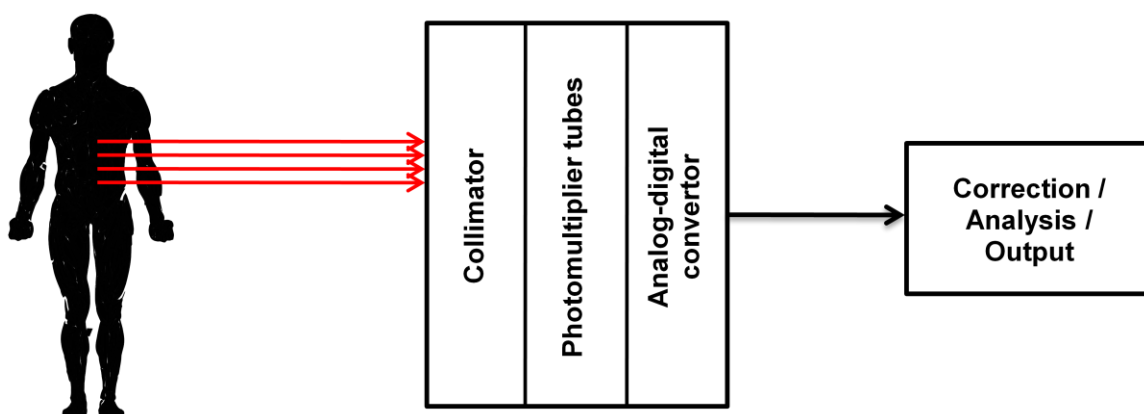
### 1.6.3 SPECT

PET and SPECT are generally distinguished by the type of radioisotope employed in their respective imaging probes. While PET makes use of positron emitting radioisotopes, which lead to the formation of two anti-parallel photons of equal energy, SPECT employs radioisotopes which emit only a single gamma-ray photon with each radioactive decay. This distinction between the numbers of emitted photons determines the type of hardware and software used to detect localized radiopharmaceuticals.<sup>77</sup>

SPECT imaging techniques, much like PET, start with the administration of a radiopharmaceutical. Following the decay of the administered radioisotope, gamma rays are collected by a collimator. This component is typically a thick sheet of a heavy metal, such as lead, that is shaped like a honeycomb with long thin channels. The collimator collects gamma rays that travel in the specific direction of the honeycomb channels, and directs them towards a crystalline material called a scintillator. The scintillator uses the

energy from the detected gamma rays to produce many optical wavelength photons, which are detected and converted to a cascade of electrons by a collection of photomultiplier tubes. The produced current is then acquired by accompanying electronics which record the occurrence of this event. Registration of multiple events then leads to the projected image of the object (Figure 1.11). Common radioisotopes used for SPECT imaging are  $^{99m}\text{Tc}$ ,  $^{111}\text{In}$ ,  $^{123}\text{I}$ , and  $^{131}\text{I}$  (Table 1.5).<sup>77</sup>

Compared to PET, SPECT uses lower energy  $\gamma$  rays, while providing the same spatial resolution (1-2 mm). Utilization of SPECT also allows for simultaneous detection of multiple isotopes with varying  $\gamma$  energies. A drawback of SPECT, however, when compared to PET, is its reduced sensitivity ( $10^{-10}$ - $10^{-11}$  M for SPECT compared to  $10^{-11}$ - $10^{-12}$  M for PET).<sup>2, 77</sup> Clinical applications of SPECT are numerous some of which have been listed in Table 1.7.



**Figure 1.11** Schematic diagram of a conventional gamma camera setup used in SPECT imaging.<sup>77</sup>

<b>Radiopharmaceutical</b>	<b>Application</b>
$^{67}\text{Ga}$ -citrate	Infection or lymphoma detection
$^{111}\text{In}$ -capromab pendetide	Prostate cancer detection
$^{201}\text{Tl}$ -TlCl	Myocardial perfusion or viability assessment
$^{99\text{m}}\text{Tc}$ -sestamibi or tetrofosmin	Myocardial perfusion or viability assessment, Parathyroid localization
$^{99\text{m}}\text{Tc}$ -MDP	Metastases or fracture detection
$^{99\text{m}}\text{Tc}$ -Red blood cells	Liver hemangioma detection
$^{99\text{m}}\text{Tc}$ -sulfur colloids	Liver/spleen assessment, lymphoscintigraphy
$^{99\text{m}}\text{Tc}$ -HMPAO	Brain perfusion assessment

**Table 1.7** Clinical applications of radiopharmaceuticals used for SPECT imaging; HMPAO = hexamethylpropyleneamine-oxine; MDP = methylene diphosphonate.<sup>89-97</sup>

## 1.7 Radioisotope production

Radioisotopes, in general, can be categorized as being neutron rich or neutron poor. Isotopes that are neutron rich are produced in a reactor, whereas those that are electron poor are produced in particle accelerators. The use of the latter, and in particular cyclotrons, is preferred over the use of reactors. This is due to several reasons which are: 1) unfavorable decay characteristics of reactor produced radioisotopes, such as particle emissions and gamma ray energies, for certain applications, 2) reactor produced radioisotopes cannot be produced with high specific activities, and most importantly 3) access to reactors is more limited when compared to cyclotrons.<sup>98</sup> As a result, the radioisotopes used in this thesis were all produced, either directly or indirectly, by cyclotron accelerators.

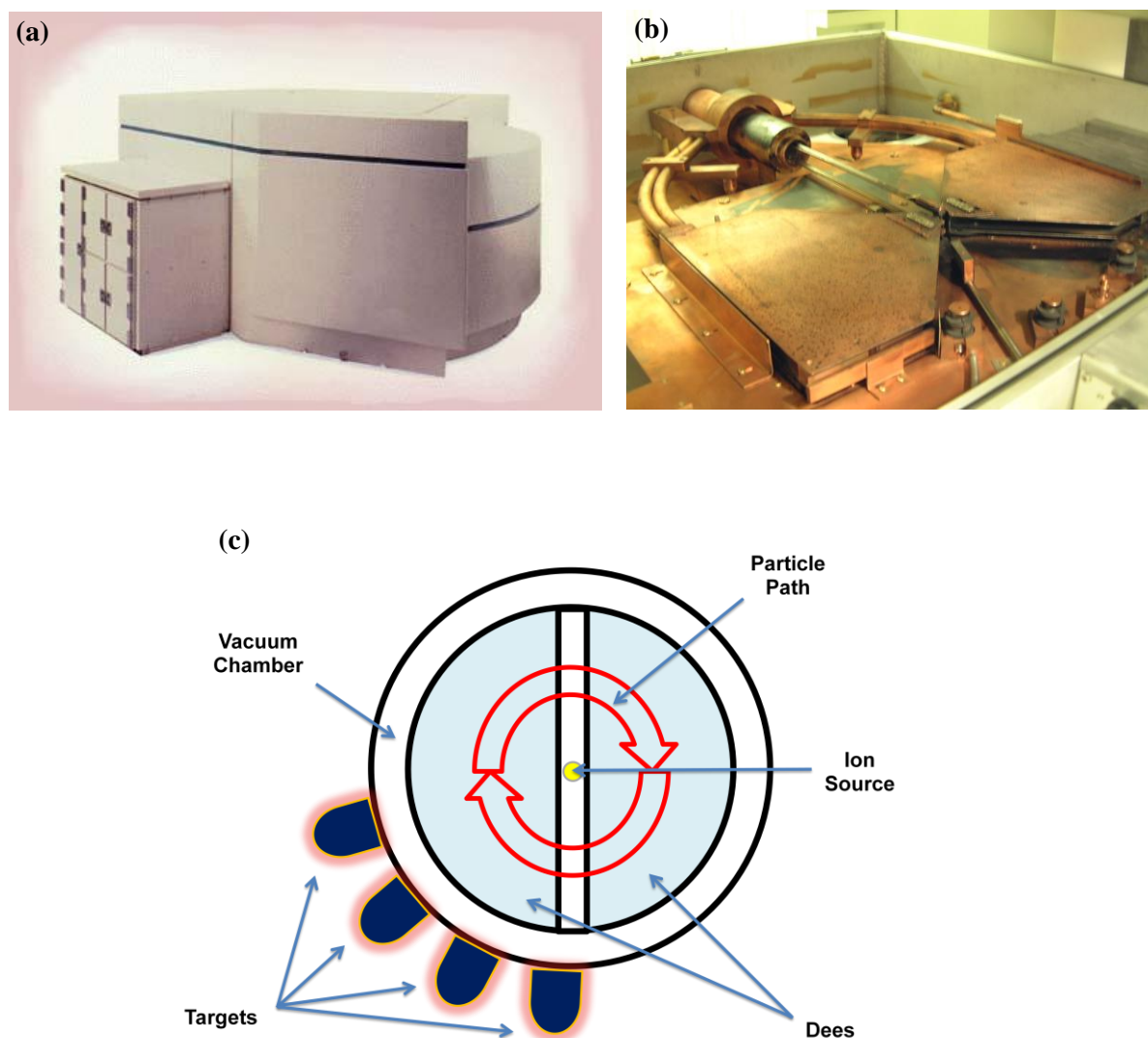
### 1.7.1 Cyclotrons

There are currently a large number of nuclear reactions that can be used in accelerators to produce radioactive materials. The bombarding particles are usually protons, deuterons, or helium particles. The energies used range from a few MeV to hundreds of MeV. In a typical reaction, the accelerated particle, along with its energy, are absorbed into the nucleus of the target materials. This energy distribution in the nucleus become homogenous (equilibrates), prior to decomposition and particle emission, thus leading to the formation of the desired radioisotope. Figure 1.12 shows the setup of a cyclotron.<sup>98</sup>

A particle accelerator is surrounded by both inner and outer shields (Figure 1.12 a). The inner shield is approximately 30 cm thick consisting of a mixture of lead, epoxy, and boron carbide, whereas the outer shield is roughly 70 cm thick and consists of polyethylene and boron carbide loaded concrete. The cyclotron core, which is always under high vacuum, consists of two D-shaped electrodes (Figure 1.12 b), to which alternating voltage is applied. With the aid of an electromagnetic field perpendicular to the electrodes, charged particles are accelerated in an outward spiral path within the hollow Ds in the high vacuum environment (Figure 1.12 c). These particles, produced at the source, can be either positively (eg.  $H^+$ ) or negatively (eg.  $H^-$ ) charged ions. In a proton cyclotron, hydrogen gas, which is directed into the cyclotron chamber, gets ionized by electrons emitted from a cathode. This results in the formation of both positively and negatively charged protons, which are separated based on the type of cyclotron and the direction of the magnetic field. The energy of the accelerated particles can reach several MeV depending on the size and design of the cyclotron. After



acceleration, these particles are then brought in contact with the target materials, causing the formation of the desired radioisotopes.<sup>78, 99</sup> Three cyclotron produced radioisotopes that will be further discussed in this thesis are listed in Table 1.8.



**Figure 1.12** A cyclotron setup with protective shields (a) closed and (b) open; courtesy of Hamilton Health Sciences; (c) demonstrates components of the cyclotron core.<sup>100</sup>

<b>Radionuclide</b>	<b>Nuclear Reaction</b>	<b>Half life</b>
Fluorine-18	$^{18}\text{O}(\text{p},\text{n})^{18}\text{F}$	109.8 min
Indium-111	$^{111}\text{Cd}(\text{p},\text{n})^{111}\text{In}$	2.8 days
Germanium-68	$^{69}\text{Ga}(\text{p},2\text{n})^{68}\text{Ge}^*$	272 days

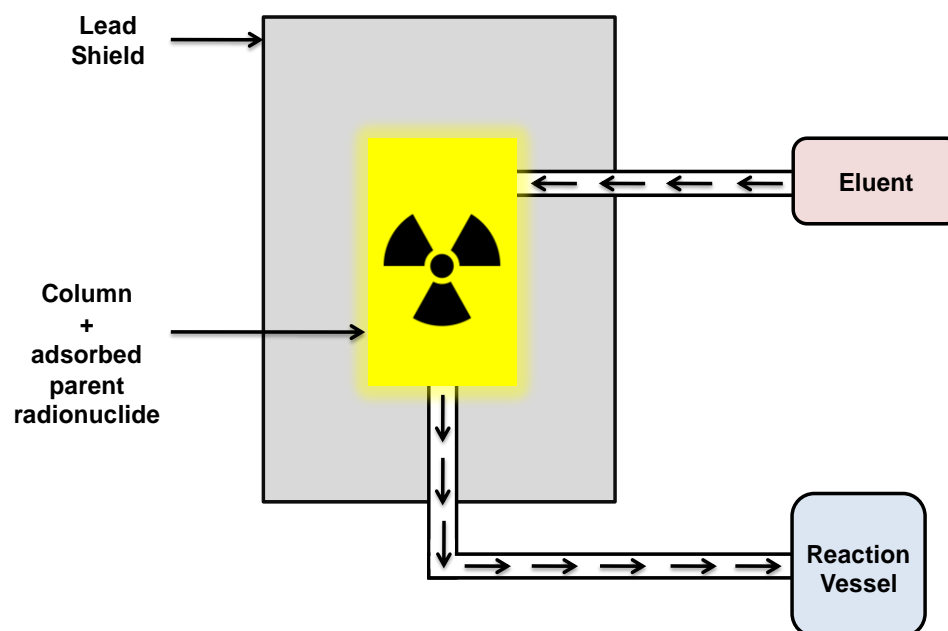
**Table 1.8** Cyclotron produced radionuclides discussed in this work; \*denotes the use of isotopically enriched materials.<sup>98</sup>

Among the available radionuclides, the use of short-lived radioisotopes has gained considerable interest, which is due to the added capability of administering larger radiopharmaceutical dosages into patients while minimizing their received radiation dose. This methodology also results in the production of high quality images. The increasing interest in short-lived isotopes has resulted in the development of radionuclide generators that serve as convenient sources for their production.<sup>98, 101</sup>

### 1.7.2 Radionuclide Generators

Generators are constructed based on the decay-growth relationship between a long-lived radionuclide and its shorter-lived daughter radionuclide. A long-lived radioisotope is allowed to decay to its short-lived daughter. Distinct differences in the chemical properties of the two nuclides are then utilized for the isolation of the daughter nuclide from the parent. Generators consist of a glass or plastic column fitted at the bottom with a fritted disk. The parent nuclide is then adsorbed onto the column packing which could be made of various materials such as cation/anion exchange resin, alumina or zirconia. Decay of the parent nuclide, and the subsequent formation of its daughter,

continues until an equilibrium is reached within several half-lives of the daughter nuclide. Once an equilibrium is reached, the half-life of the daughter would appear to be the same as that of its parent. The elution of the generator would bring out the daughter while leaving the parent nuclide adsorbed on the column. After an elution, the daughter nuclide starts to form again in the generator until an equilibrium is reached, as mentioned above, at which point another elution can be carried out. Figure 1.13 illustrates the outline of a radionuclide generator.<sup>55</sup>



**Figure 1.13** Illustration of a radionuclide generator set-up.

Generators, while simple and convenient to use, provide high yields of the daughter nuclide reproducibly and are shielded to minimize radiation exposure. The shipment of generators is facile since they are sturdy and compact, making them ideal

candidates for both research and medicinal applications. Table 1.9 provides a list of generators employed in nuclear medicine.

### 1.7.3 Optical Imaging

Optical imaging techniques, much like radionuclide imaging, are varied based on the modality of choice. Traditionally, optical methods were used for surface and subsurface fluorescence imaging using confocal imaging, multiphoton imaging,

Parent	Parent $t_{1/2}$	Daughter	Daughter $t_{1/2}$	Column Packing	Eluant
$^{99}\text{Mo}$	66 h	$^{99\text{m}}\text{Tc}$	6 h	$\text{Al}_2\text{O}_3$	0.9% NaCl
$^{113}\text{Sn}$	115 d	$^{113\text{m}}\text{In}$	99.5 min	$\text{ZrO}_2$	0.05 N HCl
$^{68}\text{Ge}$	271 d	$^{68}\text{Ga}$	68 min	$\text{Al}_2\text{O}_3$ ; $\text{SnO}_2$	0.005 M EDTA; 1 N HCl
$^{62}\text{Zn}$	9.3 h	$^{62}\text{Cu}$	9.7 min	Dowex 1 x 8	2 N HCl
$^{137}\text{Cs}$	30 y	$^{137\text{m}}\text{Ba}$	2.6 min	Ammonium molybdophosphate	0.1 N HCl + 0.1 N $\text{NH}_4\text{Cl}$
$^{81}\text{Rb}$	4.6 h	$^{81\text{m}}\text{Kr}$	13 s	BioRad AG 50	$\text{H}_2\text{O}$
$^{82}\text{Sr}$	25.5 d	$^{82}\text{Rb}$	75 s	$\text{SnO}_2$	0.9% NaCl
$^{191}\text{Os}$	15.4 d	$^{191\text{m}}\text{Ir}$	4.9 s	BioRad AG1	4% NaCl
$^{195}\text{Hg}$	41.5 h	$^{195\text{m}}\text{Au}$	30.6 s	Silica gel coated with ZnS	$\text{Na}_2\text{S}_2\text{O}_3 \cdot 5\text{H}_2\text{O}$ solution
$^{87}\text{Y}$	80 h	$^{87\text{m}}\text{Sr}$	2.8 h	Dowex 1 x 8	0.15 M $\text{NaHCO}_3$

**Table 1.9** Examples and specifications of generators used in nuclear medicine.<sup>102</sup>

microscopic imaging by intravital microscopy, or total internal reflection fluorescence microscopy. More recently, however, imaging of deeper tissues has become possible with the aid of continuous light or with intensity-modulated light and tomographic systems.<sup>103</sup> This development has also been largely due to the discovery of near infrared probes that exhibit deeper tissue penetration, which results from lower tissue light absorption at longer wavelengths.<sup>104</sup> Given all the recent improvements in probe and instrumentation development, the penetration depth for near infrared dyes is expected to reach up to several centimeters. However, given the poor depth penetration, optical techniques are still largely limited to small animal imaging as there are currently few clinical opportunities.<sup>2</sup>

Optical imaging techniques have been utilized to study gene expression, cell trafficking, and drug efficacy. Two techniques utilized in this area are fluorescence imaging (FI) and bioluminescence imaging (BI), both of which provide a cost-effective methods for high-throughput screening of biological targets and functions in small animal models such as mice. Advantages of optical imaging include its high sensitivity, ranging  $10^{-9}$  to  $10^{-12}$  M (optical fluorescence imaging), probe stability as there is no radioactive decay, and its non-ionizing nature. Equally important is the capability to follow multiple optical probes, labeled with dyes with varying fluorescence wavelengths, in the same study.<sup>2, 105</sup> The particular technique used in this thesis was fluorescence imaging which is discussed more in detail.

#### 1.7.4 Fluorescence Imaging

In FI, an excitation light source of a specified wavelength is used to excite a fluorophore. The subsequent relaxation of energetically promoted electrons then results in the emission of longer wavelength photons which are recorded by a detector. Fluorescent probes exhibit great sensitivity due to this discrete emission of light upon excitation, leading to a number of applications such as those involving *in vitro* assay procedures (eg. fluorescently tagged antibodies for antigen detection). In general, each fluorophore exhibits unique optical properties such as signal intensity, excitation/emission wavelengths, as well as quantum yields (ratio of total photon emission, over the entire range of fluorescence, to the total photon absorption), and extinction coefficients. These properties are key components in the design of optical imaging probes as they determine the type of instrumentation required. A fluorescent compound is expected to not only possess a high quantum yield, but to also exhibit a large Stoke's shift (difference in absorption and emission wavelengths). Greater Stoke's shifts minimize interferences from Rayleigh-scattered excitation light, thus resulting in higher signal to noise ratios. Another important fact to keep in mind when selecting the appropriate fluorophore, is the naturally occurring background fluorescence of the surrounding tissues, which could result in the reduction of signal to noise ratios.

Perhaps the most widely used fluorophore is the green fluorescent protein (GFP) which is often used in *in vitro* studies such as assays for reporter genes. Other common classes of fluorescent tags include the fluoresceins, rhodamines, coumarins, BODIPY, cascade blue, Lucifer yellow, phycobiliproteins and cyanine dyes. Table 1.10 lists examples of applications of optical imaging.

<b>Probe</b>	<b>Application</b>
Peptide-based NIR activatable optical probes	Cancer imaging, thrombosis, atherosclerosis, apoptosis, arthritis
Luciferase, GFP	Imaging gene expression

**Table 1.10** Examples of optical imaging applications in living subjects.<sup>106-112</sup>

## 1.8 Imaging Probe Design: Overall Picture

Combination of a targeting moiety, signaling component and imaging modality for analysis of a particular biological target encompasses the design of an imaging agent. Over the years, a large number of probes have been reported for use by various imaging modalities as mentioned above. However, it is not uncommon for a number of probes to have the same biological target. This is due to the options created from the combination of targeting moiety, signaling component and imaging modality. As a result, in order to circumvent this overlap, multimodality imaging was developed for the production of single molecules that could be used with various modalities, thus maximizing the amount of data obtained with a single tracer.

## 1.9 Multimodality Imaging

In recent years, the use of multiple modalities in conjunction has gained considerable interest. These techniques combine individual strengths of modalities, thus leading to more accurate imaging results and experiments. The first fused system was a PET/CT instrument, which was developed by Townsend and colleagues, in collaboration

with Siemens Medical, in 1998.<sup>113</sup> The success of this invention led not only to the development of other fused systems, but also extensive research in the design of novel multimodality imaging agents. In the development of multimodality imaging probes, while not necessitated by all application, use of a single probe for multiple modalities can aid in maintaining consistent pharmacokinetics and co-localization properties.<sup>113</sup> This would also prevent any additional unnecessary stress on the body, which would accompany multiple probe administration. Keeping this in mind, over the past two decades, various types of multimodality imaging agents have been reported with structures based on lipids (eg. liposomes and lipoproteins),<sup>114, 115</sup> nanoparticles (eg. quantum dots,<sup>116</sup> iron-oxide particles,<sup>117</sup> dendrimers<sup>118</sup>), macromolecules (eg. peptides),<sup>119</sup> and small molecules.<sup>113, 120</sup> Of these categories small molecules and dendrons are commonly used in the development of single and multimodality molecular imaging probes. These categories are discussed in more details below.

### **1.9.1 Dendrimers**

Dendrimers are an assembly of branched polymers that terminate in numerous functional groups (eg. hydroxyl or amine groups), which can be further utilized for ligand conjugation. The more suited biocompatibility of dendrimeric compounds (when compared to peptides, quantum dots and some small molecules), has resulted in their increasing utilization in medicinal chemistry.<sup>121</sup> Two of the most utilized applications include drug delivery (eg. cyclodextrins),<sup>122</sup> and gene delivery (eg. lysine-polyethyleneglycol-lysine dendrimers).<sup>123,124</sup> Peptide-dendrimers have shown to be

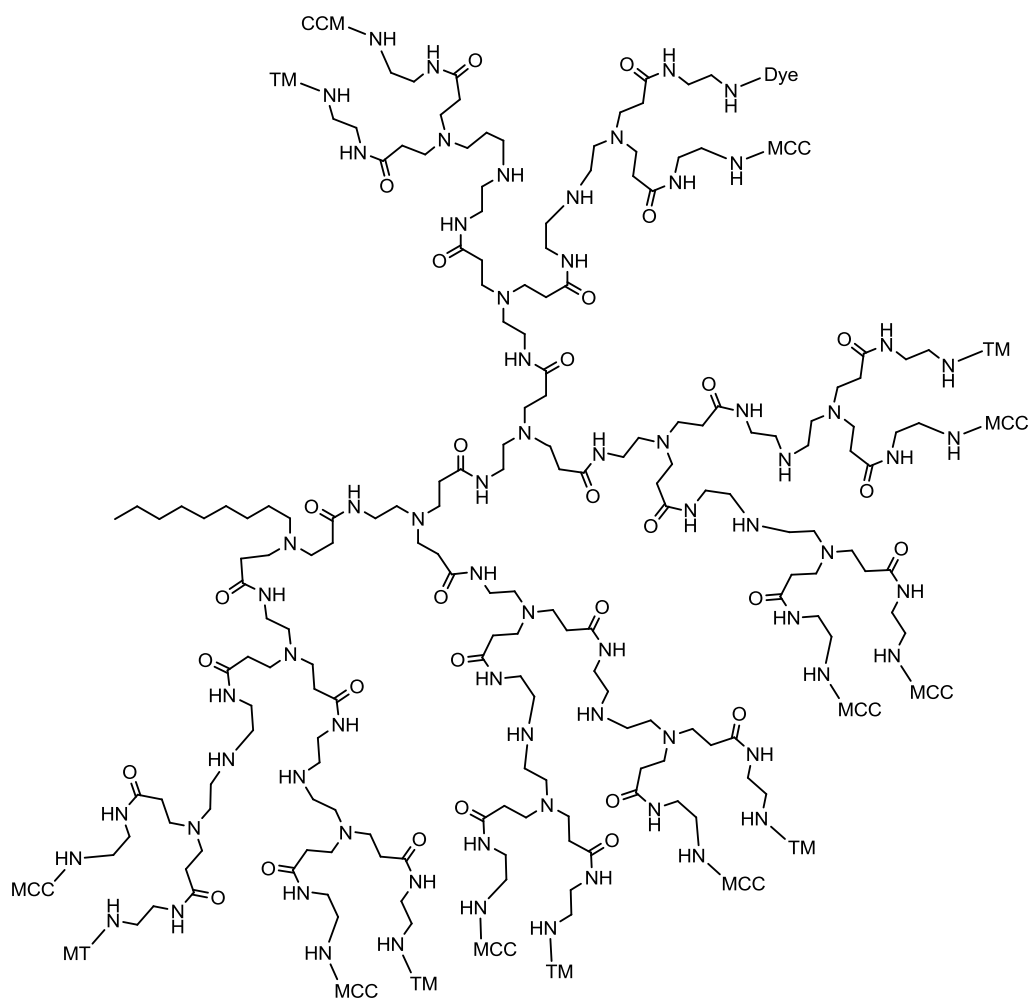


potential candidates as protein mimics, anticancer agents and vaccines. Peptide-dendrimers are typically more water soluble, less toxic to normal human cells, and more stable to proteolysis when compared to their linear analogues. Dendrimeric structures have also been frequently used in molecular imaging.<sup>125</sup>

Dendrimers with various tags have already been reported including metal-chelator complexes (eg. Gd-DTPA),<sup>118, 126, 127</sup> and fluorescent tags (eg. rhodamine,<sup>128</sup> Alexa Fluor,<sup>142</sup> and Cy5.5<sup>129</sup>). The branched chains, typically consisting of polyamidoamines (PAMAM), provide a large number of functional groups on the surface, while minimizing the overall size of the nanoparticle. For instance, the size of a third generation (being the number of repeated branched cycles) dendrimer (G3) is approximately 4 nm while that of a G8 dendrimer is roughly 10 nm. The control over the size of these particles is very important in determining the pharmacokinetic behavior of the probe in vivo. For example, the clearance of dendrimers is by the renal system for G3-4 dendrimers, kidney and liver for G5 dendrimers, and only via liver for G6-9 dendrimers. Figure 1.14 illustrates an example of a dual-modality, dendrimer-based molecular imaging probe for  $\alpha_v\beta_3$  integrins in a melanoma cell line. The probe exhibited a tumor to blood ratio of  $3.30 \pm 0.03$ , two hours post injection.<sup>118, 130</sup>

## 1.9.2 Small Molecules

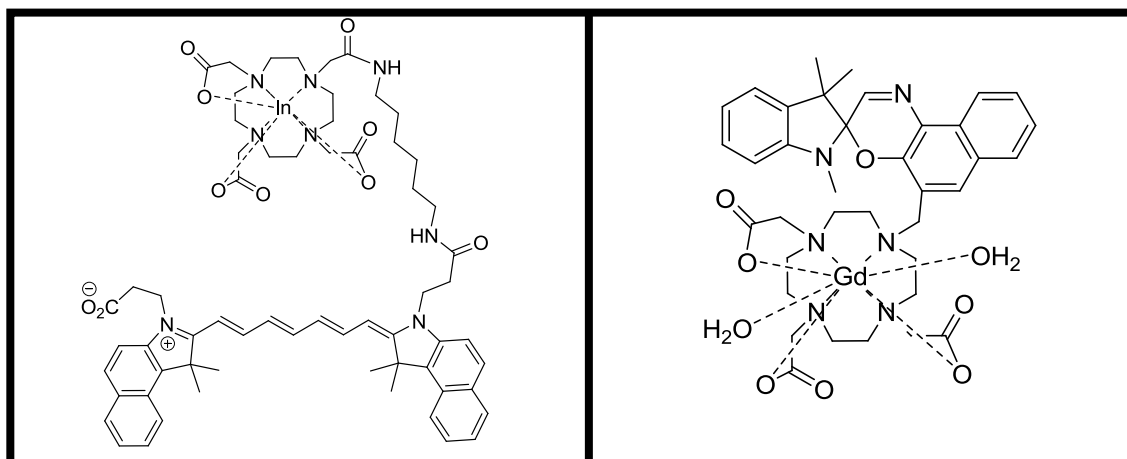
The synthesis of small molecule multimodality imaging probes is usually achieved by the direct fusion of multiple imaging probes, or by attachment of multiple



**Figure 1.14** An example of a fluorescent/MR dual-modality imaging probe with the PAMAM dendrimer core shown in black, gadolinium-EDTA complexes (MCC), cRGDfK peptide (targeting  $\alpha_v\beta_3$  integrins) TM, and Alexa Fluor 594 dye (Dye).<sup>118</sup>

imaging tags to one molecule. While this design maintains a small size for the probe overall, it may alter the pharmacokinetics of the parent molecule based on the properties of the added imaging tags. In terms of probe excretion, small molecules tend to clear via the renal system, while larger molecules (> 5 nm) typically clear through the liver. This provides a clear advantage in preventing toxicity associated with long-term liver retention. While the short circulation times of smaller probes is undesired, resulting in reduced probe uptake, rapid tissue diffusion rates have been observed and may be attractive for *in vivo* applications.<sup>113</sup>

A number of small molecule probes have already been reported including metal-chelator-dye conjugates such as Gd-DOTA-rhodamine<sup>131</sup> and Gd-DO3A-spiroanthoxazine<sup>132, 133</sup> (Figure 1.14). Although various efforts have been made in the development of MRI-optical small molecule fusions, there are major disadvantages associated with this probe design approach. The most important drawback of this methodology is the much lower sensitivity of MRI when compared to optical imaging techniques, implying that, in a given probe, higher numbers of MRI tags are required to produce the same effect as the optical probes. This drawback, however, is minimized *in vivo* due to the lowered sensitivity of optical methods compared to *in vitro* microscopy. The fusion of radioisotopes with optical tags is a more suitable methodology in designing multimodality probes because the sensitivities of the involved modalities are in the same range. Examples of developed optical/nuclear probes include <sup>111</sup>In-DOTA-cyprate<sup>134</sup> (Figure 1.15) and radioiodinated porphyrins (eg. HPPH).<sup>113, 135, 136</sup>



**Figure 1.15** Structures of  $^{111}\text{In}$ -DOTA-cypate (left) and Gd-DO3A-spiro-naphthoxazine (right).

The focus of this dissertation is primarily on the development of novel single and multimodality molecular imaging probes with an emphasis on PET, SPECT and fluorescence imaging. Chapter 2 covers the discovery of novel GLP-1-based PET and SPECT imaging probes for the non-invasive visualization of pancreatic islets *in vivo*. Here, syntheses, characterization, radiometal labeling, *in vitro* and *in vivo* evaluation (in mouse models) of novel tracers, are discussed. Chapter 3 deals with the discovery of a new approach for development of multimodality PET/fluorescence imaging probes. With the aim of eliminating the need for the attachment of multiple imaging tags in the development of multimodality agents, the use of porphyrins is suggested as a fluorescent entity that would also act as a radiometal chelator. The development of a model tracer, utilizing PPIX as the porphyrin ring of choice, is discussed entailing synthesis, characterization, radiolabeling, optical analysis, and *in vitro* characterization with a breast cancer cell line. Chapter 4 deals with the development of a screening procedure for the

discovery of novel biological targeting entities via library screening. This is the first example of a fluorescent, cell-based approach for the screening of a peptide library where peptide-based targeting entities can be identified directly, post solid-phase synthesis, without the need for further modifications. Chapter 5 concludes this dissertation by discussing future directions for the developed ideas.

### 1.10 References

1. Rudin, M.; Weissleder, R., Molecular imaging in drug discovery and development. *Nature Reviews Drug Discovery* **2003**, 2, (2), 123-131.
2. Massoud, T. F.; Gambhir, S. S., Molecular imaging in living subjects: seeing fundamental biological processes in a new light. *Genes & Development* **2003**, 17, (5), 545-580.
3. Krestin, G. P.; Bernsen, M. R., Molecular imaging in radiology: the latest fad or the new frontier? *European Radiology* **2006**, 16, (11), 2383-2385.
4. Gambhir, S. S., Molecular imaging of cancer with positron emission tomography. *Nature Reviews Cancer* **2002**, 2, (9), 683-693.
5. Weissleder, R., Molecular imaging in cancer. *Science* **2006**, 312, (5777), 1168-1171.
6. Bengel, F. M.; Schachinger, V.; Dimmeler, S., Cell-based therapies and imaging in cardiology. *European Journal of Nuclear Medicine and Molecular Imaging* **2005**, 32, S404-S416.

7. Harisinghani, M. G.; Barentsz, J.; Hahn, P. F.; Deserno, W. M.; Tabatabaei, S.; van de Kaa, C. H.; de la Rosette, J.; Weissleder, R., Noninvasive detection of clinically occult lymph-node metastases in prostate cancer. *New England Journal of Medicine* **2003**, 348, (25), 2491-U5.
8. Lardinois, D.; Weder, W.; Hany, T. F.; Kamel, E. M.; Korom, S.; Seifert, B.; von Schulthess, G. K.; Steinert, H. C., Staging of non-small-cell lung cancer with integrated positron-emission tomography and computed tomography. *New England Journal of Medicine* **2003**, 348, (25), 2500-2507.
9. Van den Abbeele, A. D.; Badawi, R. D., Use of positron emission tomography in oncology and its potential role to assess response to imatinib mesylate therapy in gastrointestinal stromal tumors (GISTs). *European Journal of Cancer* **2002**, 38, S60-S65.
10. Smith-Jones, P. M.; Solit, D. B.; Akhurst, T.; Afroze, F.; Rosen, N.; Larson, S. M., Imaging the pharmacodynamics of HER2 degradation in response to Hsp90 inhibitors. *Nature Biotechnology* **2004**, 22, (6), 701-706.
11. Orlic, D., BM stem cells and cardiac repair: where do we stand in 2004? *Cytotherapy* **2005**, 7, (1), 3-15.
12. Fayad, Z. A., MR imaging for the noninvasive assessment of atherothrombotic plaques. *Magn Reson Imaging Clin N Am* **2003**, 11, (1), 101-13.
13. Cheng, Y.; Meyers, J. D.; Broome, A.-M.; Kenney, M. E.; Basilion, J. P.; Burda, C., Deep Penetration of a PDT Drug into Tumors by Noncovalent Drug-Gold Nanoparticle Conjugates. *Journal of the American Chemical Society* 133, (8), 2583-2591.

14. SIEMENS, *Imaging Systems for Medical Diagnostics*. Publicis Corporate Publishing: 2005.
15. Weissleder, R., Scaling down imaging: Molecular mapping of cancer in mice. *Nature Reviews Cancer* **2002**, 2, (1), 11-18.
16. Funovics, M.; Weissleder, R.; Tung, C. H., Protease sensors for bioimaging. *Analytical and Bioanalytical Chemistry* **2003**, 377, (6), 956-963.
17. Grimm, J.; Wunder, A., Molekular Bildgebung: Stand der Forschung *Fortschritte auf dem Gebiet der Rontgenstrahlen* **2005**, 177, 326-337.
18. Eckelman, W. C., Mechanism of target specific uptake using examples of muscarinic receptor binding radiotracers. In *Handbook of radiopharmaceuticals* Welch, M. J.; Redvantly, C. S., Eds. Wiley: Washington, 2003; pp 487-500.
19. Logan, J., Strategies for quantifying PET imaging data from tracer studies of brain receptors and enzymes. In *Handbook of Radiopharmaceuticals*, Welch, M. J.; Redvantly, C. S., Eds. Wiley: Washington, 2003; pp 501-528.
20. Hwang, D.; Bergmann, S. R., Radiopharmaceuticals for studying the heart. In *Handbook of Radiopharmaceuticals*, Welch, M. J.; Redvantly, C. S., Eds. Wiley: Washington, 2003; pp 529-556.
21. Hustinx, R.; Alavi, A., Tumor Imaging. In *Handbook of Radiopharmaceuticals* Welch, M. J.; Redvantly, C. S., Eds. Wiley: Washignton, 2003; pp 629-642.
22. Knight, L. C., Radiolabeled peptides for tumor imaging. In *Handbook of Radiopharamceuticals*, Welch, M. J.; Redvantly, C. S., Eds. Wiley: Washington, 2003; pp 643-684.

23. Zalutsky, M. R.; Lewis, J. S., Radiolabeled Antibodies for Tumor Imaging and Therapy. In *Handbook of Radiopharmaceuticals*, Welch, M. J.; Redvantly, C. S., Eds. Wiley: Washington, 2003; pp 685-714.
24. Wagner, H. N.; Zsolt, S., Dynamic neurotransmitter interactions measured with PET. In *Handbook of Radiopharmaceuticals* Welch, M. J.; Redvantly, C. S., Eds. Wiley: Washington, 2003; pp 603-628.
25. Urano, Y.; Asanuma, D.; Hama, Y.; Koyama, Y.; Barrett, T.; Kamiya, M.; Nagano, T.; Watanabe, T.; Hasegawa, A.; Choyke, P. L.; Kobayashi, H., Selective molecular imaging of viable cancer cells with pH-activatable fluorescence probes. *Nature Medicine* **2009**, 15, (1), 104-109.
26. Kirchmair, J.; Distinto, S.; Schuster, D.; Spitzer, G.; Langer, T.; Wolber, G., Enhancing drug discovery through in silico screening: Strategies to increase true positives retrieval rates. *Current Medicinal Chemistry* **2008**, 15, (20), 2040-2053.
27. Haberkorn, U.; Altmann, A., Radionuclide imaging in the post-genomic era. *Journal of Cellular Biochemistry* **2002**, 1-10.
28. Weissleder, R.; Ntziachristos, V., Shedding light onto live molecular targets. *Nature Medicine* **2003**, 9, (1), 123-128.
29. Begley, D. J.; Brightman, M. W., Structural and functional aspects of the blood-brain barrier. *Progress in Drug Research, Vol 61* **2003**, 61, 39-78.
30. Jain, R. K., Transport of molecules, particles, and cells in solid tumors. *Annual Review of Biomedical Engineering* **1999**, 1, 241-263.



31. Luyt, L. G., The Design of Radiolabeled Peptides for Targeting Malignancies. In *Monoclonal Antibody and Peptide-Targeted Radiotherapy of Cancers*, Reilly, R., Ed. Raymond M. Reilly 2010.
32. Klabunde, T.; Hessler, G., Drug design strategies for targeting G-protein-coupled receptors. *Chembiochem* **2002**, 3, (10), 929-944.
33. Reubi, J. C., Peptide receptors as molecular targets for cancer diagnosis and therapy. *Endocrine Reviews* **2003**, 24, (4), 389-427.
34. Tyndall, J. D. A.; Pfeiffer, B.; Abbenante, G.; Fairlie, D. P., Over one hundred peptide-activated G protein-coupled receptors recognize ligands with turn structure. *Chemical Reviews* **2005**, 105, (3), 793-826.
35. Reile, H.; Armatis, P. E.; Schally, A. V., Characterization of high-affinity receptors for bombesin/gastrin releasing peptide on the human prostate-cancer cell-lines PC-3 and DU-145 - Internalization of receptor-bound (125)I-(Tyr(4)) bombesin by tumor-cells *Prostate* **1994**, 25, (1), 29-38.
36. Reubi, J. C.; Schaer, J. C.; Waser, B., Cholecystokinin (CCK)-A and CCK-B gastrin receptors in human tumors. *Cancer Research* **1997**, 57, (7), 1377-1386.
37. Wicki, A.; Wild, D.; Storch, D.; Seemayer, C.; Gotthardt, M.; Behe, M.; Kneifel, S.; Mihatsch, M. J.; Reubi, J. C.; Macke, H. R.; Christofori, G., [Lys(40)(Ahx-DTPA-In-111)NH<sub>2</sub>]-Exendin-4 is a highly efficient radiotherapeutic for glucagon-like peptide-1 receptor-targeted therapy for insulinoma. *Clinical Cancer Research* **2007**, 13, (12), 3696-3705.
38. Salazar-Onfray, F.; Lopez, M.; Lundqvist, A.; Aguirre, A.; Escobar, A.; Serrano, A.; Korenblit, C.; Petersson, M.; Chhajlani, V.; Larsson, O.; Kiessling, R., Tissue

- distribution and differential expression of melanocortin I receptor, a malignant melanoma marker. *British Journal of Cancer* **2002**, 87, (4), 414-422.
39. Reubi, J. C.; Waser, B.; Friess, H.; Buchler, M.; Laissue, J., Neurotensin receptors: a new marker for human ductal pancreatic adenocarcinoma. *Gut* **1998**, 42, (4), 546-550.
40. Zhang, K. J.; An, R.; Gao, Z. R.; Zhang, Y. X.; Aruva, M. R., Radionuclide imaging of small-cell lung cancer (SCLC) using Tc-99m-labeled neurotensin peptide 8-13. *Nuclear Medicine and Biology* **2006**, 33, (4), 505-512.
41. Reubi, J. C.; Gugger, M.; Waser, B.; Schaer, J. C., Y-1-mediated effect of neuropeptide Y in cancer: Breast carcinomas as targets. *Cancer Research* **2001**, 61, (11), 4636-4641.
42. Korner, M.; Waser, B.; Reubi, J. C., High expression of neuropeptide Y1 receptors in Ewing sarcoma tumors. *Clinical Cancer Research* **2008**, 14, (16), 5043-5049.
43. Froidevaux, S.; Eberle, A. N., Somatostatin analogs and radiopeptides in cancer therapy. *Biopolymers* **2002**, 66, (3), 161-183.
44. Hennig Vvo M, J. A. L.; Horisberger, U.; Reubi, J.-C., Substance-P receptors in human primary neoplasms: Tumoral and vascular localization. *International Journal of Cancer* **1995**, 61, (6), 786-792.
45. Folkman, J., Angiogenesis in cancer, vascular, rheumatoid and other disease. *Nature Medicine* **1995**, 1, (1), 27-31.
46. Ahlskog, J.; Paganelli, G.; Neri, D., Vascular tumor targeting. *Quarterly Journal of Nuclear Medicine and Molecular Imaging* **2006**, 50, (4), 296-309.

47. Cai, W. B.; Rao, J. H.; Gambhir, S. S.; Chen, X. Y., How molecular imaging is speeding up antiangiogenic drug development. *Molecular Cancer Therapeutics* **2006**, 5, (11), 2624-2633.
48. Fasman, G. D., Practical handbook of biochemistry and molecular biology  
*Fasman, G. D. (Ed.). Practical Handbook of Biochemistry and Molecular Biology. IX+601p. Crc Press, Inc.: Boca Raton, Florida, USA. Illus 1989, IX+601P.*
49. Cleland, W. W., Dithiothreitol new protective reagent for SH groups *Biochemistry* **1964**, 3, (4), 480-&.
50. Brinkley, M., A brief survey of methods for preparing protein conjugates with dyes, haptens, and cross-linking reagents. *Bioconjugate Chemistry* **1992**, 3, (1), 2-13.
51. Lund, F.; Jogestrand, T., Video fluorescein imaging of the skin: description of an overviewing technique for functional evaluation of regional cutaneous blood perfusion in occlusive arterial disease of the limbs. *Clinical Physiology* **1997**, 17, (6), 619-633.
52. Ragin, A. D.; Morgan, R. A.; Chmielewski, J., Cellular import mediated by nuclear localization signal peptide sequences. *Chemistry & Biology* **2002**, 9, (8), 943-948.
53. Kaufman, C. L.; Williams, M.; Ryle, L. M.; Smith, T. L.; Tanner, M.; Ho, C., Superparamagnetic iron oxide particles transactivator protein-fluorescein isothiocyanate particle labeling for in vivo magnetic resonance imaging detection

- of cell migration: Uptake and durability. *Transplantation* **2003**, 76, (7), 1043-1046.
54. Carion, O.; Mahler, B.; Pons, T.; Dubertret, B., Synthesis, encapsulation, purification and coupling of single quantum dots in phospholipid micelles for their use in cellular and in vivo imaging. *Nature Protocols* **2007**, 2, (10), 2383-2390.
55. Saha, G. B., Fundamentals of Nuclear Pharmacy. In Fifth Edition ed.; Springer-Verlag: New York, 2004.
56. Baidoo, K. E.; Scheffel, U.; Stathis, M.; Finley, P.; Lever, S. Z.; Zhan, Y. G.; Wagner, H. N., High-affinity no-carrier-added Tc-99m-labeled chemotactic peptides for studies of inflammation in vivo. *Bioconjugate Chemistry* **1998**, 9, (2), 208-217.
57. Zamora, P. O.; Gulhke, S.; Bender, H.; Diekmann, D.; Rhodes, B. A.; Biersack, H. J.; Knapp, F. F., Experimental radiotherapy of receptor-positive human prostate adenocarcinoma with Re-188-RC-160, a directly-radiolabeled somatostatin analogue. *International Journal of Cancer* **1996**, 65, (2), 214-220.
58. Okarvi, S. M., Recent progress in fluorine-18 labelled peptide radiopharmaceuticals. *European Journal of Nuclear Medicine* **2001**, 28, (7), 929-938.
59. Fichna, J.; Janecka, A., Synthesis of target-specific radiolabeled peptides for diagnostic Imaging. *Bioconjugate Chemistry* **2003**, 14, (1), 3-17.

60. Anderson, G. W.; Callahan, F. M.; Zimmerman, J. E., Use of esters of N-hydroxysuccinimide in peptide synthesis *Journal of the American Chemical Society* **1964**, 86, (9), 1839-&.
61. Grumbach, I. M.; Veh, R. W., Sulfo-N-hydroxysuccinimide activated long-chain biotin - a new microtitre plate assay for the determination of its stability at different pH values and its reaction-rate with protein-bound amino-groups *Journal of Immunological Methods* **1991**, 140, (2), 205-210.
62. Liu, S.; Edwards, D. S., Tc-99m-Labeled small peptides as diagnostic radiopharmaceuticals. *Chemical Reviews* **1999**, 99, (9), 2235-2268.
63. Thakur, M. L., Radiolabeled peptides - now and the future *Nuclear Medicine Communications* **1995**, 16, (9), 724-732.
64. Meares, C. F., Chelating agents for the binding of metal ions to antibodies. *Int J Rad Appl Instrum B* **1986**, 13, (4), 311-8.
65. McMurry, T. J.; Pippin, C. G.; Wu, C. C.; Deal, K. A.; Brechbiel, M. W.; Mirzadeh, S.; Gansow, O. A., Physical parameters and biological stability of yttrium(III) diethylenetriaminepentaacetic acid derivative conjugates. *Journal of Medicinal Chemistry* **1998**, 41, (18), 3546-3549.
66. Hnatowich, D. J.; Layne, W. W.; Childs, R. L.; Lanteigne, D.; Davis, M. A.; Griffin, T. W.; Doherty, P. W., Radioactive labeling of antibody - a simple and efficient method *Science* **1983**, 220, (4597), 613-615.
67. deJong, M.; Bakker, W. H.; Krenning, E. P.; Breeman, W. A. P.; vanderPluijm, M. E.; Bernard, B. F.; Visser, T. J.; Jermann, E.; Behe, M.; Powell, P.; Macke, H. R., Yttrium-90 and indium-111 labelling, receptor binding and biodistribution of

- [DOTA(0),D-Phe(1),Tyr(3)]octreotide, a promising somatostatin analogue for radionuclide therapy. *European Journal of Nuclear Medicine* **1997**, 24, (4), 368-371.
68. McMurry, T. J.; Brechbiel, M.; Kumar, K.; Gansow, O. A., Convenient synthesis of bifunctional tetraaza macrocycles *Bioconjugate Chemistry* **1992**, 3, (2), 108-117.
69. Otte, A.; Jermann, E.; Behe, M.; Goetze, M.; Bucher, H. C.; Roser, H. W.; Heppeler, A.; MuellerBrand, J.; Maecke, H. R., DOTATOC: a powerful new tool for receptor-mediated radionuclide therapy. *European Journal of Nuclear Medicine* **1997**, 24, (7), 792-795.
70. Oberg, K.; Eriksson, B., Nuclear medicine in the detection, staging and treatment of gastrointestinal carcinoid tumours. *Best Practice & Research Clinical Endocrinology & Metabolism* **2005**, 19, (2), 265-276.
71. Wang, X. Y.; Jin, T. Z.; Comblin, V.; Lopezmut, A.; Merciny, E.; Desreux, J. F., A kinetic investigation of the lanthanide DOTA chelates - stability and rates of formation and of dissociation of a macrocyclic Gadolinium(III) polycarboxylic MRI contrast agent *Inorganic Chemistry* **1992**, 31, (6), 1095-1099.
72. Broan, C. J.; Cox, J. P. L.; Craig, A. S.; Katakya, R.; Parker, D.; Harrison, A.; Randall, A. M.; Ferguson, G., Structure and solution stability of indium and gallium complexes of 1,4,7-triazacyclononanetriacetate and of yttrium complexes of 1,4,7,10-tetraazacyclododecanetetraacetate and related ligands - kinetically stable complexes for use in imaging and radioimmunotherapy - x-ray molecular-

- structure of the indium and gallium complexes of 1,4,7-triazacyclononane-1,4,7-triacetic acid. *Journal of the Chemical Society-Perkin Transactions 2* **1991**, (1), 87-99.
73. Clarke, E. T.; Martell, A. E., Stabilities of the fe(iii), ga(iii) and in(iii) chelates of n,n',n''-triazacyclononanetriacetic acid. *Inorganica Chimica Acta* **1991**, 181, (2), 273-280.
74. Anderson, C. J.; Welch, M. J., Radiometal labeled agents (non-technetium) for diagnostic imaging. *Chemical Reviews* **1999**, 99, (9), 2219-2234.
75. Bass, L. A.; Wang, M.; Welch, M. J.; Anderson, C. J., In vivo transchelation of copper-64 from TETA-octreotide to superoxide dismutase in rat liver. *Bioconjugate Chemistry* **2000**, 11, (4), 527-532.
76. Weissleder, R., Molecular imaging: Exploring the next frontier. *Radiology* **1999**, 212, (3), 609-614.
77. WERNICK, M. N.; AARSVOLD, J. N., Introduction to Emission Tomography. In *Emission Tomography: The Fundamentals of PET and SPECT*, WERNICK, M. N.; AARSVOLD, J. N., Eds. Elsevier Academic Press: Oxford, 2004; pp 11-22.
78. Zaidi, H.; Hasegaway, B. H., Overview of Nuclear Medical Imaging: Physics and Instrumentation. In *Quantitative Analysis in Nuclear Medicine Imaging*, Zaidi, H., Ed. Springer Science & Business Media, Inc.: New York, 2006; pp 1-34.
79. Juweid, M. E.; Cheson, B. D., Current concepts - Positron-emission tomography and assessment of cancer therapy. *New England Journal of Medicine* **2006**, 354, (5), 496-507.

80. Chen, Y. J.; Cairns, R.; Papandreou, I.; Koong, A.; Denko, N. C., Oxygen Consumption Can Regulate the Growth of Tumors, a New Perspective on the Warburg Effect. *Plos One* **2009**, 4, (9).
81. Grosu, A. L.; Weber, W. A.; Riedel, E.; Jeremic, B.; Nieder, C.; Franz, M.; Gumprecht, H.; Jaeger, R.; Schwaiger, M.; Molls, M., L-(methyl-11C) methionine positron emission tomography for target delineation in resected high-grade gliomas before radiotherapy. *International Journal of Radiation Oncology Biology Physics* **2005**, 63, (1), 64-74.
82. Veas, H.; Buchegger, F.; Albrecht, S.; Khan, H.; Husarik, D.; Zaidi, H.; Soloviev, D.; Hany, T. F.; Miralbell, R., F-18-choline and/or C-11-acetate positron emission tomography: detection of residual or progressive subclinical disease at very low prostate-specific antigen values (< 1 ng/mL) after radical prostatectomy. *Bju International* **2007**, 99, (6), 1415-1420.
83. Laverman, P.; Boerman, O. C.; Corstens, F. H. M.; Oyen, W. J. G., Fluorinated amino acids for tumour imaging with positron emission tomography. *European Journal of Nuclear Medicine and Molecular Imaging* **2002**, 29, (5), 681-690.
84. Miyakubo, M.; Oriuchi, N.; Tsushima, Y.; Higuchi, T.; Koyama, K.; Arai, K.; Paudyal, B.; Iida, Y.; Hanaoka, H.; Ishikita, T.; Nakasone, Y.; Negishi, A.; Mogi, K.; Endo, K., Diagnosis of maxillofacial tumor with L-3-[F-18]-fluoro-alpha-methyltyrosine (FMT) PET: a comparative study with FDG-PET. *Annals of Nuclear Medicine* **2007**, 21, (2), 129-135.
85. Kauhanen, The clinical value of [F-18]fluoro-dihydroxyphenylalanine positron emission tomography in primary diagnosis, staging, and restaging of



- neuroendocrine tumors (vol 16, pg 255, 2009). *Endocrine-Related Cancer* **2009**, 16, (2), 661-661.
86. Yeh, S. H.; Liu, R. S.; Wu, L. C.; Yang, D. J.; Yen, S. H.; Chang, C. W.; Yu, T. W.; Chou, K. L.; Chen, K. Y., Fluorine-18 fluoromisonidazole tumour to muscle retention ratio for the detection of hypoxia in nasopharyngeal carcinoma. *European Journal of Nuclear Medicine* **1996**, 23, (10), 1378-1383.
87. Moresco, R. M.; Casati, R.; Lucignani, G.; Carpinelli, A.; Schmidt, K.; Todde, S.; Colombo, F.; Fazio, F., Systemic and cerebral kinetics of 16-alpha[f-18]fluoro-17-beta-estradiol - a ligand for the in-vivo assessment of estrogen-receptor binding parameters. *Journal of Cerebral Blood Flow and Metabolism* **1995**, 15, (2), 301-311.
88. Shani, J.; Wolf, W., Model for prediction of chemotherapy response to 5-fluorouracil based on differential distribution of 5-[f-18]fluorouracil in sensitive versus resistant lymphocytic-leukemia in mice. *Cancer Research* **1977**, 37, (7), 2306-2308.
89. Edwards, C. L.; Hayes, R. L., Tumor scanning with <sup>67</sup>Ga citrate. *Journal of Nuclear Medicine* **1969**, 10, (2), 103-&.
90. Nagda, S. N.; Morideen, N.; Lo, S. S.; Khan, U.; Dillehay, G.; Wagner, R.; Campbell, S.; Flanigan, R., Long-term follow-up of In-111-capromab pendetide (ProstaScint) scan as pretreatment assessment in patients who undergo salvage radiotherapy for rising prostate-specific antigen after radical prostatectomy for prostate cancer. *International Journal of Radiation Oncology Biology Physics* **2007**, 67, (3), 834-840.

91. Stegger, L.; Schafers, K.; Kopka, K.; Wagner, S.; Hermann, S.; Kies, P.; Law, M.; Schober, O.; Schafers, M., Molecular cardiovascular imaging using scintigraphic methods. *European Radiology* **2007**, *17*, (6), 1422-1432.
92. Miller, T. D.; Christian, T. F.; Hopfenspirger, M. R.; Hodge, D. O.; Gersh, B. J.; Gibbons, R. J., Infarct size after acute myocardial-infarction measured by quantitative tomographic Tc-99m sestamibi imaging predicts subsequent mortality. *Circulation* **1995**, *92*, (3), 334-341.
93. Zaret, B. L.; Rigo, P.; Wackers, F. J. T.; Hendel, R. C.; Braat, S. H.; Iskandrian, A. S.; Sridhara, B. S.; Jain, D.; Itti, R.; Serafini, A. N.; Goris, M. L.; Lahiri, A.; Halders, S.; Koppejans, L.; Cajob, I.; Willems, P.; Bontemps, L.; Egroizard, P.; Sayegh, Y.; Fraysse, M.; Benoit, T. R.; Lellerlo, B.; Foulon, J.; Kline, R.; Morrissette, G.; Price, L.; Jackson, R.; Spies, S.; Bellow, S.; Leonard, S.; Bull, C.; Sridhara, B.; Raval, U.; Crawley, J.; Smith, T.; Iskandrian, A.; Heo, J.; Unteeker, W.; Feinsmith, N.; Cave, V.; Wasserleben, V.; McDougall, R.; Blake, L.; Gurevich, N.; Fujii, C.; Ezuddin, S.; Sequeira, R.; Lowery, M.; Wackers, F. J.; Mattera, J.; McMahon, M.; Saari, M., Myocardial perfusion imaging with Tc-99m tetrofosmin - comparison to (Tl)-T-201 imaging and coronary angiography in a phase-iii multicenter. *Circulation* **1995**, *91*, (2), 313-319.
94. Clarke, S. E. M.; Lazarus, C. R.; Wraight, P.; Sampson, C.; Maisey, M. N., Pentavalent [Tc-99m]DMSA, [i-131]MIBG, and [Tc-99m]MDP-an evaluation of 3 imaging techniques in patients with medullary carcinoma of the thyroid. *Journal of Nuclear Medicine* **1988**, *29*, (1), 33-38.

95. Murata, Y.; Yamada, I.; Umehara, I.; Ishii, Y.; Okada, N., Perfusion and blood-pool scintigraphy in the evaluation of head and neck hemangiomas. *Journal of Nuclear Medicine* **1997**, 38, (6), 882-885.
96. Pandit-Taskar, N.; Dauer, L. T.; Montgomery, L.; St Germain, J.; Zanzonico, P. B.; Divgi, C. R., Organ and fetal absorbed dose estimates from Tc-99m-sulfur colloid lymphoscintigraphy and sentinel node localization in breast cancer patients. *Journal of Nuclear Medicine* **2006**, 47, (7), 1202-1208.
97. Donnemiller, E.; Heilmann, J.; Wenning, G. K.; Berger, W.; Decristoforo, C.; Moncayo, R.; Poewe, W.; Ransmayr, G., Brain perfusion scintigraphy with Tc-99m-HMPAO or Tc-99m-ECD and I-123-beta-CIT single-photon emission tomography in dementia of the Alzheimer-type and diffuse Lewy body disease. *European Journal of Nuclear Medicine* **1997**, 24, (3), 320-325.
98. Schlyer, D. J., *Production of Radionuclides in Accelerators*. John Wiley & Sons, Ltd: 2005; p 1-70.
99. Saha, G. B., *Basics of PET Imaging*. Second Edition ed.; Springer Science and Business Media: Cleveland, 2010.
100. Brown, T.; LeMay, E. H.; Bursten, B. E., *Chemistry: The Central Science*. Pearson Publications Company: 2006.
101. Hnatowich, D. J., Review of radiopharmaceutical development with short-lived generator-produced radionuclides other than Tc-99m. *International Journal of Applied Radiation and Isotopes* **1977**, 28, (1-2), 169-&.
102. Firestone, R. B.; Browne, E., Table of radioactive isotopes *Abstracts of Papers of the American Chemical Society* **1985**, 190, (SEP), 98-NUL.

103. Ntziachristos, V., Fluorescence molecular imaging. *Annu Rev Biomed Eng* **2006**, 8, 1-33.
104. Weissleder, R., A clearer vision for in vivo imaging. *Nature Biotechnology* **2001**, 19, (4), 316-317.
105. Brovko, L., *Bioluminescence and Fluorescence for In Vivo Imaging*. SPIE Press: Washington, 2010.
106. Tung, C. H., Fluorescent peptide probes for in vivo diagnostic imaging. *Biopolymers* **2004**, 76, (5), 391-403.
107. Achilefu, S.; Jimenez, H. N.; Dorshow, R. B.; Bugaj, J. E.; Webb, E. G.; Wilhelm, R. R.; Rajagopalan, R.; Jöhler, J.; Erion, J. L., Synthesis, in vitro receptor binding, and in vivo evaluation of fluorescein and carbocyanine peptide-based optical contrast agents. *Journal of Medicinal Chemistry* **2002**, 45, (10), 2003-2015.
108. Tung, C. H.; Ho, N. H.; Tang, Q.; Jaffer, F. A.; Reed, G. L.; Weissleder, R., Novel factor XIII probes for blood coagulation imaging. *Chembiochem* **2003**, 4, (9), 897-899.
109. Lai, W. F. T.; Chang, C. H.; Tang, Y.; Bronson, R.; Tung, C. H., Early diagnosis of osteoarthritis using cathepsin B sensitive near-infrared fluorescent probes. *Osteoarthritis and Cartilage* **2004**, 12, (3), 239-244.
110. Chen, J. Q.; Tung, C. H.; Mahmood, U.; Ntziachristos, V.; Gyurko, R.; Fishman, M. C.; Huang, P. L.; Weissleder, R., In vivo imaging of proteolytic activity in atherosclerosis. *Circulation* **2002**, 105, (23), 2766-2771.

111. Messerli, S. M.; Prabhakar, S.; Tang, Y.; Shah, K.; Cortes, M. L.; Murthy, V.; Weissleder, R.; Breakefield, X. O.; Tung, C. H., A novel method for imaging apoptosis using a caspase-1 near-infrared fluorescent probe. *Neoplasia* **2004**, *6*, (2), 95-105.
112. Tung, C. H.; Gerszten, R. E.; Jaffer, F. A.; Weissleder, R., A novel near-infrared fluorescence sensor for detection of thrombin activation in blood. *Chembiochem* **2002**, *3*, (2-3), 207-211.
113. Louie, A. Y., Multimodality Imaging Probes: Design and Challenges. *Chemical Reviews* *110*, (5), 3146-3195.
114. Glickson, J. D.; Lund-Katz, S.; Zhou, R.; Choi, H.; Chen, I. W.; Li, H.; Corbin, I.; Popov, A. V.; Cao, W. G.; Song, L. P.; Qi, C. Z.; Marotta, D.; Nelson, D. S.; Chen, J.; Chance, B.; Zheng, G., Lipoprotein nanoplatform for targeted delivery of diagnostic and therapeutic agents. *Molecular Imaging* **2008**, *7*, (2), 101-110.
115. Al-Jamal, W. T.; Kostarelos, K., Liposome-nanoparticle hybrids for multimodal diagnostic and therapeutic applications. *Nanomedicine (Lond)* **2007**, *2*, (1), 85-98.
116. Jaiswal, J. K.; Mattoussi, H.; Mauro, J. M.; Simon, S. M., Long-term multiple color imaging of live cells using quantum dot bioconjugates. *Nature Biotechnology* **2003**, *21*, (1), 47-51.
117. Banerjee, S. S.; Chen, D. H., A multifunctional magnetic nanocarrier bearing fluorescent dye for targeted drug delivery by enhanced two-photon triggered release. *Nanotechnology* **2009**, *20*, (18).
118. Boswell, C. A.; Eck, P. K.; Regino, C. A. S.; Bernardo, M.; Wong, K. J.; Milenic, D. E.; Choyke, P. L.; Brechbiel, M. W., Synthesis, characterization, and

- biological evaluation of integrin alpha(v)beta(3)-targeted PAMAM dendrimers. *Molecular Pharmaceutics* **2008**, 5, (4), 527-539.
119. Huber, M. M.; Staubli, A. B.; Kustedjo, K.; Gray, M. H. B.; Shih, J.; Fraser, S. E.; Jacobs, R. E.; Meade, T. J., Fluorescently detectable magnetic resonance imaging agents. *Bioconjugate Chemistry* **1998**, 9, (2), 242-249.
120. Li, C.; Wang, W.; Wu, Q. P.; Shi, K.; Houston, J.; Sevick-Muraca, E.; Dong, L.; Chow, D.; Charnsangavej, C.; Gelovani, J. G., Dual optical and nuclear imaging in human melanoma xenografts using a single targeted imaging probe. *Nuclear Medicine and Biology* **2006**, 33, (3), 349-358.
121. Dykes, G. M., Dendrimers: a review of their appeal and applications. *Journal of Chemical Technology and Biotechnology* **2001**, 76, (9), 903-918.
122. Challa, R.; Ahuja, A.; Ali, J.; Khar, R. K., Cyclodextrins in drug delivery: an updated review. *AAPS PharmSciTech* **2005**, 6, (2), E329-57.
123. Choi, J. S.; Lee, E. J.; Choi, Y. H.; Jeong, Y. J.; Park, J. S., Poly(ethylene glycol)-block-poly(L-lysine) dendrimer: Novel linear polymer/dendrimer block copolymer forming a spherical water-soluble polyionic complex with DNA. *Bioconjugate Chemistry* **1999**, 10, (1), 62-65.
124. Lee, M.; Kim, S. W., Polyethylene glycol-conjugated copolymers for plasmid DNA delivery. *Pharmaceutical Research* **2005**, 22, (1), 1-10.
125. Sadler, K.; Tam, J. P., Peptide dendrimers: applications and synthesis. *J Biotechnol* **2002**, 90, (3-4), 195-229.
126. Xu, H.; Regino, C. A. S.; Koyama, Y.; Hama, Y.; Gunn, A. J.; Bernardo, M.; Kobayashi, H.; Choyke, P. L.; Brechbiel, M. W., Preparation and preliminary

- evaluation of a biotin-targeted, lectin-targeted dendrimer-based probe for dual-modality magnetic resonance and fluorescence Imaging. *Bioconjugate Chemistry* **2007**, 18, 1474-1482.
127. Kobayashi, H.; Kawamoto, S.; Brechbiel, M. W.; Bernardo, M.; Sato, N.; Waldmann, T. A.; Tagaya, Y.; Choyke, P. L., Detection of lymph node involvement in hematologic malignancies using micromagnetic resonance lymphangiography with a gadolinium-labeled dendrimer nanoparticle. *Neoplasia* **2005**, 7, (11), 984-991.
128. Wei, Y. Q.; Laurent, R.; Majoral, J. P.; Caminade, A. M., Synthesis and characterization of phosphorus-containing dendrimers bearing rhodamine derivatives as terminal groups. *Arkivoc*, 318-327.
129. Talanov, V. S.; Regino, C. A. S.; Kobayashi, H.; Bernardo, M.; Choyke, P. L.; Brechbiel, M. W., Dendrimer-based nanoprobe for dual modality magnetic resonance and fluorescence imaging. *Nano Letters* **2006**, 6, (7), 1459-1463.
130. Tomalia, D. A.; Reyna, L. A.; Svenson, S., Dendrimers as multi-purpose nanodevices for oncology drug delivery and diagnostic imaging. *Biochemical Society Transactions* **2007**, 35, 61-67.
131. Sturzu, A.; Kalbacher, H.; Echner, H.; Klose, U.; Gharabaghi, A.; Heckl, S., Imaging of human glioma cells by means of a Syndecan-4 directed DOTA-conjugate. *Amino Acids* 38, (5), 1415-1421.
132. Yuan, W. F.; Sun, L.; Tang, H. H.; Wen, Y. Q.; Jiang, G.; Huang, W.; Jiang, L.; Song, Y. L.; Tian, H.; Zhu, D. B., A novel thermally stable spironaphthoxazine

- and its application in rewritable high density optical data storage. *Advanced Materials* **2005**, 17, (2), 156-+.
133. Chu, N. Y. C., Photochromism of spiroindolinonaphthoxazine .1. photophysical properties. *Canadian Journal of Chemistry-Revue Canadienne De Chimie* **1983**, 61, (2), 300-305.
134. Edwards, W. B.; Xu, B.; Akers, W.; Cheney, P. P.; Liang, K.; Rogers, B. E.; Anderson, C. J.; Achilefu, S., Agonist-antagonist dilemma in molecular imaging: Evaluation of a monomolecular multimodal imaging agent for the somatostatin receptor. *Bioconjugate Chemistry* **2008**, 19, (1), 192-200.
135. Tu, C.; Nagao, R.; Louie, A. Y., Multimodal Magnetic-Resonance/Optical-Imaging Contrast Agent Sensitive to NADH. *Angewandte Chemie-International Edition* **2009**, 48, (35), 6547-6551.
136. Pandey, S. K.; Gryshuk, A. L.; Sajjad, M.; Zheng, X.; Chen, Y. H.; Abouzeid, M. M.; Morgan, J.; Charamisinau, I.; Nabi, H. A.; Oseroff, A.; Pandey, R. K., Multimodality agents for tumor imaging (PET, fluorescence) and photodynamic therapy. A possible "see and treat" approach. *Journal of Medicinal Chemistry* **2005**, 48, (20), 6286-6295.



## CHAPTER 2. Design, Synthesis and In Vitro Characterization of Glucagon-Like Peptide-1 Derivatives for Pancreatic Beta Cell Imaging

*A section of this chapter has been published in the journal of bioorganic and medicinal chemistry*

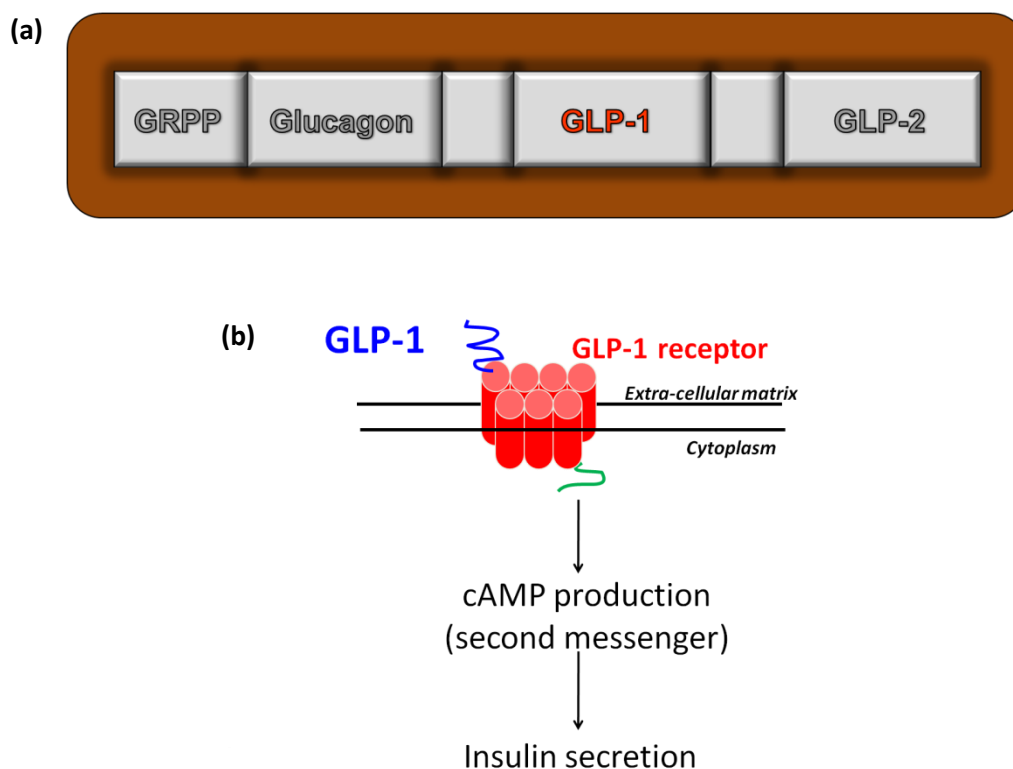
Behnam Azad, B. et al. *Bioorg. Med. Chem.* **2010**, *18*, 1265-1272

### 2.1 Introduction

Diabetes mellitus is a metabolic disorder characterized by chronic hyperglycemia and disturbance of carbohydrate, fat, and protein metabolism resulting from defects of insulin secretion, insulin action or both.<sup>1</sup> The relative contribution of these variables, however, varies between different types of diabetes. Several processes are involved in the development of diabetes including destruction of insulin-producing pancreatic beta cells, as well as enhanced resistance to insulin action. It is this insensitivity or lack of insulin, which results in abnormalities typically observed in carbohydrate, fat and protein metabolism.<sup>2</sup> Diabetes has emerged as a major health problem worldwide with an estimated 285 million people suffering from the disease in 2010. The growth of type 2 diabetes is expected to increase this number to over 400 million in the next twenty years. Considering the projected statistics, the ability to non-invasively monitor the onset of diabetes, and its progression into type 2 diabetes, could aid in enhancing our understanding of the involved processes, thus allowing for earlier diagnosis and treatment.

Glucagon-Like Peptide-1 (GLP-1) is a peptide hormone produced by intestinal L-cells in response to nutrient ingestion.<sup>3</sup> It is produced through the post-translational processing of its larger precursor, proglucagon, by the enzyme prohormone convertase 1/3 and exists largely as the C-terminally amidated form, GLP-1 (7-36).<sup>4</sup>

Other products of this enzymatic degradation are: 1) GLP-2, a peptide involved in growth of epithelial cells, 2) glucagon for maintaining blood glucose levels, and 3) glicentin related pancreatic peptide (GRPP), a glucagon precursor (Figure 2.1a ). As GLP-1 binds to its receptor on the pancreatic beta cell, signaling events trigger the release of insulin (Figure 2.1b) in a glucose-dependent manner known as the “incretin effect”.<sup>5</sup> GLP-1 receptor signaling events also lead to the enhancement of beta cell survival through stimulation of beta cell growth and differentiation, which plays a role in regeneration of beta cell mass.<sup>6</sup> Therefore, GLP-1 may potentially be a viable and powerful candidate in the treatment of Type 2 diabetes.



**Figure 2.1** An illustration showing (a) major proglucagon degradation products and (b) role of GLP-1 in insulin production.

The structure of the GLP-1 receptor classifies it as part of the Family B (II) Glucagon-Secretin G Protein-Coupled Receptor (GPCR) super family. The structural characteristics of the receptors in this family include a long extracellular N-terminal domain, disulfide bridged cysteine residues in the extracellular domains, and several glycosylation sites.<sup>7</sup> Structure-function studies of the GLP-1R have shown that the helical region of GLP-1 interacts with the extracellular N-terminal domain of the GLP-1R, while the N-terminal 8 amino acids of GLP-1 interact with residues in the extracellular regions and transmembrane helices of the receptor.<sup>8</sup> Such a complex receptor/ligand interaction demands consideration of only a limited number of sites on the ligand that can be modified for the generation of an imaging probe with GLP-1 as a targeting component.

Since the structural and biochemical characteristics of the interaction between GLP-1 and its receptor have been determined, GLP-1 may be a suitable peptide with which to develop peptide-based imaging probes for the detection and monitoring of pancreatic beta cell mass *in vivo*, and thus the onset and progression of diabetes. One limiting factor is the short biological half life of GLP-1 (1-2 min) due to rapid enzymatic degradation,<sup>7</sup> as the alanine residue at position 8 is a cleavage site for the plasma protease dipeptidyl peptidase-IV (DPP-IV). Thus, in order to develop GLP-1-based therapeutics and diagnostics, it is important to increase the biological half life of the parent peptide, which can be done through modification of <sup>8</sup>Ala to <sup>8</sup>D-Ala.<sup>9,10</sup> An alternate approach can be the use of exendin-4, a 39-amino acid peptide originally isolated from *Heloderma suspectum*,<sup>11</sup> which is a more potent and stable GLP-1R agonist with a plasma half life of approximately 26 min, largely due to the substitution of a glycine residue for alanine at position 8.

Considering that GLP-1 receptors are expressed on beta cells in high density, we propose that the use of radiolabeled GLP-1, in conjunction with non-invasive imaging techniques SPECT or PET, can provide a method of studying beta cell mass *in vivo*. This hypothesis is supported by a recent report on the generation of the probe [ $^{40}\text{Lys}$  (Ahx-DTPA- $^{111}\text{In}$ )NH $_2$ ]exendin-4, which was shown to target the GLP-1 receptor for the molecular imaging of insulinomas in transgenic Rip1Tag2 mice.<sup>12</sup> In terms of GLP-1 peptides, until now, radioiodination has been the only method reported for GLP-1 radiolabeling. However, iodinated peptides, such as [ $^{123}\text{I}$ ]GLP-1 for detection of insulinomas, have been reported to be unsuitable as a result of the instability of the radioiodine label *in vivo*.<sup>13</sup> Here we report radiometal and radiofluorinated derivatives of GLP-1 with increased structural stability and optimal binding affinity for beta cell imaging.

### 2.1.1 Selection of Suitable Metals

Radiometal-labeled ligands have commonly been used in molecular imaging with both PET and SPECT modalities. Radiopharmaceuticals labeled with metal radionuclides are typically injected into patients in order to diagnose and monitor biological processes in cancers, infections, thrombosis, kidney / liver abnormalities, as well as cardiological and neurological disorders. Radiometal agents are also used to monitor cancer therapy and targeted radiotherapy treatments. Metals utilized in radiopharmaceuticals range in half-life from 10 min for  $^{62}\text{Ga}$  to several days in case of  $^{67}\text{Ga}$ , thus providing a wide range of options to meet such criteria.<sup>14</sup>

Design of radiometal-based imaging agents requires sufficient understanding of the redox properties, stability, stereochemistry, charge and lipophilicity of radiometal complexes because, in most cases, this information would help explain the observed *in vivo* behavior of the developed compounds. For instance, the clearance path of negatively charged compounds is typically through the kidneys, while positively charged compounds tend to accumulate in the heart. In brain imaging, having an overall neutral complex is a requirement for crossing the blood brain barrier. Lipophilic complexes have been commonly observed to clear through the hepatobiliary system with fatty tissue accumulation. Stereochemistry plays an important role, in terms of ligand receptor interaction, when targeting surface receptors.<sup>14</sup>

### 2.1.2 Coordination Chemistry of Indium and Gallium

Under physiological conditions, the oxidation state of the group 13 metals indium and gallium is +3, making it the only relevant oxidation state for radiopharmaceutical sciences. Complexation of ligands to In and Ga is carried out based on the hardness/softness of the acid/base.<sup>15</sup> While gallium, being slightly harder than indium, would chelate oxygen, nitrogen or sulfur atoms, indium would prefer neutral nitrogen or negatively charged sulfur atoms. Coordination spheres of gallium could include 3, 4, 5, or 6 ligands while indium coordination could include up to seven ligands due to its larger ionic radius. Octahedral complexes of both metals, however, have been reported to be thermodynamically and biologically more stable.<sup>14, 16-18</sup>

A major consideration in the chemistry of trivalent indium and gallium is their pH dependent hydrolysis. Free hydrated Ga(III) is only stable under acidic conditions with

the insoluble  $\text{Ga}(\text{OH})_3$  forming as the major product between pH 3 and 9.5. Reactions carried out in solutions with  $\text{pH} > 9.5$  result in the formation of soluble gallate ions  $[\text{Ga}(\text{OH})_4^-]$ . Similarly, free indium(III) is stable in slightly acidic pH solutions ( $\text{pH} = 4-5$ ) when it exists as a hexaqua ion, while it undergoes extensive hydrolysis below pH 3.4, and forms soluble hydroxides under basic conditions.<sup>19</sup> Considering that the rate of hydrolysis is much faster than that for metal-complexation, a careful selection of ligands and optimization of pH levels is a significant requirement. In general, indium(III) and gallium(III) complexes have been reported to exhibit high thermodynamic stability and biological inertness (no exchange with transferrin), especially in cases utilizing multidentate chelators.<sup>14, 18</sup>

### 2.1.3 Indium and Gallium Radioisotopes

The metals gallium and indium have several medically useful radioisotopes that can be used for diagnostic imaging, the most widely used of which are Ga-67 and In-111.<sup>20</sup> The later has been employed in tumor imaging ( $^{111}\text{In}$ -DTPA-octreotide),<sup>21</sup> tumor pre-targeting ( $^{111}\text{In}$ -DTPA-biotin),<sup>22</sup> folate receptors imaging ( $^{111}\text{In}$ -DTPA-folate),<sup>23</sup> somatostatin receptor imaging ( $^{111}\text{In}$ -DOTA-CCK-8),<sup>24</sup> thrombus ( $^{111}\text{In}$ -oxine),<sup>25</sup> and inflammation ( $^{111}\text{In}$ -white blood cells)<sup>26</sup> imaging.<sup>14</sup>

The use of Ga-68 for positron diagnostic imaging has also gained significant interest owing to its convenient half-life and its wide availability from radionuclide generators.<sup>27-31</sup> An example of gallium based imaging agents is  $^{68}\text{Ga}$ -Citrate which has been used in quantification of pulmonary vascular permeability.<sup>32</sup> The use of PET allows quantification that otherwise would not be possible with  $^{67}\text{Ga}$  and gamma scintigraphy.

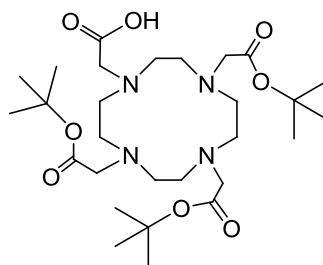
There have also been advances in development of radiotracers for myocardial (eg.  $^{68}\text{Ga}$ -[(4,6-MeOssal)<sub>2</sub>BAPEN]<sup>+</sup>),<sup>33</sup> brain (eg.  $^{68}\text{Ga}$ -THM<sub>2</sub>BED),<sup>34</sup> tumor (eg.  $^{68}\text{Ga}$ -octreotide),<sup>35</sup> and Thrombus (eg.  $^{68}\text{Ga}$ -platelets)<sup>36</sup> imaging.

As a result, this work employed both indium-111 and gallium-68 in the development of SPECT and PET oriented molecular imaging probes for beta cell imaging. Indium-111, produced by the  $^{112}\text{Cd}$  (p,2n) $^{111}\text{In}$  nuclear reaction,<sup>37</sup> was purchased, whereas gallium-68 was obtained from an in house Eckert and Ziegler  $^{68}\text{Ge}/^{68}\text{Ga}$  radionuclide generator coupled to a modular lab unit for automated synthesis.

#### 2.1.4 Radiometal-Chelator Selection

One class of chelators commonly used for the radiometal labeling of peptides are cyclen derivatives, such as DOTA,<sup>38-40</sup> which are inert and thermodynamically stable, making them good candidates for radiolabeling of peptides and antibodies.<sup>40, 41</sup> Examples of chelator-conjugated peptides include DOTA-labelled somatostatin analogues (eg. DOTA-NOC (1-Nal3-octreotide),<sup>42</sup> and RGD peptides.<sup>43</sup> A review by De León-Rodríguez and Kovacs was recently published on DOTA-peptide conjugates and their applications.<sup>40</sup> To date, DOTA has not been employed as a chelator for the radiolabeling of GLP-1. The conjugation of DOTA to a peptide using solid-phase chemistry, the most suitable synthetic approach for peptides, requires ligands that are compatible with the organic solvents commonly used in solid-phase peptide synthesis (SPPS). The commercially available tris-tBu-DOTA (Figure 2.2), satisfies these requirements and can be conjugated, via an unprotected carboxylic acid, to free amino groups using tetramethyluronium coupling agents such as HBTU (O-benzotriazole-N,N,N',N'-

tetramethyl-uronium-hexafluoro-phosphate) or HATU (2-(1H-7-azabenzotriazol-1-yl)-1,1,3,3-tetramethyl uronium hexafluorophosphate methanaminium). Both indium and gallium have been shown to form stable complexes with cyclen derivatives. Therefore tris-tBu-DOTA was selected for chelation of both metals.



**Figure 2.2** Structure of tris-tBu-DOTA.

### 2.1.5 Radiofluorination

Considering the rapid blood clearance of peptides, high signal to noise ratios can often be achieved in reasonably short time periods. As a result, short-lived PET isotopes are potential candidates for labeling of bioactive peptides. Fluorine-18, in particular, is an ideal candidate for such applications with a half-life of 110 minutes, which is also sufficient for tracer transport. This isotope can be produced in large quantities and exhibits a low positron energy (0.64 MeV), reducing radiation dose to patients while still providing high resolution images. Table 2.1 lists commonly used radiofluorinated peptide-based compounds in oncology.<sup>44-52</sup>



<b>Radiotracer</b>	<b>Application</b>
[[ <sup>18</sup> F]-Nle <sup>4</sup> , D-Phe <sup>7</sup> ]- $\alpha$ -MSH	$\alpha$ -MSH receptors (eg. melanomas)
[ <sup>18</sup> F]-NT(8-13)	NT receptors
[ <sup>18</sup> F]SAA-RGD	$\alpha_v\beta_3$ integrin expression
[ <sup>18</sup> F]Fluorobenzoyl-RGD	Integrin receptors
[ <sup>18</sup> F]C-peptide	Specific cell-membrane receptors
[ <sup>18</sup> F]-ET-1	Endothelin receptors
[ <sup>18</sup> F]FNleLFNleYK	Infection/inflammation

**Table 2.1** Examples of <sup>18</sup>F-labeled peptide-based imaging tracers.

Ideal conditions for radiofluorination procedures are given in Table 2.2. The initial step in all fluorination reactions involves the pre-activation of cyclotron-produced aqueous [<sup>18</sup>F]fluoride by evaporation from an added base (K<sub>2</sub>CO<sub>3</sub>/Kryptofix-222 and Bu<sub>4</sub>N<sup>+</sup>). Subsequent reactions are then carried out under strong basic conditions, which are not suitable for compounds containing amine/thiol reactive groups or complex bioactive molecules. Although, fluorine-18 labeling procedures for peptides are often time-consuming and laborious, efficient radiolabeling reactions have been reported using the prosthetic group approach.<sup>44</sup> This is especially significant considering that the direct fluorination of biomolecules is not possible, leading to denaturing and decomposition of labile substrates.<sup>53</sup> Prosthetic groups can be conjugated by various means such as acylation (eg. methyl 2-[<sup>18</sup>F]fluoropropionate),<sup>54</sup> amidation (eg. 1-[4-(<sup>18</sup>F)Fluoromethyl]benzoyl]-aminobutane-4-amine),<sup>55</sup> imidation (eg. 3-[<sup>18</sup>F]Fluoro-5-nitrobenzimidate),<sup>56</sup> alkylation (eg. *N*-(*p*-[<sup>18</sup>F]Fluorophenyl)maleimides),<sup>57</sup> and photochemical conjugation (4-Azidophenacyl-[<sup>18</sup>F]fluoride).<sup>58</sup> Among all prosthetic groups reported to date, use of *N*-succinimidyl 4-[<sup>18</sup>F]fluorobenzoate ([<sup>18</sup>F]SFB) appears to be the most suitable approach in radiofluorination of biomolecules as it has been

reported to result in higher yields and biologically more stable products.<sup>58</sup> As a result, the prosthetic group methodology with [<sup>18</sup>F]SFB was employed in this work for the development of GLP-1 based, Fluorine-18 PET tracers.<sup>44</sup>

Simple, quick and efficient procedure
Few preparation steps
No influence of the labeling agent on the biological activity of the targeting entity
Mild reaction conditions (eg. pH, temperature) to prevent decomposition
Simple radiosynthesis of the prosthetic group
Sufficient chemical reactivity of the prosthetic group
Formation of desired products at tracer concentrations
Minimal side-reactions
Few purification steps
High specific activity product

**Table 2.2** Basic requirements of ideal radiofluorination procedures.<sup>44</sup>

This work utilized both radiometal and radiofluorinated derivatives of GLP-1 in order to develop probes with enhanced structural stability and optimal binding affinity for beta cell imaging. Furthermore, various GLP-1 derivatives were prepared in order to determine the best substitution site for the prosthetic group or chelator to maintain optimal binding affinity for GLP-1 receptors.

## 2.2. Experimental Procedures

Common solvents and reagents were purchased from VWR, Fisher Scientific, or Sigma-Aldrich and used as received, unless stated otherwise. Sterile, deionized water was used in all aqueous procedures. All Fmoc protected amino acids, except Fmoc-Lys(mtt)-OH (Nova Biochem), and HBTU were obtained from Peptides International. Fmoc-Rink amide MBHA resin (4-(2',4'-Dimethoxyphenyl)-(9-Fluorenylmethoxycarbonyl)-aminomethyl)-phenoxy-acetamido-norleucyl-4-Methyl Benzhydrylamine resin), and

Boc-His(Boc)-OH-DCHA (dicyclohexylamine) were obtained from Nova Biochem. The hydrophilic linker 2-[2-(2-aminoethoxy)ethoxy]acetic acid (AEEA) was synthesized in our laboratory.<sup>59</sup> DOTA-tris(tBu)-ester was obtained from CheMatech. Indium trichloride tetrahydrate (99.99%) was obtained from Strem Chemicals. Indium-111 and [<sup>125</sup>I]-exendin were obtained from MDS Nordion and PerkinElmer Inc. respectively. [<sup>18</sup>F]Fluoride was obtained from Hamilton Health Sciences. RP-C18 Sep-Pak SPE cartridges were obtained from Waters. CHO/GLP-1R and INS-1 832/13 cells were provided by Dr. Michael Wheeler from University of Toronto and Dr. Christopher Newgard from Duke University respectively. Gallium-68 generator and all automated synthesis modules were purchased from Eckert and Ziegler.

### 2.2.1 Peptide Syntheses

Fmoc-based solid-phase peptide synthesis was carried out using an APEX 396 autosynthesizer (AAPPTec) with 0.05 meq of 0.27 mmol/g Fmoc-Rink amide mBHA resin and a 3-fold excess of the protected amino acids. Fmoc removal, carried out with 20% piperidine in DMF (*N,N*-dimethylformamide) over two cycles (10 and 20 min), was followed by amino acid activation with 3 eq HBTU and 6 eq DIPEA (*N,N*-diisopropylethylamine) (10 min) and subsequent coupling over 30 and 120 min cycles.

Methyl trityl deprotection was carried out in a glass peptide reaction vessel using 5% triisopropylsilane (v/v) + 2% trifluoroacetic acid (v/v) in CH<sub>2</sub>Cl<sub>2</sub> over 3 min and repeated 10 times. Coupling of DOTA/AEEA to this site, or the coupling of DOTA to AEEA, followed the same methodology used in amino acid coupling, however the coupling times were increased to 18 and 24 hours for AEEA and DOTA respectively. In

preparation of fluorescent GLP-1 analogues, conjugation of FITC to Mtt-protected 37Lys was carried out using a 4 fold excess of FITC and DIPEA in DMF. This conjugation reaction was monitored using Kaiser tests and was completed in 23 hours. Microcleaved samples were also used to monitor reaction progress and peptide purity via HPLC.

Full deprotection of synthesized peptides was accomplished using a solution of 88% TFA (v/v) + 5% H<sub>2</sub>O (v/v) + 5% phenol (m/v) + 2% triisopropylsilane (v/v) over 6 hours. The cleaved peptides were then precipitated using *tert*-butyl methyl ether (TBME) and centrifuged (2200 rpm for 15 min). After removing the resulting supernatant, the peptide pellet was rinsed with TBME, vortexed and centrifuged again (2200 rpm for 15 min). The supernatant was removed, then the peptide pellet was dissolved in water, frozen at 78 °C and lyophilized.

### 2.2.2 Purification by RP-HPLC / ESI-MS

Peptides were analyzed using a reverse-phase analytical HPLC column (Grace Vydac Protein/Peptide RP-C18 column 4.6 x 250 mm, 5 μm). This system was equipped with a Waters 600 controller, Waters Prep degasser, and Waters MassLynx software (version 4.1). Employed mobile phases were 0.1% CF<sub>3</sub>CO<sub>2</sub>H in water (eluent A) and 0.1% CF<sub>3</sub>CO<sub>2</sub>H in CH<sub>3</sub>CN (eluent B). The linear gradient used was 30-50% of B with a flow rate of 1.5 mL min<sup>-1</sup> over 20 min. The column eluate was monitored using a Waters 2998 Photodiode array detector set at 220 and 254 nm.

Peptides were purified using a reverse-phase preparative HPLC column (Grace Vydac Protein/Peptide RP-C18 column 22.0 x 250 mm, 10 μm) on the same system

mentioned above. The detection method along with eluents and gradients were the same as those stated above, with the exception of the flow rate being set at 20 mL min<sup>-1</sup>. The collected fraction was then lyophilized to a solid and subsequently analyzed by ESI-MS (electrospray ionization mass spectrometry) (Waters Micromass Quattro Micro<sup>TM</sup> API). Purity of final products was determined by analytical RP-HPLC (reverse-phase high performance liquid chromatography).

### 2.2.3 <sup>113/115</sup>In Labeling

In a typical reaction, 5 mg of the GLP-1 analogue, 3 mL of pH 5 NaOAc / HOAc buffer, and 7 mg of InCl<sub>3</sub>·4H<sub>2</sub>O (0.02 mmol) were placed in a 25 mL glass round bottom flask. The reactants were dissolved by sonication at 25 °C. The reaction was then carried out at 70 °C for 30 min. The resulting reaction mixture was allowed to cool before purification by a light C18 RP sep-pak<sup>®</sup> (conditioned with 3 mL of ethanol and 10 mL of H<sub>2</sub>O). After passing the reaction mixture through the sep-pak<sup>®</sup>, 10 mL of water was used as eluent in order to wash out residual unreacted InCl<sub>3</sub>·4H<sub>2</sub>O. A 10 mL aliquot of 0.1% TFA in CH<sub>3</sub>CN was used to wash out the labeled product. The resulting solution was then mixed with 10 mL of H<sub>2</sub>O (to lower the % component of acetonitrile), frozen at -78 °C and subsequently lyophilized.

#### 2.2.4 <sup>111</sup>In Radiolabeling

To a clean conical glass vial was added 20  $\mu$ L of the prepared GLP-1 analogue (1 mg/ mL of pH 5 NaOAc / HOAc buffer). This aliquot was dissolved in 200  $\mu$ L of the buffer (10 fold dilution to obtain  $\mu$ M concentrations), to which 5.63 mCi of <sup>111</sup>InCl<sub>3</sub> was added. The reaction mixture was then heated at 70 °C for 30 minutes, before purification by a RP-C18 SPE Sep-Pak cartridge (conditioned with 5 mL of ethanol and 15 mL of water). After passing the reaction mixture through the sep-pak<sup>®</sup>, 10 mL of water was used as eluent in order to wash out residual unreacted InCl<sub>3</sub>. A 5 mL aliquot of EtOH was used to wash out the radiolabeled product. The Sep-Pak eluate was evaporated on a rotary evaporator prior to *in vitro* studies. The reaction progress and product purity was analyzed using analytical RP-HPLC (Waters Symmetry, 4.6 x 150 mm, 5 Å, C-18 column) coupled to a gamma detector. This system employed a Waters 1525 Binary HPLC pump, Waters 2487 dual  $\lambda$  absorbance detector, Waters In-Line degasser and Breeze software (version 3.30).

#### 2.2.5 <sup>69/71</sup>Ga Labeling

In a typical reaction, 10 mg of GLP-1 analogue was dissolved in pH 4 NaOAc / HOAc buffer. Chelation was carried out using a two-fold excess of anhydrous GaCl<sub>3</sub> at 75 °C over 30 minutes. Resulting mixture was cooled prior to purification by a plus C18 RP sep-pak<sup>®</sup> (conditioned with 6 mL of ethanol and 25 mL of water). After passing the reaction mixture through the sep-pak<sup>®</sup>, 10 mL of water was used as eluent in order to wash out residual unreacted GaCl<sub>3</sub>. A 6 mL aliquot of EtOH was used to wash out the

labeled product. The resulting solution was then dried on a rotary evaporator, mixed with 10 mL of H<sub>2</sub>O, frozen at -78 °C and subsequently lyophilized overnight.

### 2.2.6 <sup>68</sup>Ga Radiolabeling

To a clean glass microwave vessel was added 100 μL of GLP-1 analogue solution (1 mg/mL in pH 3.5 HEPES buffer). This aliquot was dissolved in 900 μL of the buffer (10 fold dilution to obtain final solution with μM concentrations), to which 3 mCi <sup>68</sup>GaCl<sub>3</sub> was added, freshly eluted from the Ge-68/Ga-68 generator using 3 mL of 0.1 M HCl. Purification and isolation of <sup>68</sup>Ga was achieved using a Phenomenix Strata-X-C 33u polymeric strong cation exchange column (30 mg/mL) with 0.05 N HCl in Acetone as the eluent. The reaction mixture was then heated in the reactor of the automated synthesis module at 80 °C for 30 minutes, prior to sep-pak<sup>®</sup> purification using a light RP-tC18 SPE Sep-Pak cartridge<sup>®</sup> (conditioned with 3 mL of ethanol and 10 mL of water). After passing the reaction mixture through the sep-pak<sup>®</sup>, 3 mL of water was used as eluent in order to wash out residual unreacted <sup>68</sup>Ga materials. A 2 mL aliquot of EtOH was used to wash out the radiolabeled product. After evaporation of the solvent on a V-10 1.6 Biotage<sup>®</sup> vortex and vacuum evaporation system. The reaction progress and product purity was analyzed using analytical RP-HPLC (Sunfire<sup>™</sup> RP-C18 column 4.6 x 150 mm, 5 μm) coupled to a gamma detector, prior to further use in animal studies. HPLC system employed a Waters 1525 Binary HPLC pump, Waters 2487 dual λ absorbance detector, Waters In-Line degasser and Breeze software (version 3.30).

### 2.2.7 Synthesis of Modified GLP-1 analogue (9)

GLP-1 derivatives were prepared using Fmoc solid phase methodology as previously mentioned. Glycine 37 was replaced with Fmoc-Lys(Alloc)-OH, while Fmoc-Lys(Mtt)-OH residues used in positions 26 and 34 were acylated. In a typical experiment, 0.05 meq of peptide-loaded resin was swollen in DMF. Methyl trityl deprotection of Lys 26 and 34 side chains was carried out in a glass peptide reaction vessel using 5% triisopropylsilane (v/v) + 2% trifluoroacetic acid (v/v) in CH<sub>2</sub>Cl<sub>2</sub> over 3 min (repeated x10 ). The resin was washed thoroughly with DMF and DCM respectively. A 7 mL solution of 10% acetic acid anhydride in DMF was then added to the resin followed by shaking over 15 min (repeated x5). Completion of acylation reaction (ie. presence of free amines) was monitored by Kaiser tests. DOTA coupling then proceeded as stated previously.

### 2.2.8 Synthesis of [<sup>19</sup>F]FB-GLP-1

Synthesis of [<sup>19</sup>F]Fluorobenzoic acid (4-FB) was carried out using a solid-phase methodology. In a typical synthesis, 0.05 meq of fully protected GLP-1 analogue on rink amide resin was swollen in DMF over 10 min. Methyl trityl deprotection at position 37 was carried out in a glass peptide reaction vessel using 5% triisopropylsilane (v/v) + 2% trifluoroacetic acid (v/v) in CH<sub>2</sub>Cl<sub>2</sub> over 3 min (repeated 10 times). In certain instances Lys(alloc)-OH was employed in position 37. Alloc deprotection was carried out by initial treatment of the resin with 20 eq of PhSiH<sub>3</sub> in DCM for 3 min. This was followed by addition of 0.25 eq of Pd(PPh<sub>3</sub>)<sub>4</sub> in DCM and mixing over 30 min. This process was repeated twice prior to prosthetic group conjugation.



Coupling of 4-FB to this site was carried out using 4 eq of 4-FB and HATU and 6 eq of DIPEA in 5 mL of DMF over 4 hours. Microcleaved samples were used to monitor reaction progress and peptide purity via HPLC. Full deprotection was accomplished using a solution of 88% TFA (v/v) + 5% H<sub>2</sub>O (v/v) + 5% phenol (m/v) + 2% triisopropylsilane (v/v) over 6 hours. The cleaved peptides were then precipitated using TBME and centrifuged (2200 rpm for 20 min). After removing the resulting supernatant, the peptide pellet was rinsed with TBME, vortexed and centrifuged again (2200 rpm for 20 min). The supernatant was removed, peptide pellet dissolved in water, frozen at -78 °C and lyophilized overnight. Purification of the peptide was carried out using a reverse-phase preparative HPLC column (Grace Vydac Protein/Peptide RP-C18 column 22.0 x 250 mm, 10 μm).

### **2.2.9 Synthesis of *t*-butyl-*N,N,N*-trimethylammoniumbenzoate triflate**

In a typical reaction, 700 mg of 4-dimethylaminebenzoic acid was added to 50 mL of THF and cooled to 0 °C for 15 min. This was followed by drop wise addition of 1.3 mL of trifluoroacetic anhydride and stirring for 35 minutes. After addition of 8 mL of *t*-BuOH in one portion, the mixture was warmed up to room temperature and stirred over 2 hours. This mixture was then poured into 250 mL of saturated NaHCO<sub>3</sub> and extracted (3x) with dichloromethane. Organic layers were combined, evaporated using a rotary evaporator, dried with MgSO<sub>4</sub> and passes through a silica gel plug. The product was subsequently eluted using 60 mL of DCM, and evaporated to give a yellow oil. This oil was redissolved in nitromethane and cooled to -30 °C for 20 min. A 500 μL aliquot of methyl triflate was then added drop wise to the reaction mixture, which was warmed up

to 0 °C and stirred over 1 hour. The reaction mixture was poured into 200 mL of diethyl ether causing the precipitation of the desired product as a white powder, which was isolated by suction filtration and washed with cold diethyl ether. The dried product was analyzed using  $^1\text{H}$  NMR and was shown to not require further purification. Typically 1 g of product was obtained indicating a 68% yield.

#### 2.2.10 Synthesis of 4- $^{18}\text{F}$ FB and 4- $^{18}\text{F}$ SFB

Prior to the start of reaction, the obtained  $^{18}\text{F}$ Fluoride sample was dried via azeotropic evaporation with anhydrous acetonitrile. A typical reaction involved the addition of 5 mg (13 mmol) of the triflate salt to 1 mL of anhydrous  $\text{CH}_3\text{CN}$  containing 80 mCi of  $^{18}\text{F}$ Fluoride. The mixture was heated at 90 °C over 10 min. A 500  $\mu\text{L}$  aliquot of 1 M HCl was added and the reaction mixture heated at 100 °C for 5 min. After cooling, the mixture was diluted with 12 mL of deionized water and passed through a RP-C18 light Chromafix cartridge. The product was eluted with 7 mL of acetonitrile, followed by addition of 500  $\mu\text{L}$  of 45%  $\text{Me}_4\text{NOH}$ . The solvent mixture was evaporated at 100 °C under a nitrogen stream and product was assayed and analyzed using an analytical RP-HPLC (Waters Symmetry, 4.6 x 150 mm, 5 Å, C-18 column) coupled to a gamma detector. Decay-corrected radiochemical yields were  $35\pm 5\%$  with radiochemical purities  $> 98\%$ .

The synthesis of Succinimydyl 4- $^{18}\text{F}$ Fluorobenzoic acid involved the activation of  $^{18}\text{F}$ FB with 15 mg of TSTU in 500  $\mu\text{L}$  of anhydrous acetonitrile at 90 °C over 4 min. After cooling and addition of 10 mL of 5% aqueous acetic acid, the reaction mixture was passed through a RP-C18 Chromafix cartridge. Unreacted materials were washed out of

the cartridge using 2 mL of a 65:35 water:acetonitrile solution. The product was eluted with 3 mL of acetonitrile, dried using a rotator evaporator, assayed and analyzed using an analytical RP-HPLC (Waters Symmetry, 4.6 x 150 mm, 5 Å, C-18 column) coupled to a gamma detector. Activation by HATU was carried out using the same methodology.

#### **2.2.11 Solid-phase Synthesis of 37-Lys-[<sup>18</sup>F]FB-GLP-1(7-37)**

Coupling of [<sup>18</sup>F]FB was carried out on resin using Mtt-deprotected GLP-1 derivative, with HATU in DMF at 50 °C over 15 min. Resin batch was then drained, washed with DCM, and assayed. Complete deprotection and cleavage from the resin was then achieved using 90% TFA and scavengers at 50 °C over 20 min. The resulting cocktail was then evaporated on a rotary evaporator, counted and analyzed by analytical HPLC as mentioned above. In the case of [<sup>18</sup>F]SFB, the reaction was carried out (on resin), in 500 µL of DMF at 50 °C over 15 min. Deprotection, cleavage from resin and subsequent analysis steps were carried out as mentioned above.

#### **2.2.12 Binding Assays**

All GLP-1 receptor binding studies were conducted using Chinese hamster ovary cells stably transfected with the human GLP-1 receptor (CHO/GLP-1R), generously donated by Dr. Michael Wheeler (University of Toronto). Receptor binding was measured by the displacement of [<sup>125</sup>I]-exendin-4 with increasing concentrations of the synthesized <sup>113/115</sup>Indium or <sup>69/71</sup>Ga-labeled GLP-1 analogues, using a previously published method.<sup>60</sup> Briefly, CHO/GLP-1R cells were cultured in Dulbecco's Modified

Eagle's Medium (DMEM, Invitrogen) containing 10% fetal bovine serum (Invitrogen). On the day of the experiment, cells were rinsed 2X with warm Hank's buffered saline solution (HBSS) and dissociated in HBSS containing 2 mM EDTA. Approximately one million cells were incubated for 60 min at 37 °C in binding buffer (DMEM containing 0.1% Trasylol (Bayer) and 0.1% bovine serum albumin (Sigma), pH 7.4), 0.77  $\mu\text{mol}$  [ $^{125}\text{I}$ ]exendin-4 (Amersham) and variable concentrations of each GLP-1 analogue ( $10^{-5}$  to  $10^{-11}$  M). After incubation, cells were centrifuged at 2800 rpm for 15 min. After removal of the supernatants, the cell pellets were washed with 200  $\mu\text{L}$  of cold binding buffer and re-centrifuged before the final pellet was counted in a gamma counter. Binding curves and  $\text{IC}_{50}$  (half maximal inhibitory concentration) values were generated using MS Excel, Sigma Plot, and Origin Lab 8.

### **2.2.13 cAMP Studies**

Activation of the GLP-1 receptor by the peptide analogues was assessed by stimulation of cAMP using a previously published method.<sup>60</sup> Briefly, CHO/GLP1R cells were plated at a density of  $1 \times 10^5$  cells/well in a 24-well plate 48 hours prior to the day of the experiment. Cells were incubated for 30 min at 37 °C in DMEM containing 1  $\mu\text{M}$  3-isobutyl-1-methylxanthine (IBMX; Sigma) and 10 nM of the peptide analogues. Media were removed, cells were rinsed twice with cold HBSS and scraped in 200  $\mu\text{L}$  of 80% ethanol. cAMP levels were measured using a cAMP radioimmunoassay kit (Perkin Elmer, Shelton CT) as per the manufacturer's instructions. Differences between basal and stimulated cAMP levels were analysed using a one-way ANOVA followed by Student's

t-test, and differences in fold stimulation were determined using a one-way ANOVA followed by Tukey's post-hoc test. Significance was set at  $p < 0.05$  for all analyses.

#### **2.2.14 *In Vitro* Imaging**

INS-1 832/13 cells were plated in 6-well plates at a density of one million cells per well. Two wells did not receive any radiolabeled peptide; two wells were incubated with 50  $\mu\text{Ci}$  [ $^{111}\text{In}$ ]-8 for 30 min at 37 °C; and two wells were incubated with 50  $\mu\text{Ci}$  [ $^{111}\text{In}$ ]-8 and 1  $\mu\text{M}$  cold exendin-4. After the incubation period, media were removed, cells were rinsed twice with cold HBSS and covered with 500  $\mu\text{L}$  culture media. Cells were imaged for 30 min with a GE Millenium II gamma camera using a medium-energy general purpose collimator. Images were acquired and analyzed using GE Xeleris software.

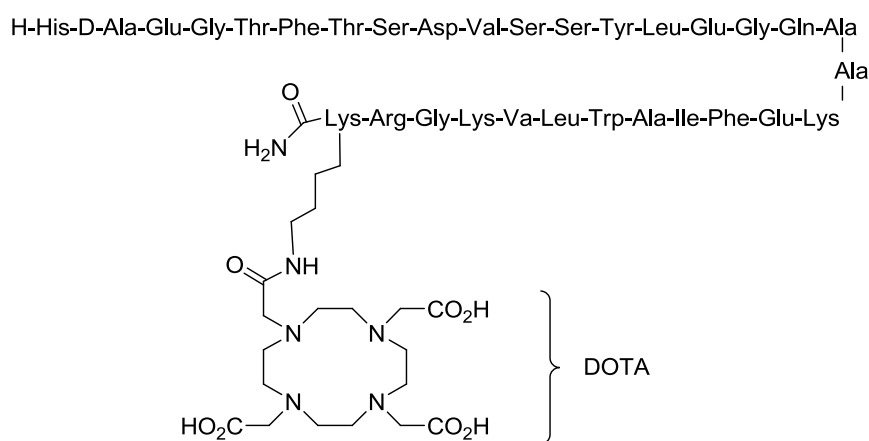
#### **2.2.15 *In Vivo* Imaging**

*In vivo* imaging studies were conducted in C57BL/6 mice following tail vein injection of 0.3-3.5 MBq of  $^{111}\text{In}$ - or  $^{68}\text{Ga}$ -7. Mice were euthanized 3 min or 4 hours post injection. The pancreata and other organs were then removed and assayed. Biodistribution was calculated as % injected dose/g.

## 2.3 Results and Discussion

### 2.3.1 Design of GLP-1 Analogues

The objective of this study was to develop novel GLP-1 analogues exhibiting optimal binding affinity for GLP-1 receptors thus allowing for the imaging of pancreatic islets. The primary difficulty in attaching DOTA to GLP-1 is interference with peptide-receptor binding caused by the addition of a metal-complex to the peptide structure. Therefore, an integral part of this research project was the determination of optimal attachment sites for the metal chelator in order to circumvent negative impacts on the binding affinity of the peptide. Figure 2.3 illustrates one of the peptide derivatives before labeling. Improvement in structural stability of the developed GLP-1 analogues was achieved by substitution of L-Ala at position 8 with D-Ala, which is a modification previously reported to increase the resistance of this peptide to degradation by DPP-IV.<sup>9</sup> Other substitutions at this position, namely <sup>8</sup>Aib, <sup>8</sup>Gly, <sup>8</sup>Ser, and <sup>8</sup>Thr, have also been reported to increase the structural stability of GLP-1; however, the latter three substitutions have a negative impact on the binding affinity and potency of the peptide as an endocrine hormone.<sup>61</sup>



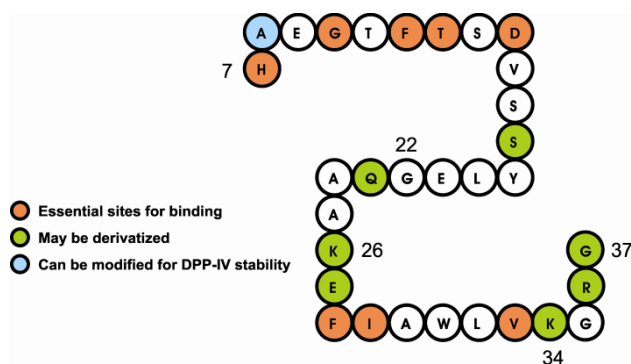
**Figure 2.3** Structure of <sup>37</sup>Lys-DOTA-GLP-1.

A report by Lee and coworkers showed that covalent coupling of PEG (polyethylene glycol) to specific sites on GLP-1 may improve the overall therapeutic effect of the peptide while maintaining its biological activity.<sup>62</sup> For instance, PEGylated GLP-1 conjugates, PEG<sub>2K</sub>-N<sup>ter</sup>-GLP-1 and PEG<sub>2K</sub>-<sup>26/34</sup>Lys-GLP-1, were prepared and analyzed *in vitro*. The latter was a mixture of derivatized peptide at positions 26 and 34 which could not be separated. The pharmacokinetic profile of each peptide was studied *in vivo*, with the finding that while PEGylation at <sup>34</sup>Lys did not increase the biological half-life of the peptide, it did increase its potency *in vivo*.<sup>62</sup> Another report by Madsen and coworkers explored the structure-activity relationship of Liraglutide analogues, coupled to fatty acids, with respect to potency on cloned human GLP-1 receptors. The authors noted that in most cases, long and bulky fatty acids decreased the potency of the peptide.<sup>59</sup> Knudsen et al. reported that GLP-1 can be derivatized at the C-terminal part of the peptide, with both short/long fatty acids and amino-acid derived spacers, and still maintain its potency.<sup>63</sup>

In order to reduce any steric effects imposed by the macrocyclic DOTA ring on the binding site of the peptide derivatives, a short polyethyleneglycol chain, 2-[2-(2-aminoethyl)ethoxy]acetic acid (AEEA), was employed as a spacer to separate the metal-chelator complex from the main peptide chain. Considering that this spacer was to be used at varying sites on the peptide chain, a short PEG-length was selected in order to minimize negative impacts on the binding affinity of the peptide.<sup>63</sup> The AEEA spacer was synthesized according to a published procedure.<sup>64</sup>

There have been a number of reports identifying the key residues within the sequence of GLP-1(7-37) that are critical for optimal binding and proper biological

functionality. Deletion of the N-terminal 8 amino acids, or substitution of residues within the N-terminal 10 amino acids, resulted in a dramatic reduction in receptor affinity<sup>8, 60</sup>. Alanine scanning experiments have shown that amino acids in positions 7, 10, 12, 13 and 15 were directly involved in receptor binding and activation, whereas those in positions 28 and 29 maintained the secondary structure of the peptide necessary for receptor recognition.<sup>65</sup> These studies therefore highlight the importance of the N-terminal region of GLP-1 in binding to and activating its receptor. Leger and coworkers synthesized a number of GLP-1 HSA (human serum albumin) analogues and subsequently tested the stabilizing effect of bioconjugation in the presence of DPP-IV, as well as receptor binding and activation.<sup>66</sup> From this study, they concluded that the C-terminus is the best point of modification both in terms of stability, especially with D-Ala at position 8, and biological activity.<sup>66</sup> Figure 2.4 summarizes the results that have been reported on structure-activity relationships of GLP-1.<sup>67</sup>



**Figure 2.4** A schematic of the structure activity relationship of GLP-1.

According to the reported Ala scans, structural modification at positions 14, 16-18, 20, 22, 27 and 30-35 may be possible without having a major impact on the binding

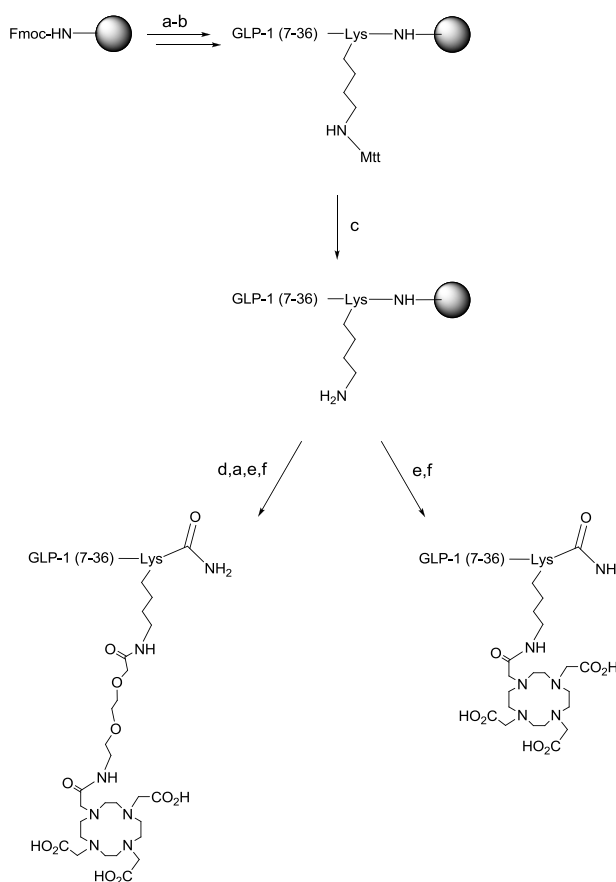


affinity of the peptide. The HSA study showed that the only site suitable for side group modification with bulky ligands is position 37 (C-terminus).<sup>66</sup> However, a report on GLP-1 PEGylation,<sup>62</sup> indicated that positions 26 and 34 could also be functionalized with bulky ligands without a major impact on binding affinity of the peptide. Therefore, based on the structure-activity relationships reported to date along with the reported modifications discussed above, we selected positions 22, 26, 34 and 37 as sites for the attachment of DOTA to GLP-1. To the best of our knowledge, substitution of large ligands at position 22 has not been previously reported. The modification of the peptide at positions 22 and 37 required substitution of Gly (originally at this site), with Lys, whereas those at positions 26 and 34 already contained a Lys residue.

### 2.3.2 Synthesis of Indium-GLP-1 Analogues

GLP-1 analogues were synthesized using standard Fmoc-SPPS methods with an automated multi-well synthesizer. A representative synthetic route is described in Scheme 2.1, illustrating the preparation of <sup>37</sup>Lys-DOTA-GLP-1(7-37) and the related analogue containing a spacer between the peptide and the DOTA, <sup>37</sup>Lys-AEEA-DOTA-GLP-1(7-36). N-Fmoc removal was achieved using 20% v/v piperidine in DMF with the Kaiser test being used to identify the presence of free primary amino groups, hence determining the proper duration for Fmoc deprotection. Amino acids with reactive side chains were protected with acid labile orthogonal protecting groups such as OtBu, tBu, Trt and Pbf. The site of DOTA attachment, the  $\epsilon$ -amine of a lysine side chain positioned at amino acid 22, 26, 34, or 37, was protected with the temporary protecting group 4-methyltrityl (Mtt), which was later removed using a solution of 2% TFA in DCM

(dichloromethane) with triisopropylsilane as a scavenger. Other lysine residues in the peptide main chain were protected with Boc groups, which are much less acid labile. Small samples of the peptide in preparation were taken at varying intervals and, after full deprotection, were subsequently analyzed using ESI-MS and RP HPLC. Typical yields obtained for the purified GLP-1 analogues were 10-15%. The purity of the peptides along



**Scheme 2.1** Employed synthetic pathway for the preparation of <sup>37</sup>Lys-DOTA-GLP-1 and <sup>37</sup>Lys-AEEA-DOTA-GLP-1(7-37): (a) 20% pip/DMF; (b) Fmoc Amino Acid, HBTU, DIPEA; (c) 2% TFA, triisopropylsilane; (d) Fmoc-AEEA-OH, HBTU, DIPEA; (e) DOTA(tBu)<sub>3</sub>, HBTU, DIPEA; (f) 88% TFA + scavengers.

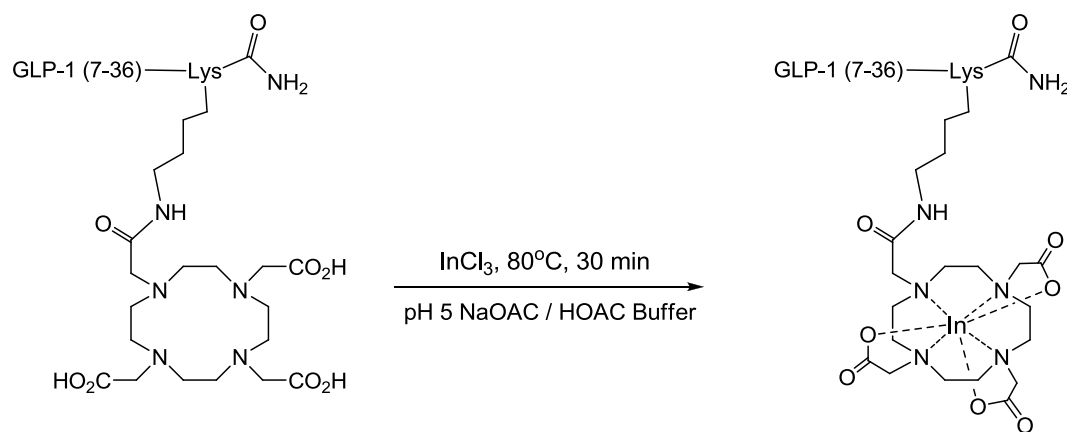
with their respective ESI-MS characterization are given in Table 2.3. While purification of most products resulted in purities in excess of 90%, due to the difficult nature of preparing these lengthy sequences and the very similar HPLC retention times of peptide byproducts formed during syntheses, compound **5** was obtained with only an 85% purity.

Initial labeling experiments were carried out using naturally occurring indium-113/115 (Scheme 2.2), in order to obtain  $IC_{50}$  values, synthesize HPLC standards, and determine radiolabeling conditions while preventing unnecessary exposure to radiation. High temperatures are required for this reaction in order to speed up the formation of the product. In addition, a sodium acetate buffer was employed in order to maintain the pH at the desired level, thus preventing the formation of insoluble indium oxides.<sup>68</sup> Products were purified using preparative HPLC and subsequently characterized using ESI-MS, which in all instances indicated complete labeling of peptides. Final compounds were analyzed by RP-HPLC for purity determination prior to biological evaluation.

In total, eight novel GLP-1 analogues containing indium were prepared, with four positional variations (22, 26, 34, 37), each position being prepared with and without the AEEA spacer. Figure 2.5 illustrates examples of UV and MS spectra obtained for compound **7**.

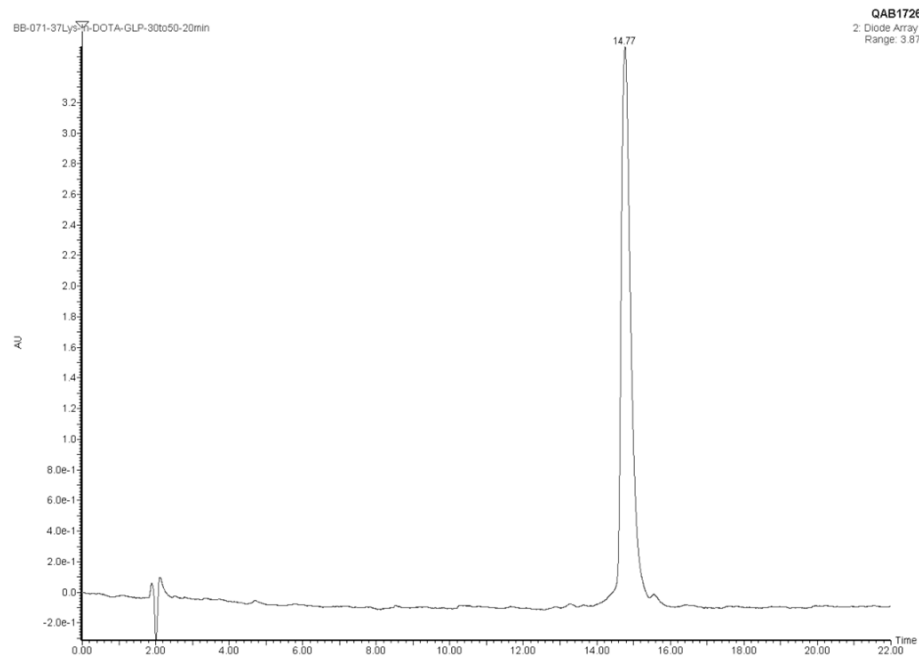
#	Peptide	Purity (%)	Calculated (m/z)	Observed (m/z)
1	$^{22}\text{Lys-In-DOTA-GLP-1(7-36)}$	90.0	1290.2 $[\text{M}+3\text{H}]^{3+}$	1290.3 $[\text{M}+3\text{H}]^{3+}$
2	$^{22}\text{Lys-AEEA-In-DOTA-GLP-1(7-36)}$	98.0	1339.4 $[\text{M}+3\text{H}]^{3+}$	1340.3 $[\text{M}+3\text{H}]^{3+}$
3	$^{26}\text{Lys-In-DOTA-GLP-1(7-36)}$	95.0	1266.6 $[\text{M}+3\text{H}]^{3+}$	1265.8 $[\text{M}+3\text{H}]^{3+}$
4	$^{26}\text{Lys-AEEA-In-DOTA-GLP-1(7-36)}$	90.0	1314.9 $[\text{M}+3\text{H}]^{3+}$	1314.6 $[\text{M}+3\text{H}]^{3+}$
5	$^{34}\text{Lys-In-DOTA-GLP-1(7-36)}$	85.3	1266.6 $[\text{M}+3\text{H}]^{3+}$	1266.3 $[\text{M}+3\text{H}]^{3+}$
6	$^{34}\text{Lys-AEEA-In-DOTA-GLP-1(7-36)}$	97.0	1314.9 $[\text{M}+3\text{H}]^{3+}$	1314.6 $[\text{M}+3\text{H}]^{3+}$
7	$^{37}\text{Lys-In-DOTA-GLP-1(7-37)}$	98.0	1309.3 $[\text{M}+3\text{H}]^{3+}$	1309.5 $[\text{M}+3\text{H}]^{3+}$
8	$^{37}\text{Lys-AEEA-In-DOTA-GLP-1(7-37)}$	95.3	1357.6 $[\text{M}+3\text{H}]^{3+}$	1357.4 $[\text{M}+3\text{H}]^{3+}$

**Table 2.3** Analysis of synthesized In-GLP-1 analogues by ESI-MS and RP HPLC.

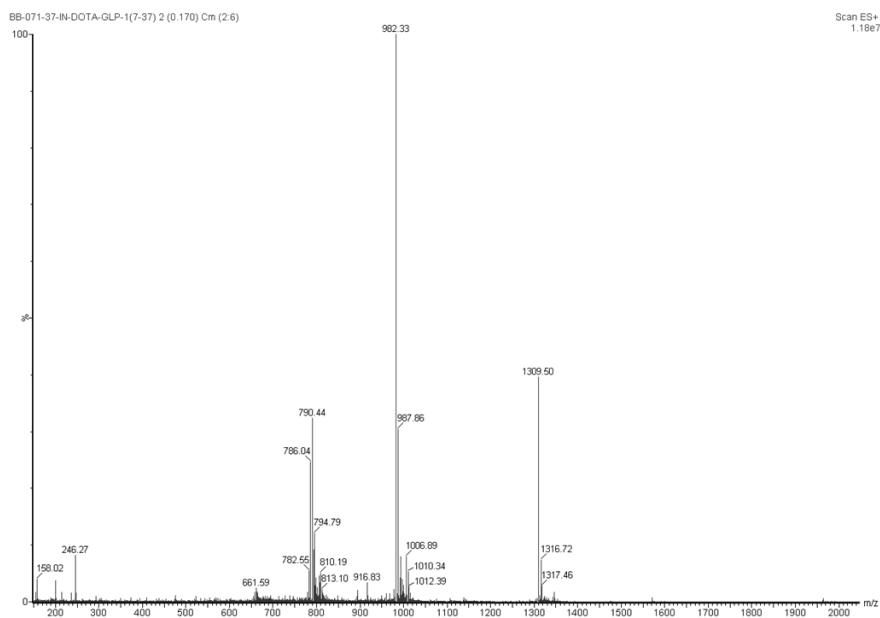


**Scheme 2.2** Indium labeling of DOTA-GLP-1 derivatives.

(a)



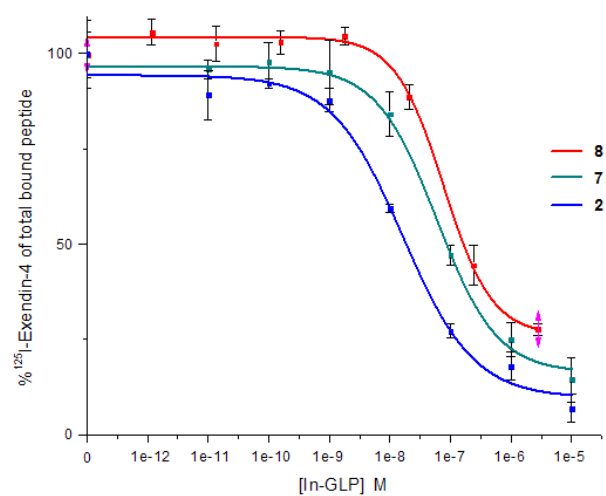
(b)



**Figure 2.5** (a) UV and (b) MS spectra obtained for compound **7** post purification.

### 2.3.3 *In Vitro* Studies

The purified GLP-1 analogues, labeled with Indium-113/115, were evaluated using receptor binding assays where the displacement of [ $^{125}$ I]exendin-4 by the indium coordinated peptide, on CHO/GLP-1R cells, was used as a measure of the respective  $IC_{50}$  value. Figure 2.6 shows typical plots obtained from competitive displacement studies, in this instance for compounds **2**, **7** and **8**. Table 2.4 shows the obtained  $IC_{50}$  values of all eight peptides.



**Figure 2.6** Competitive Displacement of compounds **2**, **7** and **8** vs. [ $^{125}$ I]-exendin-4 on CHO/GLP-1R cells.

Compd	IC <sub>50</sub> (nM)	cAMP (pmol/well)
<b>GLP-1 (7-37)</b>	5 ± 3	-
<b>1</b>	598 ± 45	-
<b>2</b>	93 ± 7	118 ± 22
<b>3</b>	970 ± 73	-
<b>4</b>	2660 ± 129	-
<b>5</b>	268 ± 16	-
<b>6</b>	573 ± 39	-
<b>7</b>	63 ± 4	74 ± 10
<b>8</b>	89 ± 3	159 ± 6

**Table 2.4** Receptor binding and cAMP measurements for GLP-1 peptide analogues. The first column shows the IC<sub>50</sub> values obtained from in vitro competitive displacement studies. Peptides **2**, **7** and **8** were selected for cAMP studies. Values for cAMP were calculated as the maximal response to 10 nM peptide.

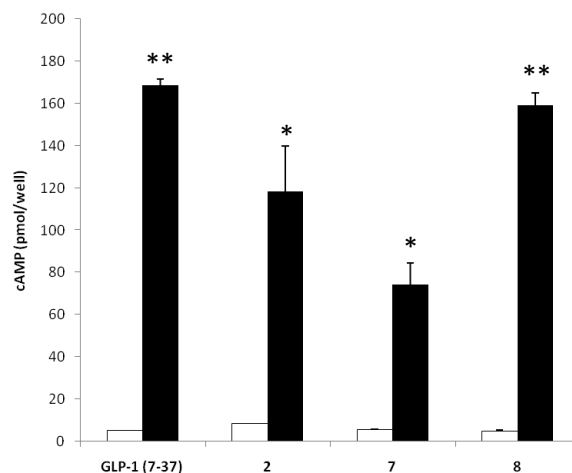
The best results for GLP-1R binding were obtained for GLP-1 derivatives modified at positions 22 and 37. For the peptide with DOTA conjugated at position 37 (**7**), a favorable IC<sub>50</sub> of 63 nM was determined, while the presence of the AEEA spacer at position 37 (**8**) decreased the binding affinity of the peptide to 89 nM. This was an unexpected outcome as the C-terminus of the peptide is the least sterically hindered position along the peptide chain. Although side chain modification at position 22 has not been recommended in the past literature, our results indicate that, when coupled with the proper spacer, modification at this position has minimal negative effect on the binding affinity of the peptide, as indicated by **2** with an IC<sub>50</sub> of 93 nM. Considering that the original residue at this position, <sup>22</sup>Gly, is predicted to disrupt the helical structure of

GLP-1,<sup>69-71</sup> it is possible that its replacement with <sup>22</sup>Lys may decrease the helical distortion, thereby allowing the addition of the metal complex with only minimal impact on its binding affinity to the GLP-1 receptor. The use of the AEEA spacer was also observed to have a negative impact on the binding affinity of the peptide when it was coupled to the Lys side chain at positions 26 and 34. This could have been caused by destabilization of the helical conformation of the GLP-1 derivatives as a result of steric hindrance or strain caused by the AEEA chain.

#### **2.3.4 cAMP Studies**

The production of intracellular cAMP is a measure of GLP-1R activation.<sup>72</sup> As GLP-1 binds to its receptor on the beta cell, intracellular  $G\alpha_s$  is activated, resulting in the stimulation of transmembrane adenylyl cyclases (tmACs) and elevation of cAMP levels.<sup>73</sup> This in turn promotes glucose-dependent insulin secretion. In this study, the ability of peptides **2**, **7**, and **8** to activate GLP-1 receptors was assessed by measuring cAMP levels in response to 10 nM of peptide using a previously published method.<sup>60</sup> As shown in Figure 2.7, all three peptides significantly increased cytoplasmic cAMP concentrations in CHO/GLP1R cells. Peptide **8** increased cAMP levels to the same extent as native GLP-1 (32.6-fold vs. 33.3-fold, respectively), while the response to peptide **2** (14.4-fold) and peptide **7** (13.8-fold) was not as great ( $p < 0.05$  compared to the fold increase by native GLP-1). These experiments therefore demonstrate that these analogues can act as GLP-1R agonists.



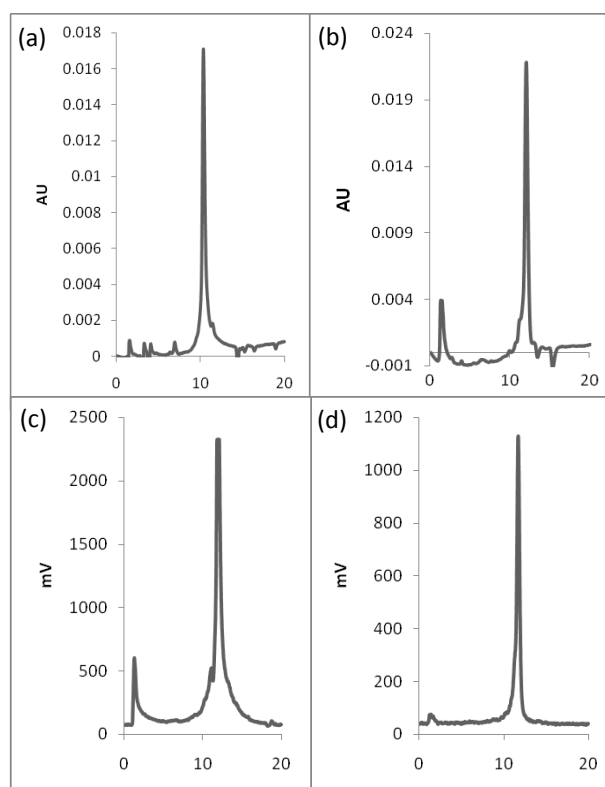


**Figure 2.7** *In vitro* cAMP accumulation in CHO/GLP-1R cells at basal level (white bars) and following stimulation (black bars) with 10 nM of GLP-1, **2**, **7**, or **8** ( $n = 3$  for each peptide). \*\*,  $p < 0.001$ ; \*,  $p < 0.05$  (compared to basal).

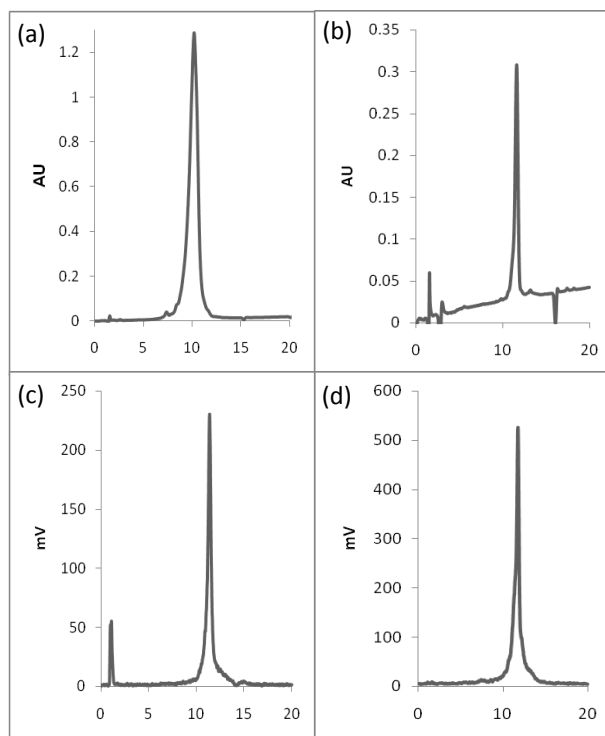
### 2.3.5 <sup>111</sup>In-Labeling

Based on the accumulated biological data for these novel GLP-1 analogues, compound **8** was selected for radiolabelling with In-111 and subsequent evaluation in insulinoma cells. Radiolabeling was carried out in pH 5 NaOAc/HOAc buffer over 30 minutes at 70 °C. The decay corrected radiochemical yield for the preparation of [<sup>111</sup>In]-**8** was 60% and the radiopurity was 98%. Monitoring of the reaction progress and characterization of the <sup>111</sup>In-labelled peptide were carried out using RP-HPLC with <sup>113/115</sup>In-labeled peptide **8** used as a non-radioactive standard for chromatographic comparison of retention time. Figure 2.8 shows the UV and radiochromatograms corresponding to this reaction. To further demonstrate the ability to radiolabel these

DOTA-GLP-1 derivatives, the radiolabeling of **2** was also carried out under the same conditions as mentioned above. The radiochemical yield and purity in this case were 84% and 97% respectively. Figure 2.9 shows the UV and radiochromatograms corresponding to the preparation of [ $^{111}\text{In}$ ]-**2**.



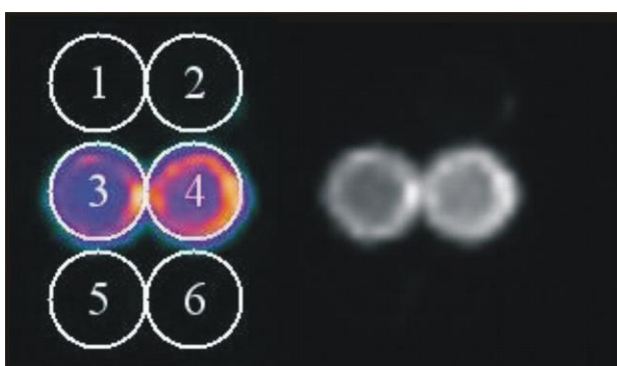
**Figure 2.8** The HPLC (a) UV chromatogram of the standard unlabeled **8**; (b) UV chromatogram of [ $^{113/115}\text{In}$ ]-**8**; (c) radiochromatogram of [ $^{111}\text{In}$ ]-**8** before purification; and (d) radiochromatogram of [ $^{111}\text{In}$ ]-**8** after Sep-Pak purification.



**Figure 2.9** The HPLC (a) UV chromatogram of the standard unlabeled **2**; (b) UV chromatogram of  $[^{113/115}\text{In}]\text{-2}$ ; (c) Radiochromatogram of  $[^{111}\text{In}]\text{-2}$  before purification; and (d) the radiochromatogram of  $[^{111}\text{In}]\text{-2}$  after Sep-Pak purification.

To demonstrate that our  $[^{111}\text{In}]$ -labeled peptides can be used for imaging, an *in vitro* imaging study was carried out using  $[^{111}\text{In}]\text{-8}$  and the clonal insulin-producing beta cell line INS-1 832/13, which expresses the GLP-1 receptor endogenously. The planar gamma camera image in Figure 2.10 demonstrated specific binding of the GLP-1 analogue, as it was displaced by exendin-4. In this image, wells 1 and 2, containing the binding buffer and INS-1 832/13 cells, were used as a control to measure the background

noise. Wells 3 and 4, containing INS-1 832/13 cells and [ $^{111}\text{In}$ ]-**8**, indicated uptake of the hot peptide. The image of wells 5 and 6 clearly indicated displacement of the hot peptide by exendin-4 thus further proving that the GLP-1 derivative was taken up by GLP-1R on the surface of the INS-1 832/13 cells. This imaging study proved [ $^{111}\text{In}$ ]-**8** to be a potential SPECT imaging agent for monitoring pancreatic beta cell mass *in vivo*.

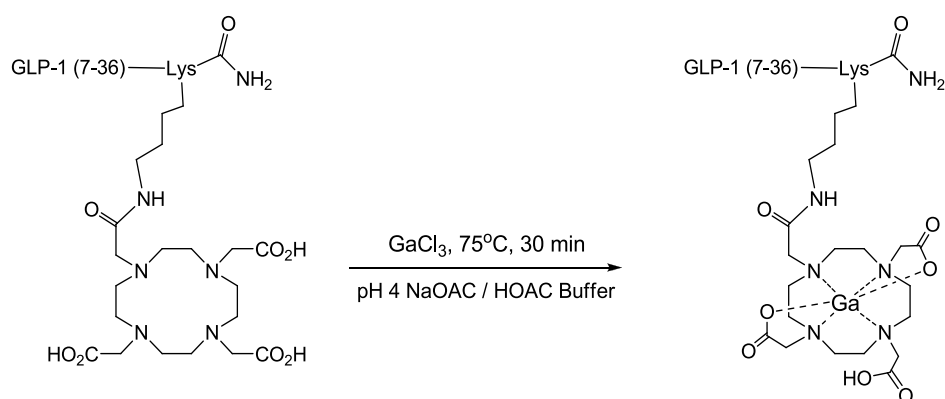


**Figure 2.10** *In vitro* gamma camera imaging study with INS-1 832/13 cells. Wells 1 and 2 = background control (no probe added); 3 and 4 = [ $^{111}\text{In}$ ]-**8**; 5 and 6 = [ $^{111}\text{In}$ ]-**8** +  $10^{-6}$  M unlabelled exendin-4 (cold exendin-4 block). Left image, color contoured; right image, grey-scale.

### 2.3.6 Synthesis of Gallium-GLP-1 Analogues

Previous *in vitro* analysis of indium-GLP-1 analogues indicated compounds **2**, **7** and **8** to be potential candidates for *in vivo* SPECT imaging of pancreatic islets. Development of  $^{68}\text{Ga}$ -GLP-1 analogues was undertaken in order to acquire PET radiotracers for pancreatic islet imaging. In doing so, both naturally occurring  $^{69/71}\text{Ga}$ -

and radioactive  $^{68}\text{Ga}$ -labeled analogues were synthesized with compound **7**. This analogue was selected over compound **8** owing to near identical binding affinities and shorter synthesis time.  $^{69}\text{Ga}$ -**7** was used as an HPLC standard for the radioactive labeling experiments. Scheme 2.3 illustrates typical conditions for  $^{69/71}\text{Ga}$ -DOTA chelation. Characterization of compounds was carried out using an LCMS (ESI) as described for indium analogues.

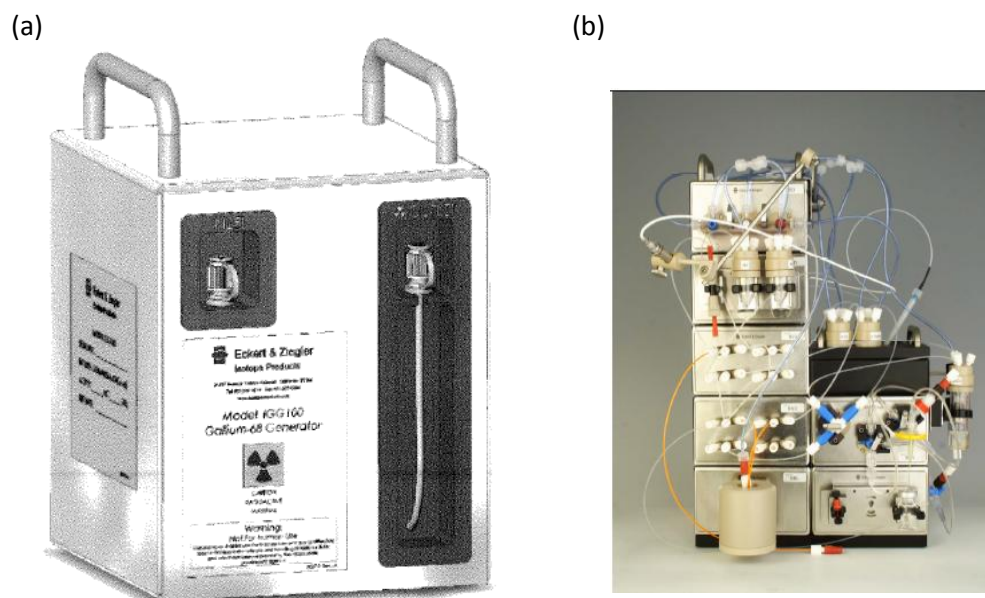


**Scheme 2.3** Synthetic scheme for  $^{69/71}\text{Ga}$ -labeling of GLP-1 analogues.

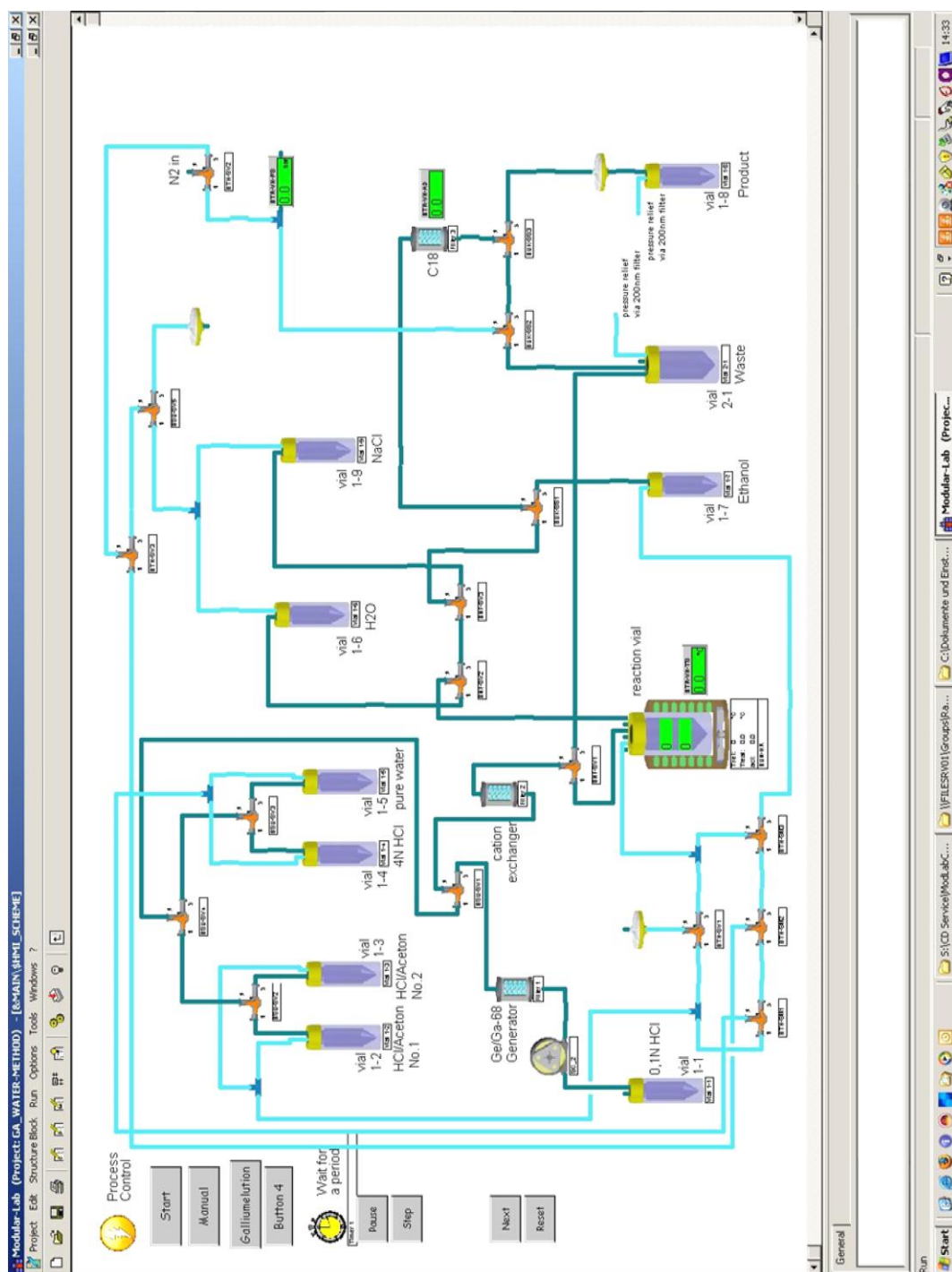
### 2.3.7 Gallium-68 Radiolabeling of GLP-1 analogues

The radiometal labeling of GLP-1 compounds was carried out using an Eckert and Ziegler  $^{68}\text{Ge}/^{68}\text{Ga}$  generator connected to a series of synthesis modules, which are remotely controlled by the user via a process computer (Figure 2.11). This remote access allows for control of specific instructions pertaining to a synthetic pathway. Scheme 2.4


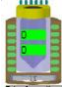
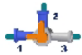




shows a graphical representation of a program written for radiolabeling of GLP-1 analogues. Table 2.5 lists the components and their function.



**Figure 2.11** Depiction of an Eckert and Ziegler modular lab system for  $^{68}\text{Ga}$ -radiolabeling experiments; (a)  $^{68}\text{Ge}/^{68}\text{Ga}$  generator; (b) modular lab automated synthesis unit.



**Scheme 2.4** Schematic of a program written for  $^{68}\text{Ga}$ -labeling of GLP-1 analogues.

Component	Symbol
Vial	
Heater Reactor Module	
Three way valves	
Cation exchange column or Sep-Pak <sup>®</sup>	
Squeeze pump	
Sterile filters	
Monitoring screens	

**Table 2.5** Description of modular part notations used in Scheme 2.4.

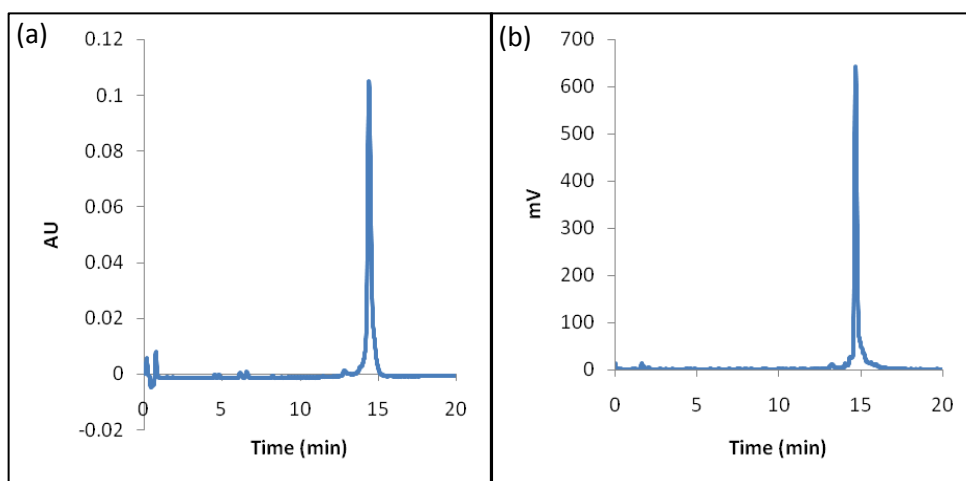
All solutions in this system, exception 0.1 N HCl in vial 1-1 which is transferred by a pressure pump, are transferred via pressure variance. In a typical experiment, gallium-68 is eluted from the generator using a squeeze pump and 3 mL of 0.1 N HCl (vial 1-1). This eluate, which may contain breakthrough of other impurities such as <sup>68</sup>Ge, is then loaded onto a Phenomenix Strata-X-C 33u polymeric strong cation exchange column for purification. Gallium-68 is then eluted out of the cation exchange cartridge using 0.4 mL of 0.05 N HCl in 98% acetone (vial 1-3), and carried to the reaction vessel containing the solution of GLP-1 analogue. After a designated duration of heating, the



reaction mixture is transferred to a RP-C18 Sep-Pak<sup>®</sup>. A 2 mL aliquot of sterile H<sub>2</sub>O (vial 1-6) is then passed through this cartridge in order to elute impurities such as unreacted Ga-68. The final product is then isolated and eluted using EtOH (vial 1-7) into a clean sealed glass vessel (vial 1-8). A small aliquot of sterile NaCl solution (0.1-0.5 mL) can also be added to the final product if required for *in vivo* studies. A small sample of the final product is diluted with water (10 fold dilution) prior to analysis by RP-HPLC. The solvent is then evaporated on a Biotage<sup>®</sup> rapid solvent evaporator system prior to being assayed. The choice of solvent and quantities of GLP-1 analogues were optimized in order to maximize radiochemical yields (Table 2.6). Radiochemical yields were observed to increase proportionally with increasing peptide amounts. Considering that the use of larger peptide quantities results in lower specific activities, the maximum quantity of peptide used was set at 100 µg. Ideal radiolabeling conditions were found to be in a pH 3.5 HEPES buffer utilizing 100 µg of peptide. Figure 2.12 shows typical chromatograms of labeled peptides.

<b>Solvent</b>	<b>Peptide (µg)</b>	<b>Volume (mL)</b>	<b>DC-RCY (%)</b>
HEPES	10	1	0.0
	20	1	0.8
	50	1	12.7
	100	1	74.8
H <sub>2</sub> O	100	1	11.0
NaOAc/HOAc Buffer pH 4	100	1	26

**Table 2.6** Optimization of radiometal labeling conditions for GLP-1 analogues.

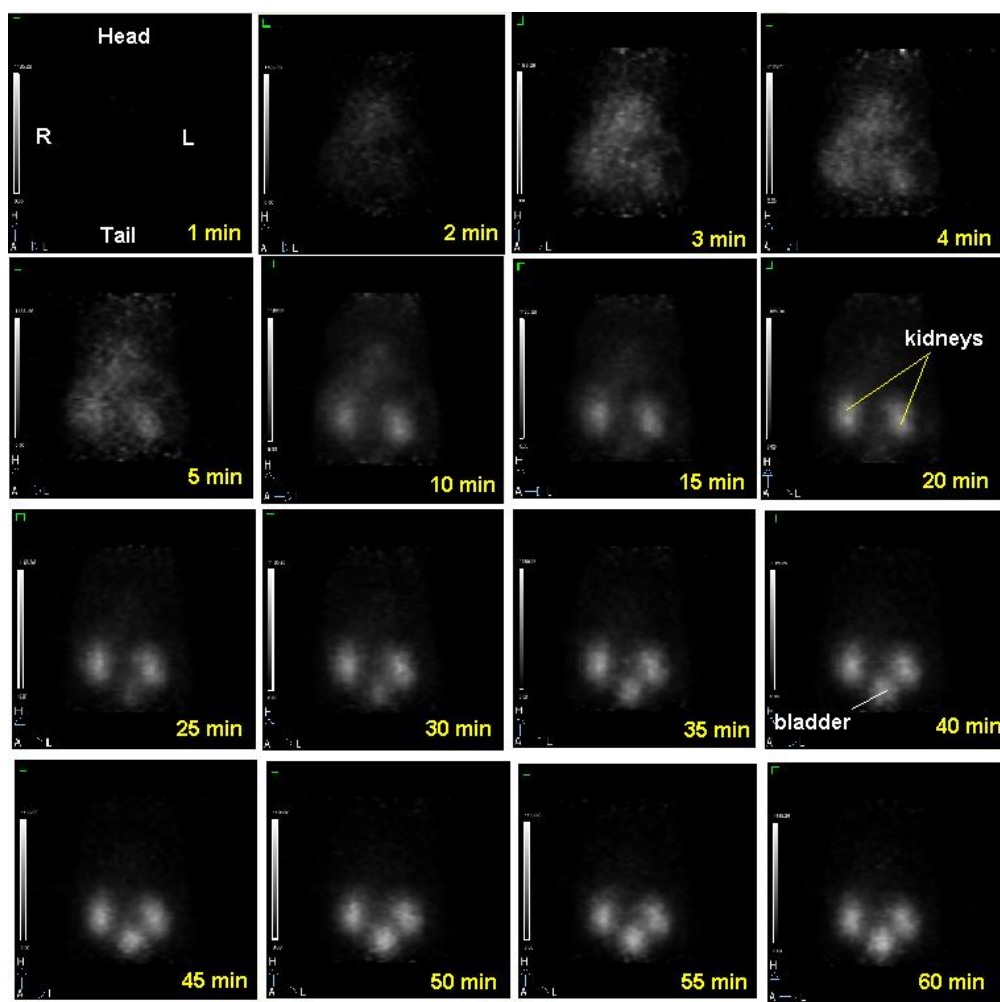


**Figure 2.12** HPLC chromatograms of GLP-1 analogue **7**; (a) UV trace of  $^{69/71}\text{Ga-7}$  and (b) radiochromatogram of  $^{68}\text{Ga-7}$  post purification.

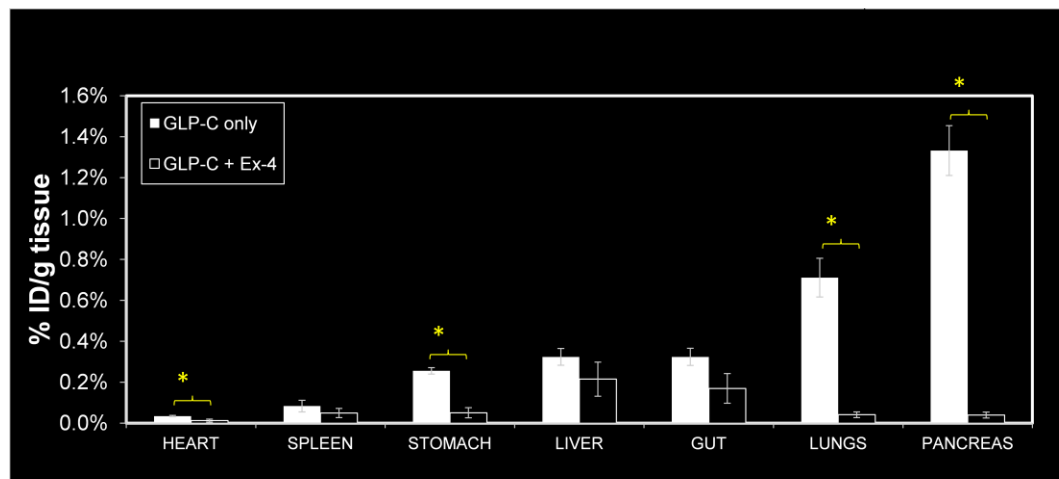
### 2.3.8 *In Vivo* Studies

Both SPECT ( $^{111}\text{In-7}$ ) and PET ( $^{68}\text{Ga-7}$ ) candidates were studied *in vivo* in C57BL/6 mice. Figure 2.13 shows PET images obtained over 60 min after intravenous injection of  $^{68}\text{Ga-7}$ . Unfortunately, pancreatic islets could not be visualized owing to tracer accumulation in kidneys, which resulted in high background signal levels. In a typical study, kidney uptake was observed 4 min post injection, while clearance from bladder was visible 25 min post injection. Biodistribution data indicated reasonable uptake levels in the pancreas (Figure 2.14), thus confirming the normalization of probe signal from the pancreas by the kidney uptake. Lower levels of probe uptake were also observed in the stomach, liver, lungs and heart. In these studies, specific binding was confirmed by a follow-up injection of excess exendin-4 immediately after injection of the

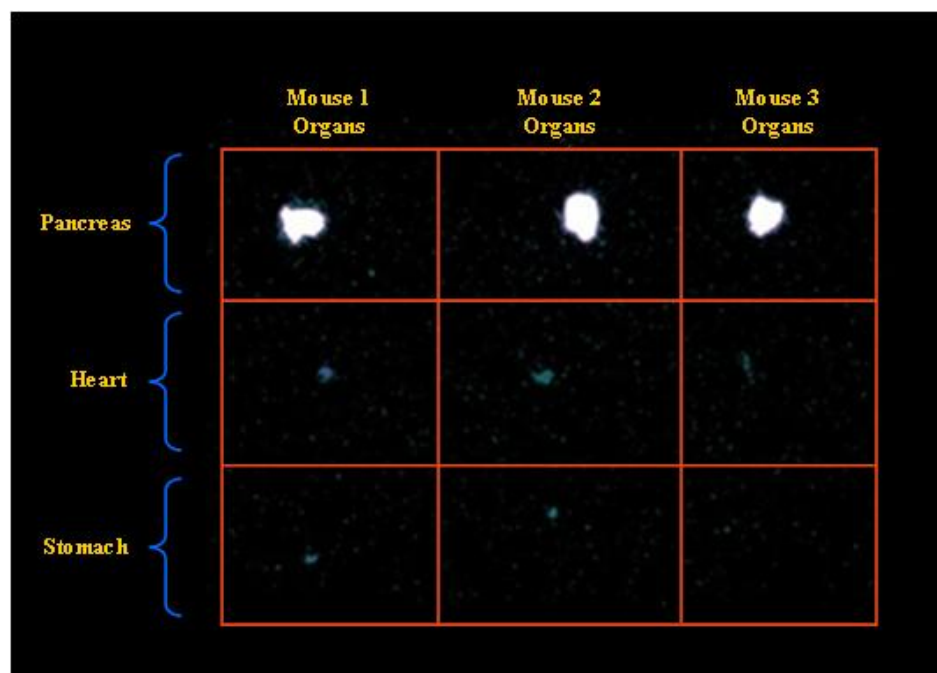
radiolabeled probe. The replacement of the GLP-1 analogue indicated specific binding of the probe, as also evident in other organs expressing the GLP-1 receptors. Removed pancreata were also visualized externally using a gamma camera to further confirm the presence of radiolabeled probe (Figure 2.15).



**Figure 2.13** PET images obtained over 60 min after intravenous injection of  $^{68}\text{Ga}$ -7 into a C57BL/6 mouse; accumulation of radiotracer in kidneys and bladder is observed after 4 min and 25 min respectively.



**Figure 2.14** Biodistribution of  $^{68}\text{Ga-7}$  in C57BL/6 mice (n=6), 4 hours post injection; blocking was carried out with excess Exendin-4.



**Figure 2.15** Ex-vivo gamma camera images of pancreata, hearts and stomachs obtained from three C57BL/6 mice 4 hours after injection of  $^{68}\text{Ga-7}$ .

Considering that the use of  $^{111}\text{In}$ -**7** and  $^{68}\text{Ga}$ -**7** was shown not to be ideal for *in vivo* pancreatic islet visualization, alternate methods of imaging the islets were sought. The first methodology involved further modification of the peptide backbone in order to reduce probe accumulation in kidneys, thus increasing signal to noise ratios. The second methodology utilized the radiohalogen fluorine-18, thus circumventing the need for radiometals and radiometal chelators.

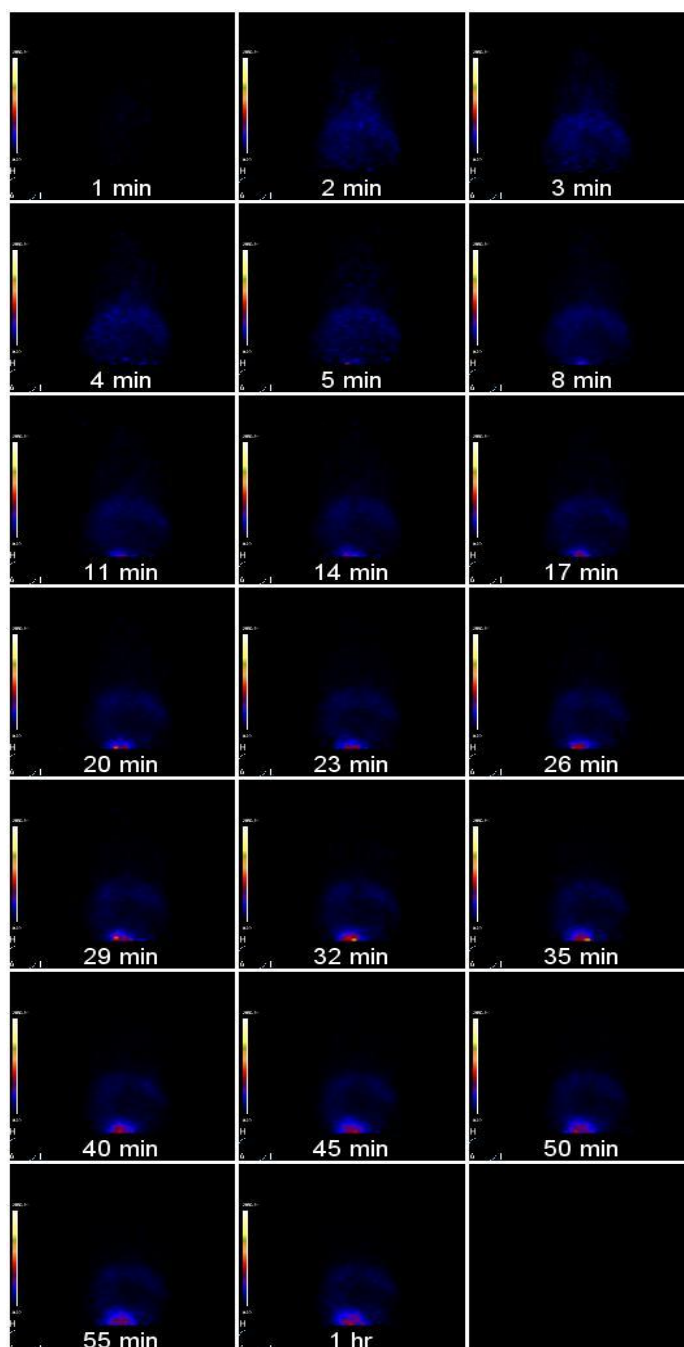
### 2.3.9 Modifying the GLP-1 Peptide Backbone

High uptake of imaging probes in kidneys has been an ongoing problem in oncology both in terms of therapeutics as well as imaging strategies.<sup>74, 75</sup> Previous reports by Pimm et al. and Behr et al. indicated the cause of this uptake to primarily be the presence of positive charged basic amino acids such as lysine and arginine.<sup>76, 77</sup> As a result, many attempts have been made by various research groups to neutralize positive charges in an effort to lower the isoelectric points of compounds under study, thus reducing probe residence time in the kidneys. Examples of such studies include the use of 2,3,5,6-tetrafluorophenyl glycolate or acylation to neutralize positive charges in anti-Tac disulfide-bonded variable region side-chain Fv fragments, which led to lower kidney accumulation while maintaining tumor uptake ratios.<sup>78-80</sup> Another example included the lowering of renal accumulation of  $^{111}\text{In}$ -DTPA-conjugated peptides such as Octreotide, which was accomplished by increasing negative charges along the peptide backbone (eg. substitution of phenylalanine by aspartic acids).<sup>81, 82</sup> In accordance with this theory, it was speculated that acylation of lysine residues and substitution of arginine residues for glycine, may aid in reducing charges in compound **7**'s backbone. The selection of

residues for acylation/substitution was made not only with regards to charge, but also to residues reported to be essential for binding (Figure 2.4). With the above consideration,  $^{37}\text{Gly}$  was replaced with  $^{37}\text{Lys}$  (later used for DOTA conjugation), while Lysine residues at positions 34 and 26 were acylated. Prepared compounds were synthesized using Fmoc solid phase strategies. Purification and analysis of peptides was carried out as stated previously.

In this study, two peptide variations were prepared with the presence of an AEEA linker being the only differentiating factor between the two molecules. The binding affinity of peptide candidates was determined using the same previously mentioned cell-based assay methodology, incorporating CHO cells and radioiodinated exendin-4. The obtained  $\text{IC}_{50}$  values were  $84.6 \pm 6.8$  nM for peptide containing AEEA (acyl-8) and  $76.0 \pm 3.9$  nM for the peptide not possessing a PEG linker (acyl-7). It was noted that the presence of a PEG linker did not affect the binding affinity of modified peptides. As a result, acyl-7 was utilized further for *in vivo* studies. Radiochemical yield and purity of  $^{68}\text{Ga}$ -acyl-7 were  $60 \pm 5\%$  and  $> 95\%$  respectively. Figure 2.16 shows typical PET images obtained from  $^{68}\text{Ga}$ -acyl-7, clearly indicating a significant reduction in kidney probe accumulation. These results confirmed that a reduction in the overall positive charge of peptides would result in lowered probe attenuation in kidneys. Unfortunately, pancreatic beta cells were still not visible even after reducing kidney retention. A possible explanation for this observation may be mouse-model dependent GLP-1R expression. As a result, the expression of GLP-1R in various mouse models are currently being studied using both radiometal labeled  $^{68}\text{Ga}$ -7 and a dye tagged fluorescein-7 analogue. In the later case, FITC was used as the fluorescent tag of choice and was conjugated to  $^{37}\text{Lys}$  side

chain, as with DOTA. Studies to examine GLP-1R expression *in vivo* are currently ongoing.



**Figure 2.16** PET images obtained over 60 min after intravenous injection of  $^{68}\text{Ga}$ -acyl-7 into a C57BL/6 mouse; accumulation of radiotracer in kidneys was reduced while showing clearance through the bladder 5 min post injection.

### 2.3.10 Fluorination of GLP-1

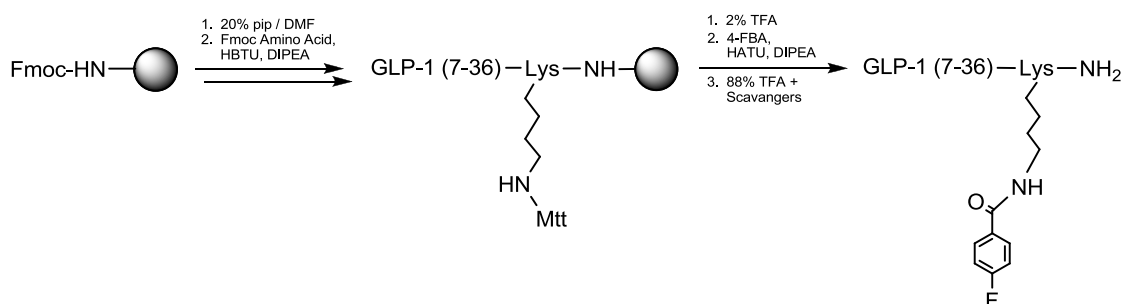
The fluorination of large molecules such as peptides is typically carried out using the prosthetic group methodology, owing to limitations imposed by the use of nucleophilic fluoride such as high proton affinity.<sup>83</sup> Among all available prosthetic groups, [<sup>18</sup>F]SFB (N-succinimidyl-4-[<sup>18</sup>F]fluorobenzoate) appears to be most suited for use with bioactive molecules and proteins, especially in terms of yields and biological stability of labeled compounds.<sup>58</sup> The synthesis of this prosthetic group involves several major steps which are 1) radiofluorination of an aromatic precursor, 2) formation of 4-[<sup>18</sup>F]fluorobenzoic acid, and 3) conversion of the free acid to the activated ester. There have been many reports on optimization of SFB synthesis with the aim of reducing synthesis time, improving activation step, minimizing purification steps and enhancing radiochemical yields.<sup>48, 58, 84, 85</sup> Wester and coworkers have reported an improved synthesis, which satisfies the requirements for radiofluorination of biological compounds.<sup>58</sup> Radiofluorination of GLP-1 analogues employed the use of both activated and non-activated [<sup>18</sup>F]fluorobenzoic acid analogues using solid phase and solution phase methodologies

#### 2.3.10.1 Solid Phase Approach

In order to examine the potential of fluorinated GLP-1 analogues as PET radiotracers for the detection of pancreatic beta cells, synthesis of non-radioactive <sup>19</sup>F-GLP-1 analogues were carried out. Considering that previous studies on metal-chelater-conjugated GLP-1 analogues revealed compound **7** to be a potential candidate for attachment of bulky groups, residue 37 was selected as a suitable position for prosthetic

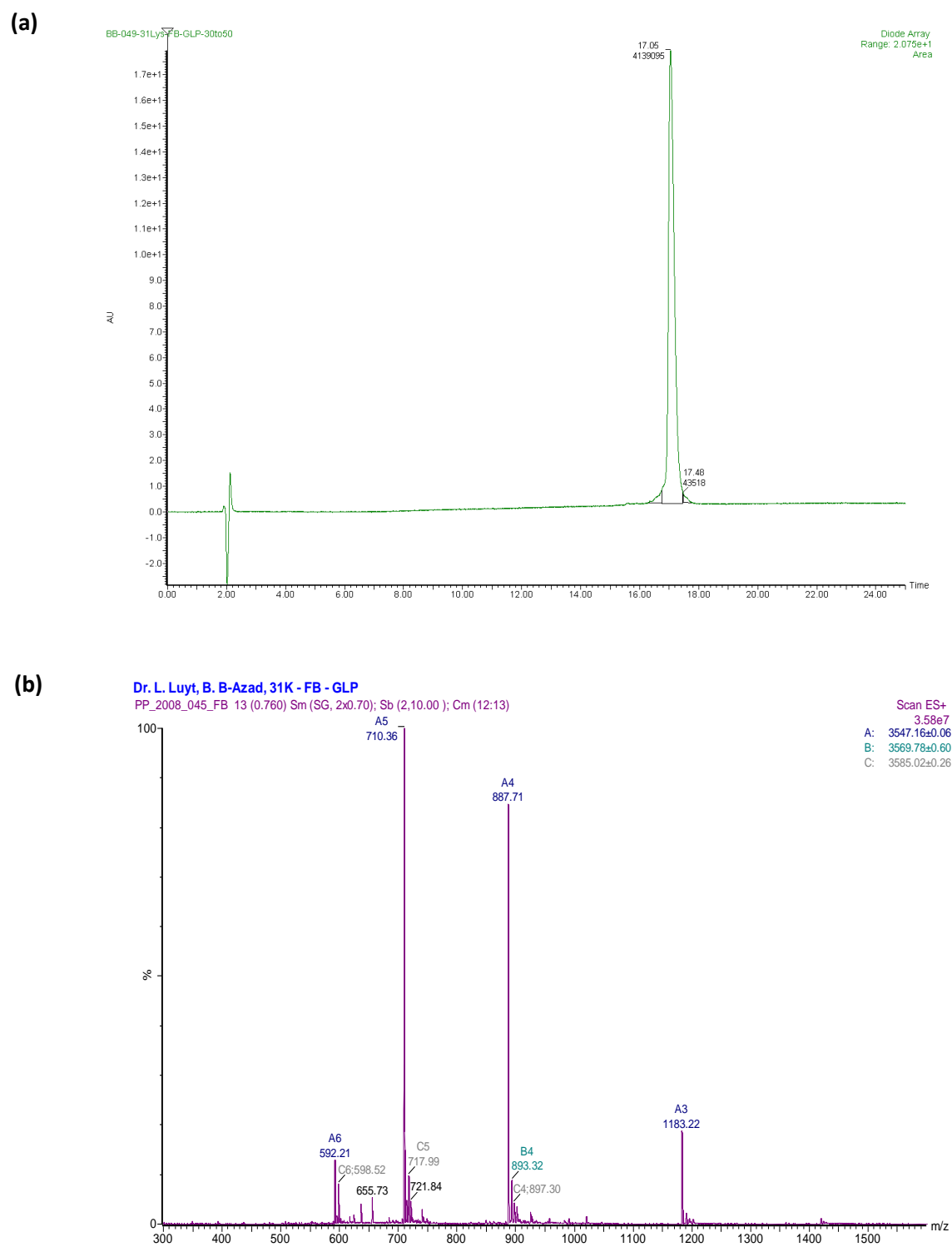


group conjugation. For this approach, 4-fluorobenzoic acid was conjugated to GLP-1 according to Scheme 2.5. Fluorinated product was analyzed and purified by HPLC and ESI-MS (Figure 2.17).

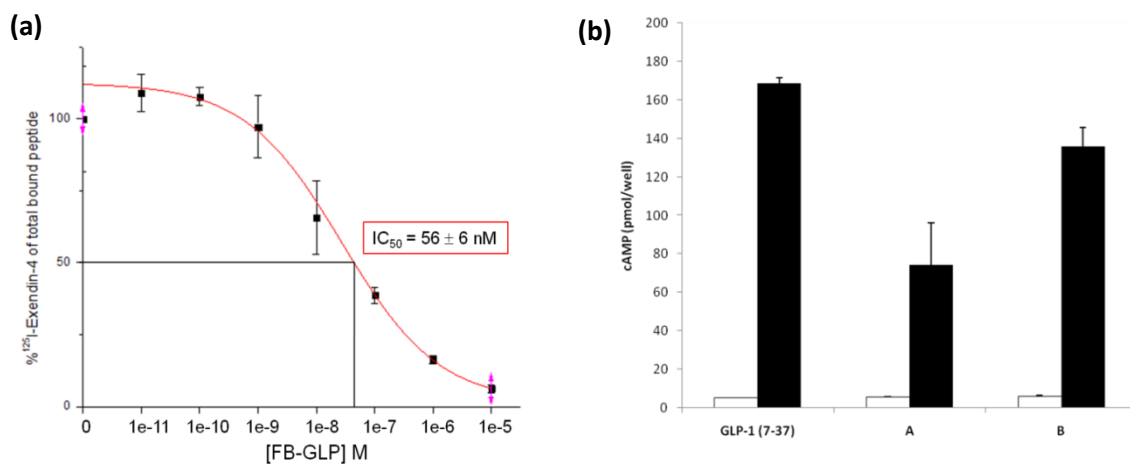


**Scheme 2.5** Synthetic scheme for  $^{37}\text{Lys}-(\text{FB})\text{-GLP-1}(7\text{-}37)$ , **9**.

A competitive cell based assay was carried out using CHO cells and radioiodinated exendin-4. This procedure was identical to those carried out for radiometal GLP-1 analogues. The binding curve obtained for this peptide Figure 2.18 (a) indicated an  $\text{IC}_{50}$  of  $56 \pm 6$  nM, which is comparable to those obtained for promising radiometal chelated GLP-1 derivatives. cAMP analysis of **9** confirmed it as a GLP-1 receptor agonist, as indicated in Figure 2.18 (b). Receptor activation seemed to be more significant in the case of **9** when compared to that of **7**.

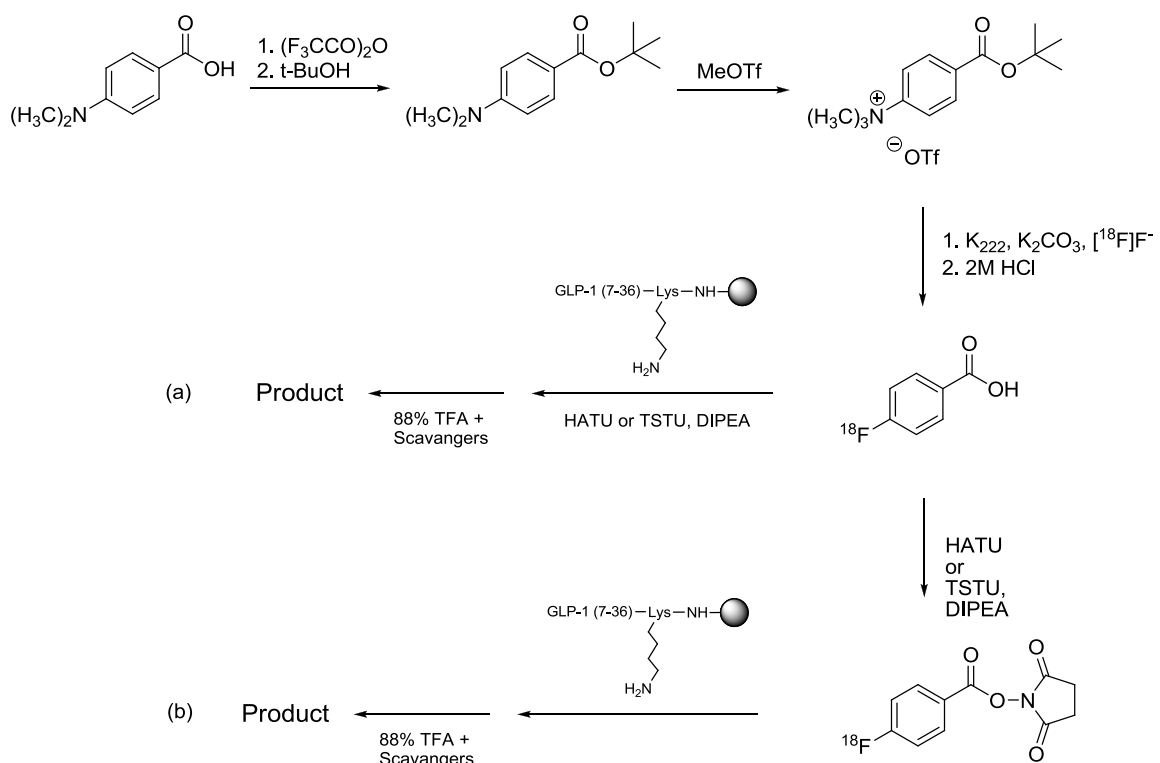


**Figure 2.17** HPLC chromatogram and ESI-MS spectrum of GLP-1 analogue **9**.

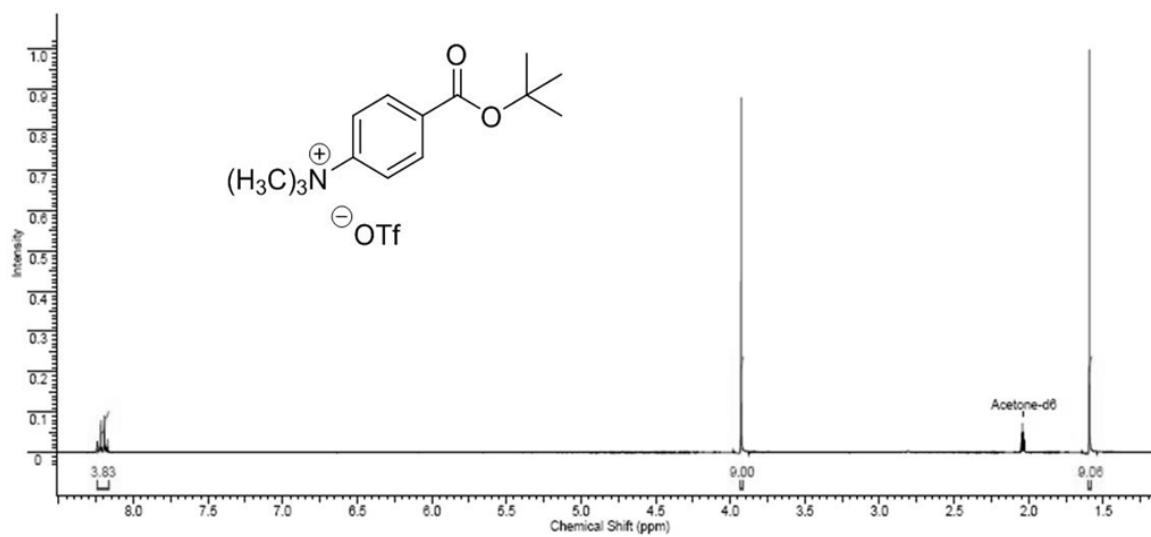


**Figures 2.18** (a) Competitive Displacement of  $^{37}\text{Lys}$ -FB GLP-1 vs.  $^{125}\text{I}$ -Exendin-4 on CHO/GLP-1R cells; (b) *in vitro* cAMP accumulation in CHO/GLP-1R cells at basal level (white bars) and following stimulation (black bars) with 10 nM of native GLP-1,  $^{37}\text{Lys}$ -In-DOTA-GLP-1(7-37) [A] and  $^{37}\text{Lys}$ -FB-GLP-1(7-37) [B].

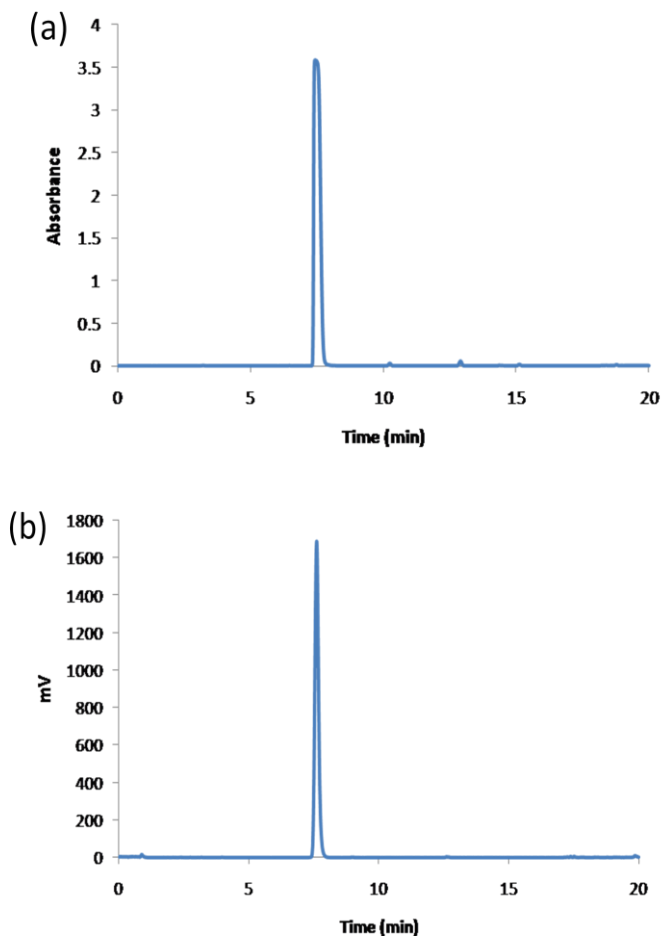
The solid phase synthetic route for the preparation of  $^{18}\text{F}$ -**9** is illustrated in Scheme 2.6. This approach required preparation of *t*-butyl-*N,N,N*-trimethylammonium benzoate triflate (TMABT) as the precursor for radiofluorination. Synthesis of TMABT started with the protection of the carboxylic acid with *t*-butyl in order to prevent side reactions in the next step. Methylation of dimethyl amine was then carried out using methyl trifluoromethanesulfonate (MeOTf), resulting in the formation of a quaternary amine suitable for nucleophilic aromatic substitution. TMABT was characterized by  $^1\text{H}$ -NMR spectroscopy (Figure 2.19). Radiofluorination of this compound and subsequent deprotection by 2 M HCl then resulted in the formation of  $^{18}\text{F}$ FB, which was isolated using a RP-Chromafix cartridge. Figure 2.20 shows a UV chromatogram of  $^{19}\text{F}$ FB and radiochromatogram of purified  $^{18}\text{F}$ FB.



**Scheme 2.6** Synthetic scheme for the radiofluorination of GLP-1 analogues using the solid phase approach.



**Figure 2.19**  $^1\text{H-NMR}$  spectrum of purified TMABT.



**Figure 2.20** HPLC chromatograms for 4-FBA; (a) UV chromatogram of 4- $^{19}\text{F}$ FBA and (b) radiochromatogram of purified 4- $^{18}\text{F}$ FBA.

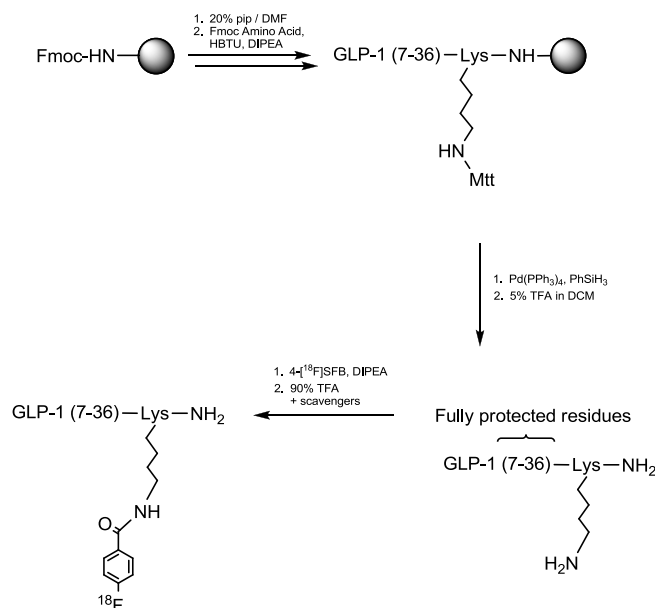
The synthesis of  $^{18}\text{F}$ FB, starting with TMABT, was optimized on a GE TRACERlab FX-N automated synthesis unit. Deprotection of  $^{18}\text{F}$ FB was optimal with 2 M HCl when carried out at 100 °C over 10 min. Decay-corrected radiochemical yields of  $^{18}\text{F}$ FB were  $35 \pm 3\%$  with radiochemical purities  $> 98\%$ . The activation of  $^{18}\text{F}$ FB, in situ (Scheme 2.6a) or in a separate step requiring further purification of  $^{18}\text{F}$ SFB (Scheme 2.6b), was carried out with both HATU and TSTU. Activated  $^{18}\text{F}$ FB was

obtained with the same radiochemical yield and purity as pre-activated [ $^{18}\text{F}$ ]FB ( $35 \pm 3\%$ ;  $> 98\%$ ).

Regardless of the route of activation, however, the extent of conjugation of  $^{18}\text{F}$ -labeled prosthetic group to GLP-1 peptide analogue was extremely low ( $< 3\%$ ) such that a radiochemical yield could not be determined. However, based on HPLC integration, a radiochemical yield of 3% was estimated. These results did not change with temperature, peptide amount (ie. number of peptide-conjugated rink amide resins), or radioactivity amounts, indicating this approach to be unsuitable for radiofluorination of GLP-1 analogues. It is speculated that poor coupling yields are due to low concentrations of both the prosthetic group as well as the peptide, in addition to steric hindrance imposed by the peptide backbone. As a result, a solution phase synthetic approach was considered.

#### **2.3.10.2 Solution Phase Methodology**

Considering results obtained from the last approach, an attempt was made to increase radiochemical yields by increasing peptide concentration in solution. This study involved the synthesis of a fully protected peptide with only one available free amine for reaction with [ $^{18}\text{F}$ ]SFB (Scheme 2.7). Solid phase Fmoc-based synthesis of GLP-1(7-37) was carried out on acid labile Sieber-amide resin, with Lys(Alloc)-OH at position 37. Palladium catalyzed removal of Alloc following by complete cleavage of the peptide from the resin using 5% TFA in DCM over 15 min. The peptide was then precipitated using *t*-butylmethyl ether (x2), and dried over night on a lyophilizer. Unfortunately, this peptide was insoluble in any solvents suitable for radiochemistry, rendering this method also unsuitable for radiofluorination of GLP-1 analogues.



**Scheme 2.7** Synthetic scheme for the radiofluorination of GLP-1 analogues using the solution phase approach.

## 2.4 Conclusion

The objective of this project was the development of novel GLP-1 analogues for the targeting of GLP-1 receptors on pancreatic beta cells. To this end, we have developed a number of GLP-1 analogues, all shown to have high affinity for GLP-1 receptors. Three of the initially developed derivatives, namely compounds **2**, **7** and **8**, showed optimal IC<sub>50</sub> values indicating that positions 22 and 37 of GLP-1 are the most suitable for indium and gallium-DOTA conjugation. While the presence of the AEEA spacer was beneficial at position 22, it had a negative impact on the binding affinity of the peptide analogues at

positions 26, 34, and 37. The SPECT images obtained from the competitive displacement study between [ $^{111}\text{In}$ ]-**7** and exendin-4 in INS-1 832/13 cells further demonstrated the potential of the developed probes to monitor beta cell mass. In vivo studies were carried out using  $^{111}\text{In}$ -**7** and  $^{68}\text{Ga}$ -**7** SPECT and PET probes, respectively. Preliminary data indicated specific uptake of the probe in the pancreas. Strong probe retention in the kidneys, however, prevented visualization of the pancreas by both PET and SPECT. Compound **7** was modified in order to reduce kidney accumulation of the radiotracer. This modification was successful as it resulted in lowering of kidney retention while maintaining similar binding affinity to GLP-1R as compound **7**. Visualization of the pancreas, however, was still not possible. After studies with radiometal-chelator-GLP-1 conjugates, attempts were made to synthesize fluorinated GLP-1 analogues. The fluorinated-GLP-1 was shown to have optimal affinity for GLP-1R while still being a receptor agonist. Both [ $^{18}\text{F}$ ]FB and activated [ $^{18}\text{F}$ ]SFB were successfully synthesized in optimal radiochemical yields for radiofluorination of GLP-1 analogues. Coupling of radiofluorinated prosthetic groups to 37Lys-GLP-1(7-37) was attempted using both solid phase and solution phase methodologies, however, these methods were found to be unsuitable owing to low yields and peptide insolubility. This research has resulted in the development of promising GLP-1 based tracers for the non-invasive imaging of pancreatic islets *in vivo*. Research on optimization of uptake and probe clearance from kidneys is currently ongoing.



## 2.5 Acknowledgements

We thank the Natural Sciences and Engineering Research Council of Canada (NSERC), the Canadian Institutes for Health Research (CIHR), and the Ontario Graduate Scholarship in Science and Technology (OGSST) for financial support. We thank Dr. Michael Wheeler (University of Toronto) and Dr. Christopher Newgard (Duke University) for providing the CHO/GLP-1R and INS-1 832/13 cells respectively. We also thank Dr. Michael Kovacs for his assistance with the radiochemistry, Becky McGirr (LHRI) for technical assistance with cell culture, and Eric Sabondjian (LHRI) for assistance with gamma camera imaging. Savita Dhanvantari is a Scholar of the Canadian Diabetes Association.

## 2.6 References

1. George, K.; Alberti, M. M., The Classification and Diagnosis of Diabetes Mellitus. In *Textbook of Diabetes*, HOLT, R. I. G.; COCKRAM, C. S.; FLYVBJERG, A.; GOLDSTEIN, B. J., Eds. Wiley-Blackwell: Oxford, 2010; pp 24-31.
2. Alberti, K.; Zimmet, P. Z.; Consultation, W. H. O., Definition, diagnosis and classification of diabetes mellitus and its complications part 1: Diagnosis and classification of diabetes mellitus - Provisional report of a WHO consultation. *Diabetic Medicine* **1998**, 15, (7), 539-553.
3. Nauck, M. A.; Kleine, N.; Orskov, C.; Holst, J. J.; Willms, B.; Creutzfeldt, W., Normalization of fasting hyperglycemia by exogenous glucagon-like peptide-1 (7-

- 36 amide) in type-2 (non-insulin-dependent) diabetic-patients. *Diabetologia* **1993**, 36, (8), 741-744.
4. Dhanvantari, S.; Brubaker, P. L., Proglucagon processing in an islet cell line: Effects of PC1 overexpression and PC2 depletion. *Endocrinology* **1998**, 139, (4), 1630-1637.
  5. Meier, J. J.; Nauck, M. A., Glucagon-like peptide 1(GLP-1) in biology and pathology. *Diabetes-Metabolism Research and Reviews* **2005**, 21, (2), 91-117.
  6. Buteau, J., GLP-1 receptor signaling: effects on pancreatic beta-cell proliferation and survival. *Diabetes & Metabolism* **2008**, 34, S73-S77.
  7. Estall, J. L.; Drucker, D. J., Glucagon and glucagon-like peptide receptors as drug targets. *Current Pharmaceutical Design* **2006**, 12, (14), 1731-1750.
  8. Al-Sabah, S.; Donnelly, D., A model for receptor-peptide binding at the glucagon-like peptide-1 (GLP-1) receptor through the analysis of truncated ligands and receptors. *British Journal of Pharmacology* **2003**, 140, (2), 339-346.
  9. Deacon, C. F.; Knudsen, L. B.; Madsen, K.; Wiberg, F. C.; Jacobsen, O.; Holst, J. J., Dipeptidyl peptidase IV resistant analogues of glucagon-like peptide-1 which have extended metabolic stability and improved biological activity. *Diabetologia* **1998**, 41, (3), 271-278.
  10. Siegel, E. G.; Scharf, G.; Gallwitz, B.; Mentlein, R.; Morys-Wortmann, C.; Folsch, U. R.; Schmidt, W. E., Comparison of the effect of native glucagon-like peptide I and dipeptidyl peptidase IV-resistant analogues on insulin release from rat pancreatic islets. *European Journal of Clinical Investigation* **1999**, 29, (7), 610-614.

11. Raufman, J. P.; Singh, L.; Singh, G.; Eng, J., Truncated glucagon-like peptide-1 interacts with exendin receptors on dispersed acini from guinea-pig pancreas - identification of a mammalian analog of the reptilian peptide exendin-4. *Journal of Biological Chemistry* **1992**, 267, (30), 21432-21437.
12. Wild, D.; Behe, M.; Wicki, A.; Storch, D.; Waser, B.; Gotthardt, M.; Keil, B.; Christofori, G.; Reubi, J. C.; Macke, H. R., [Lys(40) (Ahx-DTPA-In-111)NH<sub>2</sub>]exendin-4, a very promising ligand for glucagon-like peptide-1 (GLP-1) receptor targeting. *Journal of Nuclear Medicine* **2006**, 47, (12), 2025-2033.
13. Gotthardt, M.; Fischer, M.; Naeher, I.; Holz, J. B.; Jungclas, H.; Fritsch, H. W.; Behe, M.; Goke, B.; Joseph, K.; Behr, T. M., Use of the incretin hormone glucagon-like peptide-1 (GLP-1) for the detection of insulinomas: initial experimental results. *European Journal of Nuclear Medicine and Molecular Imaging* **2002**, 29, (5), 597-606.
14. Anderson, C. J.; Welch, M. J., Radiometal labeled agents (non-technetium) for diagnostic imaging. *Chemical Reviews* **1999**, 99, (9), 2219-2234.
15. Pearson, R. G., HARD AND SOFT ACIDS AND BASES. *Journal of the American Chemical Society* **1963**, 85, (22), 3533-&.
16. Sun, Y. Z.; Anderson, C. J.; Pajeau, T. S.; Reichert, D. E.; Hancock, R. D.; Motekaitis, R. J.; Martell, A. E.; Welch, M. J., Indium(III) and gallium(III) complexes of bis(aminoethanethiol) ligands with different denticities: Stabilities, molecular modeling, and in vivo behavior. *Journal of Medicinal Chemistry* **1996**, 39, (2), 458-470.

17. Sun, Y. Z.; Anderson, C. J.; Pajean, T. S.; Reichert, D. E.; Hancock, R. D.; Motekaitis, R. J.; Martell, A. E.; Welch, M. J., Indium(III) and gallium(III) complexes of bis(aminoethanethiol) ligands with different denticities: Stabilities, molecular modeling, and in vivo behavior (vol 39, pg 458, 1996). *Journal of Medicinal Chemistry* **1996**, 39, (12), 2434-2434.
18. Martell, A. E.; Hancock, R. D., *Metal Complexes in Aqueous Solutions*. Plenum Press: New York, 1996.
19. Welch, M. J.; Redvanly, C. S., *Handbook of radiopharmaceuticals : radiochemistry and applications*. Wiley: Chichester, England ; Hoboken, NJ, 2003; p xiv, 848 p.
20. Thakur, M. L., GA-67 AND IN-111 RADIOPHARMACEUTICALS/EUTICALS. *International Journal of Applied Radiation and Isotopes* **1977**, 28, (1-2), 183-&.
21. Shi, W.; Johnston, C. F.; Buchanan, K. D.; Ferguson, W. R.; Laird, I. D.; Crothers, J. G.; McIlrath, E. M., Localization of neuroendocrine tumours with [In-111] DTPA-octreotide scintigraphy (Octreoscan): a comparative study with CT and MR imaging. *Qjm-Monthly Journal of the Association of Physicians* **1998**, 91, (4), 295-301.
22. Nakamoto, Y.; Saga, T.; Sakahara, H.; Yao, Z. S.; Zhang, M. L.; Sato, N.; Zhao, S. J.; Nakada, H.; Yamashina, I.; Konishi, J., Three-step tumor imaging with biotinylated monoclonal antibody, streptavidin and In-111-DTPA-biotin. *Nuclear Medicine and Biology* **1998**, 25, (2), 95-99.

23. Mathias, C. J.; Wang, S.; Waters, D. J.; Turek, J. J.; Low, P. S.; Green, M. A., Indium-111-DTPA-folate as a potential folate-receptor-targeted radiopharmaceutical. *Journal of Nuclear Medicine* **1998**, 39, (9), 1579-1585.
24. Aloj, L.; Caraco, C.; Panico, M.; Zannetti, A.; Del Vecchio, S.; Tesauro, D.; De Luca, S.; Arra, C.; Pedone, C.; Morelli, G.; Salvatore, M., In vitro and in vivo evaluation of In-111-DTPAGlu-G-CCK8 for cholecystokinin-B receptor imaging. *Journal of Nuclear Medicine* **2004**, 45, (3), 485-494.
25. Thakur, M. L.; Segal, A. W.; Louis, L.; Welch, M. J.; Hopkins, J.; Peters, T. J., Indium-111-labeled cellular blood components - mechanism of labeling and intracellular location in human neutrophils. *Journal of Nuclear Medicine* **1977**, 18, (10), 1022-1026.
26. Wegener, W. A.; Alavi, A., Diagnostic-imaging of musculoskeletal infection - roentgenography gallium, indium-labeled white blood-cell, gamma-globulin, bone-scintigraphy and MRI. *Orthopedic Clinics of North America* **1991**, 22, (3), 401-418.
27. Meyer, G. J.; Macke, H.; Schuhmacher, J.; Knapp, W. H.; Hofmann, M., Ga-68-labelled DOTA-derivatised peptide ligands. *European Journal of Nuclear Medicine and Molecular Imaging* **2004**, 31, (8), 1097-1104.
28. Green, M. A.; Welch, M. J., Gallium radiopharmaceutical chemistry. *Int J Rad Appl Instrum B* **1989**, 16, (5), 435-48.
29. Green, M. A.; Welch, M. J., Gallium radiopharmaceutical chemistry *Nuclear Medicine and Biology* **1989**, 16, (5), 435-&.

30. Moerlein, S. M.; Welch, M. J., The chemistry of gallium and indium as related to radiopharmaceutical production. *International Journal of Nuclear Medicine & Biology* **1981**, 8, (4), 277-287.
31. Reichert, D. E.; Lewis, J. S.; Anderson, C. J., Metal complexes as diagnostic tools. *Coordination Chemistry Reviews* **1999**, 184, 3-66.
32. Mintun, M. A.; Dennis, D. R.; Welch, M. J.; Mathias, C. J.; Schuster, D. P., Measurements of pulmonary vascular-permeability with pet and Ga-68 transferrin. *Journal of Nuclear Medicine* **1987**, 28, (11), 1704-1716.
33. Tsang, B. W.; Mathias, C. J.; Green, M. A., A Ga-68 radiopharmaceutical that is retained in myocardium - Ga-68[(4,6-MEO<sub>2</sub>SAL)<sub>2</sub>BAPEN]<sup>+</sup>. *Journal of Nuclear Medicine* **1993**, 34, (7), 1127-1131.
34. Madsen, S. L.; Welch, M. J.; Motekaitis, R. J.; Martell, A. E., <sup>68</sup>GaTHM<sub>2</sub>BED: a potential generator-produced tracer of myocardial perfusion for positron emission tomography. *Int J Rad Appl Instrum B* **1992**, 19, (4), 431-44.
35. Smithjones, P. M.; Stolz, B.; Bruns, C.; Albert, R.; Reist, H. W.; Fridrich, R.; Macke, H. R., Gallium-67/Gallium-68-[DFO]-octreotide - a potential radiopharmaceutical for pet imaging of somatostatin receptor-positive tumors - synthesis and radiolabeling in-vitro and preliminary in-vivo studies. *Journal of Nuclear Medicine* **1994**, 35, (2), 317-325.
36. Welch, M. J.; Thakur, M. L.; Coleman, R. E.; Patel, M.; Siegel, B. A.; Terpogossian, M. M., Ga-68 labeled red-cells and platelets new agents for positron tomography. *Journal of Nuclear Medicine* **1977**, 18, (6), 558-562.

37. Brown, L. C.; Beets, A. L., Cyclotron production of carrier-free indium-111. *International Journal of Applied Radiation and Isotopes* **1972**, 23, (2), 57-&.
38. Albert, R.; Smith-Jones, P.; Stolz, B.; Simeon, C.; Knecht, H.; Bruns, C.; Pless, J., Direct synthesis of [DOTA-DPhe(1)]-octreotide and [DOTA-DPhe(1),Tyr(3)]-octreotide (SMT487): Two conjugates for systemic delivery of radiotherapeutical nuclides to somatostatin receptor positive tumors in man. *Bioorganic & Medicinal Chemistry Letters* **1998**, 8, (10), 1207-1210.
39. Schottelius, M.; Schwaiger, M.; Wester, H. J., Rapid and high-yield solution-phase synthesis of DOTA-Tyr(3)-octreotide and DOTA-Tyr(3)-octreotate using unprotected DOTA. *Tetrahedron Letters* **2003**, 44, (11), 2393-2396.
40. De Leon-Rodriguez, L. M.; Kovacs, Z., The synthesis and chelation chemistry of DOTA-peptide conjugates. *Bioconjugate Chemistry* **2008**, 19, (2), 391-402.
41. Liu, S.; He, Z. J.; Hsieh, W. Y.; Fanwick, P. E., Synthesis, characterization, and X-ray crystal structure of In(DOTA-AA) (AA = p-aminoanilide): A model for In-111-labeled DOTA-biomolecule conjugates. *Inorganic Chemistry* **2003**, 42, (26), 8831-8837.
42. Wild, D.; Schmitt, J. S.; Ginj, M.; Macke, H. R.; Bernard, B. F.; Krenning, E.; de Jong, M.; Wenger, S.; Reubi, J. C., DOTA-NOC, a high-affinity ligand of somatostatin receptor subtypes 2, 3 and 5 for labelling with various radiometals. *European Journal of Nuclear Medicine and Molecular Imaging* **2003**, 30, (10), 1338-1347.
43. Dijkgraaf, I.; Rijnders, A. Y.; Soede, A.; Dechesne, A. C.; van Esse, G. W.; Brouwer, A. J.; Corstens, F. H. M.; Boerman, O. C.; Rijkers, D. T. S.; Liskamp,

- R. M. J., Synthesis of DOTA-conjugated multivalent cyclic-RGD peptide dendrimers via 1,3-dipolar cycloaddition and their biological evaluation: implications for tumor targeting and tumor imaging purposes. *Organic & Biomolecular Chemistry* **2007**, 5, (6), 935-944.
44. Okarvi, S. M., Recent progress in fluorine-18 labelled peptide radiopharmaceuticals. *European Journal of Nuclear Medicine* **2001**, 28, (7), 929-938.
45. Vaidyanathan, G.; Zalutsky, M. R., Fluorine-18-labeled [Nle(4),D-Phe(7)]-alpha-MSH, an alpha-melanocyte stimulating hormone analogue. *Nuclear Medicine and Biology* **1997**, 24, (2), 171-178.
46. Vaidyanathan, G.; Zalutsky, M. R., F-18 labeled chemotactic peptides - a potential approach for the pet imaging of bacterial-infection. *Nuclear Medicine and Biology* **1995**, 22, (6), 759-764.
47. Johnstrom, P.; Aigbirhio, F. I.; Clark, J. C.; Pickard, J. D.; Davenport, A. P., F-18 labelling and in vitro evaluation of BQ3020, the first PET ligand synthesised for the endothelin receptor. *Journal of Labelled Compounds and Radiopharmaceuticals* **1999**, 42, (SUPPL. 1), S105-S107.
48. Fredriksson, A.; Johnstrom, P.; Stone-Elander, S.; Jonasson, P.; Nygren, P. A.; Ekberg, K.; Johansson, B. L.; Wahren, J., Preparation of radiolabelled human C-peptide by conjugation with N-succinimidyl-4-(18F)fluorobenzoate. *Journal of Labelled Compounds and Radiopharmaceuticals* **1999**, 42, (SUPPL. 1), S546-S548.



49. Wilchek, M.; Knudsen, K. L.; Miron, T., Improved method for preparing n-hydroxysuccinimide ester-containing polymers for affinity-chromatography. *Bioconjugate Chemistry* **1994**, 5, (5), 491-492.
50. Scheunemann, M.; Maeding, P.; Steinbach, J.; Bergmann, R.; Iterbeke, K.; Tourwe, D.; Johannsen, B., Fluorine-18 labelling of neurotensin analogues for the development of tumour imaging agents. *Journal of Labelled Compounds and Radiopharmaceuticals* **1999**, 42, (SUPPL. 1), S713-S714.
51. Haubner, R.; Wester, H. J.; Mang, C.; Senekowitsch-Schmidtke, R.; Kessler, H.; Schwaiger, H., Synthesis and first evaluation of a [F-18]SAA-labeled RGD-peptide for monitoring the alpha(v)beta(3)integrin expression. *Journal of Nuclear Medicine* **2000**, 41, (5), 162.
52. Sutcliffe-Goulden, J. L.; O'Doherty, M. J.; Marsden, P. K.; Hart, I. R.; Marshall, J. F.; Bansal, S. S., Rapid solid phase synthesis and biodistribution of F-18-labelled linear peptides. *European Journal of Nuclear Medicine and Molecular Imaging* **2002**, 29, (6), 754-759.
53. Guhlke, S.; Coenen, H. H.; Stocklin, G., Fluoroacylation agents based on small nca [F-18] fluorocarboxylic acids. *Applied Radiation and Isotopes* **1994**, 45, (6), 715-727.
54. Block, D.; Coenen, H. H.; Stocklin, G., NCA F-18-fluoroacylation via fluorocarboxylic acid-esters. *Journal of Labelled Compounds & Radiopharmaceuticals* **1988**, 25, (2), 185-200.
55. Shai, Y.; Kirk, K. L.; Channing, M. A.; Dunn, B. B.; Lesniak, M. A.; Eastman, R. C.; Finn, R. D.; Roth, J.; Jacobson, K. A., F-18-labeled insulin - a prosthetic

- group methodology for incorporation of a positron emitter into peptides and proteins. *Biochemistry* **1989**, 28, (11), 4801-4806.
56. Wester, H. J.; Schottelius, M., Fluorine-18 labeling of peptides and proteins. *Ernst Schering Res Found Workshop* **2007**, (62), 79-111.
57. Shiue, C. Y.; Wolf, A. P.; Hainfeld, J. F., Synthesis of fluorine-18 labelled n-p fluorine-18 fluorophenylmaleimide and its derivatives for labeling monoclonal antibody with fluorine-18. *Journal of Labelled Compounds and Radiopharmaceuticals* **1989**, 26, 287-289.
58. Wester, H. J.; Hamacher, K.; Stocklin, G., A comparative study of NCA fluorine-18 labeling of proteins via acylation and photochemical conjugation. *Nuclear Medicine and Biology* **1996**, 23, (3), 365-372.
59. Madsen, K.; Knudsen, L. B.; Agersoe, H.; Nielsen, P. F.; Thogersen, H.; Wilken, M.; Johansen, N. L., Structure-activity and protraction relationship of long-acting glucagon-like peptide-1 derivatives: Importance of fatty acid length, polarity, and bulkiness. *Journal of Medicinal Chemistry* **2007**, 50, (24), 6126-6132.
60. Xiao, Q.; Giguere, J.; Parisien, M.; Jeng, W.; St-Pierre, S. A.; Brubaker, P. L.; Wheeler, M. B., Biological activities of glucagon-like peptide-1 analogues in vitro and in vivo. *Biochemistry* **2001**, 40, (9), 2860-2869.
61. Kim, J. G.; Baggio, L. L.; Bridon, D. P.; Castaigne, J. P.; Robitaille, M. F.; Jette, L.; Benquet, C.; Drucker, D. J., Development and characterization of a glucagon-like peptide 1-albumin conjugate - The ability to activate the glucagon-like peptide 1 receptor in vivo. *Diabetes* **2003**, 52, (3), 751-759.

62. Lee, S. H.; Lee, S.; Youn, Y. S.; Na, D. H.; Chae, S. Y.; Byun, Y.; Lee, K. C., Synthesis, characterization, and pharmacokinetic studies of PEGylated glucagon-like peptide-1. *Bioconjugate Chemistry* **2005**, 16, (2), 377-382.
63. Knudsen, L. B.; Nielsen, P. F.; Huusfeldt, P. O.; Johansen, N. L.; Madsen, K.; Pedersen, F. Z.; Thogersen, H.; Wilken, M.; Agerso, H., Potent derivatives of glucagon-like peptide-1 with pharmacokinetic properties suitable for once daily administration. *Journal of Medicinal Chemistry* **2000**, 43, (9), 1664-1669.
64. Aldrich, J. V.; Kumar, V. Methods of synthesizing and using derivatives of [2-(2-aminoethoxy(ethoxy) acetic acid 7038078, 2006.
65. Adelhorst, K.; Hedegaard, B. B.; Knudsen, L. B.; Kirk, O., Structure-activity studies of glucagon-like peptide-1. *Journal of Biological Chemistry* **1994**, 269, (9), 6275-6278.
66. Leger, R.; Thibaudeau, K.; Robitaille, M.; Quraishi, O.; van Wyk, P.; Bousquet-Gagnon, N.; Carette, J.; Castaigne, J. P.; Bridon, D. P., Identification of CJC-1131-albumin bioconjugate as a stable and bioactive GLP-1(7-36) analog. *Bioorganic & Medicinal Chemistry Letters* **2004**, 14, (17), 4395-4398.
67. Wettergren, A.; Schjoldager, B.; Mortensen, P. E.; Myhre, J.; Christiansen, J.; Holst, J. J., Truncated GLP-1 (Proglucagon 78-107-amide) inhibits gastric and pancreatic functions in man. *Digestive Diseases and Sciences* **1993**, 38, (4), 665-673.
68. Szilagyi, E.; Toth, E.; Kovacs, Z.; Platzek, J.; Raduchel, B.; Brucher, E., Equilibria and formation kinetics of some cyclen derivative complexes of lanthanides. *Inorganica Chimica Acta* **2000**, 298, (2), 226-234.

69. Neidigh, J. W.; Fesinmeyer, R. M.; Prickett, K. S.; Andersen, N. H., Exendin-4 and glucagon-like-peptide-1: NMR structural comparisons in the solution and micelle-associated states. *Biochemistry* **2001**, 40, (44), 13188-13200.
70. Andersen, N. H.; Brodsky, Y.; Neidigh, J. W.; Prickett, K. S., Medium-dependence of the secondary structure of exendin-4 and glucagon-like-peptide-1. *Bioorganic & Medicinal Chemistry* **2002**, 10, (1), 79-85.
71. Miranda, L. P.; Winters, K. A.; Gegg, C. V.; Patel, A.; Aral, J.; Long, J. S.; Zhang, J. W.; Diamond, S.; Guido, M.; Stanislaus, S.; Ma, M.; Li, H. Y.; Rose, M. J.; Poppe, L.; Veniant, M. M., Design and synthesis of conformationally constrained glucagon-like peptide-1 derivatives with increased plasma stability and prolonged in vivo activity. *Journal of Medicinal Chemistry* **2008**, 51, (9), 2758-2765.
72. Moens, K.; Heimberg, H.; Flamez, D.; Huypens, P.; Quartier, E.; Ling, Z. D.; Pipeleers, D.; Gremlich, S.; Thorens, B.; Schuit, F., Expression and functional activity of glucagon, glucagon-like peptide I, and glucose-dependent insulinotropic peptide receptors in rat pancreatic islet cells. *Diabetes* **1996**, 45, (2), 257-261.
73. Dyachok, O.; Isakov, Y.; Sagetorp, J.; Tengholm, A., Oscillations of cyclic AMP in hormone-stimulated insulin-secreting beta-cells. *Nature* **2006**, 439, (7074), 349-352.
74. Behe, M.; Kluge, G.; Becker, W.; Gotthardt, M.; Behr, T. M., Use of polyglutamic acids to reduce uptake of radiometal-labeled minigastrin in the kidneys. *Journal of Nuclear Medicine* **2005**, 46, (6), 1012-1015.

75. de Jong, M.; Krenning, E., New advances in peptide receptor radionuclide therapy. *Journal of Nuclear Medicine* **2002**, 43, (5), 617-620.
76. Behr, T. M.; Sharkey, R. M.; Juweid, M. E.; Blumenthal, R. D.; Dunn, R. M.; Griffiths, G. L.; Bair, H. J.; Wolf, F. G.; Becker, W. S.; Goldenberg, D. M., Reduction of the renal uptake of radiolabeled monoclonal-antibody fragments by cationic amino-acids and their derivatives. *Cancer Research* **1995**, 55, (17), 3825-3834.
77. Pimm, M. V.; Gribben, S. J., Prevention of renal tubule reabsorption of radiometal (In-111) labeled fab fragment of a monoclonal-antibody in mice by systemic administration of lysine. *European Journal of Nuclear Medicine* **1994**, 21, (7), 663-665.
78. Kim, I. S.; Yoo, T. M.; Kobayashi, H.; Kim, M. K.; Le, N.; Wang, Q. C.; Pastan, I.; Carrasquillo, J. A.; Paik, C. H., Acylation with glycolate lowers pI of anti-Tac dsFv and reduces renal uptake of its Tc-99m label. *Journal of Labelled Compounds and Radiopharmaceuticals* **1997**, 40, 422-424.
79. Kim, I. S.; Yoo, T. M.; Kobayashi, H.; Kim, M.; Le, N.; Wang, Q.; Pastan, I.; Carrasquillo, J. A.; Paik, C. H., Chemical modification to reduce renal uptake of disulfide-bonded variable region fragment of anti-Tac monoclonal antibody labeled with Tc-99m. *Bioconjugate Chemistry* **1999**, 10, (3), 447-453.
80. Kobayashi, H.; Le, N.; Kim, I. S.; Kim, M. G.; Pie, J. E.; Drumm, D.; Paik, D. S.; Waldmann, T. A.; Paik, C. H.; Carrasquillo, J. A., The pharmacokinetic characteristics of glycolated humanized anti-Tac Fabs are determined by their isoelectric points. *Cancer Research* **1999**, 59, (2), 422-430.

81. Akizawa, H.; Arano, Y.; Mifune, M.; Iwado, A.; Saito, Y.; Mukai, T.; Uehara, T.; Ono, M.; Fujioka, Y.; Ogawa, K.; Kiso, Y.; Saji, H., Effect of molecular charges on renal uptake of In-111-DTPA-conjugated peptides. *Nuclear Medicine and Biology* **2001**, 28, (7), 761-768.
82. Miao, Y. B.; Owen, N. K.; Whitener, D.; Gallazzi, F.; Hoffman, T. J.; Quinn, T. P., In vivo evaluation of (188)re-labeled alpha-melanocyte stimulating hormone peptide analogs for melanoma therapy. *International Journal of Cancer* **2002**, 101, (5), 480-487.
83. Guhlke, S.; Wester, H. J.; Bruns, C.; Stocklin, G., (2-[F-18]Fluoropropionyl-(D)phe(1))-octreotide, a potential radiopharmaceutical for quantitative somatostatin receptor imaging with pet - synthesis, radiolabeling, in-vitro validation and biodistribution in mice. *Nuclear Medicine and Biology* **1994**, 21, (6), 819-825.
84. Hostetler, E. D.; Edwards, W. B.; Anderson, C. J.; Welch, M. J., Synthesis of 4-(18F)fluorobenzoyl octreotide and biodistribution in tumour-bearing Lewis rats. *Journal of Labelled Compounds and Radiopharmaceuticals* **1999**, 42, (SUPPL. 1), S720-S722.
85. Vaidyanathan, G.; Zalutsky, M. R., Improved synthesis of n-succinimidyl 4-[F-18]fluorobenzoate and its application to the labeling of a monoclonal-antibody fragment. *Bioconjugate Chemistry* **1994**, 5, (4), 352-356.

## **CHAPTER 3. Development of targeted Gallium-PPIX compounds for PET / Fluorescence dual modality imaging**

### **3.1 Introduction**

Molecular imaging, through non-invasive characterization and quantification of biological processes at cellular and sub-cellular levels, provides the potential for early detection and treatment evaluation of numerous disease processes. There are currently a number of imaging modalities available for such applications, however, the use of multiple modalities in conjunction has gained considerable interest as it provides more accurate results owing to the complementary abilities of imaging techniques. This is particularly important in diagnostic imaging considering that modalities with the highest sensitivity offer a relatively poor resolution, while those possessing high resolution suffer from poor sensitivity. Combining modalities provides a way to utilize the respective strengths from each technique, while circumventing shortcomings, leading to more reliable results.<sup>1</sup>

Considering that each modality requires its own imaging tag (eg. radioisotopes for PET, dyes for fluorescence/optical imaging, contrast agents for CT/MRI) a single imaging probe was initially required for use with each modality of interest. Following the discovery of the first fused instrument (positron emission tomography/computed tomography, or PET/CT), however, research on multimodality imaging probes expanded exponentially based on the concept that while the use of a single compound for multiple modalities is not essential for all applications, it is certainly beneficial in terms of

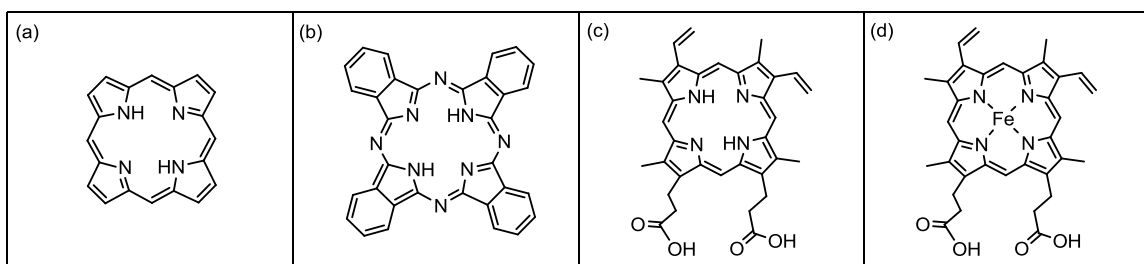
maintaining consistent pharmacokinetics and localization *in vivo*. Such agents are most commonly prepared via attachments of all required imaging tags to one molecule. Another common route is using the same core compound equipped with different tags, but synthesized individually for imaging (eg. dye-coupled compound-A vs. radiolabeled compound-A). The drawback of the first methodology is the significant structural modifications required to make a single multimodality imaging probe, which could result in changes in the expected pharmacokinetics and localization behavior of the compound. In the latter methodology, the disadvantage lies in the structural differences between probes as a result of differences in the respective imaging tags.<sup>1</sup> These structural differences, on top of altering the properties of the core molecule itself, could also lead to inconsistencies in imaging results obtained from different modalities. As a result, the development of probes that can be used for multimodality imaging without the need for further structural modification is desired. In this regard, using an identical compound for multimodality imaging would minimize discrepancies observed between modalities and, as well, aid in preserving the innate properties of the core molecule possessing the imaging tag. One class of compounds suitable for use in such applications is porphyrins.

Porphyrins, which are naturally occurring compounds shown to play an important role in living organisms, and their respective derivatives have gained considerable interest in recent years. They have been used for numerous applications, such as in light harvesting,<sup>2</sup> removal of reactive oxygen species (ROS),<sup>3</sup> methanogenesis,<sup>4</sup> electron transfer processes,<sup>5</sup> detoxification,<sup>6</sup> photodynamic therapy (PDT),<sup>7</sup> and respiration.<sup>8</sup> Two porphyrin derivatives, namely Porfimer Sodium and verteporfin are FDA-approved for PDT treatment of melanoma, as well as a number of cancers including those of lung,



digestive tract and genitourinary tract.<sup>7, 9</sup> Nuclear medicine, however, most commonly utilizes the optical properties of porphyrins as magnetic resonance imaging (MRI) contrast agents.<sup>10</sup>

Structurally, the porphyrin nucleus consists of four pyrrole rings connected by methine groups (Figure 3.1a). This ring system is very stable and exhibits aromatic characteristics. Functionalization of this ring leads to formation of other classes of porphyrins such as phthalocyanines (Figure 3.1b). Porphines typically exhibit a central cavity measuring approximately 4.1 Å in diameter, which is sufficient for coordination of a metal ion.<sup>11</sup> Transition metals have previously been reported to form very stable complexes with porphyrin rings (eg. Zn-TPP).<sup>12</sup> Examples of such complexes are naturally present in biological systems, such as haemoproteins (containing iron), chlorophylls (containing magnesium), and Vitamin B<sub>12</sub> (containing cobalt).<sup>13</sup>



**Figure 3.1** Structures of (a) porphine, (b) phthalocyanine, (c) protoporphyrin IX, and (d) heme.

One of the most abundant porphyrins is protoporphyrin (IX) (PPIX), which is naturally produced in the heme cycle and is the direct precursor of heme, with an iron core being the only differentiating factor between the two molecules (Figure 3.1c,d).

PPIX, having various applications, is most commonly used as a photosensitizer (produced by exogenous administration of aminolevulinic acid) in PDT for treatment of skin premalignant and malignant lesions.<sup>14, 15</sup> This compound has also been shown to exhibit anti-bacterial and anti-malarial activity *in vitro*.<sup>16, 17</sup> Furthermore, a recent study has reported the use of peptide conjugated PPIX as a potential probe for anti-cancer treatment.<sup>18</sup> The authors reported that the attachment of a targeting moiety did not affect the overall efficacy of PPIX, but did significantly improve its targeting and localization capabilities.

Considering the favourable fluorescence properties of porphyrins and that the porphine ring system exhibits a spatially appropriate central cavity for metal chelation, here we report the development of gallium-PPIX compounds as single molecular entities with potential application for both fluorescence microscopy and positron emission tomography (PET) imaging, without the need for further structural modification. The porphyrin ring, in this case, will act as both the fluorescent tag as well as the metal chelator, thus allowing for the same identical molecule to be used in conjunction with different modalities. The use of an identical molecule will preserve the characteristics of the core compound while reducing any inconsistencies observed in between modalities. The targeting entity was selected to be an RGD motif which has been well studied and proven to target the  $\alpha_v\beta_3$  receptors typically over-expressed in a number of cancers such as breast,<sup>19</sup> ovarian,<sup>20, 21</sup> and melanomas.<sup>22, 23</sup> The radiometal of choice was gallium-68, which is a generator produced PET radioisotope with a 68 min half-life and 89% positron abundance accompanied by low photon emission (1.077 MeV, 3.2%). The use of this radioisotope has gained considerable interest in recent years owing to improvements in

the performance of commercially available  $^{68}\text{Ge}/^{68}\text{Ga}$  generators.<sup>24-26</sup> In this paper, we report the synthesis, characterization, optical analysis, radiolabeling and *in vitro* evaluation of Ga-PPIX-RGD compounds as proof of concept for the use of porphyrins as nuclear/fluorescence dual modality imaging agents.

## 3.2 Experimental

Common solvents and reagents were purchased from VWR, Fisher Scientific, or Sigma-Aldrich and used as received, unless stated otherwise. Sterile, deionized water was used in all aqueous procedures. All Fmoc protected amino acids and coupling agents, except Fmoc-Lys(mtt)-OH (Nova Biochem), HATU (Nova Biochem), and HBTU were obtained from Peptides International. Fmoc-Rink amide MBHA resin (4-(2',4'-dimethoxyphenyl)-(9-fluorenylmethoxycarbonyl)-aminomethyl)-phenoxy-acetamidonorleucyl-4-methyl benzhydrylamine resin) was obtained from Nova Biochem. PPIX was obtained from Sigma-Aldrich. The hydrophilic linker AEEA was synthesized in our laboratory according to a previously published procedure.<sup>27</sup> RP-C18 Sep-Pak SPE cartridges were obtained from Waters.  $^{68}\text{Ge}$ - $^{68}\text{Ga}$  generator was obtained from Eckert and Ziegler.

### 3.2.1 Peptide Syntheses

Fmoc-based solid-phase peptide synthesis was carried out manually with 0.05 meq of 0.45 mmol/g Fmoc-Rink amide MBHA resin and a 3-fold excess of the protected amino acids. Fmoc removal, carried out with 20% piperidine in DMF (*N,N*-dimethylformamide) over two cycles (10 and 20 min), was followed by amino acid

activation with 3 eq HBTU and 6 eq DIPEA (*N,N*-diisopropylethylamine) (10 min) and subsequent coupling over 30 and 120 min cycles.

Coupling of AEEA to N-terminus of peptides followed the same methodology used in amino acid coupling, however, reaction time was increased to 16 hours. Coupling of PPIX was carried out using HATU, in a solution of 1:1:1 (v:v:v) DCM:DMF:DMSO and over 24 hours. Microcleaved samples were used to monitor reaction progress and peptide purity via HPLC.

Full deprotection of synthesized peptides was accomplished using a solution of 88% TFA (v/v), 5% H<sub>2</sub>O (v/v), 5% phenol (m/v), 2% triisopropylsilane (v/v) over 6 hours. The cleaved peptides were then precipitated using *tert*-butyl methyl ether (TBME) and centrifuged at 2200 rpm for 15 min. After decanting, the peptide pellet was rinsed with TBME, vortexed and centrifuged again. Following the removal of the supernatant, the peptide pellets were dissolved in water, frozen at 78 °C and lyophilized overnight.

In preparing the cyclic peptide, cRGDfV, the straight sequence was initially synthesized using standard Fmoc-based solid phase synthesis on 0.05 meq of 0.40 mmol/g Fmoc-Alloc(Wang resin)-OAll resin. Allyl ester deprotection was achieved using 20 eq PhSiH<sub>3</sub> and 0.25 eq of Pd(PPh<sub>3</sub>)<sub>4</sub> in dry DCM. Following Fmoc removal, the chain was cyclized on resin using 4 eq of HATU over 4 hours. Cleavage and full deprotection of peptides followed the above mentioned procedures.

### 3.2.2 Purification by RP-HPLC / ESI-MS

Peptides were analyzed using a reverse-phase analytical HPLC column (Sunfire™ RP-C18 column 4.6 x 150 mm, 5 μm). This system was equipped with a Waters 600

controller, Waters Prep degasser, and Waters MassLynx software (version 4.1). Employed mobile phases were 0.1% CF<sub>3</sub>CO<sub>2</sub>H in water (eluent A) and 0.1% CF<sub>3</sub>CO<sub>2</sub>H in CH<sub>3</sub>CN (eluent B). The linear gradient used was 30-50% of B with a flow rate of 1.5 mL min<sup>-1</sup> over 20 min. The column eluate was monitored using a Waters 2998 Photodiode array detector set at 220, 254 and 400 nm.

Peptides were purified using a reverse-phase preparative HPLC column (Sunfire<sup>TM</sup> Prep RP-C18 OBD<sup>TM</sup> column 19 x 150 mm, 5 μm) on the same system mentioned above. The detection method along with eluents and gradients were the same as those stated above, with the exception of the flow rate being set at 20 mL min<sup>-1</sup>. The collected fraction was then lyophilized to a solid and subsequently analyzed by ESI-MS (electrospray ionization mass spectrometry) (Waters Micromass Quattro Micro<sup>TM</sup> API). Purity of final products was determined by analytical RP-HPLC.

### 3.2.3 General procedure for synthesis of <sup>69/71</sup>Ga-Labeled peptides

In a typical reaction, 8 mg of the trimeric peptide, RGD, 3 mL of pH 5 NaOAc / HOAc buffer, and 5 mg of anhydrous GaCl<sub>3</sub> (4 fold excess) were placed in a 5 mL glass microwave reactor vessel. The reactants were dissolved by stirring at 25 °C over 5 min before the start of the reaction, which was carried out in a microwave reactor at 70 °C for 40 min. The resulting solution was then mixed with 10 mL of H<sub>2</sub>O, frozen at -78 °C and lyophilized overnight.

### 3.2.4 Optical Analyses

UV absorption data were obtained using a Varian Cary 300 Bio UV-VIS spectrophotometer. Excitation and Emission data were obtained using a Photon Technology International QM-4 SE spectrometer equipped with double excitation and emission monochromators. Extinction coefficients were calculated using the serial dilution methodology. For this study, UV absorptions at seven different concentrations (highest concentration having a UV absorption maxima of 1-2) were recorded per compound. The slope of the resulting graph of concentration versus absorption was then calculated in order to obtain the value for the molar extinction coefficient. All absorption, excitation, and emission wavelengths were obtained in DMSO. Quantum yields were calculated according to previously reported comparative methods (S. Fery-Forgues, D. Lavabre, *Journal of Chemical Education* **1999**, 76, 1260), using optically dilute samples (maximum UV absorption intensity 0.1-1) in EtOH and Rhodamine 6G as the standard.

### 3.2.5 Fluorescence Microscopy using $^{69/71}\text{Ga}$ -PPIX-AEEA-RGD (**8**)

MDA-MB-435 cells were released from the tissue-culture flask using trypsin and seeded onto coverslips in a 12-well tissue culture plate. The cells were incubated overnight in DMEM containing 10% FBS at 37 °C with 5% CO<sub>2</sub>. Subsequently, the serum-containing DMEM in each well was removed and replaced with serum-free DMEM. Cells were incubated with 67 μM of compound **5** (control) or **8** (probe) in a 37 °C incubator for 1 hour. Cells were then washed three times with PBS, fixed with 4% paraformaldehyde, and mounted with Prolong Gold antifade reagent containing DAPI (Invitrogen). Images were captured using the Zeiss AxioImager Z1 microscope, and the

average PPIX intensities in each cell was quantified using Volocity, version 4.0 (PerkinElmer).

### **3.2.6 Blocking of $^{69/71}\text{Ga}$ -PPIX-AEEA-RGD with cRGDfV**

MDA-MB-435-GFP cells were released from adhesion to tissue-cultured flask using EDTA. Subsequently, cells were resuspended in serum free DMEM and placed in microcentrifuge tubes. Incubation was carried out with  $67\mu\text{M}$  of **2** or **8** in suspension for 1 h at  $37\text{ }^\circ\text{C}$  at 56 rpm. Blocking studies were conducted in the presence of 5x excess of cRGDfV. Cells were washed three times with PBS by centrifugation, re-seeded onto coverslips, cultured in DMEM and allowed to adhere. Once the cells had adhered to the coverslips, they were washed once with PBS, fixed with 4% formaldehyde and mounted. Images were captured using the Zeiss AxioImager Z1 microscope. The average PPIX intensities in cells were quantified using Volocity, version 4.0 (PerkinElmer).

### **3.2.7 Radiolabeling to Prepare $^{68}\text{Ga}$ -8**

To a clean glass microwave vessel was added  $100\ \mu\text{L}$  of PPIX analogue solution ( $1\ \text{mg/mL}$  in pH 3.5 NaOAc / HOAc buffer). This aliquot was dissolved in  $900\ \mu\text{L}$  of the buffer (10 fold dilution to obtain final solution with  $\mu\text{M}$  concentrations), to which 3 mCi  $^{68}\text{GaCl}_3$  was added, freshly eluted from the Ge-68/Ga-68 generator using 3 mL of 0.1 M HCl. Purification and isolation of  $^{68}\text{Ga}$  was achieved using a Phenomenix Strata-X-C 33u polymeric strong cation exchange column ( $30\ \text{mg/mL}$ ), prior to transfer to the microwave vessel (eluent: 0.05 N HCl in Acetone). The reaction mixture was then heated in a microwave reactor at  $120\text{ }^\circ\text{C}$  for 45 minutes, before purification by semi-preparative

HPLC (Sunfire™ RP-C18 column 10 x 150 mm, 5 μm) The reaction progress and product purity was analyzed using analytical RP-HPLC (Sunfire™ RP-C18 column 4.6 x 150 mm, 5 μm) coupled to a gamma detector. This system employed a Waters 1525 Binary HPLC pump, Waters 2487 dual λ absorbance detector, Waters In-Line degasser and Breeze software (version 3.30).

### **3.3. Results and Discussion**

#### **3.3.1 Probe Design**

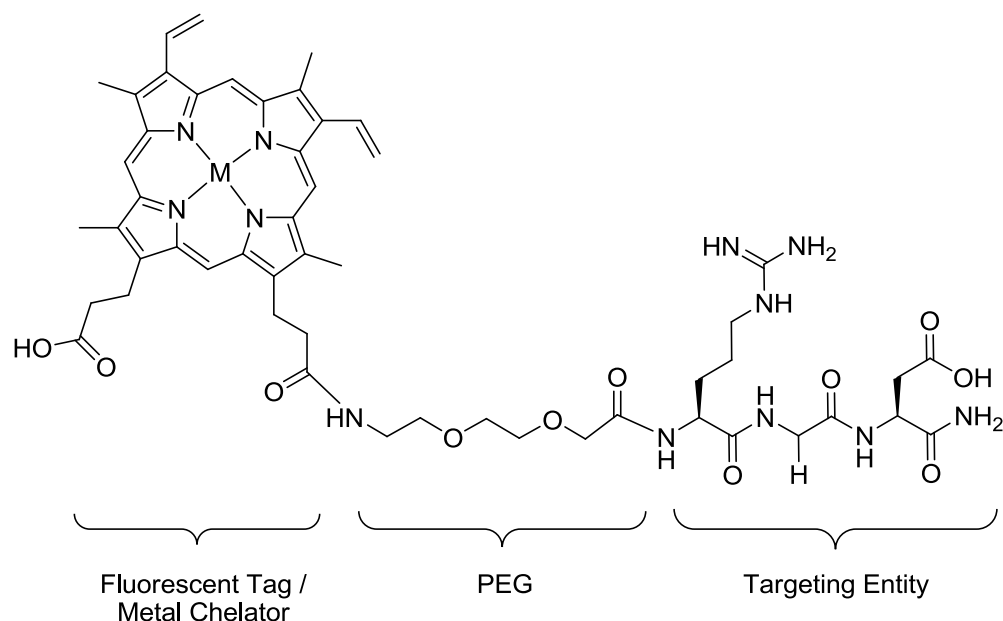
The primary objective of this project was to develop a single compound that could be used for both fluorescence and PET imaging without the need for structural modifications or attachment of multiple imaging tags. To this extent, the desired probe would employ a porphyrin ring as the inherently fluorescent metal chelator, which would be used in conjunction with a targeting entity. While PPIX has gained considerable interest owing to the versatility of its applications to various research areas, it has been underutilized as an imaging agent. This, in conjunction with its natural occurrence in biological systems, led us to select PPIX as the porphyrin ring for this study. The radiometal gallium-68, an efficient positron emitter used in conjunction with PET, was also utilized. This radiometal is produced from readily available <sup>68</sup>Ge/<sup>68</sup>Ga generators.

Considering that the focus of this project was to show the potential of porphyrins in dual modality imaging, the characteristics and behavior of the selected targeting entity had to be well known in order to reduce the number of variables affecting the outcome of this research. The tripeptide RGD was selected as the targeting entity, as it is a well established ligand for the α<sub>v</sub>β<sub>3</sub> integrin, typically over-expressed in a number of cancers



such as breast,<sup>21</sup> ovarian,<sup>20</sup> and melanomas.<sup>22, 23</sup> RGD containing compounds have been used in conjunction with several modalities such as PET (<sup>68</sup>Ga-DOTA-RGD, <sup>18</sup>F-RGD peptides),<sup>28, 29</sup> MR (Iron oxide nanoparticle-RGD, Gd-DTAP-RGD)<sup>30, 31</sup> and fluorescence imaging (quantum dot-RGD).<sup>32</sup> As a result, the RGD moiety was selected as the preferred targeting entity for the  $\alpha_v\beta_3$  receptors.

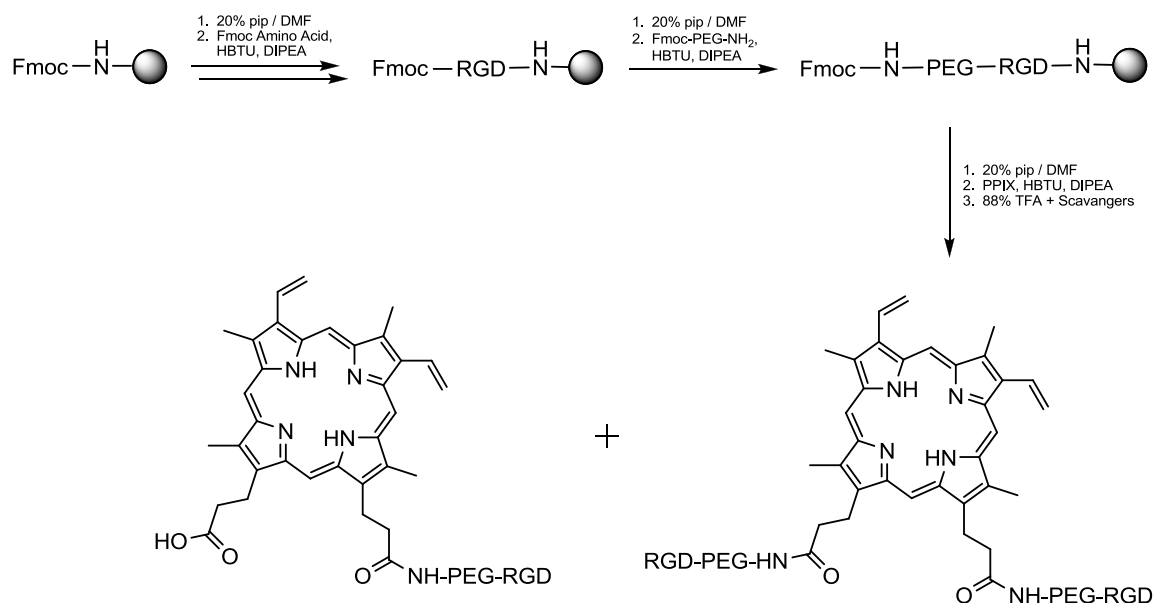
A major drawback in using porphyrin derivatives is the extreme hydrophobic nature of these compounds, which raises numerous challenges in their handling due to significantly reduced product solubility. As a result, a short polyethyleneglycol (PEG) chain was added between PPIX and RGD in order to enhance the overall solubility of the compound. The PEG linker of choice was Fmoc-AEEA, which was synthesized according to a previously published procedure.<sup>27</sup> The overall design of the probe is shown in Figure 3.2.



**Figure 3.2** Structure of the proposed imaging probe.

### 3.3.2 Synthesis of $^{69/71}\text{Ga}$ -PPIX analogues

RGD peptides were synthesized manually using standard Fmoc-SPPS methods. An example of this methodology is illustrated in Scheme 3.1. Typical yields, obtained post HPLC-purification, were 60-70% with purities over 95%. It is important to note that the formation of both PPIX-AEEA-RGD and PPIX-(AEEA-RGD)<sub>2</sub> analogues was observed at the end of the reaction. This was beneficial as this project initially aimed at studying both of these compounds in order to examine any advantages associated with having multiple targeting moieties present on the imaging probe. Use of PPIX was also advantageous towards simplifying this synthetic route due to the presence of two free carboxylic acids available for acylation. A drawback of this protocol, however, was the lack of regioselectivity involved with the acylation of PPIX, as two regioisomers could be produced. Although these isomers cannot be separated due to their very similar physical characteristics, their presence is not likely to alter the overall localization or fluorescence of PPIX conjugates in cancer cells.<sup>18</sup> As a result, other porphyrin rings could be employed if a single specific regioisomer is desired (eg. in drug development). Considering that this project also aimed to study the effects of peptide and linker addition on the optical properties of PPIX, eight PPIX analogues were synthesized containing one or more linker/peptide moieties in addition to their gallium-labeled counterparts. The purity and ESI-MS characterization of the prepared compounds are given in Table 3.1.

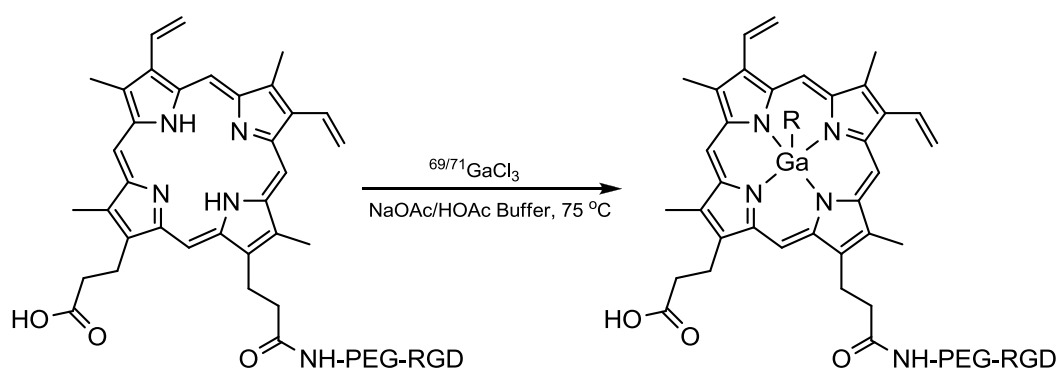


**Scheme 3.1** Synthetic pathway for the preparation of PPIX-AEEA-RGD analogues.

#	Compound	Purity (%)	Calculated m/z	Observed m/z
2	PPIX-AEEA	97.0	709.4 [M+H] <sup>+</sup>	709.2 [M+H] <sup>+</sup>
3	PPIX-(AEEA) <sub>2</sub>	96.0	853.5 [M+H] <sup>+</sup>	853.4 [M+H] <sup>+</sup>
4	PPIX-AEEA-RGD	95.0	1037.5 [M+H] <sup>+</sup>	1037.7 [M+H] <sup>+</sup>
5	PPIX-(AEEA-RGD) <sub>2</sub>	97.0	755.7 [M+2H] <sup>2+</sup>	756.6 [M+2H] <sup>2+</sup>
6	<sup>69/71</sup> Ga-PPIX-AEEA	98.0	775.3 [M+H] <sup>+</sup>	775.4 [M+H] <sup>+</sup>
7	<sup>69/71</sup> Ga-PPIX-(AEEA) <sub>2</sub>	97.0	919.3 [M+H] <sup>+</sup>	919.4 [M+H] <sup>+</sup>
8	<sup>69/71</sup> Ga-PPIX-AEEA-RGD	98.0	1104.4 [M+H] <sup>+</sup>	1104.9 [M+H] <sup>+</sup>
9	<sup>69/71</sup> Ga-PPIX-(AEEA-RGD) <sub>2</sub>	98.0	790.3 [M+H+Na] <sup>2+</sup>	790.3 [M+H+Na] <sup>2+</sup>

**Table 3.1** Analysis of synthesized PPIX-RGD analogues by RP-HPLC and ESI-MS.

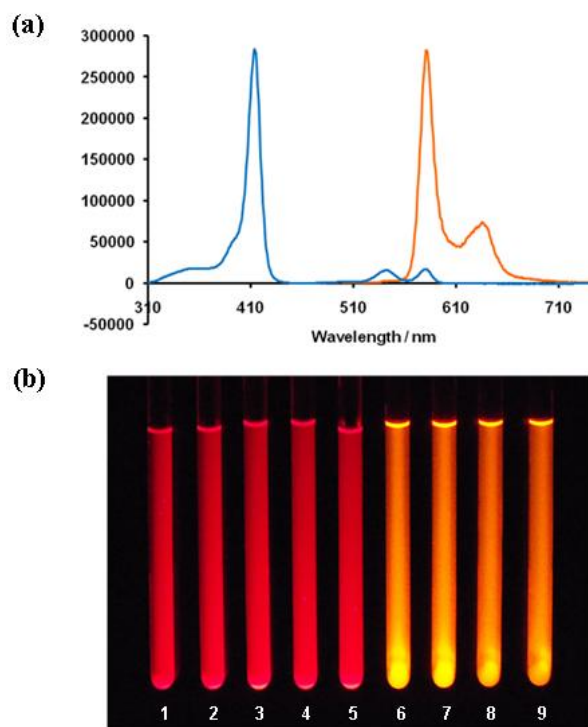
Chelation of naturally occurring gallium (Scheme 3.2) was carried out in order to prepare non-radioactive compounds for *in vitro* imaging, optical analysis, preparation of HPLC standards and determination of radiolabeling conditions, while preventing unnecessary radiation exposure. Chelation of a metal ion to the porphyrin central cavity requires high reaction temperatures. Metal chelation reactions of porphyrins using conventional heating methods have been reported to require very long reaction times, often continuing overnight at elevated temperatures.<sup>33</sup> Microwave reactors, however, have been reported to facilitate metal chelation reactions leading to significantly reduced reaction times.<sup>34-37</sup> As a result, this study employed the use of a microwave reactor in order to facilitate reaction rates. In addition, a pH 3.5 sodium acetate/acetic acid buffer was employed in order to minimize formation of insoluble gallium hydrolysis products.<sup>38</sup> It was noted that chelation efficiencies improved with increasing reaction time, reaching 95% completion after 40 minutes of heating at 75°C. Products were purified using preparative HPLC and subsequently analyzed using ESI-MS.



**Scheme 3.2** Synthetic scheme for the preparation of  $^{69/71}\text{Ga}$ -PPIX-AEEA-RGD.

### 3.3.3 Optical Analysis

Optical properties of compounds **2-9** was studied and compared to the parent compound PPIX (**1**) in order to evaluate the potential for fluorescence microscopy. The observed excitation and emission wavelengths (Figure 3.3) are reported in Table 3.2. Both peptide/linker conjugation as well as gallium-chelation caused a blue shift in the excitation wavelengths from 467 nm for native PPIX to 429-437 nm for gallium coordinated **6-9**. A similar trend was observed for emission maxima with an approximate wavelength decrease of 50 nm from PPIX to the gallium congener. Maximum absorbance wavelengths did not change significantly ( $\Delta\lambda \sim 7$  nm post gallium chelation), while extinction coefficients were affected by gallium chelation with a greater than two-fold increase. The quantum yields were consistent pre and post gallium chelation, indicating that metal-dependent fluorescence-quenching is minimal in these compounds. This is a particularly important observation since a number of other metals (eg. Mg, Sn, Zn) were recently reported to quench the fluorescence of PPIX with quantum yields dropping below 5%,<sup>39</sup> while the quantum yields for **6-9** are maintained above 30% (Table 3.2).



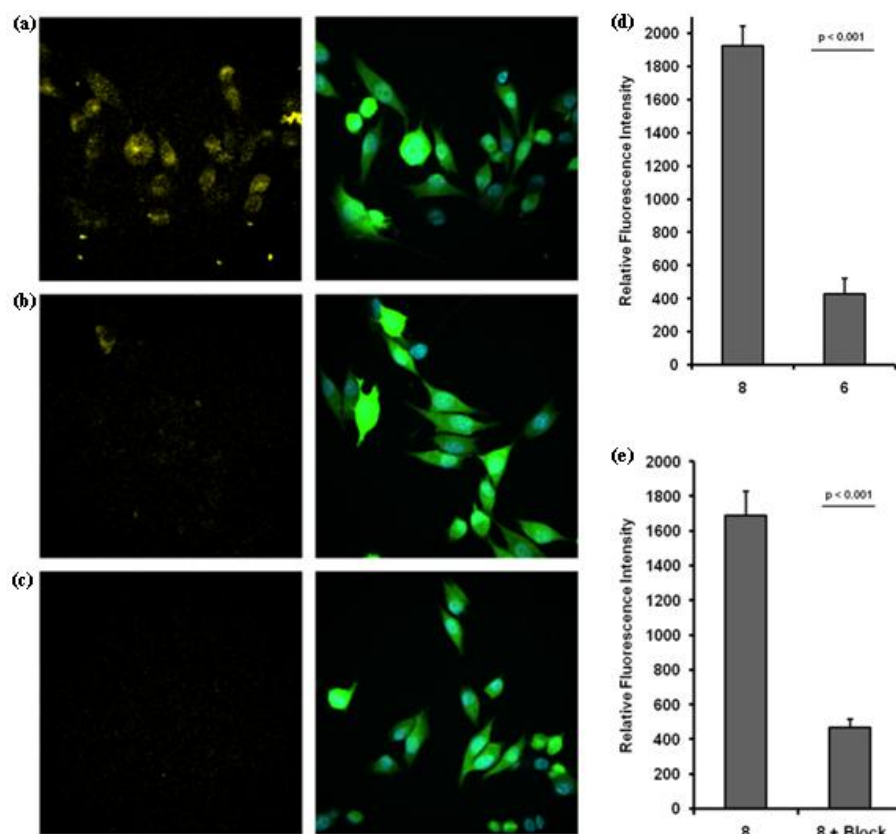
**Figure 3.3** (a) absorption (blue) / emission (orange) data obtained for **8**; (b) photo of visible emission of **1-9** under 365 nm light.

#	Compound	$\lambda_{\text{ex}}$ (nm)	$\lambda_{\text{em}}$ (nm)	$\lambda_{\text{abs}}$ (nm)	$\epsilon$ ( $\text{M}^{-1}$ )	$\Phi$
1	PPIX	467	638	406	17377	0.37
2	PPIX-AEEA	467	638	407	11415	0.34
3	PPIX-(AEEA) <sub>2</sub>	467	635	407	12554	0.32
4	PPIX-AEEA-RGD	441	633	407	15120	0.42
5	PPIX-(AEEA-RGD) <sub>2</sub>	446	632	407	11559	0.31
6	<sup>69/71</sup> Ga-PPIX-AEEA	414	585	414	42550	0.49
7	<sup>69/71</sup> Ga-PPIX-(AEEA) <sub>2</sub>	420	584	415	41599	0.33
8	<sup>69/71</sup> Ga-PPIX-AEEA-RGD	437	593	414	32226	0.42
9	<sup>69/71</sup> Ga-PPIX-(AEEA-RGD) <sub>2</sub>	429	585	413	47661	0.49

**Table 3.2** Photophysical data for PPIX derivatives **1-9**: excitation, emission, absorbance maxima wavelengths, extinction coefficients and quantum yields (experimental details provided in Supplementary Information).

### 3.3.4 *In Vitro* Imaging

In order to demonstrate the potential of these analogues for fluorescence imaging, **8** was evaluated *in vitro* using the MDA-MB-435 cancer cell line, which over-expresses the  $\alpha_v\beta_3$  integrin. For this study compound **6** was selected as the negative control, which is identical to compound **8** with the exception of lacking the RGD targeting moiety. After incubation of **8** with cells, and subsequent washing, confocal microscopy images were obtained. The cellular uptake of compound **8** was statistically significant and visually pronounced, while the signal from the negative control was nominal, with approximately a 4:1 signal ratio between **8** and **6** (Figure 3.4). Compounds **7** and **9** were very hydrophobic and therefore were not evaluated *in vitro*. In order to confirm specific uptake of **8** to MDA-MB-435 cells, a blocking experiment was carried out using a cyclic RGD pentapeptide, cRGDfV, which has high affinity for the  $\alpha_v\beta_3$  integrin.<sup>40</sup> The statistically significant displacement of **8** by the blocking moiety demonstrated specific binding of the probe to the MDA-MB-435 cell line, therefore confirming the specificity of **8** for the integrin target.

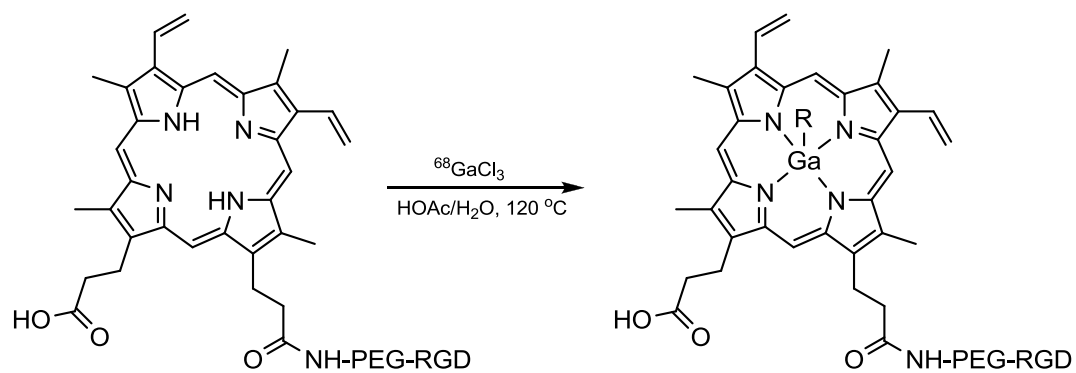


**Figure 3.4** Fluorescence microscopy of **8** in GFP-expressing MDA-MB-435 cells: (a) uptake of **8** indicated in yellow (left panel), GFP-expressing cells in green and DAPI stained nuclei in blue (right panel); (b) uptake of negative control **6** in yellow (left panel); (c) cells with no treatment (left panel); (d) quantified data for uptake of targeted **8** vs non-targeted **6**; (e) quantified data for uptake of **8** vs uptake of **8** in cells treated simultaneously with cRGDfV peptide (block).

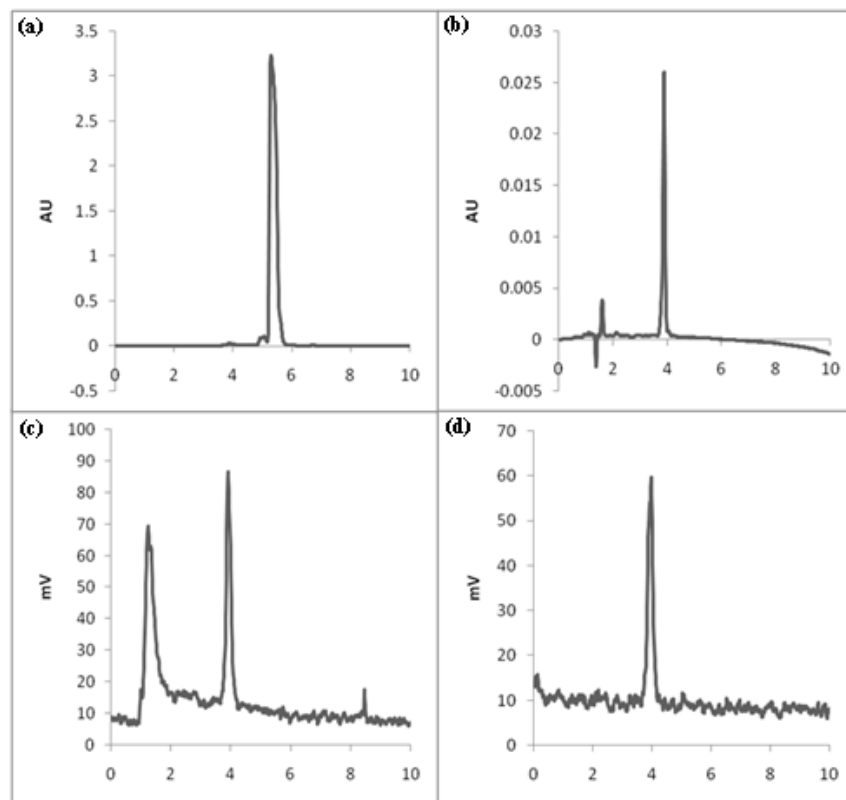


### 3.3.5 <sup>68</sup>Ga-Labeling

Radiolabeling of compound **7** with gallium-68 was carried out in a microwave reactor according to Scheme 3.3. Optimal reaction conditions were found to employ a pH 4.5 HOAc/H<sub>2</sub>O solution with a 45 minute reaction time at 120 °C. The decay corrected radiochemical yields were typically 30-35% with radiochemical purity >98%. In theory, chelation efficiency of porphyrins could be improved with increasing reaction periods and temperatures. In this case, however, peptide instability and hydrolysis of free gallium-68 were observed with further increment in both variables. Monitoring of reaction progress as well as characterization of the radiolabeled products was carried out using RP-HPLC with utilization of compound **7** as the non-radioactive standard. The desired <sup>68</sup>Ga-labeled product was identified by chromatographic comparison of retention times between radiolabeled and non-radioactive compounds. Figure 3.4 shows representative UV and radiochromatograms corresponding to this reaction. It is important to note that there is a retention time difference of 1.5 minutes between starting material PPIX-AEEA-RGD and final product <sup>68</sup>Ga-PPIX-AEEA-RGD, thus facilitating their separation by RP-HPLC at the end of reaction. It is also worth noting that the final product can also be purified using a RP-C18 Sep-pak®. In summary, this study further confirms the ability of PPIX to act as a gallium-68 radiometal chelator, as well as the potential of this probe as a PET imaging agent.



**Scheme 3.3** Radiolabeling scheme for compound **8**.



**Figure 3.5** The HPLC (a) UV chromatogram of the standard unlabeled **4**; (b) UV chromatogram of [ $^{69/71}\text{Ga}$ ]-**8**; (c) radiochromatogram of the reaction mixture pre-purification; and (d) radiochromatogram of [ $^{68}\text{Ga}$ ]-**8** post purification.

### 3.4 Conclusion

The aim of this study was to develop porphyrin-based analogues as dual modality fluorescence/PET imaging agents without requiring the attachment of multiple imaging tags to the molecule. To that end, we have developed derivatives of PPIX-RGD which can be used for both fluorescence and PET imaging without the need for modification. Metal chelation conditions were optimized for gallium labeling (both radioactive and naturally occurring) and the coordination with gallium produced strongly fluorescent molecules with quantum yields of >30%. The versatility of this approach permits the use of different targeting entities based on the desired biological target, while allowing for progression from *in vitro* evaluation (fluorescence) through to *in vivo* imaging (PET), with consistent imaging results between modalities.

### 3.5 References

1. Louie, A. Y., Multimodality Imaging Probes: Design and Challenges. *Chemical Reviews* **2010**, 110, (5), 3146-3195.
2. Nam, Y. S.; Shin, T.; Park, H.; Magyar, A. P.; Choi, K.; Fantner, G.; Nelson, K. A.; Belcher, A. M., Virus-Templated Assembly of Porphyrins into Light-Harvesting Nanoantennae. *Journal of the American Chemical Society* **132**, (5), 1462-+.

3. Khan, I.; Batinic-Haberle, I.; Benov, L. T., Effect of potent redox-modulating manganese porphyrin, MnTM-2-PyP, on the Na<sup>+</sup>/H<sup>+</sup> exchangers NHE-1 and NHE-3 in the diabetic rat. *Redox Report* **2009**, 14, (6), 236-242.
4. Zimmer, M.; Crabtree, R. H., Bending of the reduced porphyrin of factor F430 can accommodate a trigonal-bipyramidal geometry at nickel - a conformational-analysis of this nickel-containing tetrapyrrole, in relation to archaeobacterial methanogenesis. *Journal of the American Chemical Society* **1990**, 112, (3), 1062-1066.
5. Sadamoto, R.; Tomioka, N.; Aida, T., Photoinduced electron transfer reactions through dendrimer architecture. *Journal of the American Chemical Society* **1996**, 118, (16), 3978-3979.
6. Moser, J. G., Porphyrins and phthalocyanines as model compounds for detoxification of tumor chemotherapeutic drugs. *Journal of Porphyrins and Phthalocyanines* **2000**, 4, (1), 129-135.
7. Dougherty, T. J.; Gomer, C. J.; Henderson, B. W.; Jori, G.; Kessel, D.; Korblick, M.; Moan, J.; Peng, Q., Photodynamic therapy. *Journal of the National Cancer Institute* **1998**, 90, (12), 889-905.
8. Babcock, G. T., How oxygen is activated and reduced in respiration. *Proceedings of the National Academy of Sciences of the United States of America* **1999**, 96, (23), 12971-12973.
9. Sehgal, I.; Sibrian-Vazquez, M.; Vicente, M. G. H., Photoinduced cytotoxicity and biodistribution of prostate cancer cell-targeted porphyrins. *Journal of Medicinal Chemistry* **2008**, 51, (19), 6014-6020.

10. Jacques, V.; Desreux, J. F., New classes of MRI contrast agents. *Contrast Agents I* **2002**, 221, 123-164.
11. Fleische.Eb, Structure of porphyrins and metalloporphyrins. *Accounts of Chemical Research* **1970**, 3, (3), 105-112.
12. Gamboa, M.; Campos, M.; Torres, L. A., Study of the stability of 5,10,15,20-tetraphenylporphine (TPP) and metalloporphyrins NiTPP, CoTPP, CuTPP, and ZnTPP by differential scanning calorimetry and thermogravimetry. *Journal of Chemical Thermodynamics* 42, (5), 666-674.
13. Biesaga, M.; Pyrzynska, K.; Trojanowicz, M., Porphyrins in analytical chemistry. A review. *Talanta* **2000**, 51, (2), 209-224.
14. Ethirajan, M.; Chen, Y.; Joshi, P.; Pandey, R. K., The role of porphyrin chemistry in tumor imaging and photodynamic therapy. *Chemical Society Reviews* **2011**, 40, (1), 340-362.
15. Kennedy, J. C.; Pottier, R. H., Endogenous protoporphyrin-ix, a clinically useful photosensitizer for photodynamic therapy. *Journal of Photochemistry and Photobiology B-Biology* **1992**, 14, (4), 275-292.
16. Stojiljkovic, I.; Kumar, V.; Srinivasan, N., Non-iron metalloporphyrins: potent antibacterial compounds that exploit haem/Hb uptake systems of pathogenic bacteria. *Molecular Microbiology* **1999**, 31, (2), 429-442.
17. Monti, D.; Vodopivec, B.; Basilico, N.; Olliaro, P.; Taramelli, D., A novel endogenous antimalarial: Fe(II)-protoporphyrin IX alpha (heme) inhibits hemo polymerization to beta-hemo (malaria pigment) and kills malaria parasites. *Biochemistry* **1999**, 38, (28), 8858-8863.

18. Conway, C. L.; Walker, I.; Bell, A.; Roberts, D. J. H.; Brown, S. B.; Vernon, D. I., In vivo and in vitro characterisation of a protoporphyrin IX-cyclic RGD peptide conjugate for use in photodynamic therapy. *Photochemical & Photobiological Sciences* **2008**, 7, (3), 290-298.
19. Liapis, H.; Flath, A.; Kitazawa, S., Integrin alpha(v)beta(3) expression by bone-residing breast cancer metastases. *Diagnostic Molecular Pathology* **1996**, 5, (2), 127-135.
20. Carreiras, F.; Denoux, Y.; Staedel, C.; Lehmann, M.; Sichel, F.; Gauduchon, P., Expression and localization of alpha v integrins and their ligand vitronectin in normal ovarian epithelium and in ovarian carcinoma. *Gynecologic Oncology* **1996**, 62, (2), 260-267.
21. Liapis, H.; Adler, L. M.; Wick, M. R.; Rader, J. S., Expression of alpha(v)beta(3) integrin is less frequent in ovarian epithelial tumors of low malignant potential in contrast to ovarian carcinomas. *Human Pathology* **1997**, 28, (4), 443-449.
22. Natali, P. G.; Hamby, C. V.; FeldingHabermann, B.; Liang, B. T.; Nicotra, M. R.; DiFilippo, F.; Giannarelli, D.; Temponi, M.; Ferrone, S., Clinical significance of alpha(v)beta(3) integrin and intercellular adhesion molecule-1 expression in cutaneous malignant melanoma lesions. *Cancer Research* **1997**, 57, (8), 1554-1560.
23. Kageshita, T.; Hamby, C. V.; Hirai, S.; Kimura, T.; Ono, T.; Ferrone, S., Differential clinical significance of alpha(v)beta(3) expression in primary lesions of acral lentiginous melanoma and of other melanoma histotypes. *International Journal of Cancer* **2000**, 89, (2), 153-159.

24. Zoller, F.; Riss, P. J.; Montforts, F. P.; Rosch, F., Efficient post-processing of aqueous generator eluates facilitates Ga-68-labelling under anhydrous conditions. *Radiochimica Acta* **98**, (3), 157-160.
25. Al-Nahhas, A.; Win, Z.; Szyszko, T.; Singh, A.; Nanni, C.; Fanti, S.; Rubello, D., Gallium-68 PET: A new frontier in receptor cancer imaging. *Anticancer Research* **2007**, *27*, (6B), 4087-4094.
26. Khan, M. U.; Khan, S.; Ei-Refaeie, S.; Win, Z.; Rubello, D.; Al-Nahhas, A., Clinical indications for Gallium-68 positron emission tomography imaging. *Ejso* **2009**, *35*, (6), 561-567.
27. Aldrich, J. V. K., Vivek Methods of synthesizing and using derivatives of [2-(2-aminoethoxy)ethoxy] acetic acid. US-7,038,078, 2006.
28. Decristoforo, C.; Gonzalez, I. H.; Carlsen, J.; Rupprich, M.; Huisman, M.; Virgolini, I.; Wester, H. J.; Haubner, R., Ga-68- and In-111-labelled DOTA-RGD peptides for imaging of alpha v beta 3 integrin expression. *European Journal of Nuclear Medicine and Molecular Imaging* **2008**, *35*, (8), 1507-1515.
29. Kolb, H. C.; Chen, K.; Walsh, J. C.; Chen, G.; Gangadharmath, U.; Kasi, D.; Scott, R.; Haka, M.; Collier, T. L.; Padgett, H. C.; Zhu, Z.; Liang, Q.; Zhao, T.; Secrest, J.; Gomez, L. F., Synthesis and imaging of an 18F-labeled RGD peptide for detecting alpha v beta 3 integrin expression in vivo. *Journal of Labelled Compounds & Radiopharmaceuticals* **2009**, *52*, S67-S67.
30. Montet, X.; Montet-Abou, K.; Reynolds, F.; Weissleder, R.; Josephson, L., Nanoparticle imaging of integrins on tumor cells. *Neoplasia* **2006**, *8*, (3), 214-222.

31. Burtea, C.; Laurent, S.; Murariu, O.; Rattat, D.; Toubeau, G.; Verbruggen, A.; Vanstherem, D.; Elst, L. V.; Muller, R. N., Molecular imaging of alpha(v)beta(3) integrin expression in atherosclerotic plaques with a mimetic of RGD peptide grafted to Gd-DTPA. *Cardiovascular Research* **2008**, 78, (1), 148-157.
32. Cai, W. B.; Shin, D. W.; Chen, K.; Gheysens, O.; Cao, Q. Z.; Wang, S. X.; Gambhir, S. S.; Chen, X. Y., Peptide-labeled near-infrared quantum dots for imaging tumor vasculature in living subjects. *Nano Letters* **2006**, 6, (4), 669-676.
33. Coutsolelos, A.; Guillard, R.; Bayeul, D.; Lecomte, C., Gallium(iii) porphyrins - synthesis and physicochemical characteristics of halogeno gallium(iii) porphyrins x-ray crystal-structure of chloro-(5,10,15,20-tetraphenylporphyrinato) gallium(iii). *Polyhedron* **1986**, 5, (6), 1157-1164.
34. Liu, L. C.; Lee, C. C.; Hu, A. T., Synthesis of soluble metallophthalocyanines from a metal-free phthalocyanine by microwave irradiation. *Journal of Porphyrins and Phthalocyanines* **2001**, 5, (11), 806-807.
35. Shaabani, A., Synthesis of metallophthalocyanines under solvent-free conditions using microwave irradiation. *Journal of Chemical Research, Synopses* **1998**, (10), 672-673.
36. Ungurenasu, C., Improved synthesis of octaalkoxymetalphthalocyanines (MC12, M = Si,Ge,Sn) under microwave conditions. *Synthesis-Stuttgart* **1999**, (10), 1729-1730.
37. Davies, D. A.; Schnik, C.; Silver, J.; Sosa-Sanchez, J. L.; Riby, P. G., A high-yield microwave heating method for the preparation of



- (phthalocyaninato)bis(chloro)silicon(IV). *Journal of Porphyrins and Phthalocyanines* **2001**, 5, (4), 376-380.
38. Hacht, B., Gallium(III) ion hydrolysis under physiological conditions. *Bulletin of the Korean Chemical Society* **2008**, 29, (2), 372-376.
39. Hu, Y.; Geissinger, P.; Woehl, J. C., Potential of protoporphyrin IX and metal derivatives for single molecule fluorescence studies. *Journal of Luminescence* **2011**, 131, 477-481.
40. Dai, X. D.; Su, Z.; Liu, J. O., An improved synthesis of a selective alpha(v)beta(3)-integrin antagonist cyclo(-RGDfK-). *Tetrahedron Letters* **2000**, 41, (33), 6295-6298.

## **CHAPTER 4. A cell-based approach for OBOC combinatorial library screening against cell surface receptors**

### **4.1 Introduction**

An initial step in the development of drugs and therapeutic agents is the identification of compounds that bind the biological target of interest such as enzymes, or surface receptors. After identification of the molecule of interest, many analogues are still synthesized in order to optimize biological variables such as activity and lipophilicity. Discovery and optimization of potential candidates typically involves the evaluation of a large number of compounds, making this approach an extremely labor intensive and time-consuming process. In order to facilitate these demands, various chemical and biological methods have been developed for the generation of combinatorial libraries and the subsequent screening of compounds therein against biological targets of interest in order to identify high-affinity ligands.<sup>1</sup> Considered one of the most important recent advances in medicinal chemistry, this approach is currently utilized in major pharmaceuticals companies as a powerful tool for the discovery of potential agents for diagnostic and therapeutic applications.<sup>2</sup>

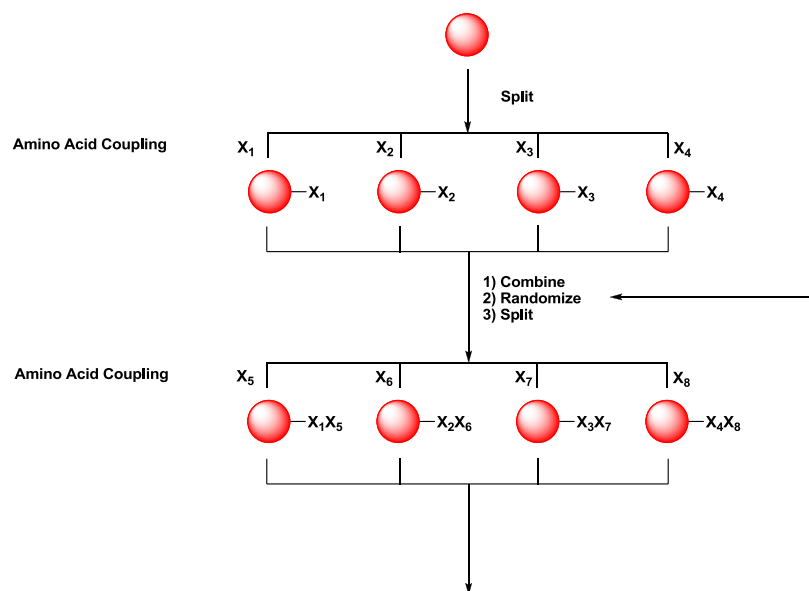
In general, all library-based methods consist of three key steps which are 1) preparation of a combinatorial library, 2) screening of compounds against biological targets, and 3) structure determination of potential imaging/drug candidates. Libraries may contain various classes of compounds including, peptides,<sup>3</sup> oligonucleotides,<sup>4</sup> proteins,<sup>5</sup> synthetic oligomers,<sup>6</sup> small molecules,<sup>1</sup> and oligosaccharides.<sup>2, 7, 8</sup> Libraries can be prepared via biological/biochemical or synthetic approaches. For instance, peptides could be either chemically synthesized or biologically expressed using a phage display

approach.<sup>9</sup> Compounds requiring chemical syntheses are commonly prepared via a solid phase methodology. Here, the solid support acts as an insoluble and inert material for the covalent attachment of compounds, thus facilitating isolation and identification processes.<sup>1</sup>

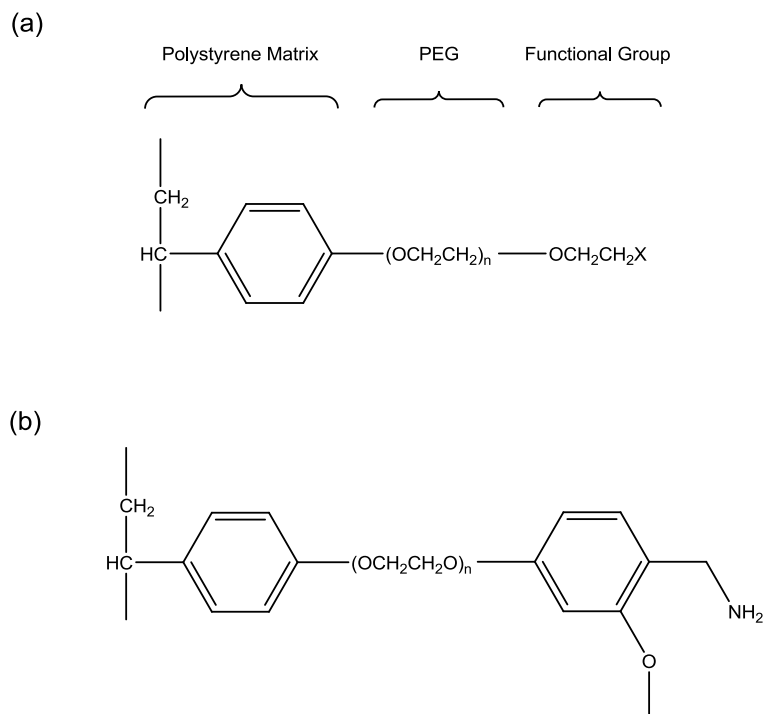
There are currently four major but distinct combinatorial library methods. The first approach is a biological library method such as phase display.<sup>10</sup> Here, peptides/proteins are expressed biologically using genetically modified plasmids. These compounds are then screened for binding against DNA or protein of interest. A second approach involves spatially addressable libraries such as the multipin system, which involves the use of separate polyethylene pins as reaction media for synthesis of individual compounds.<sup>11</sup> A third technique involves synthetic solution library methods such as affinity capillary electrophoresis (ACE).<sup>12</sup> Here, a competitive binding assay is used in conjunction with ACE, to identify high-binding ligands for the biological target of interest. The last method is based on the one-bead-one-compound (OBOC) combinatorial library approach. In this method a large number of variable peptide sequences are synthesized on solid support in a spatially independent fashion.<sup>2, 13</sup> Sequence determination of peptide candidates from this library is then carried out using mass spectrometry techniques such as MALDI-TOF/TOF.<sup>14</sup> There have also been reports on variations of this approach. An example of this variation entailed the use of peptide fragments, instead of single amino acids, in the split synthesis of larger peptides.<sup>15</sup> Considering that there are cons and pros associated with each approach mentioned above, selection of a suitable method is case-specific and relies heavily on the target, assay system and available resources. The work discussed in this dissertation utilizes an OBOC

approach, in conjunction with deconvolution methods, for screening of a peptide-based library.

OBOC libraries have been successfully applied to peptides, oligomers and small organic molecules.<sup>2</sup> Libraries employing this approach are typically prepared on resin via a split synthesis approach, which involves mixing and splitting resins following each amino acid coupling (Scheme 4.1).<sup>16</sup> Products of this process would consist of a vast number of beads, each containing only one peptide sequence, with various amino acid sequences. For instance, a library of octameric peptides prepared from a selection of 20 natural amino acids would consist of over 25 billion sequences of peptides. For this application, beaded polymers have to fulfill certain structural characteristics of which size, substitution homogeneity (i.e. number of available functional groups on the bead surface), resistance to cluster formation, and swelling abilities are most important. Examples of common beads used for such applications include Tentagel (polyoxyethylene-grafted polystyrene),<sup>17</sup> PEG-PS resin,<sup>18</sup> and ArgoGel.<sup>19</sup> TentaGel beads, which are PEG-PS based and typically utilized in bead binding assays, exhibit polyoxyethylene chains between the solid support and synthesized compounds thereby reducing steric effects imposed by the bead. PEG-PS beads possess polyoxyethylene chains as means to modify the polymer properties as they make up 70% of the resin weight. ArgoGel resins have higher substitution levels, which is made possible by branching of polyoxyethylene groups at the attachment point to the polystyrene core (Figure 4.1).



**Scheme 4.1** Synthetic pathway for a randomized combinatorial library.

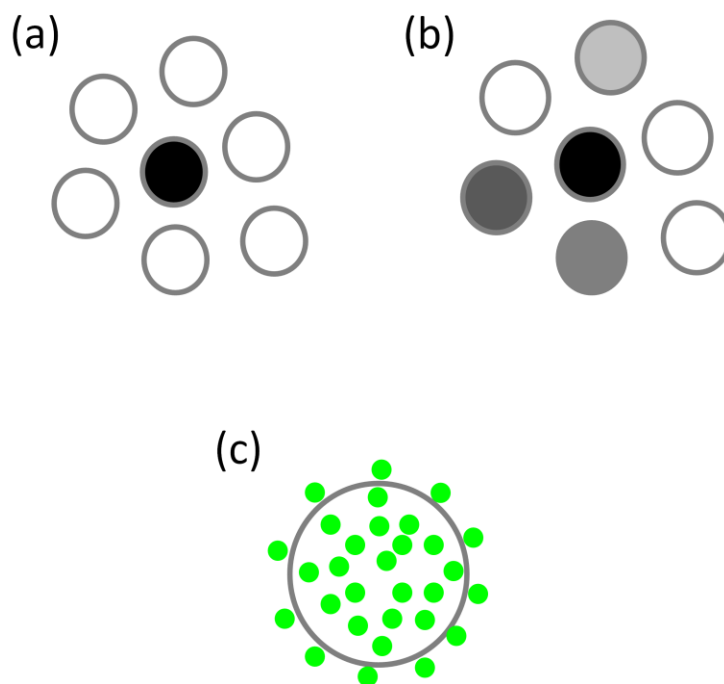


**Figure 4.1.** General structures of (a) Tentagel and PEG-PS and (b) ArgoGel-MB-NH<sub>2</sub> resins.

The binding of bead-bound compounds to biological targets can be visualized via direct or indirect routes. The direct route involves, for instance, the visualization of a colored target such as a dye<sup>20</sup> or a larger target such as a cell.<sup>21</sup> Indirect visualization, on the other hand, involves the use of reporter groups such as enzymes, radionuclides, or fluorescent probes.<sup>2</sup> In both screening processes, non-specific binding should be minimized in order to increase signal to noise ratios. Binding to an undesirable site can usually be eliminated, or at least significantly minimized, by using a high ionic strength buffer (eg. 0.3-0.4 M NaCl), with non-ionic detergent (eg. 0.1% Triton X-100) and blocking proteins (eg. bovine serum albumin).<sup>2</sup>

Various screening methods for OBOC combinatorial libraries have been reported. A common route of identifying lead compounds is a colorimetric-based enzyme-linked on-bead assay.<sup>22</sup> In this approach, peptide-conjugated beads are enzymatically phosphorylated and subsequently treated with a dye. Lead compounds which would be on colored beads are then isolated using selective antibodies. Figure 4.2a illustrates typical appearance of a cell batch in this assay with positive beads appearing darker. Beads could also vary in color pending on the extent of binding. Beads exhibiting ligands with a higher biological affinity appear darker (Figure 4.2b). Another method of screening is a whole-cell on-bead binding assay.<sup>23</sup> Direct visualization of cells (6-10  $\mu\text{m}$  in diameter) binding to ligand-conjugated beads (90-120  $\mu\text{m}$ ) is carried out under a microscope. This method was previously utilized in identifying peptides that bind integrins on prostate cancer cell lines. Figure 4.2c illustrates a typical example of this procedure for the identification of compounds binding cell surface receptors. In theory, the OBOC library approach can also be applied to viral particles, bacteria or yeast given the appropriate use

of a reporter/signaling group. Table 4.1 lists some biological targets for which OBOC libraries were utilized in finding high-affinity ligands.



**Figure 4.2** (a) Depiction of an OBOC assay with hit beads appearing dark, (b) a collection of beads with varying color intensity as reflected by ligand binding, darker colored beads exhibit higher affinity, (c) depiction of a hit bead in a whole cell on-bead binding assay, showing attachment of inherently fluorescent cells to the surface of the bead.

While the OBOC library approach allows for the ability to test a large number of compounds simultaneously but individually, owing to the spatially separable nature of compounds on beads, it would still be advantageous to combine multiple approaches in

order to solve specific problems or improve overall screening abilities. Here, we report a novel and rapid on-bead cell-based method of screening peptide libraries.

<b>Target</b>
Monoclonal antibodies
Lymphoma cells
Streptavidin/avidin
Thrombin
SH <sub>3</sub> domain
Dopamine D <sub>2</sub> receptors
Organic dyes
Prostate cancer surface integrins
Protease substrate
Protease inhibitor
Tyrosine kinase
G-protein coupled receptors
Anticancer agents
MSH
Carbonic anhydrase

**Table 4.1** A list of biological targets for which OBOC combinatorial library assays were employed in identification of high affinity ligands.<sup>2, 13, 20, 21, 23-34</sup>

## 4.2 Experimental

### 4.2.1. Materials

Common solvents and reagents were purchased from VWR, Fisher Scientific, or Sigma–Aldrich and used as received, unless stated otherwise. Sterile, deionized water was used in all aqueous procedures. Fmoc protected amino acids, HBTU, and Tentagel S



NH<sub>2</sub> resin were obtained from Peptides International. *N*-Fmoc-3-amino-3-(2-nitrophenyl) propionic acid (Fmoc-ANP) was obtained from Chem-Impex International, Inc.

#### 4.2.2. Peptide Synthesis

Fmoc-based solid-phase peptide synthesis was carried out using an APEX 396 autosynthesizer (AAPPTec, Louisville) with 0.05 meq of 0.26 mmol/g Tentagel S NH<sub>2</sub> (90 μm, 0.27 mmol/g) resin. 1.5 meq of Fmoc-ANP and subsequently, a three-fold excess of the protected amino acids were used in coupling reactions. Fmoc removal was carried out using a solution of 20% piperidine in DMF (N,N-dimethylformamide) over two cycles (10 and 20 min). Amino acid activation was carried out with 3 eq of HBTU and 6 eq of DIPEA (N,N-diisopropylethylamine), which was followed by amino acid coupling over 30 and 120 min cycles. Deprotection of peptide side chains was accomplished using a solution of 88% TFA (v/v) + 5% H<sub>2</sub>O (v/v) + 5% phenol (m/v) + 2% triisopropylsilane (v/v) over 6 h.

Cleavage of peptides from Tentagel beads was carried out using UV irradiation. All care was taken to prevent light exposure to synthesized peptides prior to ANP-linker cleavage. For this reaction, approximately 1-3 peptide conjugated Tentagel beads were placed in 200 μL of MilliQ water in an open-top 384 well polypropylene plate. UV irradiation was carried out using a 365 nm UV lamp (UV Products, Upland, CA, model EL25, 8 mWcm<sup>-2</sup>) over 2.5 hours. Water was added periodically in order to prevent wells from drying, thus reducing possible peptide decomposition. The resulting peptide-containing solution was then used for MALDI-TOF/TOF analysis.

#### 4.2.3. On-bead Cell-based Assay for Screening Peptide Library

The  $\alpha_v\beta_3$  integrin-expressing MDA-MB-435 cells were transfected with green fluorescent protein. Approximately 1000 beads containing each peptide were equilibrated with serum-free DMEM in a 12-well plate. MDA 435 cells were detached from the flask by EDTA and resuspended in serum-free DMEM. Approximately 200000 cells were added to each well, containing peptide-conjugated beads, and subsequently placed in a shaking incubator (50 rpm) for 1 hour at 37°C. Beads were then washed twice with PBS, and imaged under the Olympus IX70 inverted fluorescent microscope. Cells were fixed onto beads with 3% formaldehyde for 5 minutes at room temperature, and washed twice with PBS.

#### 4.2.4. High throughput Screening

Beads from each well were inserted into the COPAS™ large particle flow cytometer (Union Biometrica), and sorted into a 96 well plate. The fluorescence intensity threshold for sorting was defined using non-functionalized Tentagel beads. Beads with fluorescent intensity higher than the set threshold were sorted into the 96-well plate. Sorted beads were imaged using an Olympus IX70 inverted fluorescent microscope. Post imaging, beads were then treated rigorously with ethanol to remove bound cells. Rinsing with water was carried out several times prior to MALDI-TOF analysis.

#### 4.2.5. MALDI-TOF MS/MS Analysis

In a typical experiment, the exact molecular ion mass  $[M+H]^+$  of a peptide was determined using MS analysis. MS/MS spectra were subsequently recorded for the

desired molecular ion peak, previously observed by MS. This was then followed by manual deconvolution of all peptide sequences.

### **4.3 Results and Discussion**

The aim of this project was the development of an improved procedure for the screening of peptide libraries. To that end, we have devised a methodology wherein peptide-conjugated Tentagel beads are screened against cell surface receptors and subsequently sorted, while still attached to cells, based on fluorescence intensity. To the best of our knowledge, this is the first example of a screening procedure where cells that are attached to peptide-conjugated beads are directly monitored and screened for lead compounds in an automated fashion. This automated procedure is especially significant in reducing time-intensive labor associated with the manual isolation of beads coated with high-affinity or hit ligands (hit beads). Isolation of hit compounds using magnetic particles was recently reported,<sup>35</sup> however, this approach necessitates conjugation of magnetic particles (eg. quantum dots), and multiple antibodies in order to find ligands with optimal binding affinity. Addition of more variables in the screening process (i.e. multiple large entities), may reduce the overall efficiency of screening as a result of enhanced non-specific uptake. Furthermore, collection of hit beads with a magnet often results in entrapment of false beads containing non-targeting compounds, thus requiring a second screening process where beads are either manually inspected or put through a flow cytometer for secondary isolation.<sup>36</sup> As a result, having an automated procedure, which only necessitates the presence of peptide-conjugated beads and cells of interest,

would be greatly beneficial as it provides a more efficient (i.e. less labor-intensive, more time efficient, more consistent bead isolation) route for finding potential hit compounds.

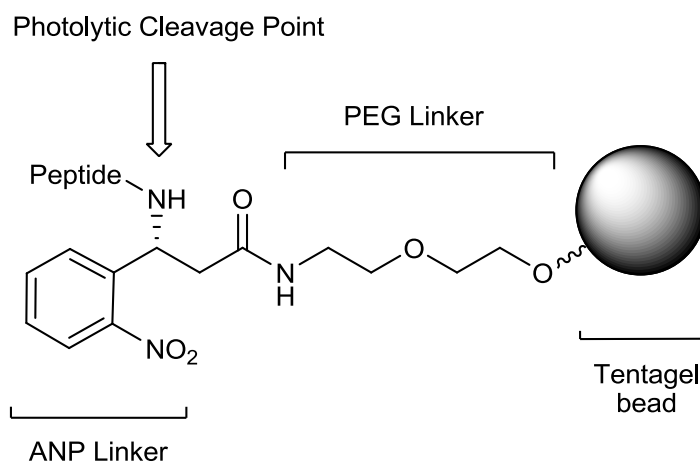
As a proof of concept for this procedure a small library of seven heptameric peptides (Table 4.2) were synthesized via Fmoc solid phase methodology, on 90  $\mu\text{m}$  Tentagel beads, which have been previously reported to be efficient solid support candidates for preparation of combinatorial libraries. The well studied  $\alpha_v\beta_3$  expressing cell-line, MDA-MB-435, was utilized in this work. In addition, the pentameric peptide GRGDS was incorporated in the sequence of all prepared peptides as it has been previously reported to bind  $\alpha_v\beta_3$  integrins.<sup>37-41</sup> The last two amino acids of the prepared peptides were selected at random in order to more closely mimic a combinatorial library. A photolabile linker (ANP) was placed between Tentagel beads and the corresponding conjugated peptides in order to facilitate peptide removal post screening. Employing this linker allows for complete removal of all acid-labile amino acid side-chain protecting groups without removing peptides. This is necessitated by the screening process, which requires the use of fully deprotected, but still resin-bound, peptides. Figure 4.3 illustrates the general design of the studied peptides.

A COPAS<sup>TM</sup> Biosorter flow cytometer (Figure 4.4) was used as means for high-speed automated analysis and sorting of cell-bead conjugates. This system was initially designed to analyze and sort living multicellular organisms based fluorescent protein expression, with rates of up to 100 organisms per second. This work employed the capabilities of this instrument for sorting and isolation of hit peptides based on the overall fluorescence intensity of cell-bead conjugates. The inherent green fluorescence of

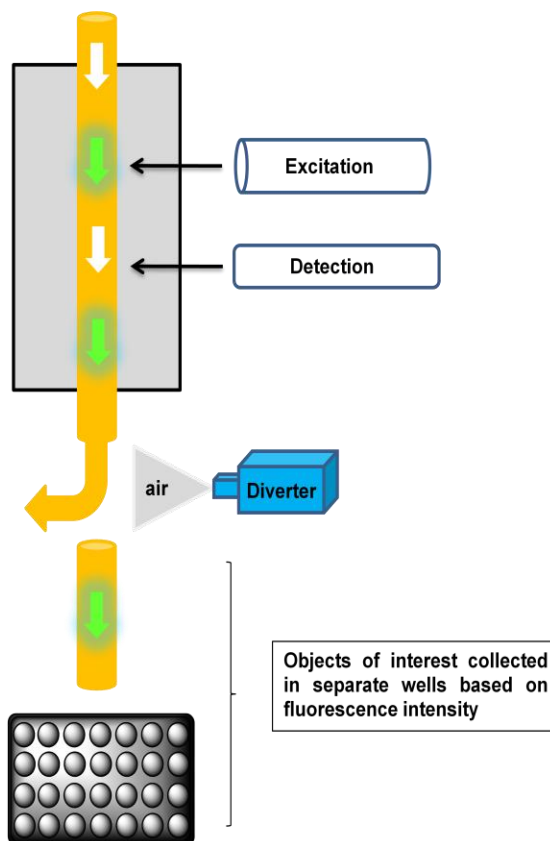
Tentagel beads, in this case, did not interfere with the isolation of beads as the signals obtained from adhesion of GFP-expressing cells was much more pronounced.

#	Sequence
1	GRGDSPS
2	GRGDSYT
3	GRGDSWK
4	GRGDShL
5	GRGDSVP
6	GRGDSTW
7	GRGDSFA
8	HMYFLLGH

**Table 4.2** List of prepared peptide sequences for cell-based screening assay.



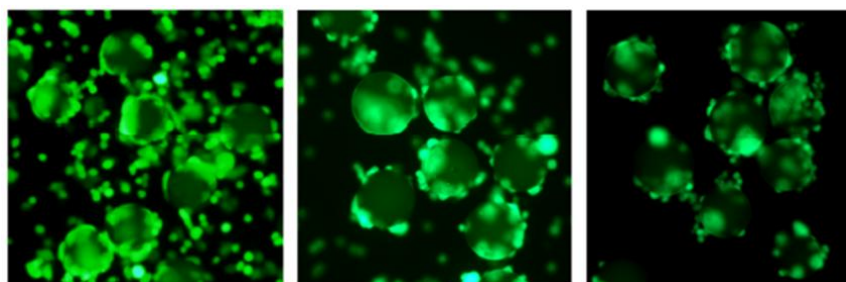
**Figure 4.3** Illustrates overall design of prepared peptides.



**Figure 4.4** An illustration of a COPAS™ Biosorter showing the mechanism of detection and isolation of fluorescent samples.<sup>42</sup>

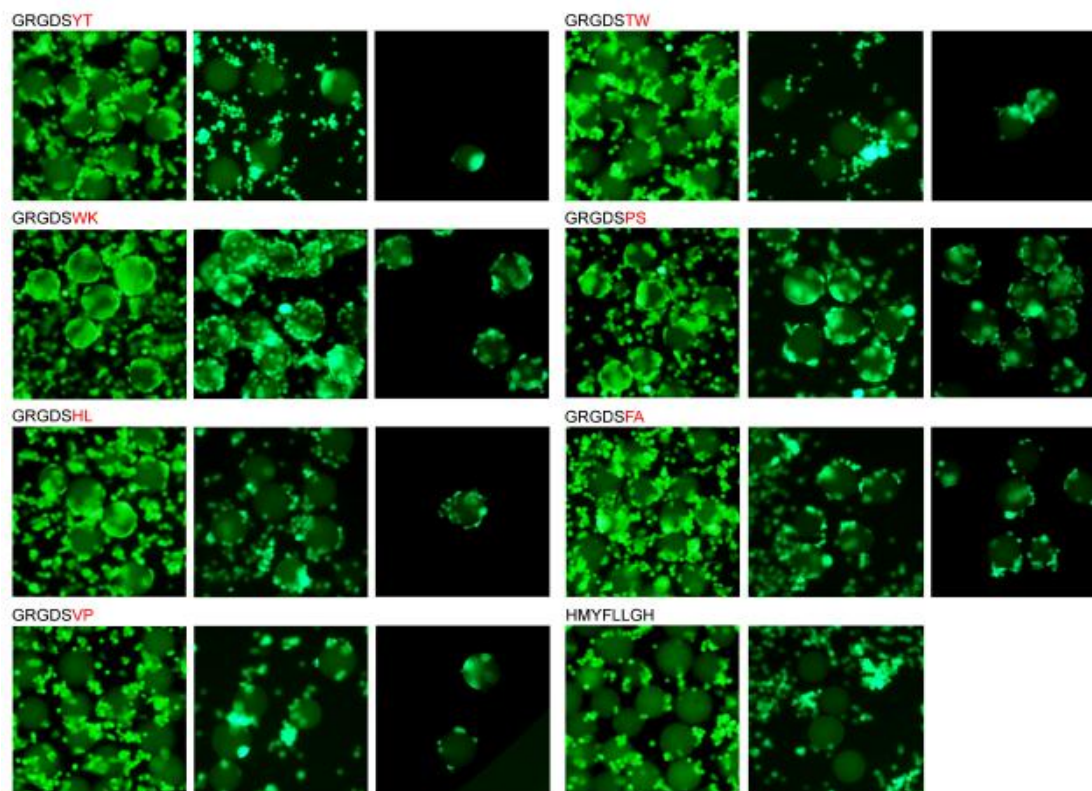
In a typical experiment, GFP-expressing cells were incubated with each peptide from the prepared library. After rinsing with PBS medium, cells were fixed onto beads using formaldehyde, which ensured the binding of cells to the surface of beads. This step was confirmed to be a necessity as untreated cells were observed to dissociate from beads during the sorting process. Cell-bound beads were then loaded onto the COPAS™ flow cytometer, which isolated hit beads based on fluorescence intensity. Peptides were then rinsed and cleaved from the resin prior to analysis by MALDI-TOF. Figure 4.5 shows images of compound **1** taken with an Olympus IX70 inverted fluorescent microscope. Images indicate a reduction of adhered cells post rinsing, which is due to the clearance of

non-specific cell uptake. Images of beads post rinsing and sorting were comparable. Using the same methodology, cell sorting, isolation and imaging for other peptide candidates in the library was carried out (Figure 4.6). As can be seen, peptides **1**, **3**, **4** and **7** exhibited highest levels of binding. Peptide **8** was used as a negative control because of its lack of affinity for  $\alpha_v\beta_3$  integrins. This was further confirmed by the COPAS<sup>TM</sup> sorter which did not isolate any **8**-bound beads.



**Figure 4.5** Images of MDA-MB-435 cells adhered to Tentagel beads containing **1** pre-wash (left), post-wash (middle) and post-sorting (right).

Considering that this is the first-reported fully automated cell-based screening assay, it was deemed necessary to confirm the ability to identify hit peptides both pre and post sorting. This was especially important in ruling out fragmentation prevention by residual formaldehyde that could be present after cell sorting. For this reason, MALDI-TOF/TOF analysis of standard peptides and those post sorting were carried out. In the former case, synthesized peptides on Tentagel beads were fully deprotected using a TFA cleavage cocktail containing scavengers. Under a light inverted microscope, 1-3 beads



**Figure 4.6** Images of MDA-MB-435 cells adhered to peptide-conjugated tentagel beads pre-wash (left columns), post-wash (middle columns) and post-sorting (right columns).

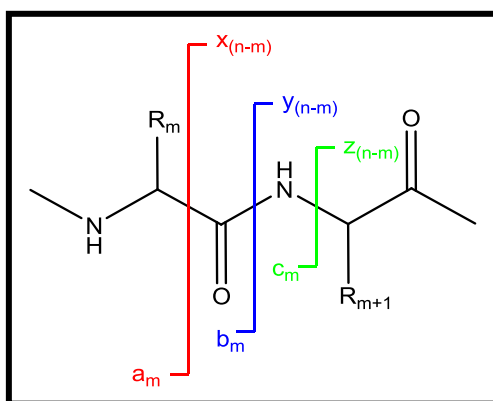
were separated and placed, with 200  $\mu$ L of MilliQ water, into one well of an open-top 384 well polypropylene plate. Removal of peptides from the resin was then carried out by exposure to a 365 nm UV light over 2.5 hours. Water was added periodically in order to prevent wells from drying, thus reducing possible peptide decomposition. The resulting peptide-containing solution was then used for MALDI-TOF/TOF analysis. As mentioned earlier, peptide-conjugated Tentagel beads were fully deprotected, but still bound to Tentagel beads, prior to analysis by the COPAS sorter. After cell sorting, removal of peptides from hit beads was accomplished using the same procedures as those used for



standard untreated beads. All peptide solutions were then analyzed by MALDI-TOF/TOF. In a typical experiment, the exact molecular ion mass  $[M+H]^+$  of a peptide is determined using MALDI-TOF analysis. MS/MS spectra are subsequently recorded for the desired molecular ion peak, previously observed by MS. This was then followed by manual deconvolution of all peptide sequences in this work. Fragments were calculated and reported according to published procedures.<sup>43</sup> Figure 4.7 illustrates commonly observed peptide fragmentation patterns. Missing fragments can be calculated only if the complementary fragment is observed. Figure 4.8 shows the MS/MS spectrum obtained for untreated **1**, which was used as a standard point of comparison to MS/MS spectra obtained post cell sorting (Figure 4.9). As it can be seen, differences between MS/MS spectra of pre- and post-sorted peptides are minimal, indicating that treatment and handling of cell-peptide-bead conjugates in this methodology does not negatively impact the peptides. In addition, successful sequencing of peptide candidates confirms the consistency in sequencing ability pre- and post-sorting (Tables 4.3 and 4.4). Tables 4.5-4.10 list calculated and observed fragmentation patterns for compounds.

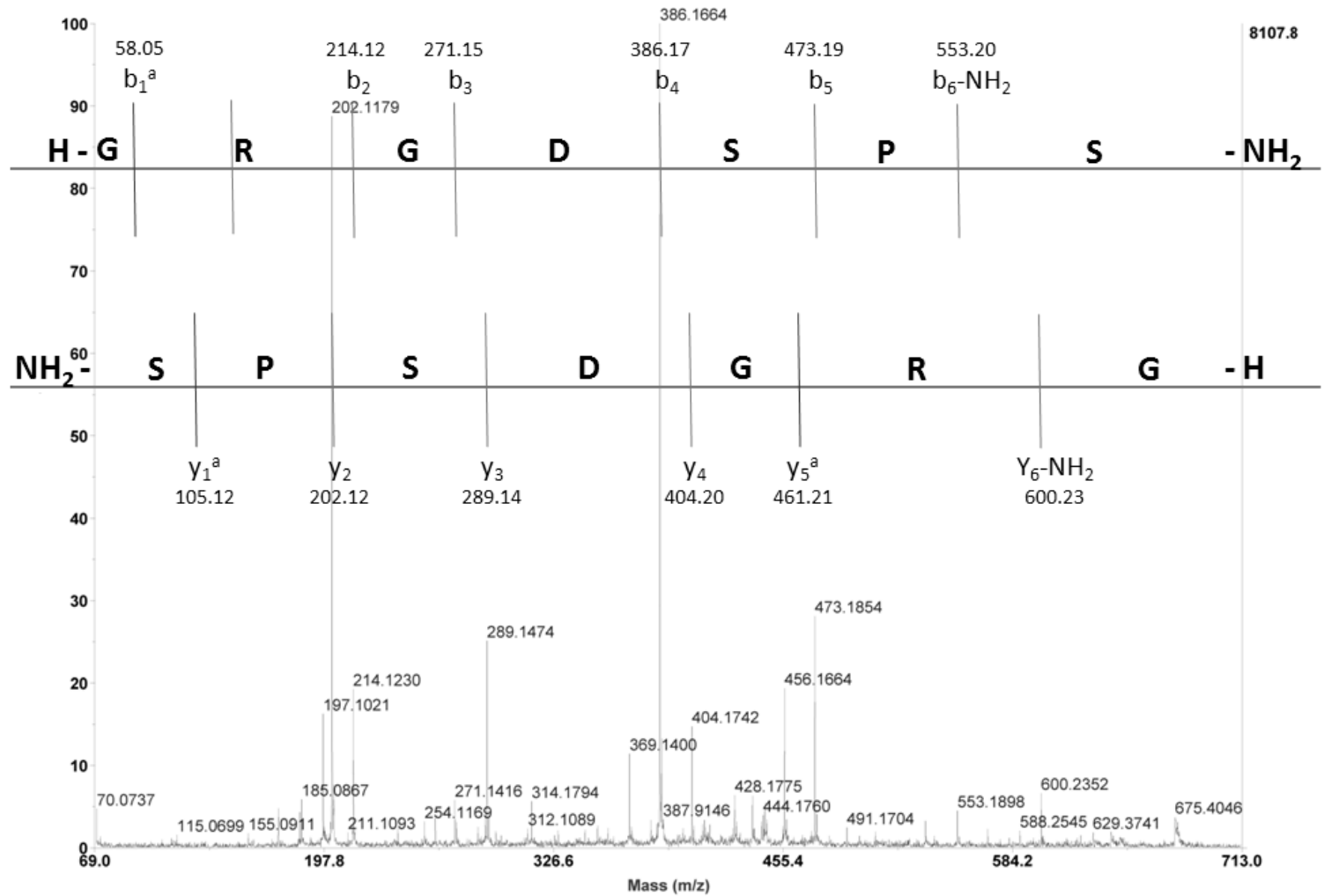
In certain cases N-terminal glycine was not observed and could not be calculated by complementarity. In these situations the combined molecular weights of the last two N-terminal residues was calculated to be that of Gly and Arg. The order of the two residues was determined by considering possible side chain fragmentation of Arg (Scheme 4.2)<sup>44</sup> as well as overall molecular weights of residues. Assuming the N-terminal peptide sequence order, RG, would indicate that the molecular weight corresponding to arginine should still be observable after glycine fragmentation. Assuming the N-terminal peptide sequence GR, on the other hand, would indicate that

upon arginine fragmentation, the remaining molecular weight (i.e. glycine), would be too low to be definitively observed, as in all cases in this study. Given the lack of evidence for the presence of arginine or any side chain fragmented derivatives, it was concluded that the likely order of sequence for the last two N-terminal residues was in fact GR.

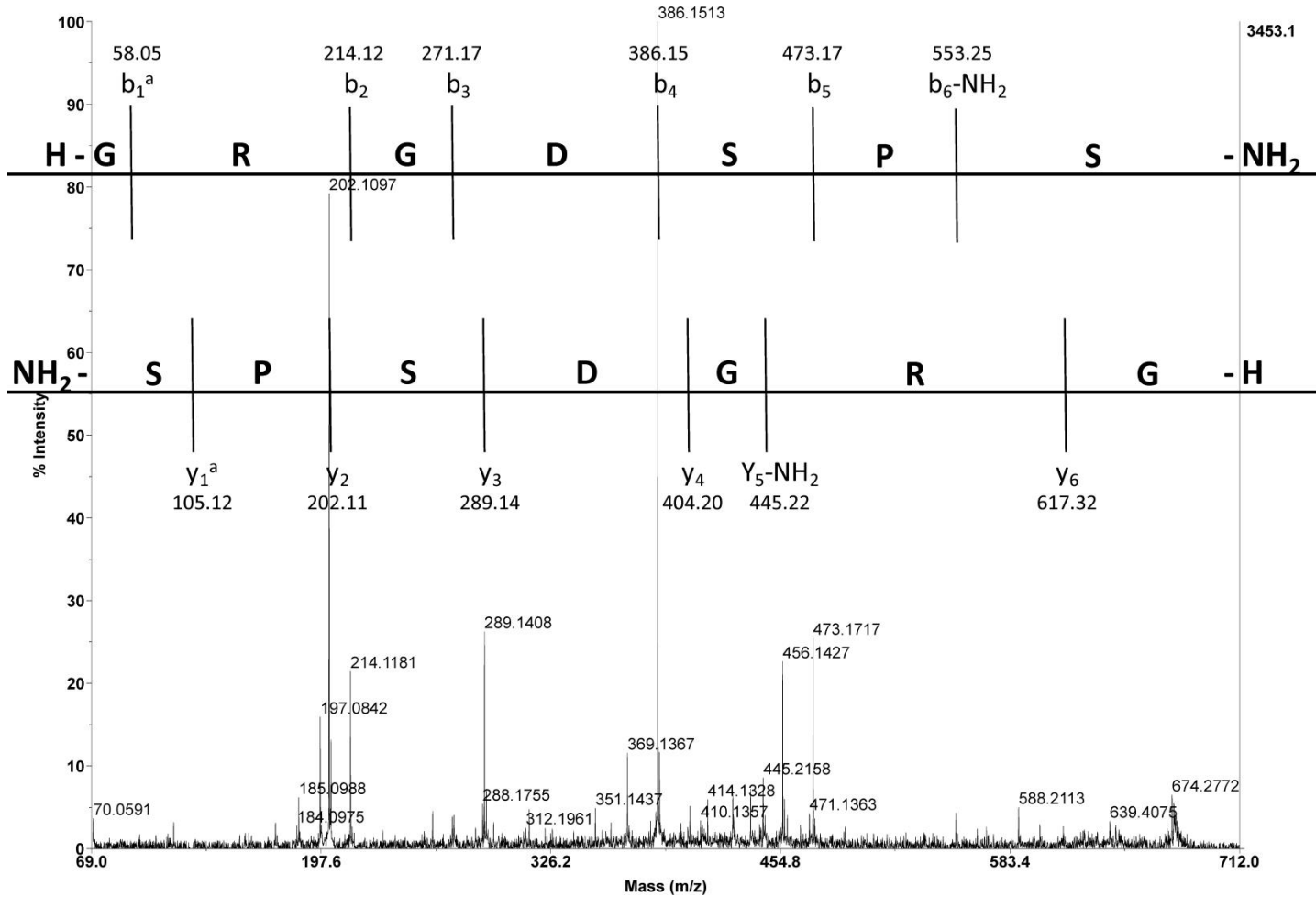


**Figure 4.7** Common peptide fragmentation patterns and the corresponding fragment notations.<sup>43</sup>

Absence of these fragments was especially apparent for peptides **3** and **6** where even the standard un-treated samples exhibited this pattern (Tables 4.6 and 4.9). Peptides **2** and **7**, on the other hand, only displayed this pattern for treated samples, as sequences for untreated peptides were completely deconvoluted (Tables 4.5 and 4.10). The cause of this incomplete fragmentation was initially postulated to result from trace amounts of formaldehyde, previously used in fixing cells, in the final peptide solution used for MALDI-TOF/TOF analysis. However, fragmentation patterns observed for peptide **4** disproved this hypothesis as the sequence of treated samples, unlike those of standards, was completely deconvoluted. This pattern, therefore, may have simply been a result of the difficult fragmentation of arginine residues.



**Figure 4.8** MS/MS spectrum of GRGDSPS peptide standard; <sup>a</sup> denotes fragments calculated by complementarity.



**Figure 4.9** MS/MS spectrum of GRGDSPS peptide post sorting; <sup>a</sup> denotes fragments calculated by complementarity.

Fragment	Expected	Found	Residue Lost
b <sub>1</sub>	58.03	58.11 <sup>a</sup>	Arg
b <sub>2</sub>	214.13	214.12	Gly
b <sub>3</sub>	271.15	271.14	Asp
b <sub>4</sub>	386.18	386.17	Ser
b <sub>5</sub>	473.21	473.19	Pro
b <sub>6</sub> - amine	553.23	553.19	Ser
y <sub>1</sub>	105.06	105.12 <sup>a</sup>	Pro
y <sub>2</sub>	202.12	202.12	Ser
y <sub>3</sub>	289.15	289.15	Asp
y <sub>4</sub>	404.18	404.17	Gly
y <sub>5</sub>	461.20	461.21 <sup>a</sup>	Arg
y <sub>6</sub> - amine	600.27	600.23	Gly

**Table 4.3** Calculated and observed fragmentation patterns for untreated GRGDSPS peptide. <sup>a</sup>Fragments were calculated by complementarity.

Fragment	Expected	Found	Residue Lost
b <sub>1</sub>	58.05	58.05 <sup>a</sup>	Arg
b <sub>2</sub>	214.15	214.13	Gly
b <sub>3</sub>	271.17	271.14	Asp
b <sub>4</sub>	386.20	386.15	Ser
b <sub>5</sub>	473.23	473.17	Pro
b <sub>6</sub> - amine	553.25	553.2	Ser
y <sub>1</sub>	105.08	105.12 <sup>a</sup>	Pro
y <sub>2</sub>	202.14	202.11	Ser
y <sub>3</sub>	289.17	289.14	Asp
y <sub>4</sub>	404.20	404.17	Gly
y <sub>5</sub> - amine	445.20	445.15	Arg
y <sub>6</sub>	617.32	617.30	Gly

**Table 4.4** Calculated and observed fragmentation patterns for GRGDSPS peptide post sorting. <sup>a</sup>Fragments were calculated by complementarity.

Fragment	Expected	Found	Residue
b <sub>1</sub>	58.05	58.08 <sup>a</sup>	Arg
b <sub>2</sub>	214.15	214.13	Gly
c <sub>3</sub>	289.20	289.16	Asp
b <sub>4</sub>	386.19	386.17	Ser
b <sub>5</sub> - amine	456.20	456.16	Tyr
c <sub>6</sub>	654.33	654.24	Thr
y <sub>1</sub>	119.10	118.16 <sup>a</sup>	Tyr
y <sub>2</sub>	282.16	282.15	Ser
y <sub>3</sub>	369.19	369.15	Asp
y <sub>4</sub>	484.22	483.22 <sup>a</sup>	Gly
y <sub>5</sub>	573.27	573.22	Arg
z <sub>6</sub>	680.33	680.26	Gly

Fragment	Expected	Found	Residue
b <sub>1</sub>	58.09	N/A	-
b <sub>2</sub>	214.19	214.13	Gly
b <sub>3</sub>	271.21	271.15	Asp
b <sub>4</sub>	386.23	386.16	Ser
b <sub>5</sub>	473.27	473.21	Tyr
b <sub>6</sub>	636.33	636.71	Thr
y <sub>1</sub>	119.14	119.09	Tyr
y <sub>2</sub>	282.20	282.16	Ser
y <sub>3</sub>	369.23	369.14	Asp
y <sub>4</sub>	484.26	484.26 <sup>a</sup>	Gly
z <sub>5</sub>	558.30	559.17	Arg
y <sub>6</sub>	697.38	N/A	-

**Table 4.5** Experimental and calculated fragmentation of untreated (left) and sorted (right) H-GRGDSYT-NH<sub>2</sub> peptide (2). <sup>a</sup> Fragments were calculated by complementarity.

Fragment	Expected	Found	Residue
b <sub>1</sub>	58.03	N/A	-
b <sub>2</sub>	214.13	214.12	Gly
b <sub>3</sub>	271.15	271.15	Asp
b <sub>4</sub>	386.18	386.16	Ser
b <sub>5</sub>	473.21	473.19	Trp
b <sub>6</sub>	659.29	659.24	Lys
z <sub>1</sub>	129.10	129.10	Trp
z <sub>2</sub>	315.18	315.19	Ser
y <sub>3</sub>	419.23	419.22	Asp
z <sub>4</sub>	517.24	517.24 <sup>a</sup>	Gly
y <sub>5</sub>	589.28	589.28 <sup>a</sup>	Arg
z <sub>6</sub>	746.38	N/A	-

Fragment	Expected	Found	Residue
b <sub>1</sub>	58.03	N/A	-
b <sub>2</sub>	214.13	214.12	Gly
b <sub>3</sub>	271.15	271.15	Asp
b <sub>4</sub>	386.18	386.16	Ser
b <sub>5</sub>	473.21	473.17	Trp
b <sub>6</sub>	659.29	659.74	Lys
z <sub>1</sub>	129.10	129.10	Trp
z <sub>2</sub>	315.18	315.15	Ser
z <sub>3</sub>	402.21	402.23 <sup>a</sup>	Asp
z <sub>4</sub>	517.24	517.24 <sup>a</sup>	Gly
y <sub>5</sub>	589.28	589.17	Arg
z <sub>6</sub>	746.38	N/A	-

**Table 4.6** Experimental and calculated fragmentation of untreated (left) and sorted (right) H-GRGDSWK-NH<sub>2</sub> peptide (3). <sup>a</sup> Fragments were calculated by complementarity.

Fragment	Expected	Found	Residue
b <sub>1</sub>	58.02	N/A	-
b <sub>2</sub>	214.12	214.13	Gly
b <sub>3</sub>	271.14	271.16 <sup>a</sup>	Asp
b <sub>4</sub>	386.17	386.16	Ser
b <sub>5</sub>	473.20	473.19	His
b <sub>6</sub>	610.26	610.21	Leu
y <sub>1</sub>	131.08	130.16 <sup>a</sup>	Leu
y <sub>2</sub>	268.14	268.18	His
y <sub>3</sub>	355.17	355.20	Asp
y <sub>4</sub>	470.23	470.22	Gly
y <sub>5</sub>	527.25	527.22	Arg
y <sub>6</sub>	683.35	N/A	-

Fragment	Expected	Found	Residue
b <sub>1</sub>	58.05	58.03 <sup>a</sup>	Arg
b <sub>2</sub>	214.15	214.08	Gly
b <sub>3</sub>	271.17	270.39	Asp
b <sub>4</sub>	386.20	386.17	Ser
b <sub>5</sub>	473.23	473.18	His
b <sub>6</sub>	610.29	610.21	Leu
y <sub>1</sub>	131.11	130.19 <sup>a</sup>	Leu
y <sub>2</sub>	268.17	268.15	His
y <sub>3</sub>	355.20	355.20	Asp
y <sub>4</sub>	470.26	470.01 <sup>a</sup>	Gly
y <sub>5</sub>	527.28	527.21	Arg
y <sub>6</sub>	683.38	682.37	Gly

**Table 4.7** Experimental and calculated fragmentation of untreated (left) and sorted (right) H-GRGDSHL-NH<sub>2</sub> peptide (4). <sup>a</sup> Fragments were calculated by complementarity.

Fragment	Expected	Found	Residue
b <sub>1</sub>	58.01	58.08 <sup>a</sup>	Arg
b <sub>2</sub>	214.11	214.14 <sup>a</sup>	Gly
b <sub>3</sub>	271.13	271.16	Asp
b <sub>4</sub>	386.16	386.16	Ser
b <sub>5</sub>	473.19	473.19	Val
b <sub>6</sub>	572.26	572.24	Pro
y <sub>1</sub>	115.07	115.08	Pro
y <sub>2</sub>	214.14	214.14	Val
y <sub>3</sub> - amine	284.14	284.13	Asp
y <sub>4</sub> - amine	399.18	399.16	Gly
y <sub>5</sub> - amine	456.20	456.16	Arg
y <sub>6</sub> - amine	612.29	612.24	Gly

Fragment	Expected	Found	Residue
b <sub>1</sub>	58.04	58.08 <sup>a</sup>	Arg
b <sub>2</sub>	214.14	214.13	Gly
b <sub>3</sub>	271.17	271.16	Asp
b <sub>4</sub>	386.19	386.16	Ser
b <sub>5</sub>	473.22	473.17	Val
b <sub>6</sub>	572.29	572.21	Pro
y <sub>1</sub>	115.10	115.08	Pro
y <sub>2</sub>	214.17	214.14 <sup>a</sup>	Val
y <sub>3</sub> - amine	284.17	283.18 <sup>a</sup>	Asp
y <sub>4</sub> - amine	399.21	399.15	Gly
y <sub>5</sub> - amine	456.23	456.17	Arg
y <sub>6</sub> - amine	612.32	612.77	Gly

**Table 4.8** Experimental and calculated fragmentation of untreated (left) and sorted (right) H-GRGDSVP-NH<sub>2</sub> peptide (5). <sup>a</sup> Fragments were calculated by complementarity.

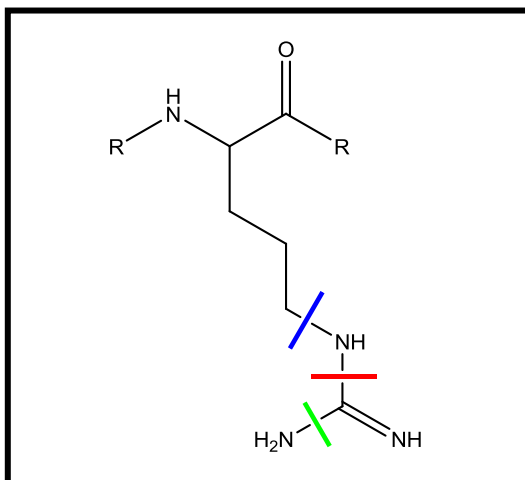
Fragment	Expected	Found	Residue	Fragment	Expected	Found	Residue
b <sub>1</sub>	58.04	N/A	-	b <sub>1</sub>	58.05	N/A	-
b <sub>2</sub>	214.14	214.12	Gly	b <sub>2</sub>	214.15	214.12	Gly
b <sub>3</sub>	271.16	271.15	Asp	b <sub>3</sub>	271.17	271.19	Asp
b <sub>4</sub>	386.19	386.17	Ser	b <sub>4</sub>	386.20	386.16	Ser
b <sub>5</sub>	473.22	473.2	Thr	b <sub>5</sub>	473.23	473.18	Thr
b <sub>6</sub>	573.26	573.22	Trp	b <sub>6</sub>	573.27	573.23	Trp
y <sub>1</sub>	204.09	204.11	Thr	y <sub>1</sub>	204.10	204.12	Thr
y <sub>2</sub>	305.14	305.15	Ser	y <sub>2</sub>	305.15	305.14	Ser
z <sub>3</sub>	407.18	407.14	Asp	z <sub>3</sub>	407.19	407.14	Asp
y <sub>4</sub> - amine	491.18	491.20	Gly	y <sub>4</sub> - amine	491.19	491.19	Gly
y <sub>5</sub>	564.22	564.27 <sup>a</sup>	Arg	y <sub>5</sub>	564.23	564.28	Arg
y <sub>6</sub>	720.32	N/A	-	y <sub>6</sub>	720.33	N/A	-

**Table 4.9** Experimental and calculated fragmentation of untreated (left) and sorted (right) H-GRGDSTW-NH<sub>2</sub> peptide (6). <sup>a</sup> Fragments were calculated by complementarity.

Fragment	Expected	Found	Residue	Fragment	Expected	Found	Residue
b <sub>1</sub>	58.03	58.05 <sup>a</sup>	Arg	b <sub>1</sub>	58.07	N/A	-
b <sub>2</sub>	214.13	214.13	Gly	b <sub>2</sub>	214.17	214.13	Gly
b <sub>3</sub>	271.15	271.15	Asp	c <sub>3</sub>	289.23	289.14	Asp
b <sub>4</sub>	386.18	386.17	Ser	b <sub>4</sub>	386.22	386.16	Ser
b <sub>5</sub>	473.21	473.20	Phe	b <sub>5</sub> - amine	456.22	456.17	Phe
b <sub>6</sub>	619.27	619.36	Ala	b <sub>6</sub>	619.31	620.26	Ala
y <sub>1</sub>	89.07	89.00 <sup>a</sup>	Phe	y <sub>1</sub>	89.11	89.13 <sup>a</sup>	Phe
y <sub>2</sub>	236.14	236.12	Ser	y <sub>2</sub>	236.18	235.12	Ser
y <sub>3</sub>	323.17	323.16	Asp	y <sub>3</sub>	323.21	323.14	Asp
y <sub>4</sub>	438.20	438.16	Gly	y <sub>4</sub>	438.24	438.28 <sup>a</sup>	Gly
y <sub>5</sub>	495.22	496.24	Arg	y <sub>5</sub>	495.26	495.26	Arg
z <sub>6</sub>	634.29	634.27	Gly	y <sub>6</sub> - amine	634.33	N/A	-

**Table 4.10** Experimental and calculated fragmentation of untreated (left) and sorted (right) H-GRGDSFA-NH<sub>2</sub> peptide (7). <sup>a</sup> Fragments were calculated by complementarity.





**Scheme 4.2** Possible fragmentation patterns of the Arginine side chain.

Considering that cells were still bound to peptide-conjugated Tentagel beads after sorting, attempts were made to facilitate cell removal via sequential heating at 60 °C and 95 °C over 10 min and 15 min, respectively. Unfortunately, this methodology prevented proper fragmentation of peptide sequences by MALDI-TOF/TOF to such an extent that no fragmentation was observed for peptides **3**, **5**, **6**, and **7**, while partial fragmentations were observed for other peptides. This could have been resulted from peptide decomposition or release from Tentagel beads. Although attempts to facilitate cell removal were not successful, complete sequencing of library peptides, without cell removal via sequential heating, proves this process to be unnecessary.

#### 4.4 Conclusions

A novel and rapid cell-based, on-bead, and fully automated screening process for one-bead one-compound libraries was developed. As proof of concept, a small library of heptameric peptides expressing the GRGDS moiety, known to bind  $\alpha_v\beta_3$  integrins, was synthesized on Tentagel beads. The peptide-conjugated beads were screened against  $\alpha_v\beta_3$  expressing MDA-MB-435 cell-line, which were transfected with GFP protein. Cells were fixed to beads via formaldehyde treatment. Automated isolation of hit beads was accomplished using a COPAS large particle flow cytometer. MALDI-TOF/TOF analysis and successful sequencing of all prepared peptides indicated efficient screening and isolation of hit beads by the COPAS flow cytometer. An attempt was made to facilitate removal of cells from beads after sorting. However, this resulted in peptide degradation/release from Tentagel beads. This process, however, was deemed unnecessary since peptide sequences were deconvoluted successfully without removing cells from the Tentagel beads.

#### 4.5 References

1. Thompson, L. A.; Ellman, J. A., Synthesis and applications of small molecule libraries. *Chemical Reviews* **1996**, 96, (1), 555-600.
2. Lam, K. S.; Lebl, M.; Krchnak, V., The "one-bead-one-compound" combinatorial library method. *Chemical Reviews* **1997**, 97, (2), 411-448.
3. Gallop, M. A.; Barrett, R. W.; Dower, W. J.; Fodor, S. P. A.; Gordon, E. M., Applications of combinatorial technologies to drug discovery .1. background and peptide combinatorial libraries. *Journal of Medicinal Chemistry* **1994**, 37, (9), 1233-1251.
4. Gold, L.; Polisky, B.; Uhlenbeck, O.; Yarus, M., Diversity of oligonucleotide function *Annual Review of Biochemistry* **1995**, 64, 763-797.
5. Barbas, C. F.; Bain, J. D.; Hoekstra, D. M.; Lerner, R. A., Semisynthetic combinatorial antibody libraries - a chemical solution to the diversity problem. *Proceedings of the National Academy of Sciences of the United States of America* **1992**, 89, (10), 4457-4461.
6. Simon, R. J.; Kania, R. S.; Zuckermann, R. N.; Huebner, V. D.; Jewell, D. A.; Banville, S.; Ng, S.; Wang, L.; Rosenberg, S.; Marlowe, C. K.; Spellmeyer, D. C.; Tan, R. Y.; Frankel, A. D.; Santi, D. V.; Cohen, F. E.; Bartlett, P. A., Peptoids - a modular approach to drug discovery. *Proceedings of the National Academy of Sciences of the United States of America* **1992**, 89, (20), 9367-9371.
7. Danishefsky, S. J.; McClure, K. F.; Randolph, J. T.; Ruggeri, R. B., A strategy for the solid-phase synthesis of oligosaccharides. *Science* **1993**, 260, (5112), 1307-1309.

8. Gordon, E. M.; Barrett, R. W.; Dower, W. J.; Fodor, S. P. A.; Gallop, M. A., Applications of combinatorial technologies to drug discovery .2. combinatorial organic-synthesis, library screening strategies, and future-directions. *Journal of Medicinal Chemistry* **1994**, 37, (10), 1385-1401.
9. Pasqualini, R.; Ruoslahti, E., Organ targeting in vivo using phage display peptide libraries. *Nature* **1996**, 380, (6572), 364-366.
10. Cwirla, S. E.; Peters, E. A.; Barrett, R. W.; Dower, W. J., Peptides on phage - a vast library of peptides for identifying ligands. *Proceedings of the National Academy of Sciences of the United States of America* **1990**, 87, (16), 6378-6382.
11. Geysen, H. M.; Meloen, R. H.; Barteling, S. J., Use of peptide-synthesis to probe viral-antigens for epitopes to a resolution of a single amino-acid. *Proceedings of the National Academy of Sciences of the United States of America-Biological Sciences* **1984**, 81, (13), 3998-4002.
12. Chu, Y. H.; Avila, L. Z.; Biebuyck, H. A.; Whitesides, G. M., Using affinity capillary electrophoresis to identify the peptide in a peptide library that binds most tightly to vancomycin. *Journal of Organic Chemistry* **1993**, 58, (3), 648-652.
13. Lam, K. S.; Salmon, S. E. Method of screening a peptide library. US 5510240, 1996.
14. Amadei, G. A.; Cho, C. F.; Lewis, J. D.; Luyt, L. G., A fast, reproducible and low-cost method for sequence deconvolution of 'on-bead' peptides via 'on-target' maldi-TOF/TOF mass spectrometry. *Journal of Mass Spectrometry* 45, (3), 241-251.

15. Erb, E.; Janda, K. D.; Brenner, S., Recursive deconvolution of combinatorial chemical libraries. *Proceedings of the National Academy of Sciences of the United States of America* **1994**, 91, (24), 11422-11426.
16. Lam, K. S.; Salmon, S. E.; Hersh, E. M.; Hruby, V. J.; Kazmierski, W. M.; Knapp, R. J., A new type of synthetic peptide library for identifying ligand-binding activity. *Nature* **1991**, 354, (6348), 82-84.
17. Quarrell, R.; Claridge, T. D. W.; Weaver, G. W.; Lowe, G., Structure and properties of TentaGel resin beads: Implications for combinatorial library chemistry. *Molecular Diversity* **1996**, 1, (4), 223-232.
18. Kates, S. A.; McGuinness, B. F.; Blackburn, C.; Griffin, G. W.; Sole, N. A.; Barany, G.; Albericio, F., "High-load" polyethylene glycol-polystyrene (PEG-PS) graft supports for solid-phase synthesis. *Biopolymers* **1998**, 47, (5), 365-380.
19. Leon, S.; Quarrell, R.; Lowe, G., Evaluation of resins for on-bead screening: A study of papain and chymotrypsin specificity using PEGA-bound combinatorial peptide libraries. *Bioorganic & Medicinal Chemistry Letters* **1998**, 8, (21), 2997-3002.
20. Lam, K. S.; Zhao, Z. G.; Wade, S.; Krchnak, V.; Lebl, M., Identification of small peptides that interact specifically with a small organic-dye. *Drug Development Research* **1994**, 33, (2), 157-160.
21. Pennington, M. E.; Lam, K. S.; Cress, A. E., The use of a combinatorial library method to isolate human tumor cell adhesion peptides. *Molecular Diversity* **1996**, 2, (1-2), 19-28.

22. Martin, S. E.; Peterson, B. R., A colorimetric enzyme-linked on-bead assay for identification of synthetic substrates of protein tyrosine kinases. *Journal of Peptide Science* **2002**, 8, (5), 227-233.
23. Lam, K. S.; Lou, Q.; Zhao, Z. G.; Smith, J.; Chen, M. L.; Pleshko, E.; Salmon, S. E., Idiotype specific peptides bind to the surface immunoglobulins of two murine B-cell lymphoma lines, inducing signal transduction. *Biomed Pept Proteins Nucleic Acids* **1995**, 1, (3), 205-10.
24. Ostergaard, S.; Hansen, P. H.; Olsen, M.; Holm, A., Novel avidin and streptavidin binding sequences found in synthetic peptide libraries. *Febs Letters* **1995**, 362, (3), 306-308.
25. Lebl, M.; Krchnak, V.; Sepetov, N. F.; Seligmann, B.; Strop, P.; Felder, S.; Lam, K. S., One-bead one-structure combinatorial libraries. *Biopolymers* **1995**, 37, (3), 177-198.
26. Combs, A. P.; Kapoor, T. M.; Feng, S. B.; Chen, J. K.; DaudeSnow, L. F.; Schreiber, S. L., Protein structure-based combinatorial chemistry: Discovery of non-peptide binding elements to Src SH3 domain. *Journal of the American Chemical Society* **1996**, 118, (1), 287-288.
27. Sasaki, S.; Takagi, M.; Tanaka, Y.; Maeda, M., A new application of a peptide library to identify selective interaction between small peptides in an attempt to develop recognition molecules toward protein surfaces. *Tetrahedron Letters* **1996**, 37, (1), 85-88.
28. Meldal, M.; Svendsen, I.; Breddam, K.; Auzanneau, F. I., Portion-mixing peptide libraries of quenched fluorogenic substrates for complete subsite mapping of

- endoprotease specificity. *Proceedings of the National Academy of Sciences of the United States of America* **1994**, 91, (8), 3314-3318.
29. Meldal, M.; Svendsen, I., Direct visualization of enzyme-inhibitors using a portion mixing inhibitor library containing a quenched fluorogenic peptide substrate .1. inhibitors for subtilisin carlsberg. *Journal of the Chemical Society-Perkin Transactions I* **1995**, (12), 1591-1596.
30. Lou, Q.; Leftwich, M. E.; Lam, K. S., Identification of GIYWHHY as a novel peptide substrate for human p60(c-src) protein tyrosine kinase. *Bioorganic & Medicinal Chemistry* **1996**, 4, (5), 677-682.
31. Quillan, J. M.; Jayawickreme, C. K.; Lerner, M. R., Combinatorial diffusion assay used to identify topically active melanocyte-stimulating hormone-receptor antagonists. *Proceedings of the National Academy of Sciences of the United States of America* **1995**, 92, (7), 2894-2898.
32. Salmon, S. E.; LiuStevens, R. H.; Zhao, Y.; Lebl, M.; Krchnak, V.; Wertman, K.; Sepetov, N.; Lam, K. S., High-volume cellular screening for anticancer agents with combinatorial chemical libraries: A new methodology. *Molecular Diversity* **1996**, 2, (1-2), 57-63.
33. Burbaum, J. J.; Ohlmeyer, M. H. J.; Reader, J. C.; Henderson, I.; Dillard, L. W.; Li, G.; Randle, T. L.; Sigal, N. H.; Chelsky, D.; Baldwin, J. J., A paradigm for drug discovery employing encoded combinatorial libraries. *Proceedings of the National Academy of Sciences of the United States of America* **1995**, 92, (13), 6027-6031.

34. Jayawickreme, C. K.; Quillan, J. M.; Graminski, G. F.; Lerner, M. R., Discovery and structure-function analysis of alpha-melanocyte-stimulating hormone antagonists. *Journal of Biological Chemistry* **1994**, 269, (47), 29846-29854.
35. Qi, X.; Astle, J.; Kodadek, T., Rapid identification of orexin receptor binding ligands using cell-based screening accelerated with magnetic beads. *Molecular Biosystems* 6, (1), 102-107.
36. Feldhaus, M. J.; Siegel, R. W.; Opresko, L. K.; Coleman, J. R.; Feldhaus, J. M. W.; Yeung, Y. A.; Cochran, J. R.; Heinzelman, P.; Colby, D.; Swers, J.; Graff, C.; Wiley, H. S.; Wittrup, K. D., Flow-cytometric isolation of human antibodies from a nonimmune *Saccharomyces cerevisiae* surface display library. *Nature Biotechnology* **2003**, 21, (2), 163-170.
37. Garrigues, H. J.; Rubinchikova, Y. E.; DiPersio, C. M.; Rose, T. M., Integrin alpha(V)beta(3) binds to the RGD motif of glycoprotein B of Kaposi's sarcoma-associated herpesvirus and functions as an RGD-dependent entry receptor. *Journal of Virology* **2008**, 82, (3), 1570-1580.
38. Schaffner-Reckinger, E., Beta3 integrins: major therapeutic targets of the near future. *Bull Soc Sci Med Grand Duche Luxemb* **2003**, (1), 23-34.
39. Pfaff, M.; Gohring, W.; Brown, J. C.; Timpl, R., Binding of purified collagen receptors (alpha-1-beta-1, alpha-2-beta-1) and rgd-dependent integrins to laminins and laminin fragments. *European Journal of Biochemistry* **1994**, 225, (3), 975-984.



40. Li, J.; Yun, H.; Gong, Y. D.; Zhao, N. M.; Zhang, X. F., Investigation of MC3T3-E1 cell behavior on the surface of GRGDS-coupled chitosan. *Biomacromolecules* **2006**, 7, (4), 1112-1123.
41. Pfaff, M.; Tangemann, K.; Muller, B.; Gurrath, M.; Muller, G.; Kessler, H.; Timpl, R.; Engel, J., Selective recognition of cyclic rgd peptides of nmr defined conformation by alpha-ii-beta-3, alpha-v-beta-3, and alpha-5-beta-1 integrins. *Journal of Biological Chemistry* **1994**, 269, (32), 20233-20238.
42. Pulak, R., Techniques for analysis, sorting, and dispensing of C-elegans on the COPAS (TM) flow-sorting system. *Methods in Molecular Biology* **2006**, 275-286.
43. Steen, H.; Mann, M., The ABC's (and XYZ's) of peptide sequencing. *Nature Reviews Molecular Cell Biology* **2004**, 5, (9), 699-711.
44. Gehrig, P. M.; Hunziker, P. E.; Zahariev, S.; Pongor, S., Fragmentation pathways of N-G-methylated and unmodified arginine residues in peptides studied by ESI-MS/MS and MALDI-MS. *Journal of the American Society for Mass Spectrometry* **2004**, 15, (2), 142-149.

## CHAPTER 5. Outlook and Concluding Remarks

The research discussed in this dissertation provides new possibilities and insights into the preparation of nuclear (PET/SPECT) and fluorescent (fluorescence microscopy) imaging probes, entailing several important findings which should be considered in the basic design of a tracer, especially when working with peptides or multiple imaging modalities. These findings include: 1) charge distribution on the peptide backbone contributes to probe clearance and uptake pathways, 2) by using porphyrin derivatives, a single molecule tracer can be developed for multimodality imaging, without requiring the use of multiple imaging tags or structural modifications, and 3) screening of OBOC libraries can be facilitated by using a fluorescent-based cell sorter, after fixing cells to beads, and utilized immediately after library preparation. Here, the significance of these findings and their contribution to the field of molecular/diagnostic imaging is discussed in more detail.

The first important finding was discovered in the development of peptide-based tracers for beta cell imaging. Nine GLP-1 analogues were initially prepared and evaluated *in vitro*. Among these, several promising candidates were identified, the most promising of which was used for *in vivo* evaluation. Although pancreatic uptake was confirmed *ex-vivo*, non-specific uptake of the tracer in kidneys prevented direct visualization of islets. Following these observations, the imaging probe was structurally modified in order to reduce kidney retention. Results obtained in this research suggested that the localization and clearance of peptide-based probes could be significantly altered based on the charge localization on the peptide backbone. This is an important observation as the non-specific uptake of tracers often interfere with proper *in vivo* evaluation of targeting agents. This

interference, as suggested by results in this dissertation, could be circumvented by perturbation of charge distribution in peptide-based agents, thereby improving images obtained in *in vivo* studies. This is especially noteworthy in the development of tracers targeting GLP-1R, considering the intended biological disease (diabetes), and the potential contribution towards the development of a cure.

Until now, there have been no reports on an imaging probe that could be used for the non-invasive and direct visualization of pancreatic islets *in vivo*. The development of a probe for this application would allow not only the visualization but also the quantification of beta cell mass during the onset of diabetes type 1 and its progression into diabetes type 2. This would serve as a more efficient route of monitoring disease progression while, perhaps, providing the experts with a better method of analysis for beta cell transfer operations, thereby providing better options for the treatment of this illness.<sup>1</sup> Visualization of beta cell mass could also prove to be a valuable diagnostic tool for monitoring of other disease processes involving GLP-1R receptors, such as pancreatic cancers (e.g. insulinomas). While the optimization process is currently ongoing, the work discussed in this dissertation provides potential imaging probe candidates that could be used for the above application.

The second finding concerns the basic design of multimodality imaging probes. In recent years, utilization of multiple imaging modalities has gained significant popularity since it provides more information on targeted biological entities. This move towards multimodality imaging requires the development of appropriate tracers for use with the intended instrumentation. A progression in this field was observed with the development of multimodality single molecule probes. However, such compounds were

commonly prepared by attachment of multiple imaging tags, which altered the innate properties of the parent molecule. This also resulted in unexpected and inconsistent *in vivo* properties, in between modalities. The use of a single molecule for multimodality imaging, without structural modifications or addition of multiple imaging tags, is the next step in the development of more efficient imaging probes. A recent report by Valliant and coworkers provided an example of this concept.<sup>2</sup> The work in this dissertation puts forth a new route for the development of such probes using porphyrins for both fluorescence and radiometal chelation. In confirming this ideology, gallium-chelated porphyrins, containing the integrin-targeting moiety RGD, were developed. Surprisingly, optical analysis of the prepared compounds indicated metal-dependent fluorescence-quenching to be minimal. This is contrary to reported literature on the negative impacts of metal chelation (Mg, Sn, Zn) on fluorescence quantum yields of PPIX.<sup>3</sup> Furthermore, *in vitro* analysis proved the potential of the developed tracers for fluorescence microscopy, while radiolabeling experiments confirmed the potential for PET imaging. This methodology could prove to be particularly beneficial in bridging the gap between the screening processes requiring initial *in vitro* evaluation, by means of fluorescence microscopy, and *in vivo* detection via nuclear imaging, with implications in the development of novel probes, drugs and therapeutics.

This work also provides a more efficient and facile route for screening peptide libraries. Although a number of screening methods have already been reported in literature,<sup>4-6</sup> there are currently no reports on a cell-based procedure which can be used with OBOC peptide libraries without the need for structural modification. As a result this procedure simplifies the screening process by providing users with the ability to evaluate

novel peptide sequences, immediately after synthesis, in a time and cost-efficient fashion. While this method was validated with a small peptide library, its application can potentially be extended to also include other compounds such as small molecules or proteins.

In overview, this dissertation provides new routes for the synthesis and screening of peptide-based agents with applications in diagnostic imaging and potentially oncology. In addition, this research not only offers new insight into pharmacokinetic control with structural modifications, but also presents novel synthetic routes for preparation of more reliable and efficient multimodality imaging agents. The results described herein will contribute to the discovery of targeting ligands in basic sciences and ultimately to the discovery of new drugs and therapeutics.

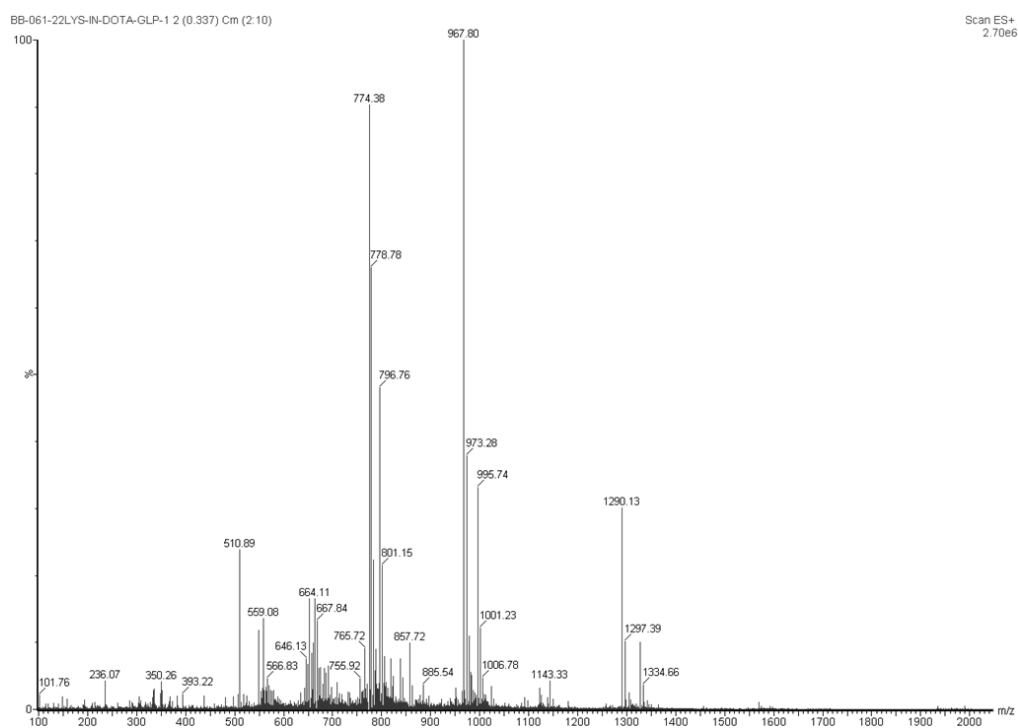
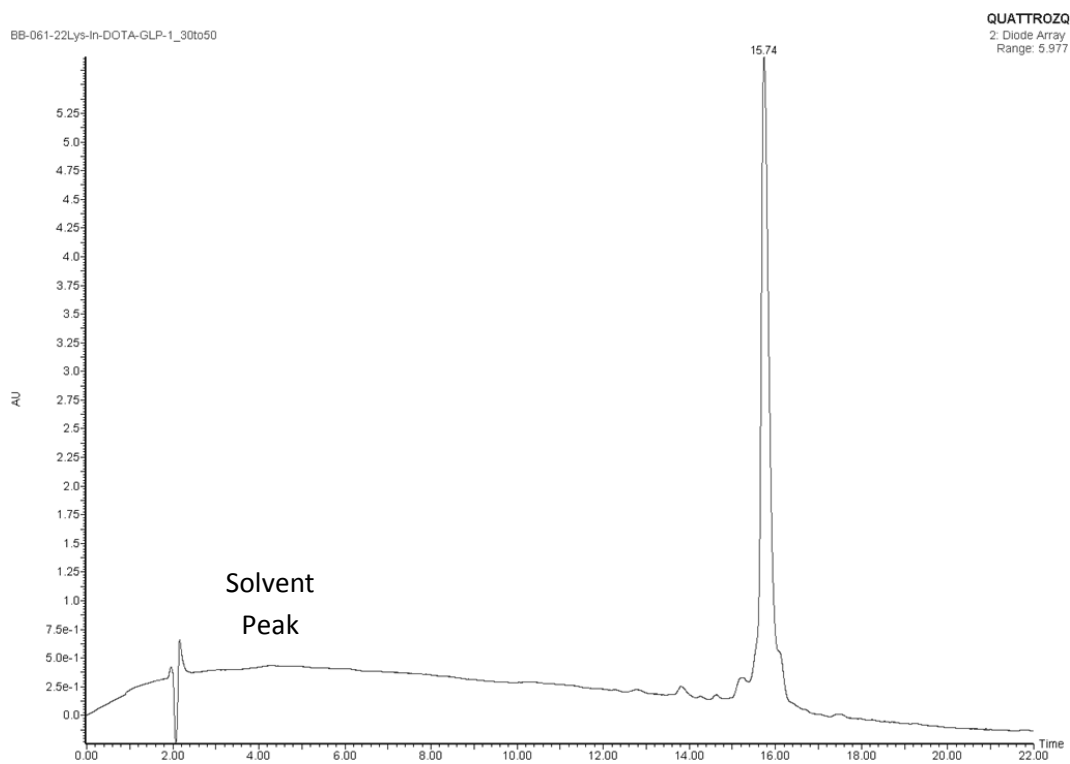
## 5.1 References

1. Hatanaka, N.; Takita, M.; Yamaguchi, T.; Kami, M.; Matsumoto, S., Interests in beta-cell replacement therapies among Japanese patients with type 1 diabetes. *Diabetes Res Clin Pract* **2010**, 89, (1), e5-8.
2. Stephenson, K. A.; Banerjee, S. R.; Besanger, T.; Sogbein, O. O.; Levadala, M. K.; McFarlane, N.; Lemon, J. A.; Boreham, D. R.; Maresca, K. P.; Brennan, J. D.; Babich, J. W.; Zubieta, J.; Valliant, J. F., Bridging the gap between in vitro and in vivo imaging: Isostructural Re and Tc-99m complexes for correlating

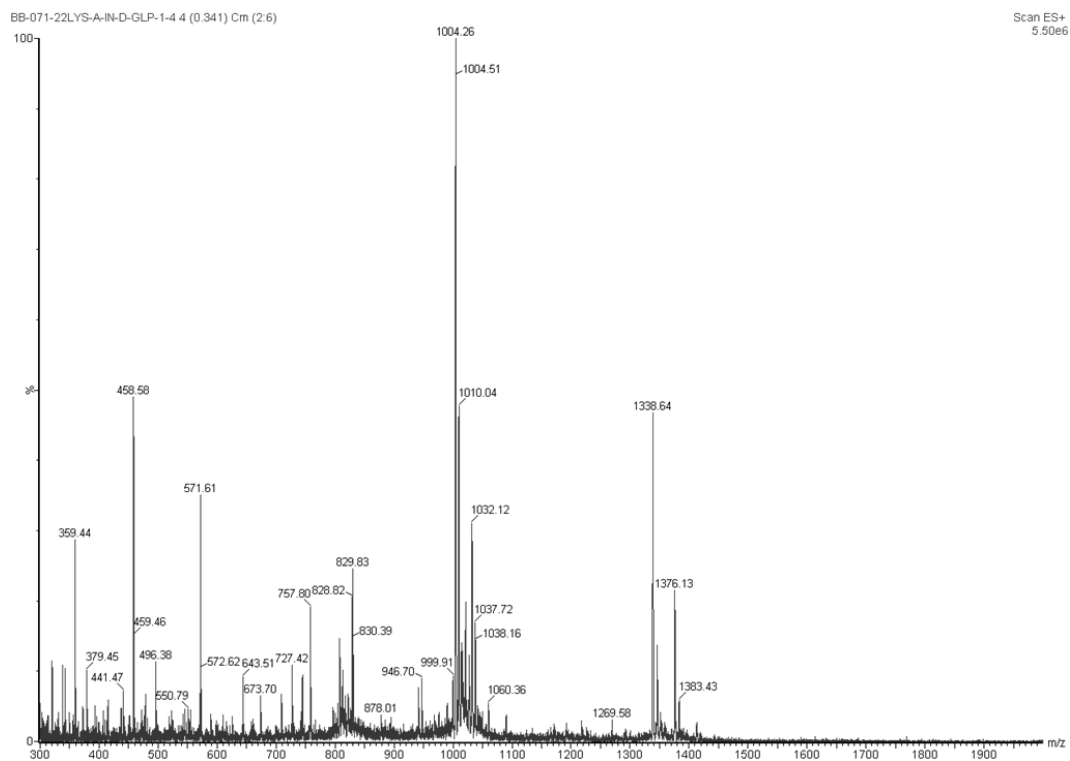
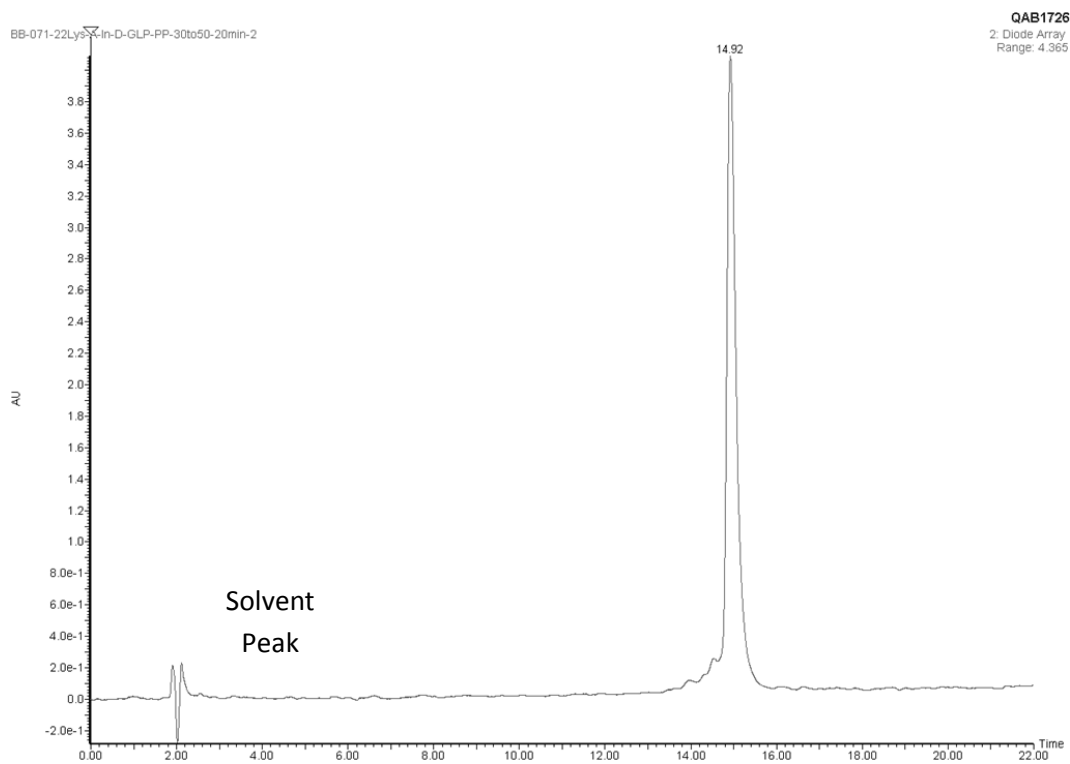
- fluorescence and radioimaging studies. *Journal of the American Chemical Society* **2004**, 126, (28), 8598-8599.
3. Hu, Y.; Geissinger, P.; Woehl, J. C., Potential of protoporphyrin IX and metal derivatives for single molecule fluorescence studies. *Journal of Luminescence* **2011**, 131, 477-481.
  4. Lam, K. S., Application of the "one-bead one-compound" combinatorial library method in basic research and drug discovery. *Abstracts of Papers of the American Chemical Society* **1996**, 211, 10-IEC.
  5. Lam, K. S.; Lebl, M.; Krchnak, V., The "one-bead-one-compound" combinatorial library method. *Chemical Reviews* **1997**, 97, (2), 411-448.
  6. Kennedy, J. P.; Williams, L.; Bridges, T. M.; Daniels, R. N.; Weaver, D.; Lindsley, C. W., Application of combinatorial chemistry science on modern drug discovery. *Journal of Combinatorial Chemistry* **2008**, 10, (3), 345-354.

## APPENDIX I - CHAPTER 2

## HPLC and MS-ESI spectra of 1 (Purity 90%)

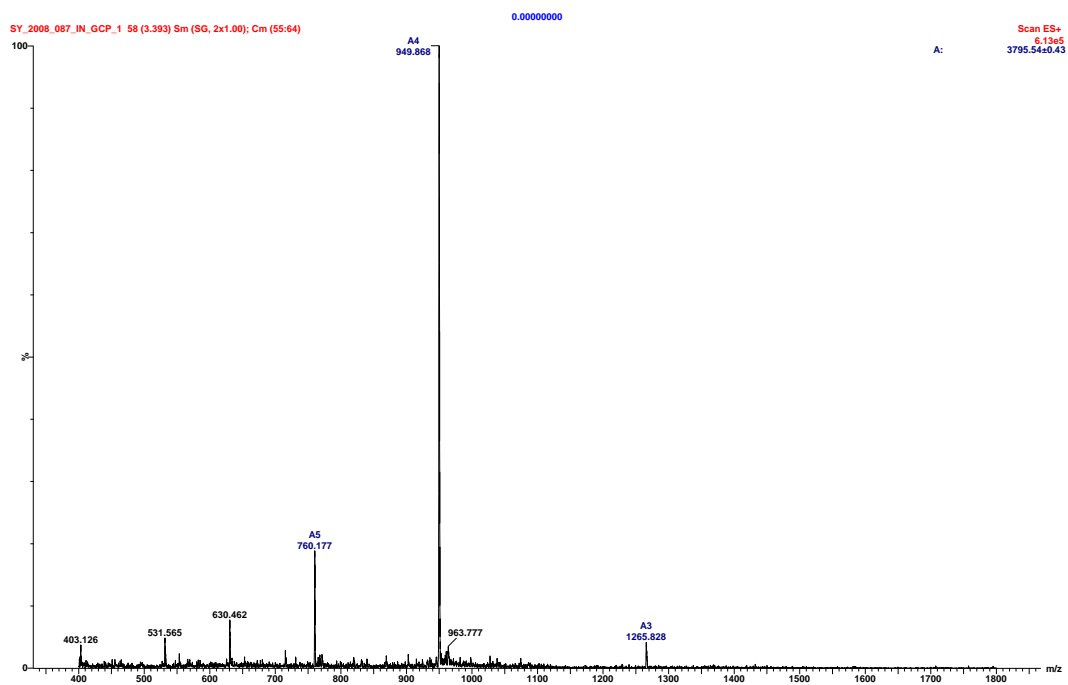
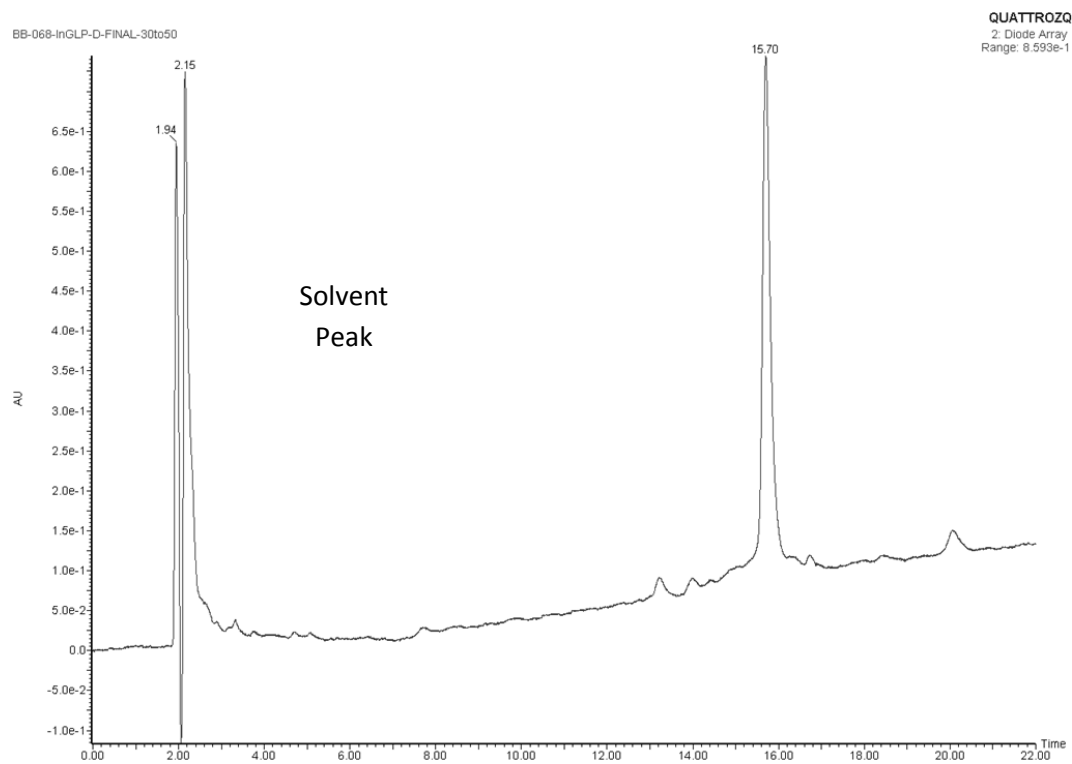


## HPLC and MS-ESI spectra of 2 (Purity 98%)

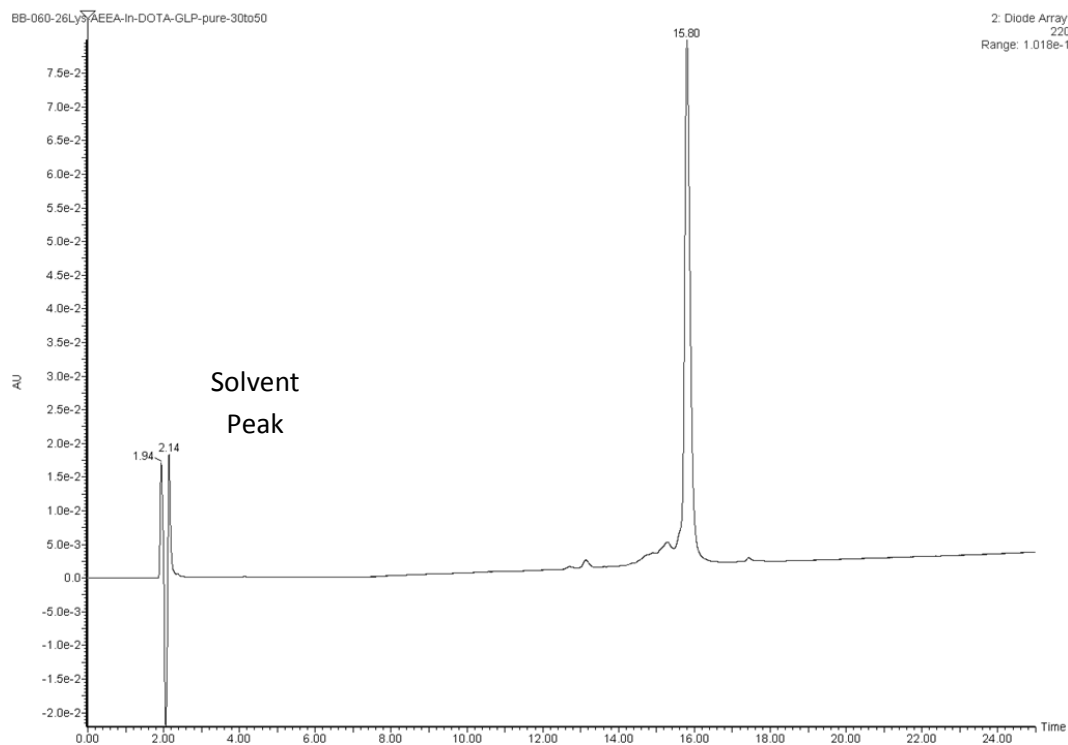




## HPLC and MS-ESI spectra of 3 (Purity 95%)

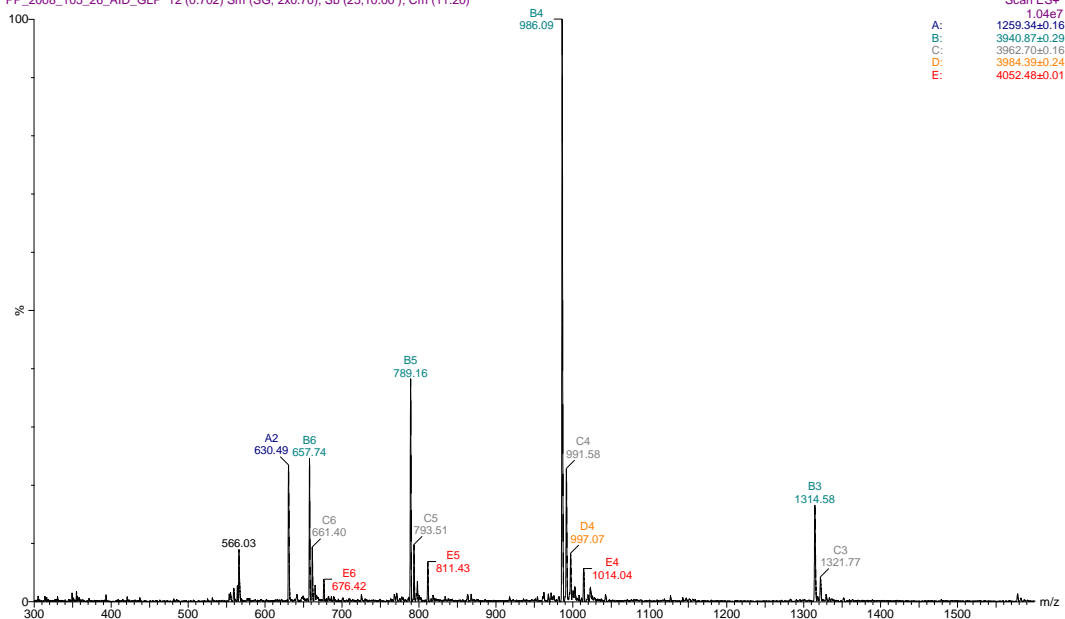


## HPLC and MS-ESI spectra of 4 (Purity 90%)

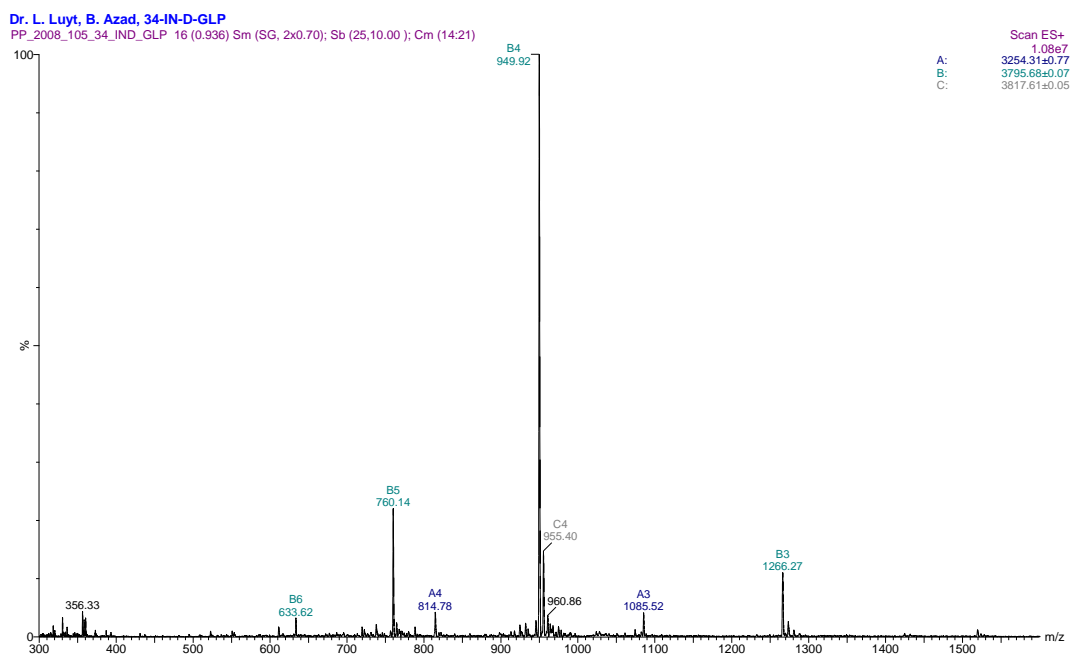
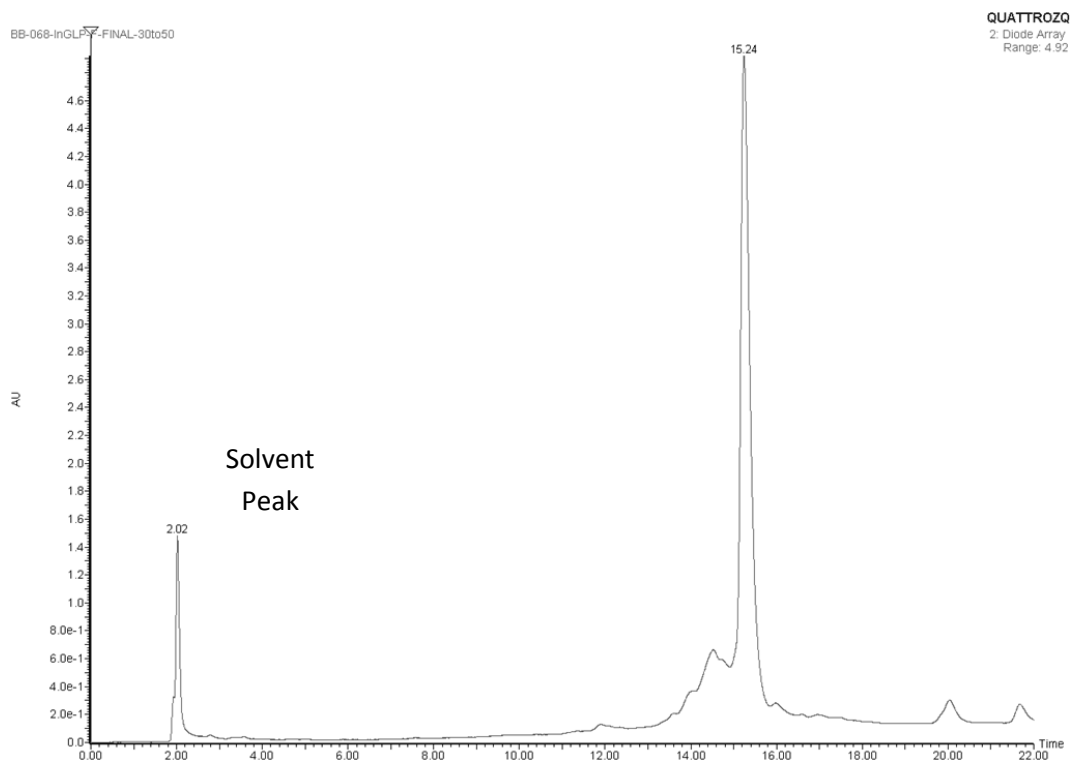


Dr. L. Luyt, B. Azad, 26-A-I-D-GLP

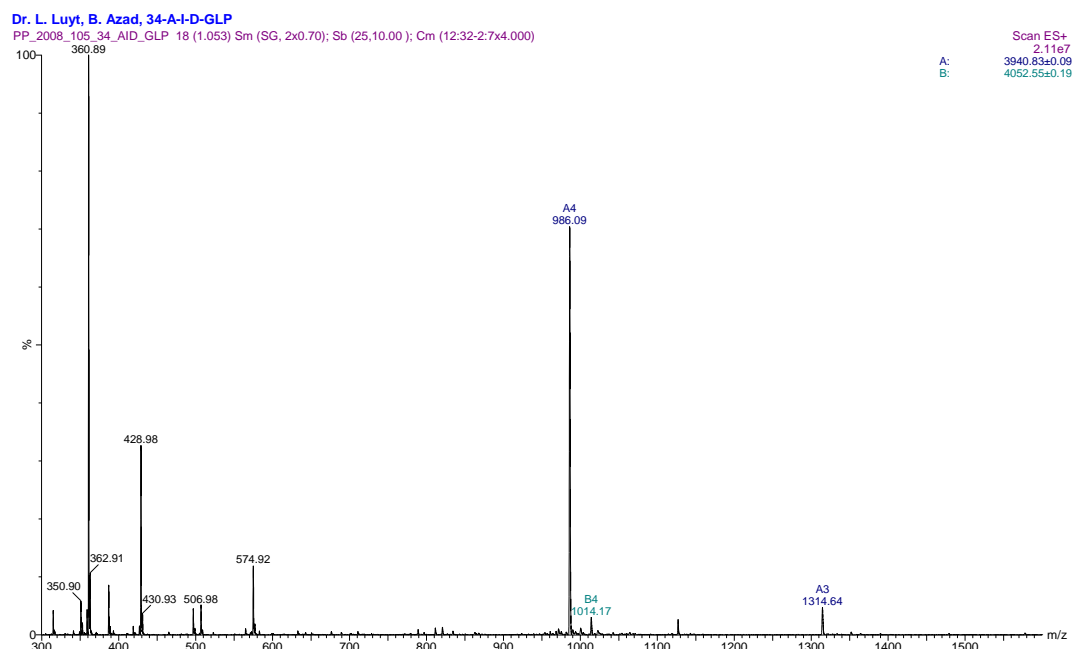
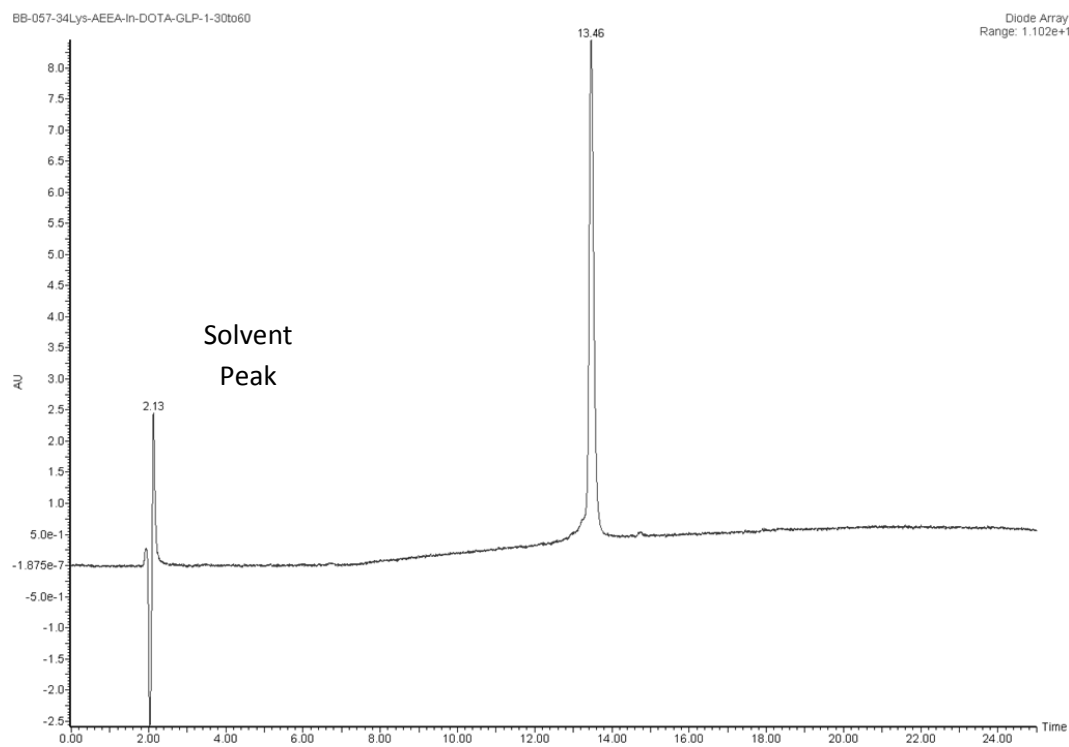
PP\_2008\_105\_26\_AID\_GLP 12 (0.702) Sm (SG, 2x0.70); Sb (25,10.00); Cm (11:20)



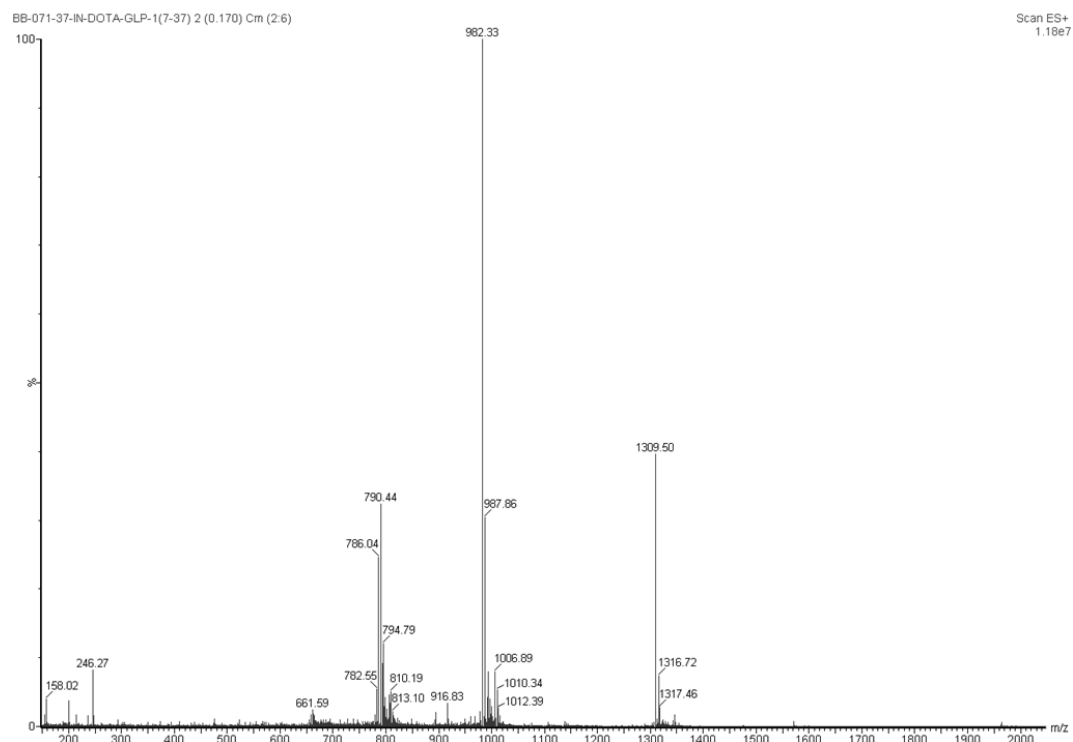
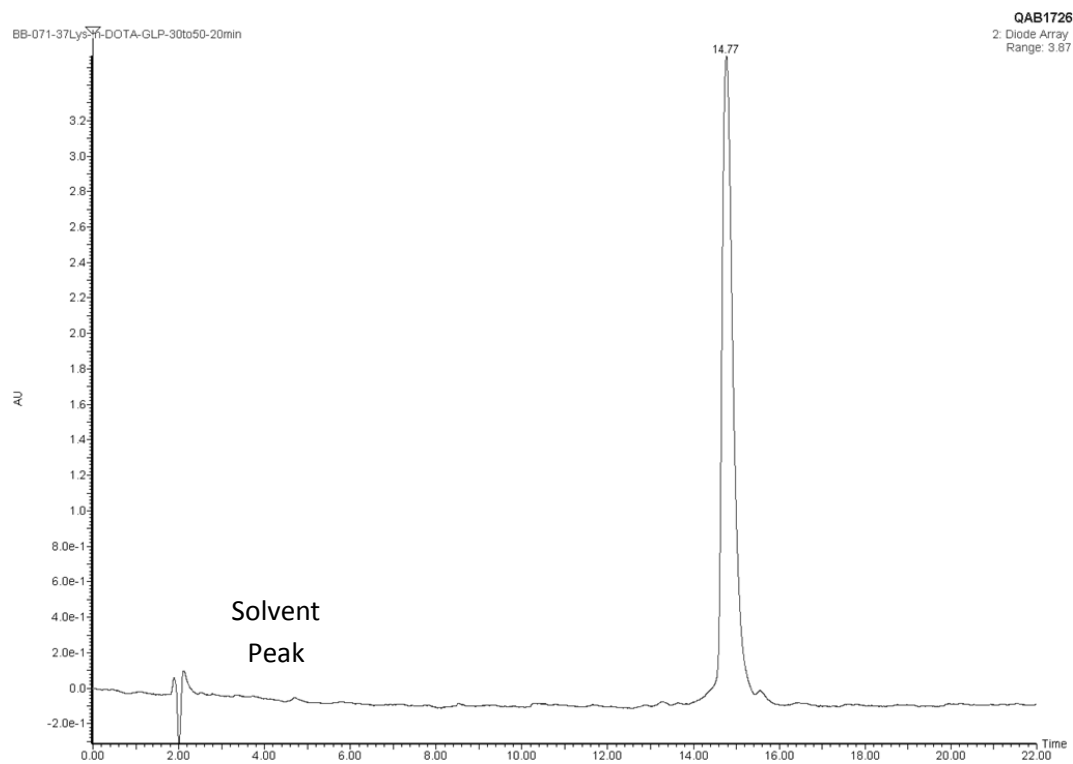
## HPLC and MS-ESI spectra of 5 (85.3%)



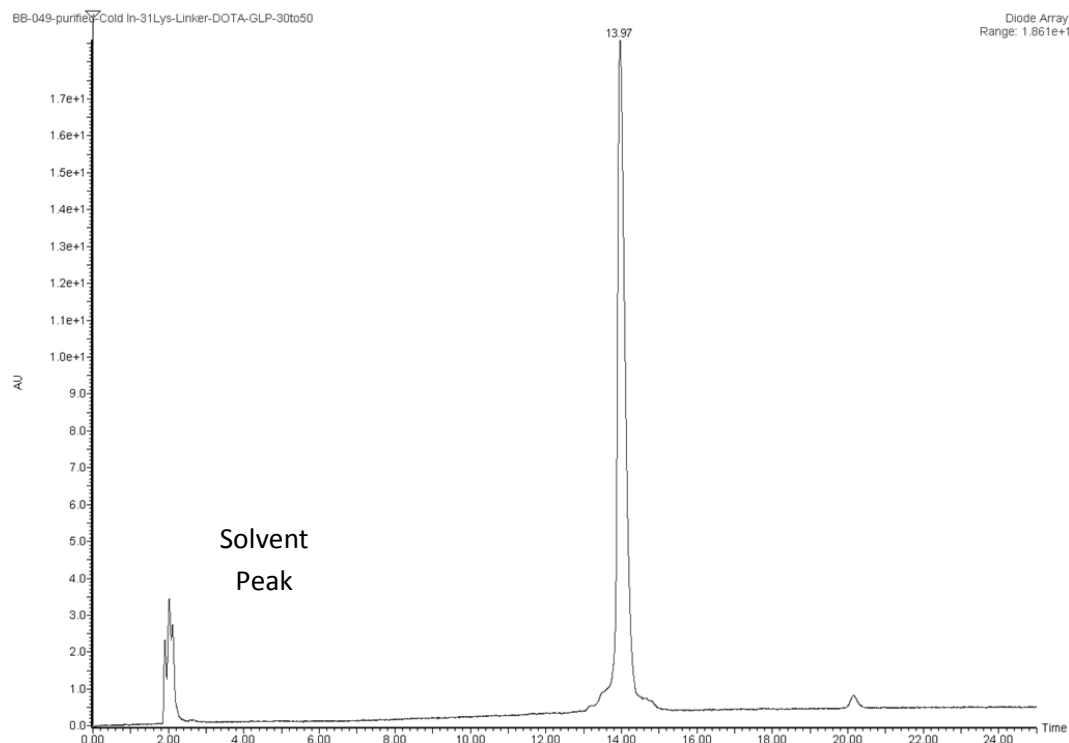
## HPLC and MS-ESI spectra of 6 (Purity 97%)



## HPLC and MS-ESI spectra of 7 (Purity 98%)

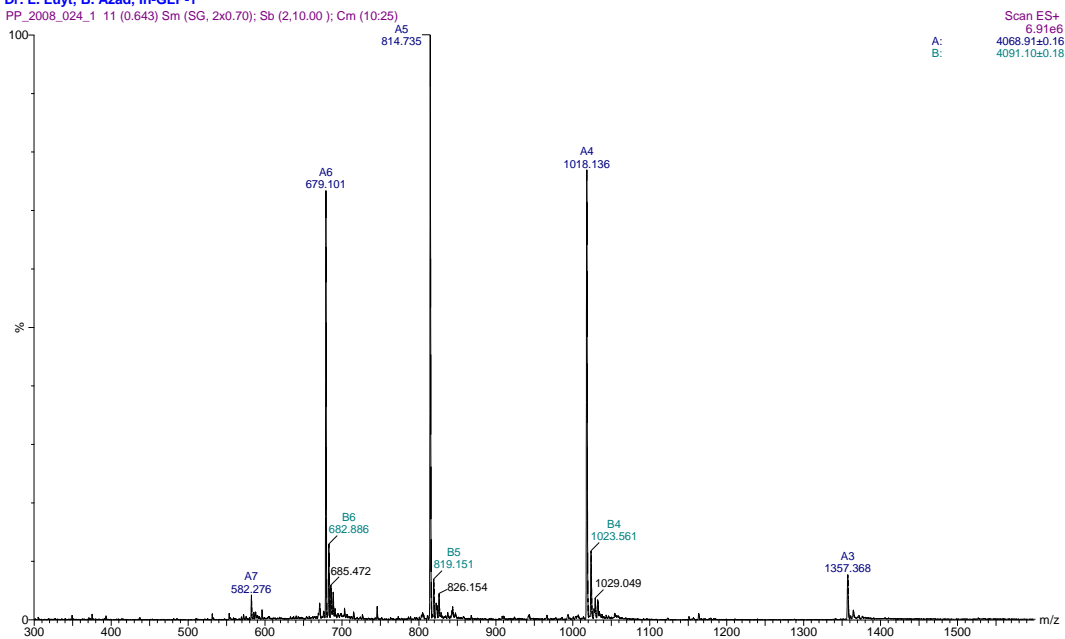


## HPLC and MS-ESI spectra of 8 (Purity 95.3%)



## Dr. L. Luyt, B. Azad, In-GLP-1

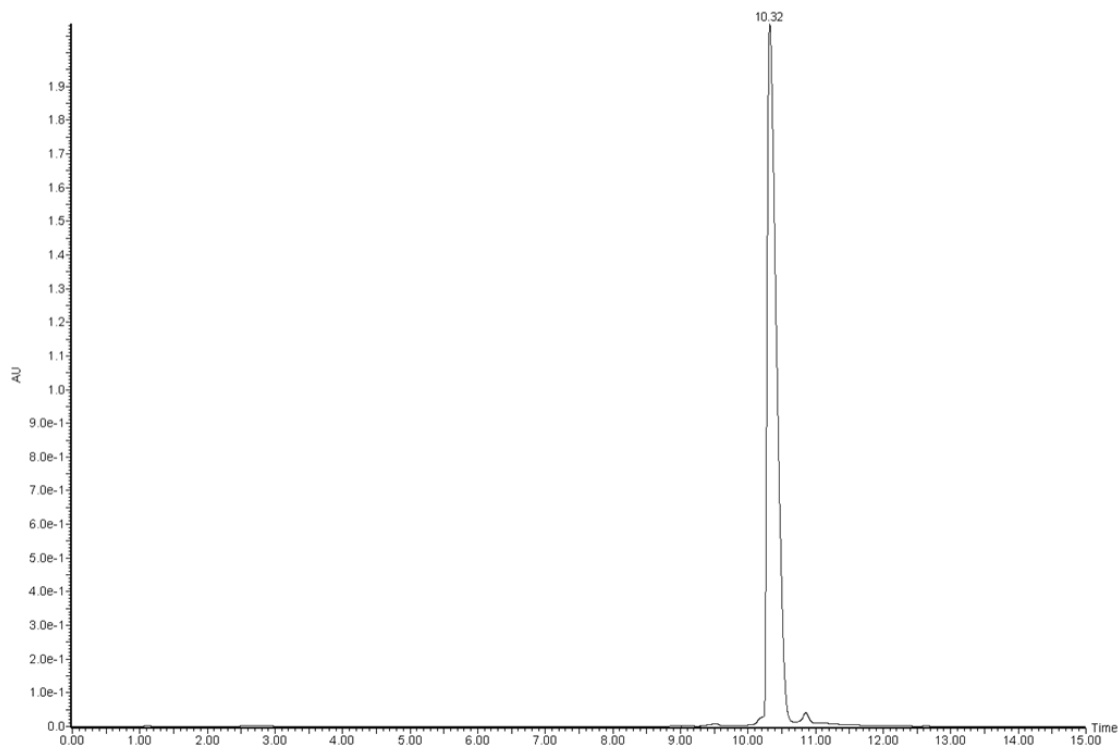
PP\_2008\_024\_1 11 (0.643) Sm (SG, 2x0.70); Sb (2,10.00); Cm (10:25)



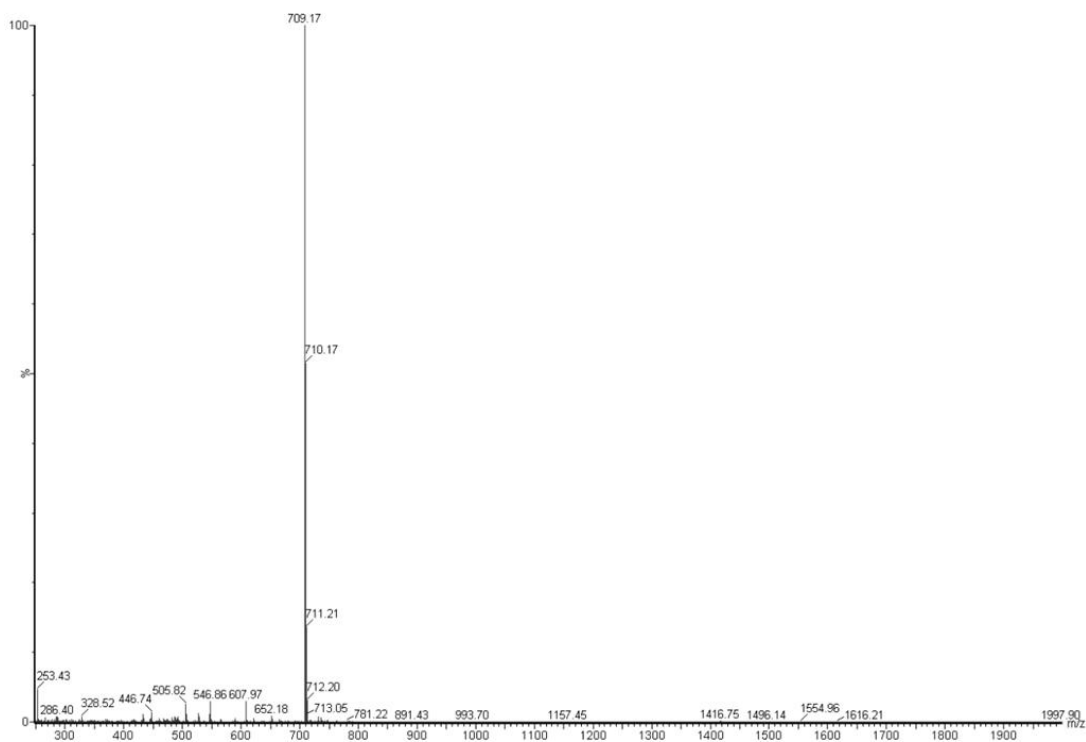
## APPENDIX II – CHAPTER 3

## UV and ESI-MS Spectra of HPLC-Purified 2

Default file

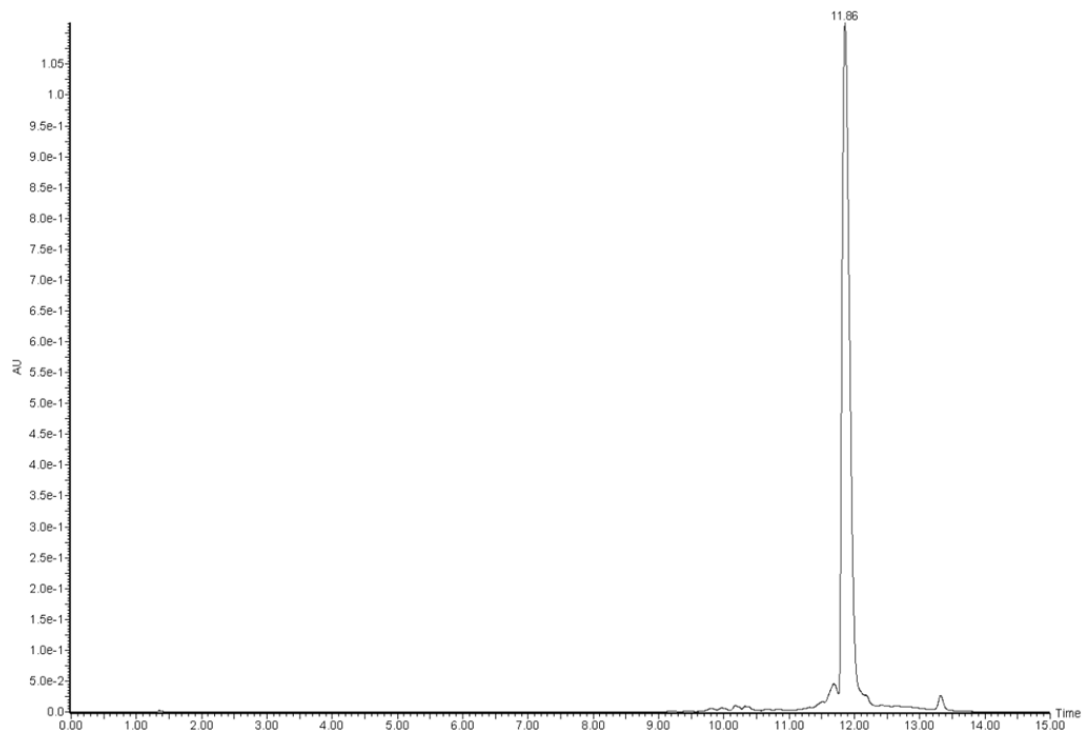


Default file

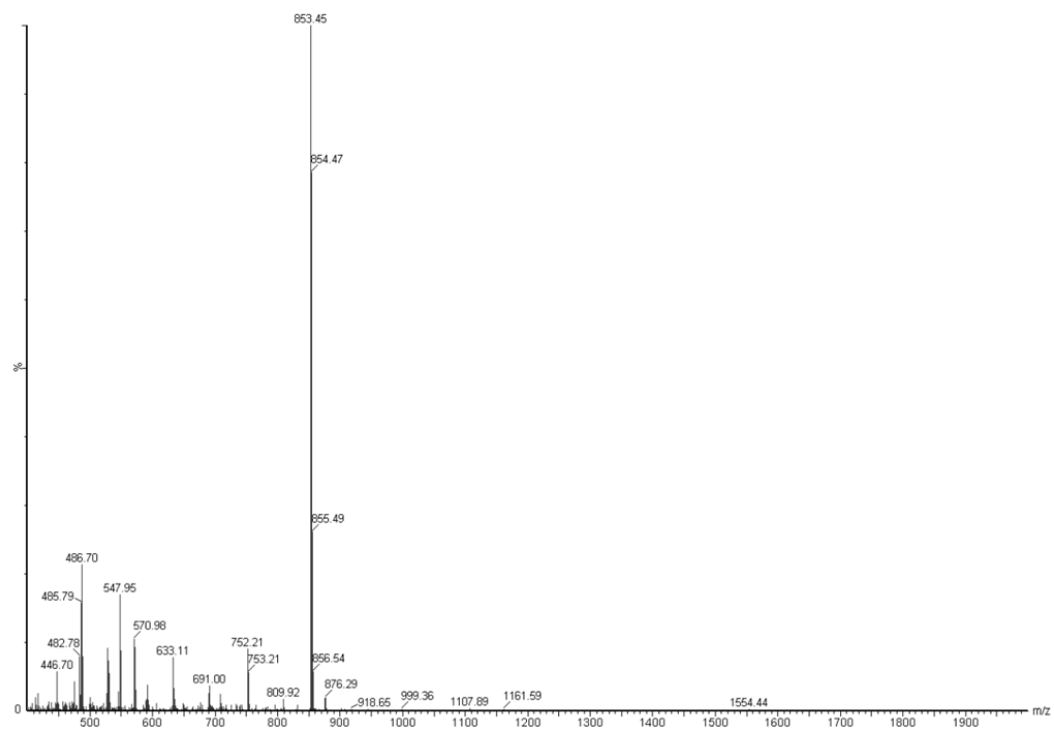


## UV and ESI-MS Spectra of HPLC-Purified 3

Default file

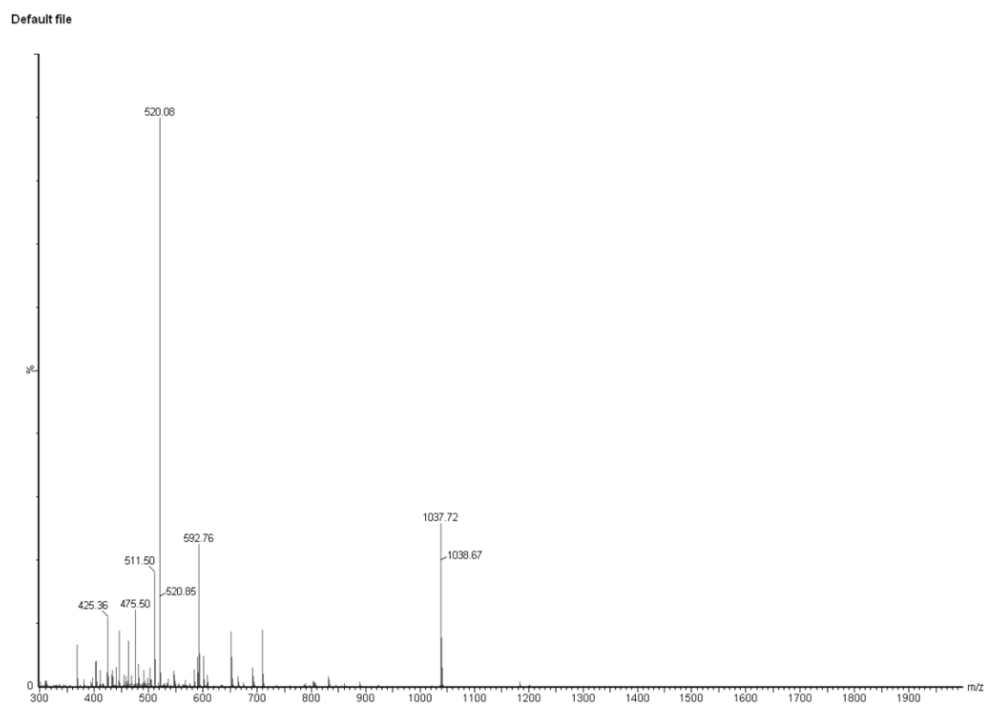
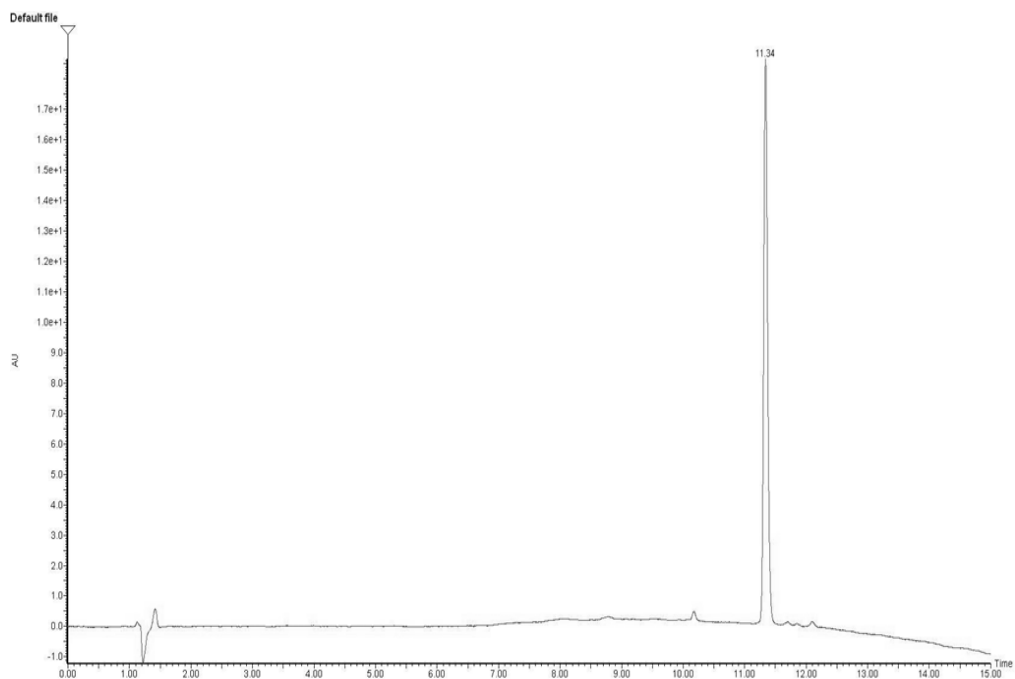


Default file

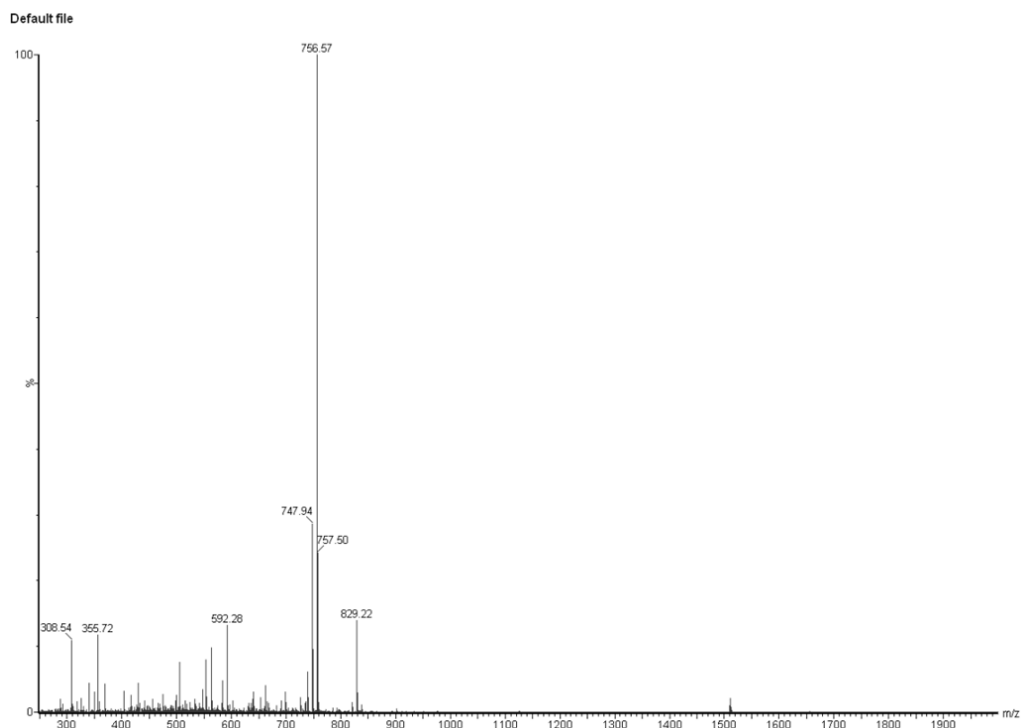
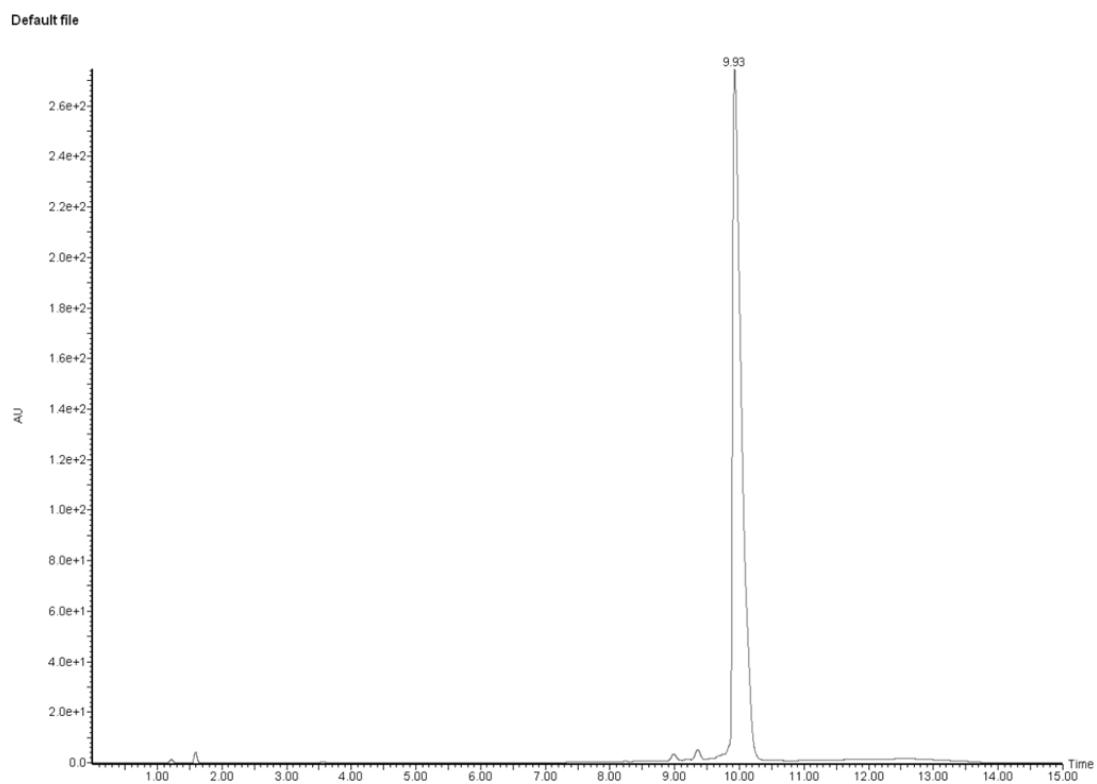




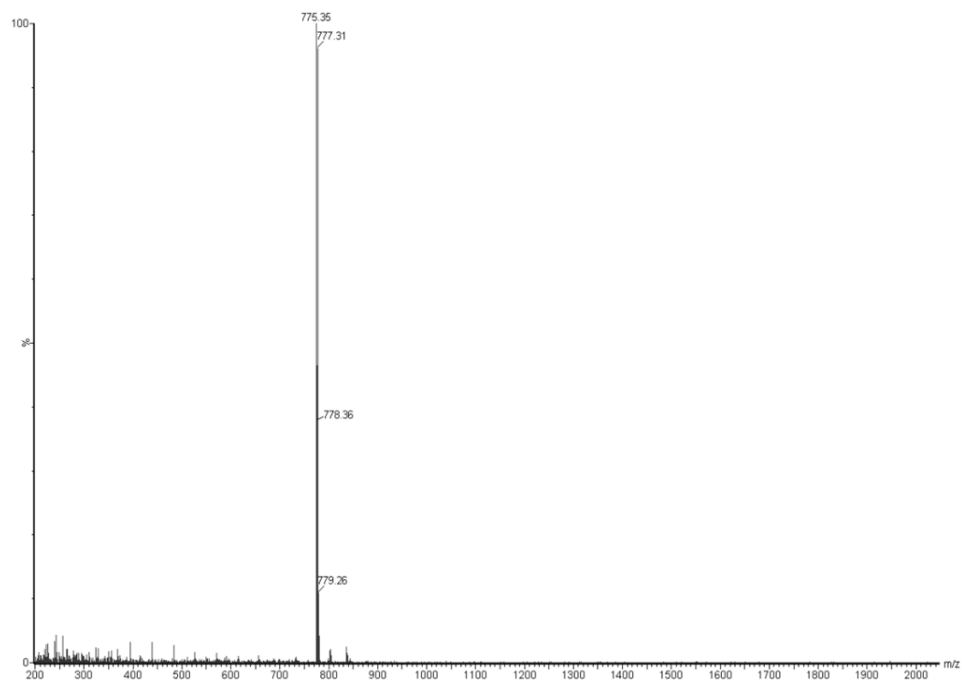
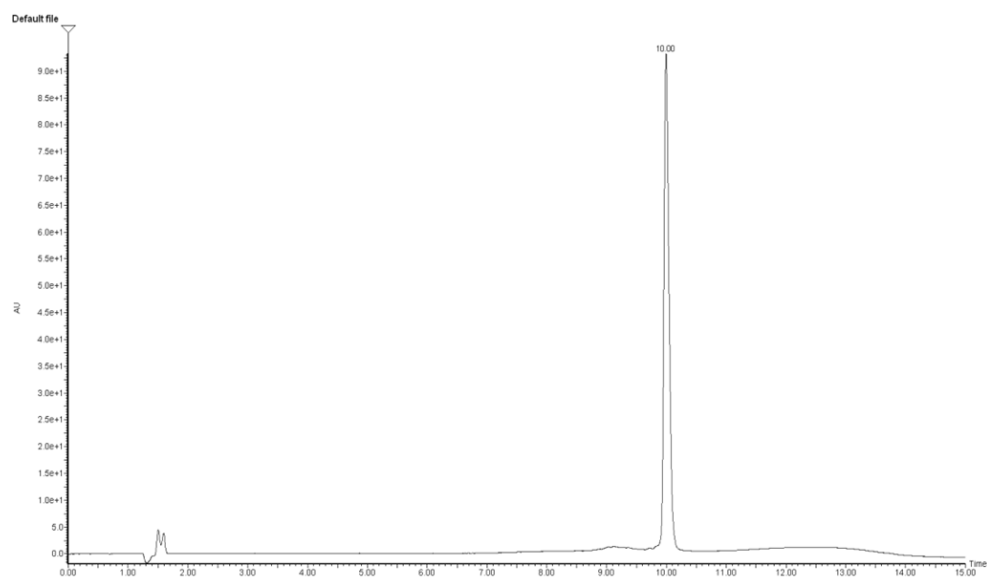
## UV and ESI-MS Spectra of HPLC-Purified 4



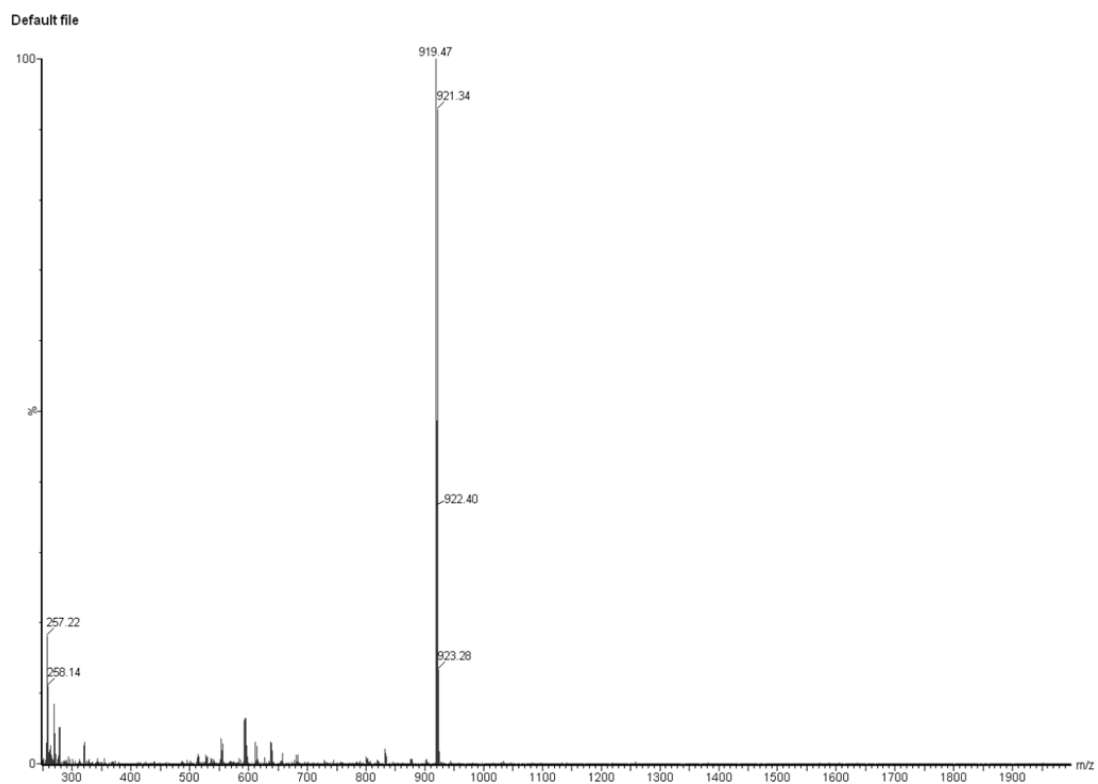
## UV and ESI-MS Spectra of HPLC-Purified 5



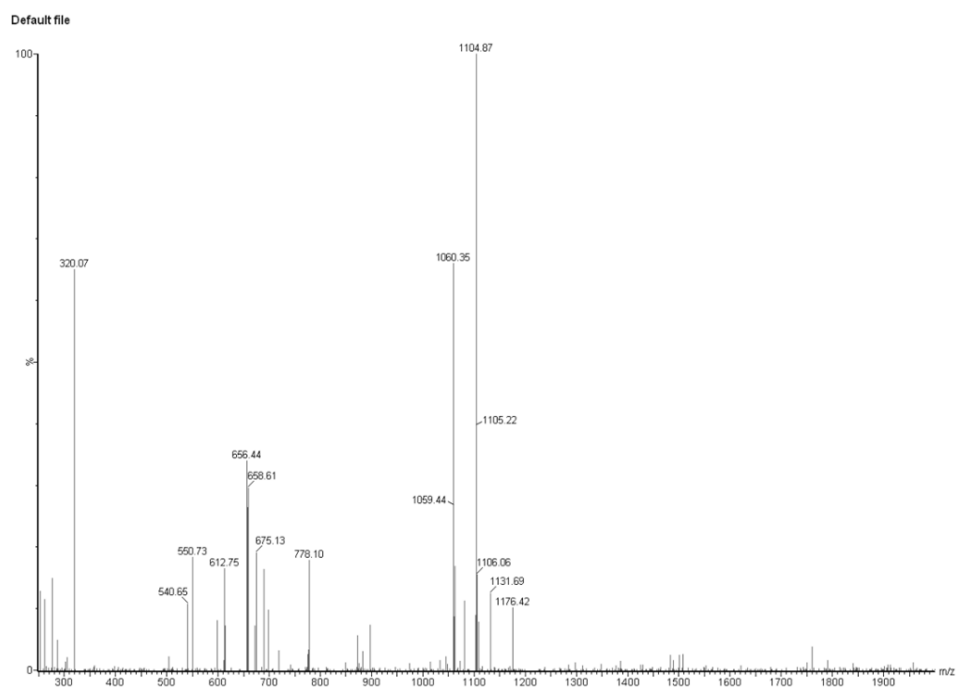
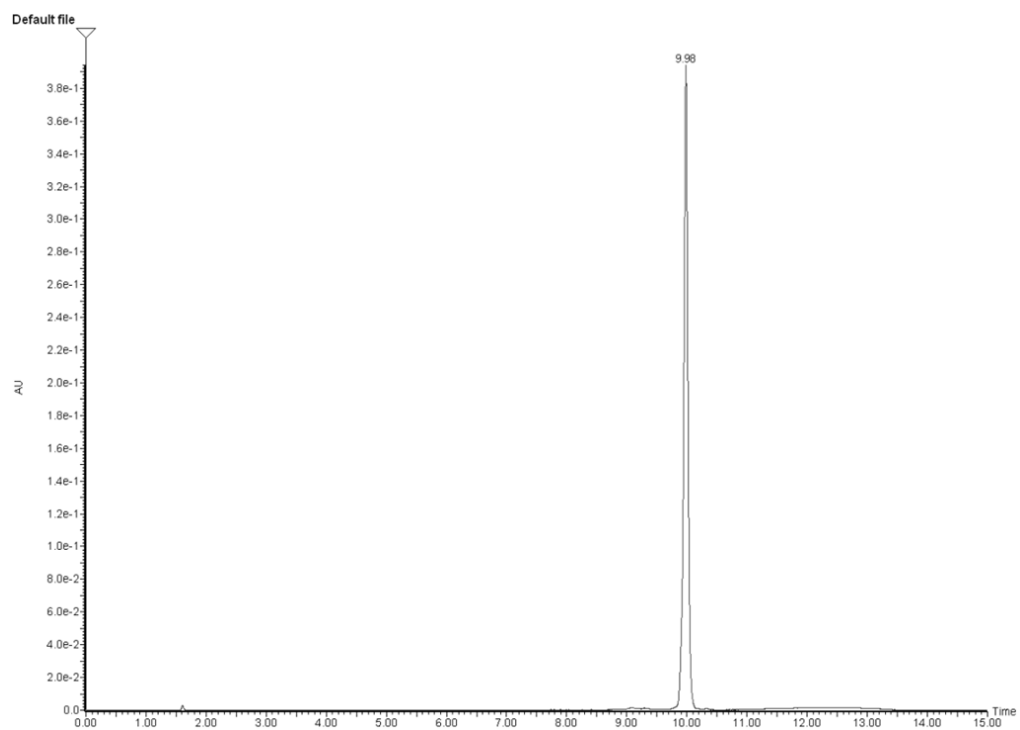
## UV and ESI-MS Spectra of HPLC-Purified 6



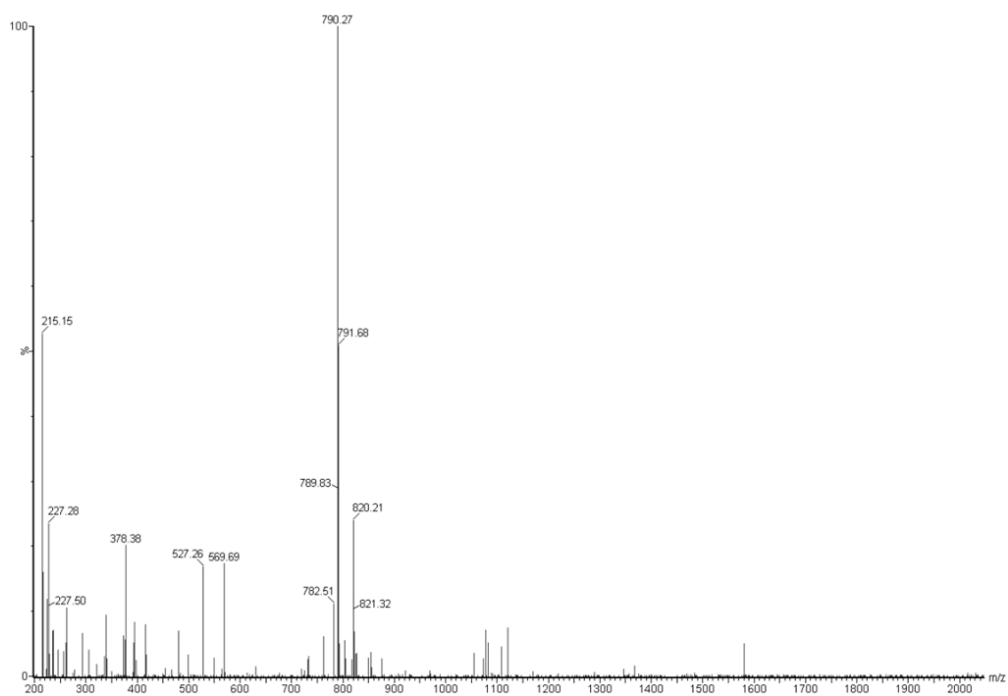
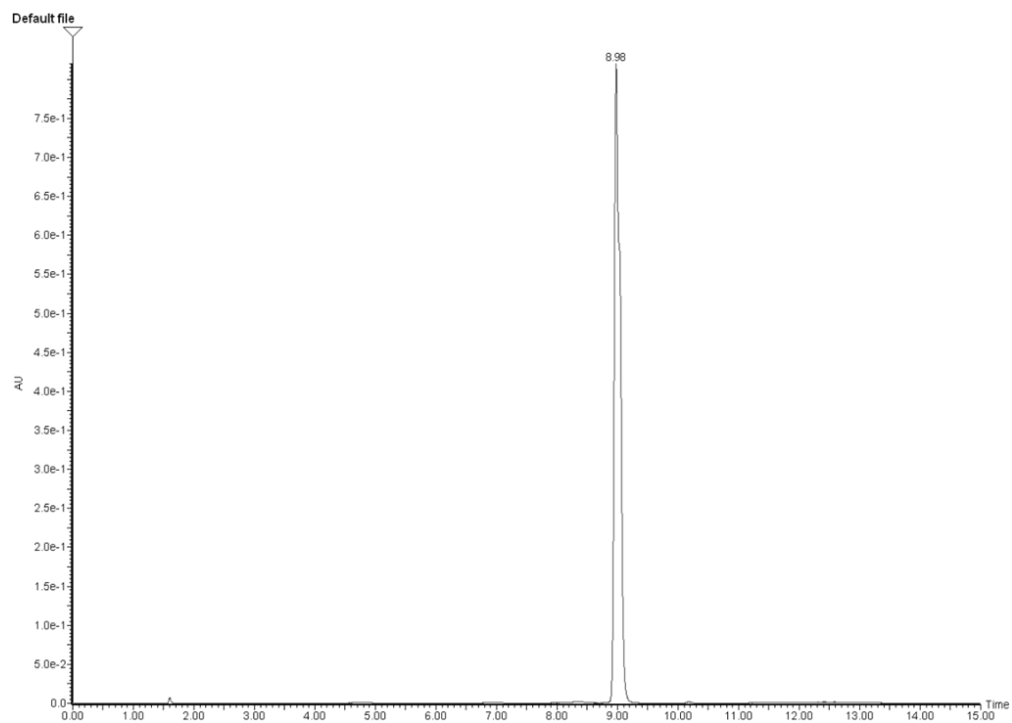
## UV and ESI-MS Spectra of HPLC-Purified 7



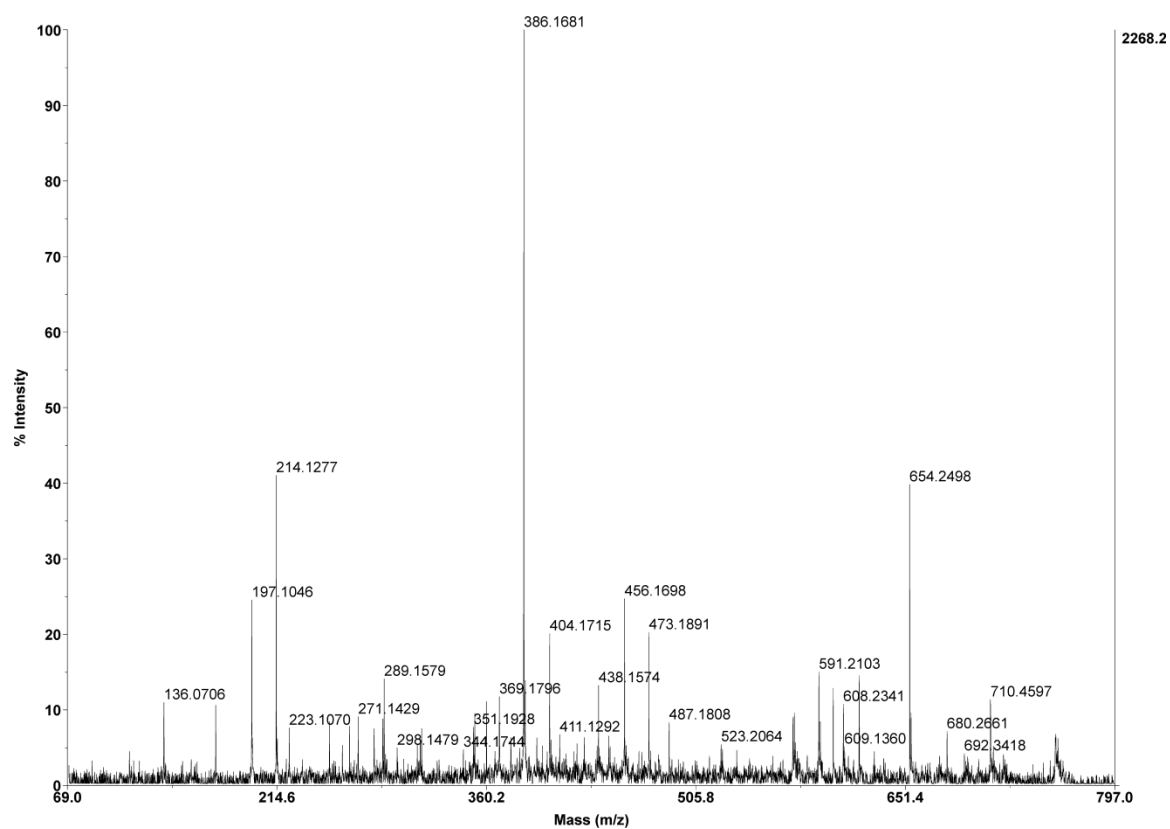
## UV and ESI-MS Spectra of HPLC-Purified 8



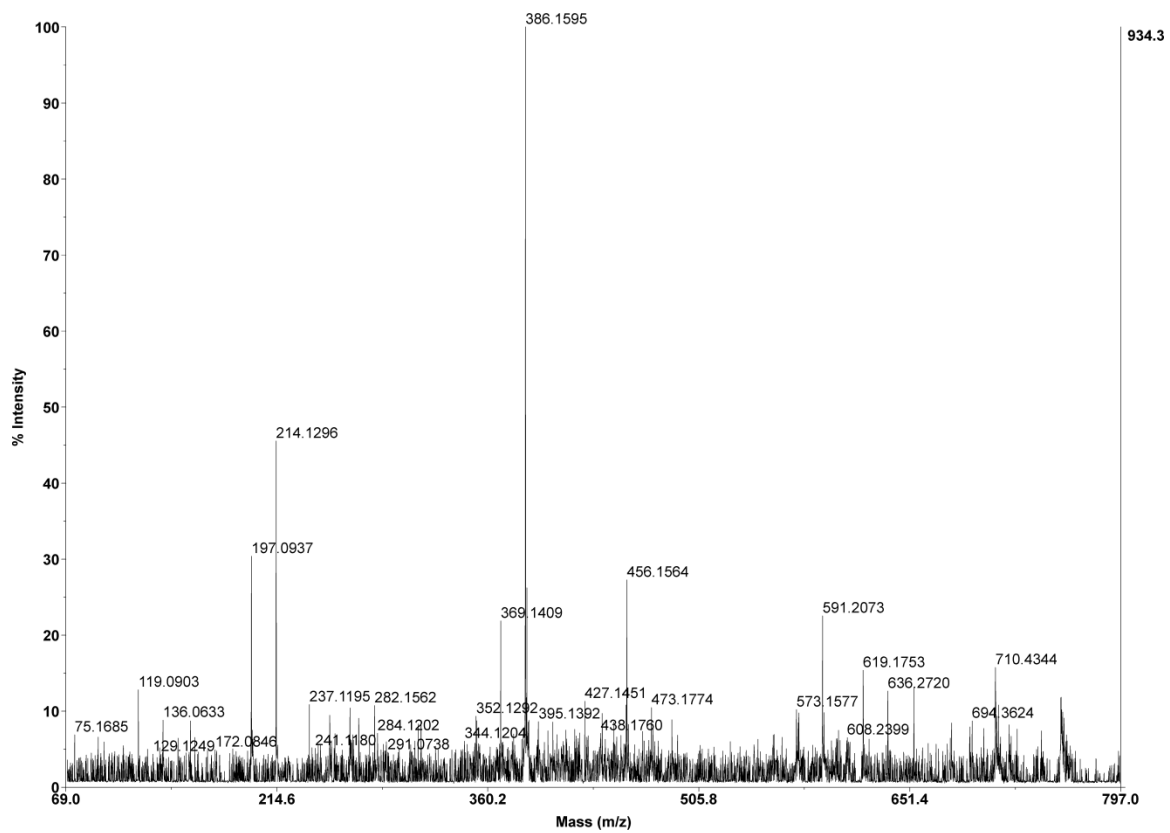
## UV and ESI-MS Spectra of HPLC-Purified 9



## APPENDIX III - CHAPTER 4

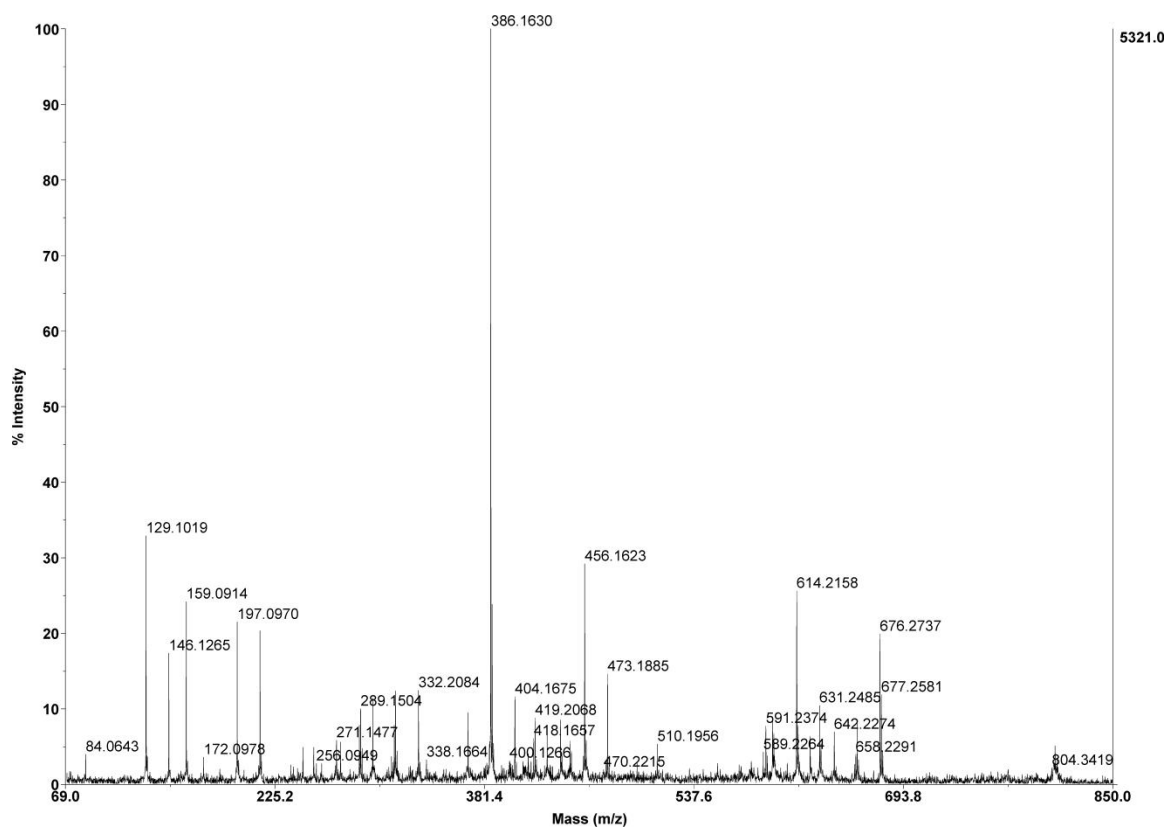


MS/MS spectrum of untreated H-GRGDSYT-NH<sub>2</sub> (2) post cleavage from tentagel resin

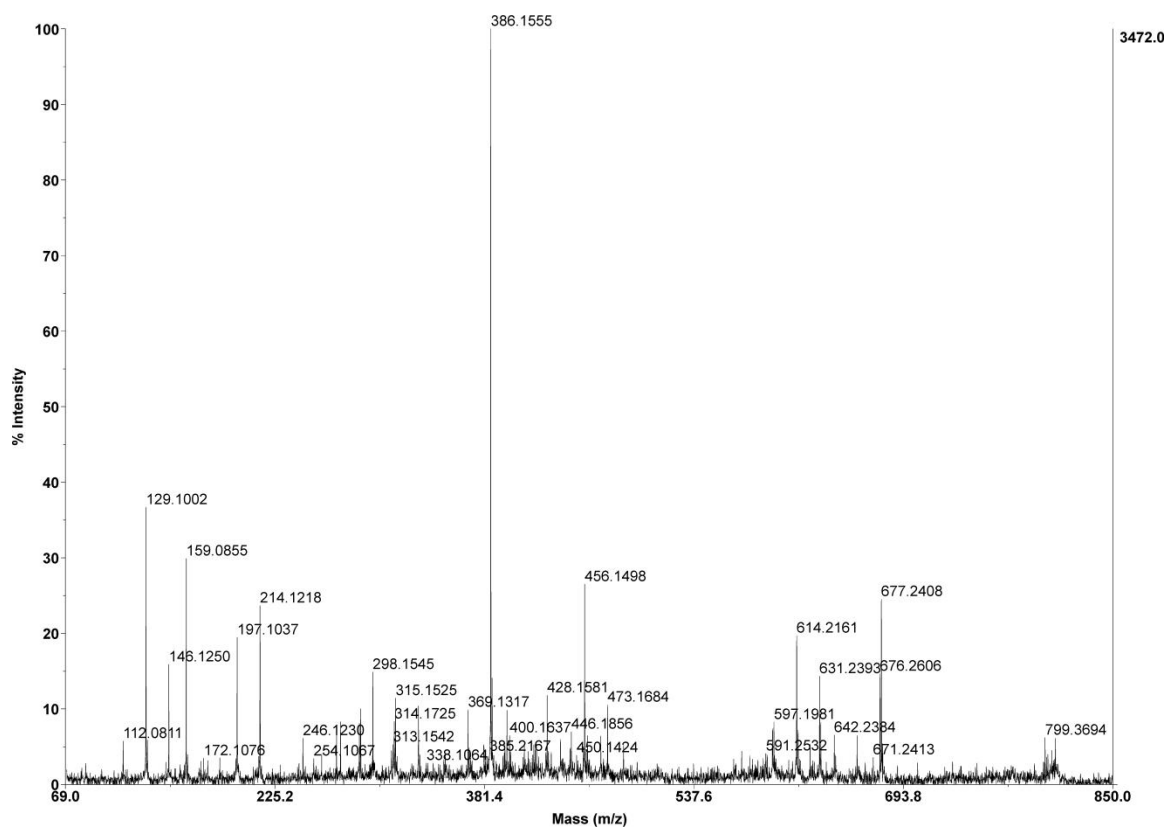


MS/MS spectrum of sorted H-GRGDSYT-NH<sub>2</sub> (2) after cleavage from tentagel resin

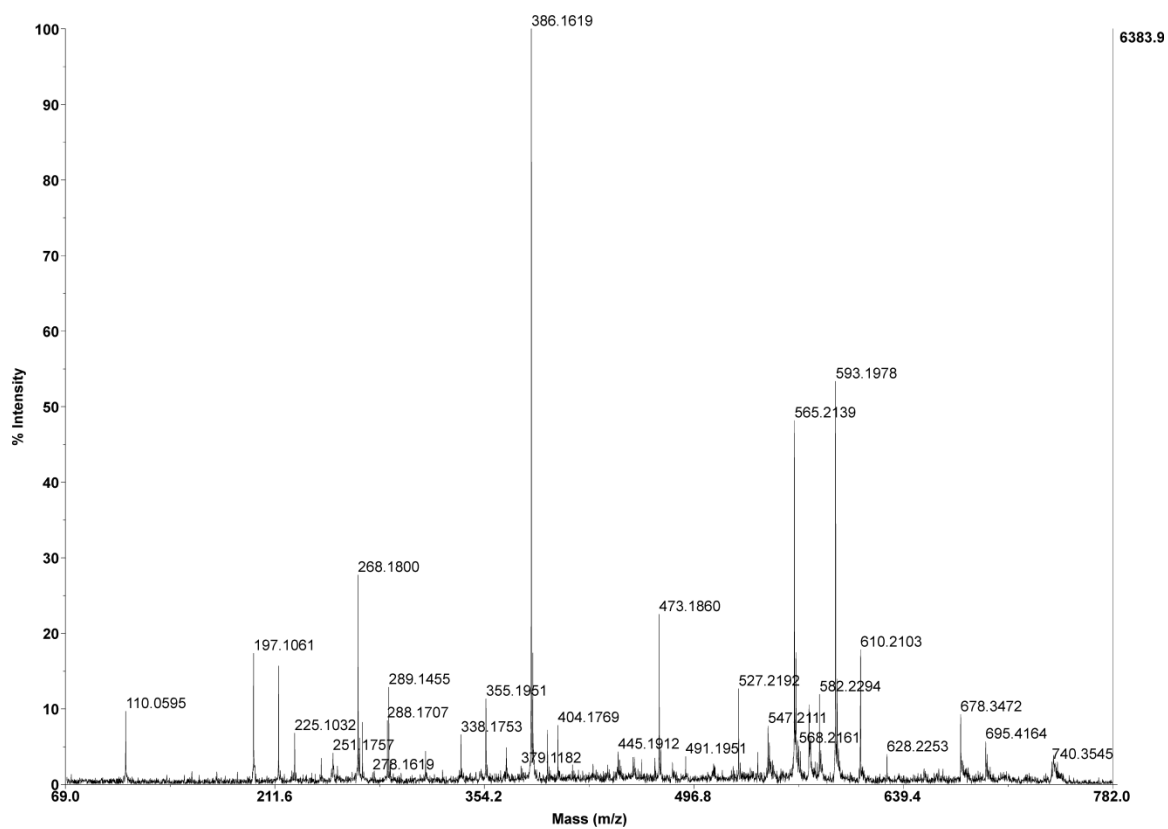




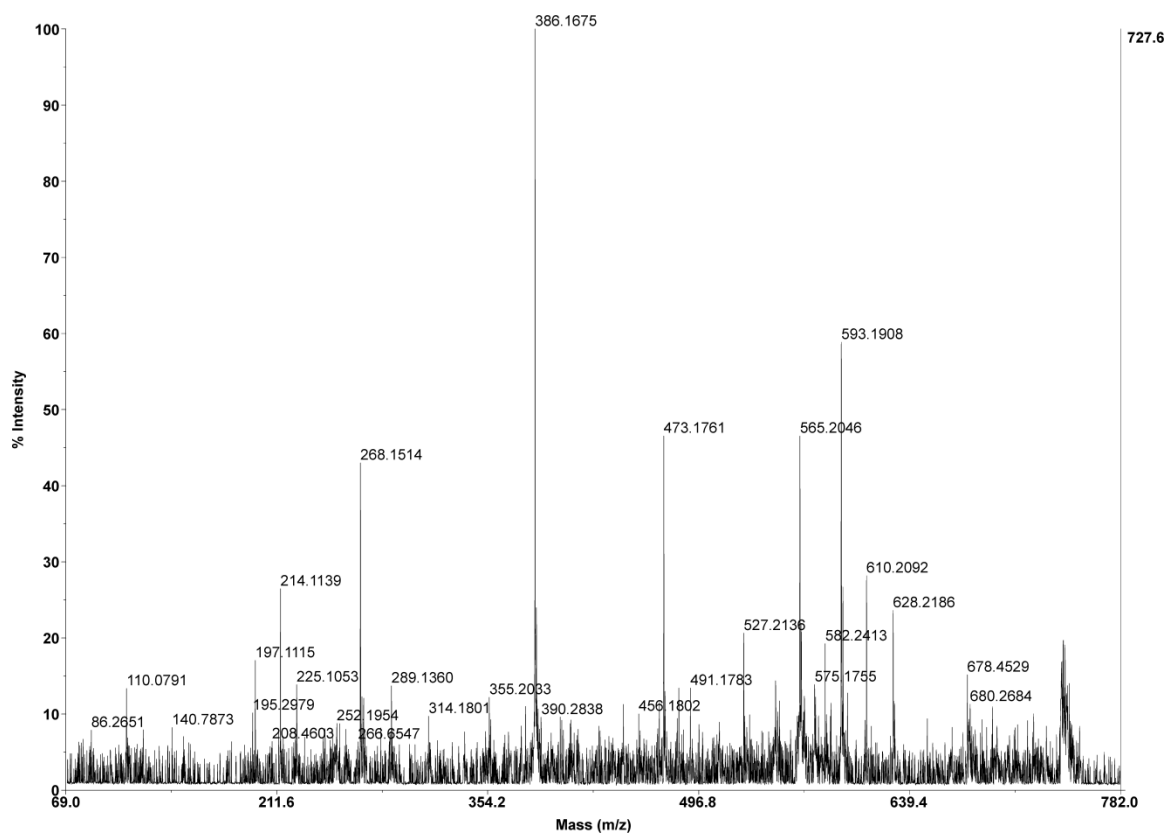
MS/MS spectrum of untreated H-GRGDSWK-NH<sub>2</sub> (**3**) after cleavage from tentagel resin



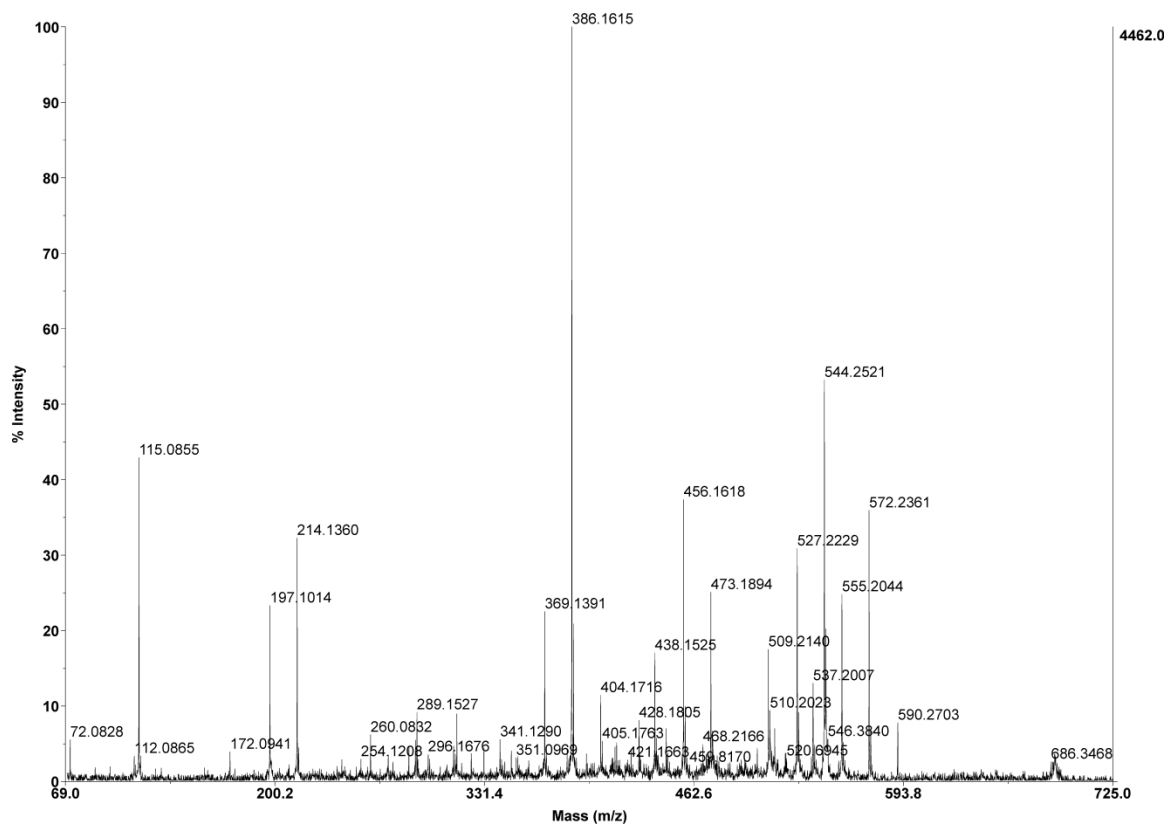
MS/MS spectrum of sorted H-GRGDSWK-NH<sub>2</sub> (**3**) after cleavage from tentagel resin



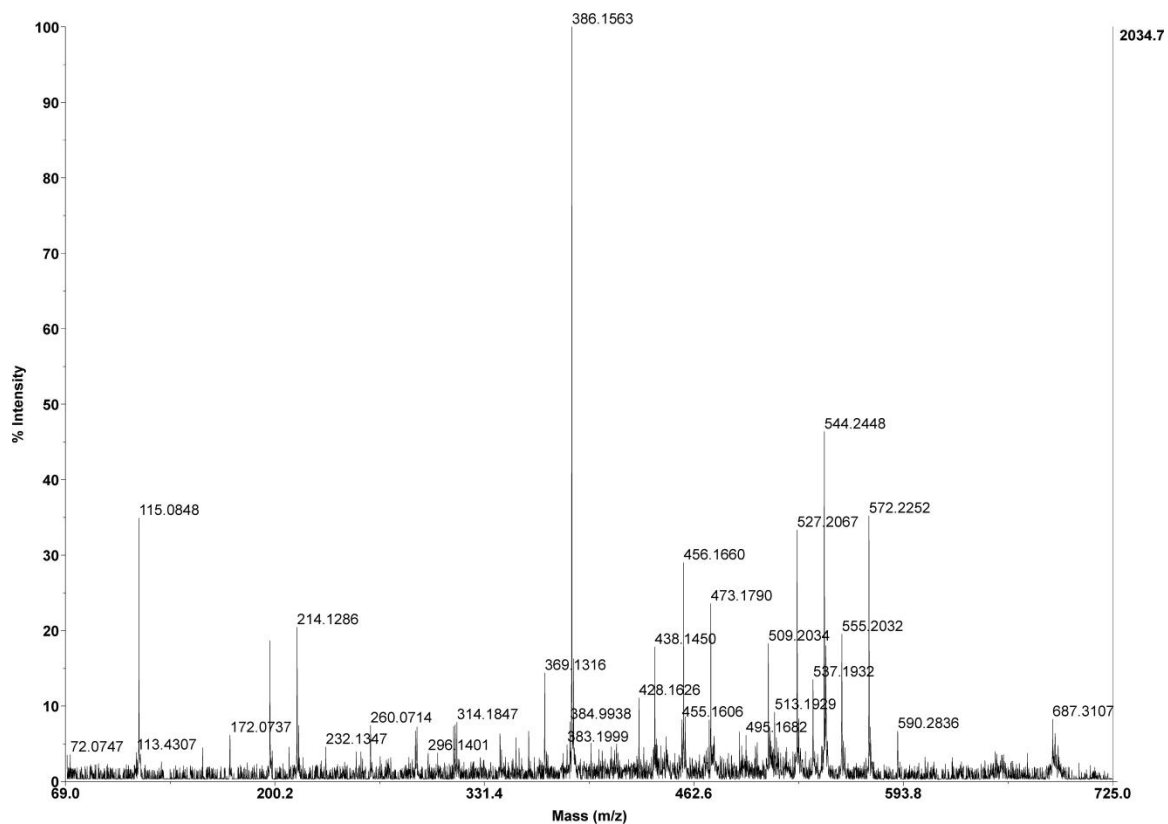
MS/MS spectrum of untreated H-GRGDSHL-NH<sub>2</sub> (**4**) after cleavage from tentagel resin



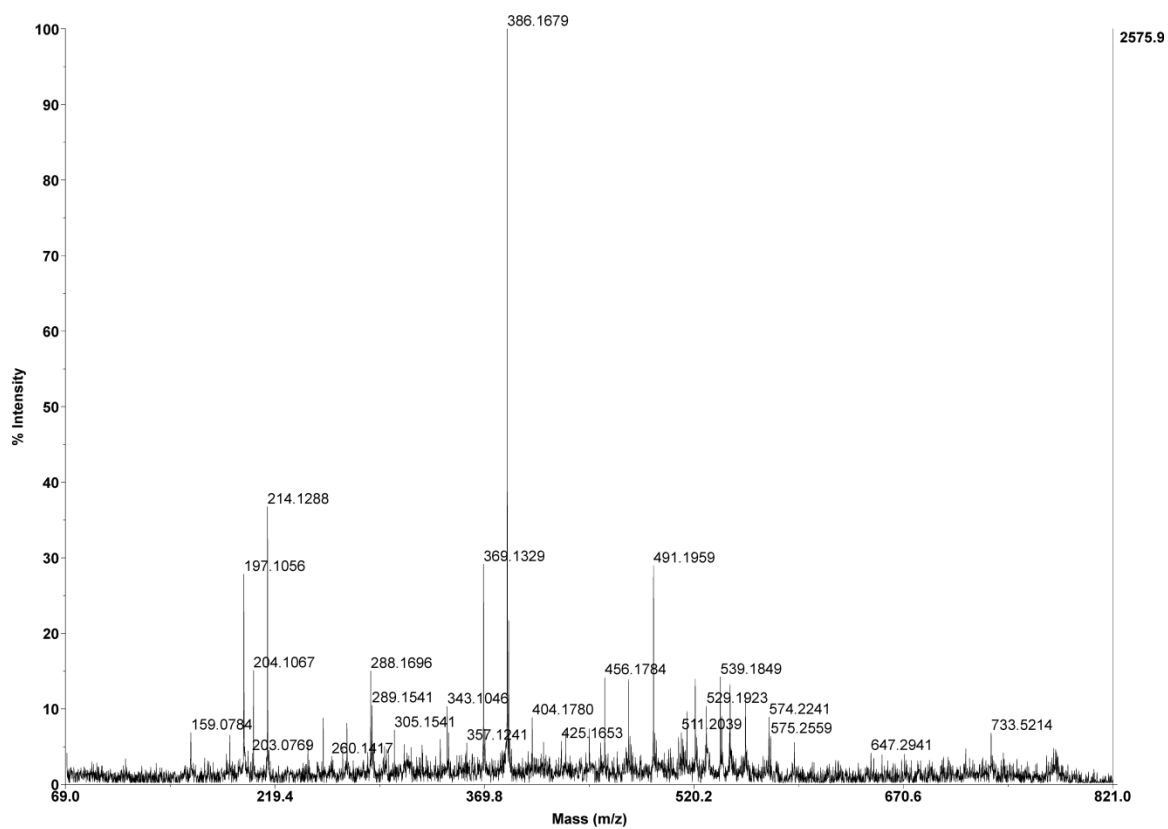
MS/MS spectrum of sorted H-GRGDSHL-NH<sub>2</sub> (**4**) after cleavage from tentagel resin



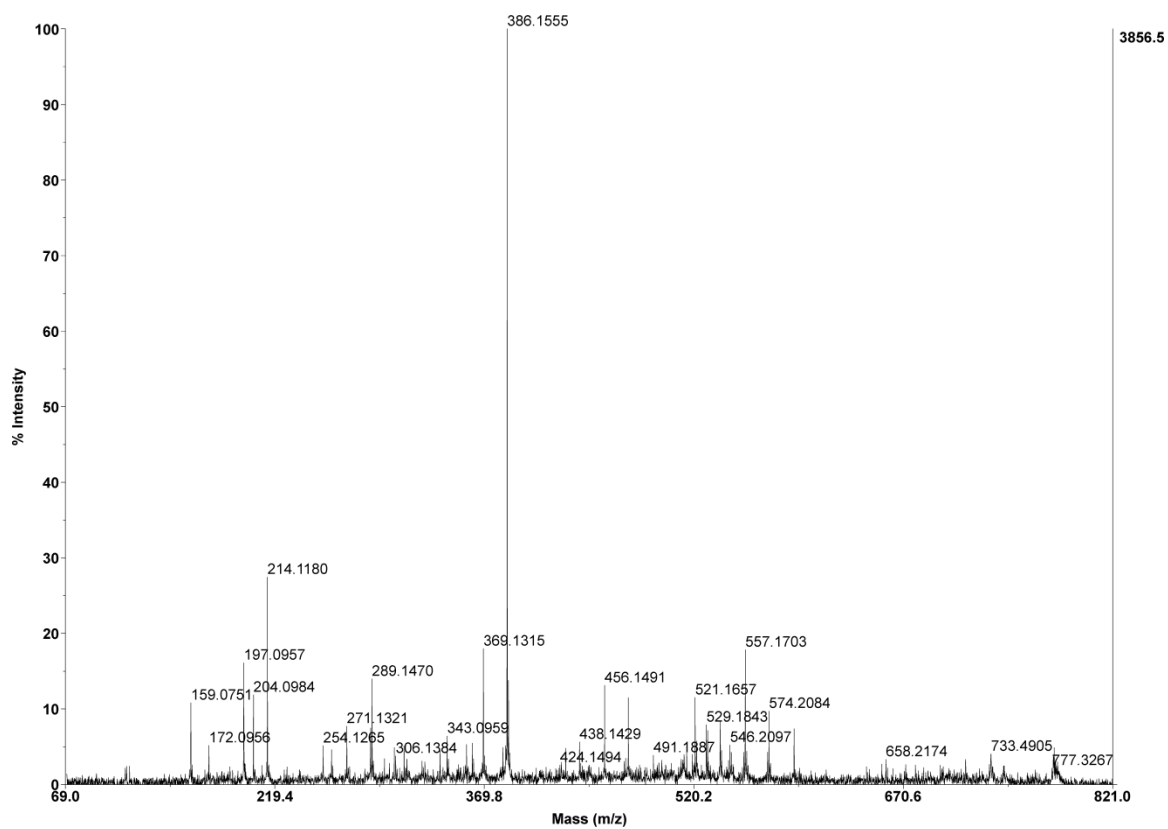
MS/MS spectrum of untreated H-GRGDSVP-NH<sub>2</sub> (**5**) after cleavage from tentagel resin



MS/MS spectrum of sorted H-GRGDSVP-NH<sub>2</sub> (**5**) after cleavage from tentagel resin

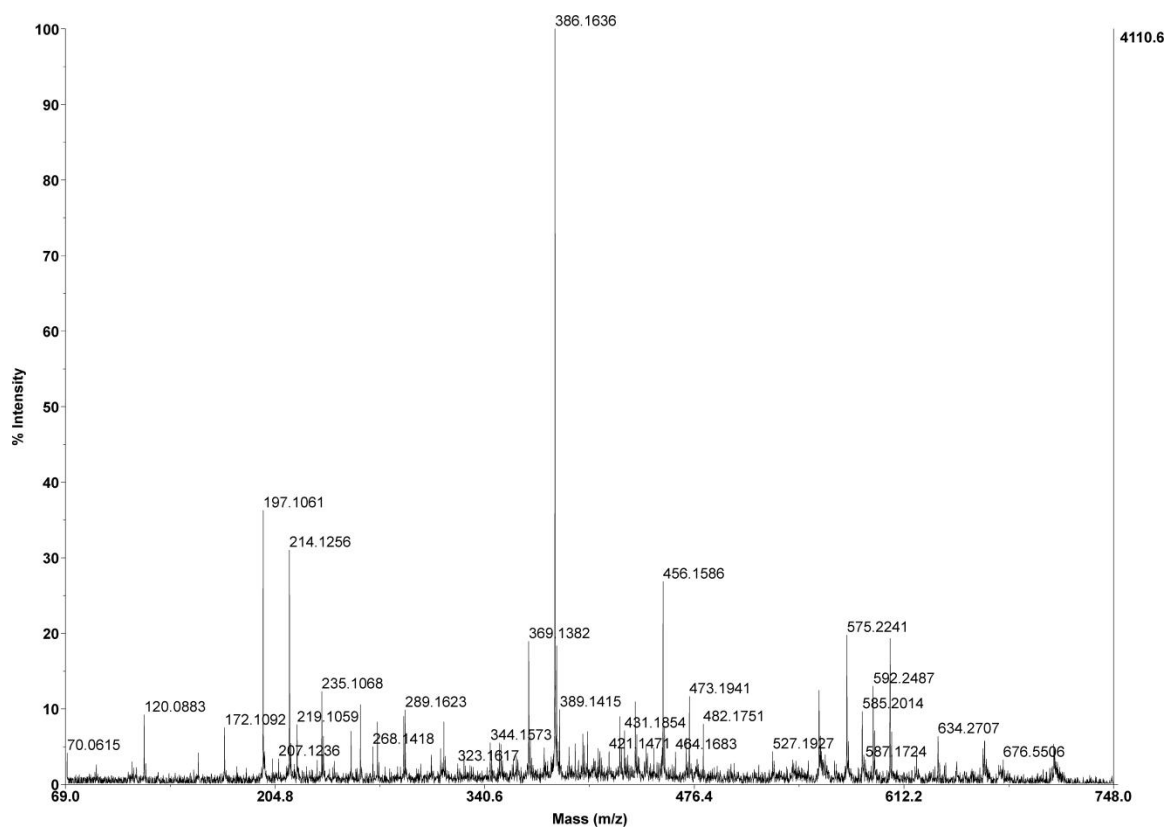


MS/MS spectrum of untreated H-GRGDSTW-NH<sub>2</sub> (**6**) after cleavage from tentagel resin

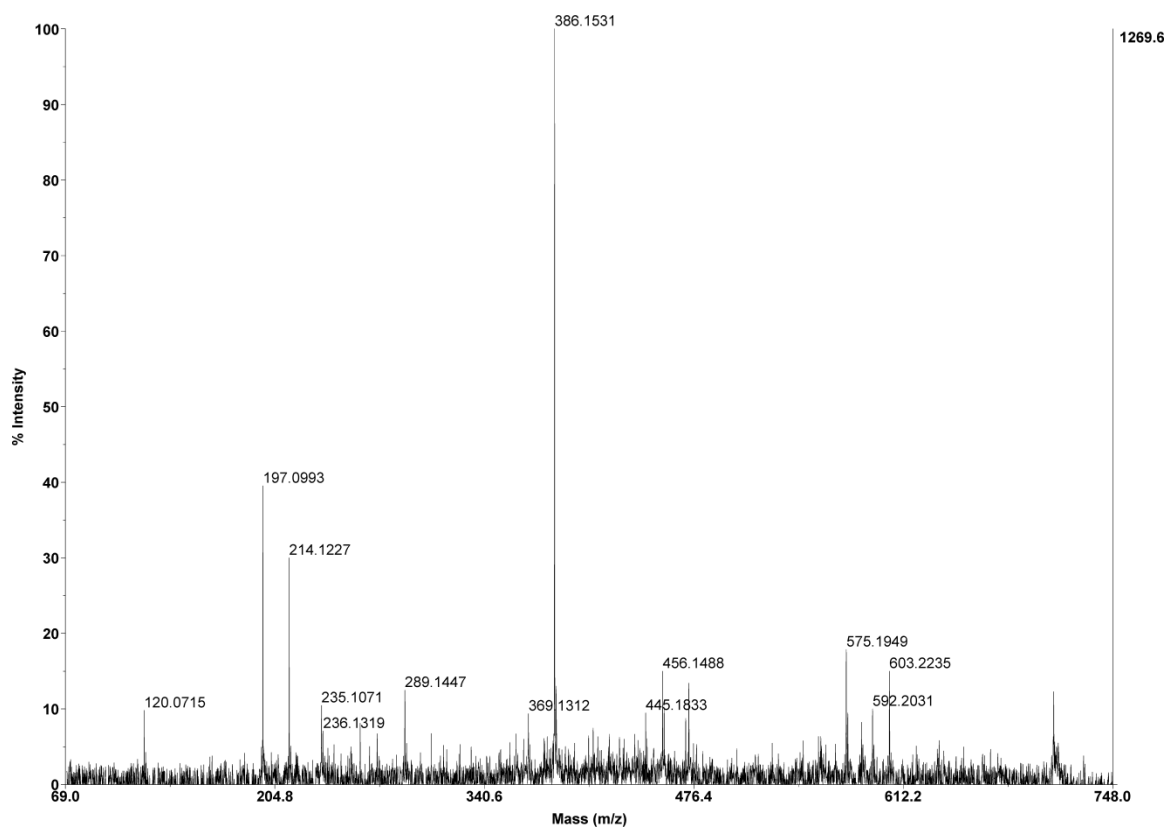


MS/MS spectrum of sorted H-GRGDSTW-NH<sub>2</sub> (**6**) after cleavage from tentagel resin





MS/MS spectrum of untreated H-GRGDSFA-NH<sub>2</sub> (**7**) after cleavage from tentagel resin



MS/MS spectrum of sorted H-GRGDSFA-NH<sub>2</sub> (7) after cleavage from tentagel resin

## APPENDIX IV - COPYRIGHT APPROVAL

Rightslink® by Copyright Clearance Center

https://s100.copyright.com/AppDispatchServlet



RightsLink®

Home

Account  
Info

Help



**Title:** Design, synthesis and in vitro characterization of Glucagon-Like Peptide-1 derivatives for pancreatic beta cell imaging by SPECT

**Author:** Babak Behnam Azad, Vanessa A. Rota, Daniel Breadner, Savita Dhanvantari, Leonard G. Luyt

**Publication:** Bioorganic & Medicinal Chemistry

**Publisher:** Elsevier

**Date:** 1 February 2010

Copyright © 2010, Elsevier

Logged in as:

Babak Behnam Azad

LOGOUT

**Order Completed**

Thank you very much for your order.

This is a License Agreement between Babak Behnam Azad ("You") and Elsevier ("Elsevier"). The license consists of your order details, the terms and conditions provided by Elsevier, and the [payment terms and conditions](#).

[Get the printable license.](#)

License Number	2653790578541
License date	Apr 21, 2011
Licensed content publisher	Elsevier
Licensed content publication	Bioorganic & Medicinal Chemistry
Licensed content title	Design, synthesis and in vitro characterization of Glucagon-Like Peptide-1 derivatives for pancreatic beta cell imaging by SPECT
Licensed content author	Babak Behnam Azad, Vanessa A. Rota, Daniel Breadner, Savita Dhanvantari, Leonard G. Luyt
Licensed content date	1 February 2010
Licensed content volume number	18
Licensed content issue number	3
Number of pages	8
Type of Use	reuse in a thesis/dissertation
Portion	full article
Format	print
Are you the author of this Elsevier article?	Yes
Will you be translating?	No
Order reference number	
Title of your thesis/dissertation	Development of Single and Multimodality Imaging Probes for PET, SPECT and Fluorescence Imaging
Expected completion date	Jul 2011
Estimated size (number of pages)	150
Elsevier VAT number	GB 494 6272 12
Permissions price	0.00 USD
VAT/Local Sales Tax	0.0 USD / 0.0 GBP
Total	0.00 USD

ORDER MORE...

CLOSE WINDOW

Copyright © 2011 Copyright Clearance Center, Inc. All Rights Reserved. [Privacy statement](#).  
Comments? We would like to hear from you. E-mail us at [customer@copyright.com](mailto:customer@copyright.com)

## APPENDIX V - ETHICS APPROVAL



October 14, 2008

**\*This is the Original Approval for this protocol\***  
 \*A Full Protocol submission will be required in 2011\*

Dear Dr. Dhanvantari:

Your Animal Use Protocol form entitled:  
 Development of GLP-1 Receptor Probes for Imaging Changes in Beta Cell Mass  
 Funding Agency CIHR - Grant #R3850A05; NSERC - Grant #R2850A04

has been approved by the University Council on Animal Care. This approval is valid from **Oct. 14, 2008 to Oct. 31, 2009**. The protocol number for this project is **#2008-117**.

1. This number must be indicated when ordering animals for this project.
2. Animals for other projects may not be ordered under this number.
3. If no number appears please contact this office when grant approval is received.  
 If the application for funding is not successful and you wish to proceed with the project, request that an internal scientific peer review be performed by the Animal Use Subcommittee office.
4. Purchases of animals other than through this system must be cleared through the ACVS office. Health certificates will be required.

#### ANIMALS APPROVED FOR 3 Years

Species	Strain	Other Detail	Pain Level	Animal # Total for 3 Years
Mouse	CD1	25-30 gms M/F	C	100
Mouse	NOD	25-30 gms M/F	C	60

#### REQUIREMENTS/COMMENTS

Please ensure that individual(s) performing procedures on live animals, as described in this protocol, are familiar with the contents of this document.

1. Please review Section L.9. for additional Occupational Health and Safety requirements.

c.c. Approved Protocol - S. Dhanvantari, D. Forder  
 Approval Letter - D. Forder

*The University of Western Ontario*  
 Animal Use Subcommittee / University Council on Animal Care  
 Health Sciences Centre, • London, Ontario • CANADA – N6A 5C1  
 PH: 519-661-2111 ext. 86770 • FL 519-661-2028 • www.uwo.ca / animal

## CURRICULUM VITAE

**Name:** Babak Behnam Azad

**Post-secondary Education and Degrees:**

The University of Western Ontario  
London, Ontario, Canada  
2007-2011 Ph.D.

McMaster University  
Hamilton, Ontario, Canada  
2005-2007 M.Sc.

McMaster University  
Hamilton, Ontario, Canada  
2000-2005 Hon. B.Sc.

**Honours and Awards:** Ontario Graduate Scholarship in Science and Technology  
2008-2009

**Related Work Experience:**

Teaching Assistant  
The University of Western Ontario  
2007-2011

McMaster University  
2003-2007

Research Associate  
McMaster Hospital  
2005-2007

Research Student  
McMaster University  
2003-2004

Laboratory Manager  
McMaster University  
2002

### **Publications:**

**Behnam Azad, B.;** Rota, V.; Breadner, D.; Dhanvantari, S. and Luyt, L. Design, synthesis and in vitro characterization of Glucagon-Like Peptide-1derivatives for pancreatic beta cell imaging by SPECT, *Bioorganic and Medicinal Chemistry*, **2010**, *18*, 1265-1272.

**Behnam Azad, B.;** Ashique, R.; Schrobilgen, G. J. and Chirakal, R. “Oxygen Difluoride: a Highly Selective Electrophilic Fluorinating Agent for *m*-tyrosine”, *Journal of Fluorine Chemistry*, **2008**, *129*, 22-27.

**Behnam Azad, B.;** Schrobilgen, G. J. and Chirakal, R., “Trifluoromethanesulfonic Acid, An Alternative Solvent Medium for the Direct Electrophilic Fluorination of Aromatic Amino Acids: New Syntheses of [<sup>18</sup>F]6-Fluoro-L-DOPA and [<sup>18</sup>F]6-Fluoro-D-DOPA”, *Journal of Labelled Compounds and Radiopharmaceuticals*, **2007**, *50* (14), 1236-1242.

### **Presentations**

**Behnam Azad, B.;** Cho, C-F.; Lewis, J. D. and Luyt, L. “Development of a Dual Modality Imaging Probe for PET and Fluorescence Imaging”, Pacificchem (Oral), Hawaii, Dec. 15-20, **2010**.

**Behnam Azad, B.;** V. Rota; S. Dhanvantari; M. Kovacs and L. Luyt, “Fluorine-18 Labeled GLP-1 Peptides for Beta Cell Imaging”, International Society of Radiopharmaceutical Sciences (Poster), Edmonton, Alberta, July 23-27, **2009**.

**Behnam Azad, B.;** Ashique R.; and Chirakal, R. V. “Temperature Effect on the Stereospecificity of nucleophilic Fluorination: Formation of [<sup>18</sup>F]*trans*-4-Fluoro-L-Proline during the synthesis of [<sup>18</sup>F]*cis*-4-Fluoro-L-Proline”, International Society of Radiopharmaceutical Sciences (Poster), Edmonton, Alberta, July 23-27, **2009**.

**Behnam Azad, B.;** Breadner, D.; Tai; J. H.; Dhanvantari, S.; Luyt, L. “Glucagon-Like Peptide-1 Derivatives for SPECT Imaging of Pancreatic Islets”, World Molecular Imaging Congress (Poster), Nice, France, Sept. 10-13, **2008**.